

CRANFIELD UNIVERSITY

FEDERICO LUPPI

INERT AND NITRATED CROSS-LINKED β -CYCLODEXTRIN
BINDERS FOR ENERGETIC APPLICATIONS

CRANFIELD DEFENCE AND SECURITY
PhD in Defence and Security

PhD
Academic Year: 2015 - 2019

Supervisor: Eleftheria Dossi
Associate Supervisor: Mike Williams
March 2019

CRANFIELD UNIVERSITY

CRANFIELD DEFENCE AND SECURITY
PhD in Defence and Security

PhD

Academic Year 2015 - 2019

FEDERICO LUPPI

Inert and Nitrated Cross-linked β -Cyclodextrin Binders for Energetic
Applications

Supervisor: Eleftheria Dossi
Associate Supervisor: Mike Williams
March 2019

This thesis is submitted in partial fulfilment of the requirements for
the degree of PhD

***(NB. This section can be removed if the award of the degree is
based solely on examination of the thesis)***

© Cranfield University 2019. All rights reserved. No part of this
publication may be reproduced without the written permission of the
copyright owner.

Abstract

This PhD project focuses on the synthesis of new inert and nitrated cross-linked cyclodextrin systems as binders for energetic formulations. Three diglycidyl ethers with polyethylene glycol segments differing in length were used to cross-link β -cyclodextrin. The physicochemical properties of the compounds were investigated by proton nuclear magnetic resonance spectroscopy, differential scanning calorimetry, thermogravimetric analysis and dynamic mechanical analysis. The polyethylene glycol chains linked to the rigid β -cyclodextrin conferred low glass transition temperatures (≥ -20 °C) on the inert binders and also on their nitrated derivatives (≥ -14 °C). This is the first time that nitrated β -cyclodextrin derivatives have shown viscoelastic behaviour at temperatures below 0 °C. The viscoelasticity of both the inert and nitrated compounds increased with the amount of polyethylene glycol chains in the system. Inert binders with higher polyethylene glycol: β -cyclodextrin units ratios were softer and exhibited self-healing behaviour. The thermo-mechanical characterisation of these binders revealed that the system was exposed to mechanical stress below the glass transition temperature, and the stress was directly related to the proportion of the soft polyethylene glycol segments. The nitrated cross-linked derivatives were characterised by decomposition temperatures of ~ 200 °C and thermal degradation energies of $1400\text{--}2100$ J g⁻¹ strictly dependent on the degree of cross-linking and nitration. Self-healing properties were confirmed in nitrated products with a high polyethylene glycol segments content. Nitrated samples with polyethylene glycol segments: β -cyclodextrin units ratios $>3.8:1$ were safer to handle in the laboratory as determined by small-scale hazard and compatibility tests with various energetic fillers. Additionally, preliminary Energetic Materials Testing Assessment Policy (EMTAP) tests confirmed the samples were not sensitive to electrostatic discharge up to 4.5 J but were sensitive to impact, with a figure of insensitiveness of 29. The nitrated samples were unstable at temperatures >80 °C. The materials developed during this PhD project could facilitate the manufacturing and storage of new binders and may offer a suitable replacement for nitrocellulose and other binders in

energetic formulations. The stabilisation of the nitrated cross-linked binders should be prioritised in future work.

Keywords: β -cyclodextrin, polyethylene glycol, cross-linking, thermal stability

This PhD was funded through the Weapons Science and Technology Centre (WSTC) by the UK Defence Science and Technology Laboratory (DSTL)

Acknowledgements

To the Centre for Defence Chemistry and my family. Many Thanks!

I am grateful to my father and mother, who have provided me thorough emotional support and a moral compass in my life. I am also grateful to my childhood friends who have supported me along the way.

Special gratitude goes out to the staff of the Centre for Defence Chemistry. A special mention goes to my supervisor Eleftheria Dossi, who guided and advised me over the past four years, helping me to overcome all the obstacles I have met. Thank you to my adoptive mentor Guillaume Kister for having guided me as if I was one of his own PhD students. I am also grateful to the other CfDC university staff: Jeff Pons, Ian Wilson, Dan McAteer, Matt Parker, Lisa Humphreys, Matt Weaver, Peter Wilkinson, Nicola Darcy, Susan Waring, Mark Carpenter, Nathalie Mai, Philp Gill, Roger Cox, Mike Williams, Sally Gaulter, Chris Stennet, Matt Goldsmith, Scott Clews, Susan Hardy and Patricia Pye for their unfailing support and assistance.

And finally, last but by no means least, also to my friends, it was great sharing the burden of the many challenges we and I have faced. To Hamish, Alejandro, Erick, Andrea, Antonio and Christine:

Ubi amici, ibidem opes. (*Plauto*)

TABLE OF CONTENTS

Abstract	i
Acknowledgements	iii
LIST OF FIGURES	vii
LIST OF TABLES	xiv
LIST OF EQUATIONS	xvi
LIST OF ABBREVIATIONS	1
1 Overview	4
1.1 Objectives	5
1.2 Academic contributions	7
1.3 Thesis structure	7
2 Introduction	9
2.1 Insensitive munitions	9
2.2 Polymers and their properties	10
2.3 Polymers as binders in energetic formulations	12
2.4 Cyclodextrins	19
2.4.1 Properties of CDs	21
2.4.2 Synthesis of cyclodextrins	30
2.4.3 Cross-linking of cyclodextrins	30
2.4.4 Energetic applications of unlinked/cross-linked cyclodextrins	34
3 Experimental	41
3.1 Materials	41
3.2 Methods	41
3.2.1 NMR spectroscopy	41
3.2.2 FTIR spectroscopy	41
3.2.3 Gel permeation chromatography	41
3.2.4 Differential scanning calorimetry and thermal gravimetric analysis ..	42
3.2.5 Dynamic mechanical analysis	42
3.2.6 Optical microscopy	43
3.2.7 Scanning electron microscopy	44
3.3 Procedures	44
3.3.1 Triethylene glycol diglycidyl ether ^[120]	44
3.3.2 Hexaethylene glycol diglycidyl ether ^[120]	44
3.3.3 Cross-linked cyclodextrins (β CXCDs)	45
3.3.4 Nitrated cross-linked cyclodextrins (β NCXCDs)	45
3.3.5 Hazard testing	46
3.3.6 Compatibility tests	47
3.3.7 Stability analysis	48
4 Synthesis and characterisation of inert β CXCDs	49
4.1 Synthesis and chemical characterisation	49
4.1.1 Effect of the NaOH concentration	53

4.1.2 Effect of the reaction time.....	54
4.1.3 Effect of the temperature.....	55
4.1.4 Effect of β CD alkoxide formation.....	56
4.1.5 Effect of the volume of NaOH solution	56
4.1.6 Effect of cross-linker: β CD ratio.....	57
4.1.7 Effect of the duration of cross-linker addition	59
4.2 The synthesis of β CXCDs.....	60
4.3 Thermal and thermo-mechanical characterisation of β CXCDs	78
4.3.1 Thermo-mechanical characterisation of the starting materials	79
4.3.2 Thermal and thermo-mechanical characterisation of inert β CXCDs	93
4.4 Conclusions	112
5 Synthesis and characterisation of energetic cross-linked β NCXCDs	115
5.1 Attempts to nitrate the insoluble β CXCD precursors.....	117
5.2 Attempts to nitrate the soluble β CXCD precursors	119
5.3 Synthesis and chemical characterisation of β NCXCDs	121
5.4 Thermal and thermo-mechanical characterisation of energetic β NCXCDs	133
5.4.1 Thermal characterisation of β NCXCDs prepared from insoluble precursors	134
5.4.2 Thermal characterisation of β NCXCDs prepared from soluble precursors	137
5.4.3 Thermo-mechanical characterisation of β NCXCDs	144
5.4.4 Qualitative analysis of the self-healing properties of β NCPCD34... ..	145
5.5 Conclusions	145
6 Compatibility, hazard and stability studies.....	147
6.1 Compatibility tests – β CXCDs.....	147
6.2 Compatibility tests – β NCXCDs	155
6.3 Hazard tests – β NCXCDs	164
6.3.1 EMTAP tests	169
6.4 Stability of β NCXCDs determined by heat flow calorimetry	171
6.5 Conclusion	173
7 Conclusion and recommendations	177
REFERENCES.....	183

LIST OF FIGURES

Figure 2.1 Chemical structure of triethylene glycol diglycidyl ether	19
Figure 2.2 Chemical structure of α , β and γ CDs [40].....	20
Figure 2.3 Distribution of the CD publications by application (1996–2013) according to <i>CD News</i> [38].	21
Figure 2.4 Structures of (a) α -D-glucopyranoside, the repeating unit of CD, and (b) the toroid representation of CDs, with primary and secondary hydroxyl groups in red and blue, respectively. H1, H2 and H4 are external to the toroid, whereas H3 and H5 are internal	22
Figure 2.6 Schematic representation of a polyrotaxane formed by several CDs threaded on a polymer chain with ending caps.....	24
Figure 2.7 The ^1H -NMR spectra of CD (a) in D_2O and (b) in DMSO-d_6 [63].	28
Figure 2.8 The infrared spectrum of βCD	29
Figure 4.1 Dialysis apparatus for the purification of βCXCDs	59
Figure 4.2 Cross-linking apparatus for the synthesis of βCXCDs	61
Figure 4.3 Physical characteristics of βCPCD . (a) Malleable IP13. (b) Powdery IP17.	64
Figure 4.4 Proposed chemical structure of the βCXCD products based on IP13 incorporating PEG segments, underlining the co-existence of PEG units as spacers and as entanglements.....	65
Figure 4.5 Comparative ^1H NMR spectra of (a) sample IP13 (PEG: βCD ratio = 3.8:1), (b) PEGDGE, and (c) βCD in DMSO-d_6 with assignments of signals. The DMSO reference peak is at 2.5 ppm. R= H, cross-linker $\text{C}_a\text{-OR}$ = H or βCD	66
Figure 4.6 Comparative ^1H NMR spectra of (a) IP13 (PEG: βCD ratio = 3.8:1), (b) mixture of degraded/non degraded PEGDGE, and (c) PEGDGE in DMSO-d_6	68
Figure 4.7 (a) The ^1H -NMR spectrum of IP13 (PEG: βCD ratio = 3.8:1) in D_2O and (b) the proposed chemical structure of βCXCDs highlighting the two different situations for the anomeric H-1, when in unit 1 or unit 2 of βCXCDs	69
Figure 4.8 The ^1H -NMR spectrum of IP13 (PEG: βCD ratio = 3.8:1) in D_2O . Int_1 = anomeric H-1, Int_3 = CH_2 of PEG.....	71
Figure 4.9 Comparative ^1H -NMR spectra of βCPCD samples (IP13, IP15–IP17) with different PEG: βCD ratios. Lower ratios enhance the visibility of the βCD proton (marked with the arrow).....	72

Figure 4.10 Comparative FTIR spectra of β CD (black curve), β CPCD sample IP13 (red curve), and PEGDGE (blue curve).....	73
Figure 4.11 GPC analysis of β CD compared to polyethylene glycol/polyethylene oxide standards.	74
Figure 4.12 GPC analysis of PEGDGE compared to polyethylene glycol/polyethylene oxide standards.	74
Figure 4.13 Analysis of β CXCDs by GPC compared to polyethylene glycol/polyethylene oxide standards. (a) Sample IP22 (PEG: β CD ratio = 2.9). (b) Sample IH2 (HEG: β CD ratio = 3.2). (c) Sample IT2 (TEG: β CD ratio = 3.1).	76
Figure 4.14 Analysis of β CTCDs by GPC compared to polyethylene glycol/polyethylene oxide standards. (a) Sample IT1 (TEG: β CD ratio = 3.6). (b) Sample IT2 (TEG: β CD ratio = 3.1). (c) Sample IT3 (TEG: β CD ratio = 2.4). (d) Sample IT4 (TEG: β CD ratio = 1.9).....	77
Figure 4.15 Combined TGA and DSC analysis of β CD ($10\text{ }^{\circ}\text{C min}^{-1}$, 25–500 $^{\circ}\text{C}$, aluminium crucible).....	79
Figure 4.16 The decomposition of β CD observed by melting point analysis. At 317 $^{\circ}\text{C}$, melting and caramelisation are dominant, but above 328 $^{\circ}\text{C}$ charring prevails.	80
Figure 4.17 DSC heating curves of β CD ($10\text{ }^{\circ}\text{C min}^{-1}$) from –100 to 100 $^{\circ}\text{C}$ in the first cycle (black), from –100 to 120 $^{\circ}\text{C}$ in the second cycle (blue), and from –100 to 140 $^{\circ}\text{C}$ in the third cycle (red).	81
Figure 4.18 DMA showing variation in the storage modulus (E' , solid lines) and $\tan\delta$ (dashed lines) of β CD ($10\text{ }^{\circ}\text{C min}^{-1}$, 1 Hz, third temperature cycle, –100 to 140 $^{\circ}\text{C}$, aluminium pocket).....	82
Figure 4.19 Combined DSC/TGA thermograms of the cross-linkers TEGDGE (black), HEGDGE (blue) and PEGDGE (red), from 30 to 500 $^{\circ}\text{C}$ ($10\text{ }^{\circ}\text{C min}^{-1}$, third temperature cycle, aluminium crucible).	83
Figure 4.20 DSC thermogram of the cross-linkers: heating (solid) and cooling (dashed) of TEGDGE (black), HEGDGE (blue) and PEGDGE (red) from –100 to 120 $^{\circ}\text{C}$ ($10\text{ }^{\circ}\text{C min}^{-1}$, third temperature cycle, aluminium crucible).	85
Figure 4.21 DMA showing variation in the storage modulus (E' , solid lines) and $\tan\delta$ (dashed lines) of PEGDGE ($10\text{ }^{\circ}\text{C min}^{-1}$, 1 Hz, third temperature cycle from –100 to 100 $^{\circ}\text{C}$, aluminium pocket).	87
Figure 4.22 DMA showing variation in the storage modulus (E') of PEGDGE with frequency ($10\text{ }^{\circ}\text{C min}^{-1}$, 1 and 10 Hz, third temperature cycle from –100 to 100 $^{\circ}\text{C}$, aluminium pocket).....	89
Figure 4.23 DMA showing variation in the storage modulus (E' , solid lines) and $\tan\delta$ (dashed lines) of HEGDGE ($10\text{ }^{\circ}\text{C min}^{-1}$, 1 Hz, third temperature cycle from –100 to 100 $^{\circ}\text{C}$, aluminium pocket).	90

Figure 4.24 DMA showing variation in the storage modulus (E' , solid lines) of HEGDGE with the frequency ($10\text{ }^{\circ}\text{C min}^{-1}$, 1 and 10 Hz, third temperature cycle from -100 to $100\text{ }^{\circ}\text{C}$, aluminium pocket).	91
Figure 4.25 DMA showing variation in the storage modulus (E' , solid lines) and $\tan\delta$ (dashed lines) of TEGDGE ($10\text{ }^{\circ}\text{C min}^{-1}$, 1 Hz, third temperature cycle from -100 to $100\text{ }^{\circ}\text{C}$, aluminium pocket).	92
Figure 4.26 DMA showing variation in the storage modulus (E' , solid lines) and $\tan\delta$ (dashed lines) of TEGDGE in an extended temperature scan ($10\text{ }^{\circ}\text{C min}^{-1}$, 1 Hz, third temperature cycle from -140 to $100\text{ }^{\circ}\text{C}$, aluminium pocket).....	93
Figure 4.27 Combined DSC analysis and TGA of IP18 (PEG: β CD ratio = 4.1:1, red line) and its precursors β CD (blue) and PEGDGE (green) over the temperature range 30 – $500\text{ }^{\circ}\text{C}$ ($10\text{ }^{\circ}\text{C min}^{-1}$, aluminium crucible).	97
Figure 4.28 DSC analysis showing the plasticising effect of water in IP18 from -100 to $120\text{ }^{\circ}\text{C}$ ($10\text{ }^{\circ}\text{C min}^{-1}$, third temperature cycle, aluminium crucible).	98
Figure 4.29 DSC analysis of β CXCD products with high XEG: β CD ratios, namely IT1 (3.6:1, black line), IH1 (4.0:1, blue line) and IP13 (3.8:1, red line) from -100 to $120\text{ }^{\circ}\text{C}$ ($10\text{ }^{\circ}\text{C min}^{-1}$, third temperature cycle, aluminium crucible).....	99
Figure 4.30 Photographs of β CPCD samples supported by (a) an aluminium pocket, (b) a stainless-steel mesh, and (c) an aluminium pocket wrapped in PTFE tape.	100
Figure 4.31 DMA showing variation in the storage modulus (E' , solid lines) and $\tan\delta$ (dashed lines) of sample IP9 ($10\text{ }^{\circ}\text{C min}^{-1}$, 1 Hz, third temperature cycle from -100 to $140\text{ }^{\circ}\text{C}$, aluminium pocket).	102
Figure 4.32 DMA showing variation in the storage modulus (E') and $\tan\delta$ of sample IP9 (PEG: β CD ratio = 3.5, solid and dotted red lines) and IP17 (PEG: β CD ratio = 1.6, solid and dotted blue lines) ($10\text{ }^{\circ}\text{C min}^{-1}$, 1 Hz, third temperature cycle from -100 to $140\text{ }^{\circ}\text{C}$, aluminium pocket).....	103
Figure 4.33 DMA showing variation in the storage modulus (E' , solid lines) and $\tan\delta$ (dashed lines) of IP9 ($10\text{ }^{\circ}\text{C min}^{-1}$, 1 Hz, third temperature cycle, -100 to $140\text{ }^{\circ}\text{C}$, stainless-steel mesh).....	105
Figure 4.34 DMA showing variation in the storage modulus (E' , solid lines) and $\tan\delta$ (dashed lines) of IP9 ($10\text{ }^{\circ}\text{C min}^{-1}$, 1 Hz, third temperature cycle, -100 to $140\text{ }^{\circ}\text{C}$, aluminium pocket and PTFE tape).....	106
Figure 4.35 Optical microscope images of IP9 (PEG: β CD ratio = 3.5) during the first temperature cycle from -100 to $100\text{ }^{\circ}\text{C}$. The top row (a-d) shows the cooling phase captured at $25\text{ }^{\circ}\text{C}$, $-55\text{ }^{\circ}\text{C}$, $-78\text{ }^{\circ}\text{C}$ and $-80\text{ }^{\circ}\text{C}$ and the bottom row (e-h) shows the heating phase captured at $2\text{ }^{\circ}\text{C}$, $43\text{ }^{\circ}\text{C}$, $67\text{ }^{\circ}\text{C}$ and $87\text{ }^{\circ}\text{C}$	107

Figure 4.36 Optical microscope images of IP9 (PEG:βCD ratio = 3.5) during the second temperature cycle from –100 to 100°C. The top row (a-d) shows the cooling phase captured at 100 °C, 25 °C, –61 °C and –88 °C and the bottom row (e-h) shows the heating phase captured at 5 °C, 43 °C, 68 °C and 84 °C.....	107
Figure 4.37 Self-healing of IP13 (PEG:βCD ratio = 3.8). (a) Sample after solvent evaporation. (b) Sample after cutting. (c) The parts are placed in contact. (d) The sample is heated to 70 °C for 30 min and pulled by the extremities.	108
Figure 4.38 Scanning electron micrograph of βCD crystals.	109
Figure 4.39 Scanning electron micrographs of the βCTCDs (a) IT1 (b) IT2 (c) IT3 and (d) IT4.....	110
Figure 4.40 Scanning electron micrographs of the βCHCDs (a) IH1 and (b) IH4, and the βCPCDs (c) IP19 and (d) IP17.	111
Figure 4.41 DMA showing variation in the storage modulus (E', solid lines) and tanδ (dashed lines) of sample IP17 (10% w/w) formulated with 90% w/w melamine (10 °C min ⁻¹ , 1 Hz, third temperature cycle from –100 to 140 °C, aluminium pocket).	112
Figure 5.1 Physical appearance of the insoluble IP26 and IT5–IT7 precursors.	118
Figure 5.2 Nitrated product degraded by the use of NaOH during purification.	121
Figure 5.3 The ¹ H NMR spectra of (a) βNCD [116] and (b) NP1 in DMSO-d ₆	123
Figure 5.4 Comparative ¹ H-NMR spectra of (a) inert precursor IP18 (PEG:βCD ratio = 2.5:1) and (b) its nitrated product NP1, both in DMSO-d ₆	124
Figure 5.5 The ¹ H NMR spectra of products (a) NP1, (b) NH1 and (c) NT1 in DMSO-d ₆ . The XEG:βCD ratios were previously determined by NMR spectroscopy.	125
Figure 5.6 The ¹ H NMR spectra of products (a) NP1, (b) NP2, (c) NP3 and (d) NP4, which show a gradually decreasing PEG:βCD ratio.	126
Figure 5.7 Comparative FTIR spectra of sample NP1 (solid line) and its inert precursor IP18 (dashed line).	129
Figure 5.8 Comparative FTIR spectra of sample NP1 (solid line) and βNCD (dashed line).....	130
Figure 5.9 Comparative GPC analysis of βNXCDs: (a) NP1 (PEG:βCD ratio = 3.8), (b) NH1 (HEG:βCD ratio = 4.0), and (c) NT1 (TEG:βCD ratio = 3.8).	132

Figure 5.10 Comparative GPC chromatograms of β NPCDs with decreasing PEG: β CD ratios: (a) NP1 (PEG: β CD ratio = 3.8), (b) NP2 (PEG: β CD ratio = 2.6), (c) NP3 (PEG: β CD ratio = 2.1), and (d) NP4 (PEG: β CD ratio = 1.6).	133
Figure 5.11 DSC thermogram of NP9, from 30 to 300 °C (10 °C min ⁻¹ , aluminium crucible).....	135
Figure 5.12 DSC thermogram of NT7, from 30 to 500 °C (10 °C min ⁻¹ , aluminium crucible).....	135
Figure 5.13 DSC thermogram of NT9 from -100 to 100 °C (10 °C min ⁻¹ , third temperature cycle, aluminium crucible).	137
Figure 5.14 DSC thermogram of NP1 from 25 to 300 °C (10 °C min ⁻¹ , aluminium crucible).....	140
Figure 5.15 DSC thermogram of NP1 from -100 to 100 °C showing the pronounced glass transition of the highly cross-linked products (10 °C min ⁻¹ , aluminium crucible).....	141
Figure 5.16 Plot of T _g against XEG: β CD ratio for β CHCDs (blue line) and β CPCDs (orange line).	142
Figure 5.17 DMA showing variation in the storage modulus (E', solid lines) and tan δ (dashed lines) of NP1 (10 °C min ⁻¹ , 1 Hz, third temperature cycle from -100 to 140 °C, aluminium pocket).....	144
Figure 5.18 Self-healing ability of NP1 (PEG: β CD ratio = 4:1).	145
Figure 6.1 DSC thermogram of HMX (blue line), IP19 (red line), and a 50/50 (w/w) mixture (black line) from 30 to 300 °C (1 mg, 2 °C min ⁻¹ , aluminium crucible).....	149
Figure 6.2 DSC thermogram of RDX (blue line), IP19 (red line), and a 50/50 (w/w) mixture (black line) from 30 to 300 °C (1 mg, 2 °C min ⁻¹ , aluminium crucible).....	150
Figure 6.3 DSC thermogram of PETN (blue line), IP19 (red line), and a 50/50 (w/w) mixture (black line) from 30 to 300 °C (1 mg, 2 °C min ⁻¹ , aluminium crucible).....	150
Figure 6.4 DSC thermogram of ADN (blue line), IP19 (red line), and a 50/50 (w/w) mixture (black line) from 30 to 300 °C (1 mg, 2 °C min ⁻¹ , aluminium crucible).....	151
Figure 6.5 DSC thermogram of KClO ₃ (blue line), IP19 (red line), and a 50/50 (w/w) mixture (black line) from 30 to 400 °C (1 mg, 2 °C min ⁻¹ , aluminium crucible).....	152
Figure 6.6 DSC thermogram of KNO ₃ (blue line), IP19 (red line), and a 50/50 (w/w) mixture (black line) from 30 to 300 °C (1 mg, 2 °C min ⁻¹ , aluminium crucible).....	152

Figure 6.7 DSC thermogram of NH_4ClO_4 (blue line), IP19 (red line), and a 50/50 (w/w) mixture (black line) from 30 to 500 °C (1 mg, 2 °C min ⁻¹ , aluminium crucible).....	153
Figure 6.8 DSC thermogram of NH_4NO_3 (blue line), IP19 (red line), and a 50/50 (w/w) mixture (black line) from 30 to 300 °C (1 mg, 2 °C min ⁻¹ , aluminium crucible).....	154
Figure 6.9 DSC thermogram of red phosphorus (blue line), IP19 (red line), and a 50/50 (w/w) mixture (black line) from 30 to 550 °C (1 mg, 2 °C min ⁻¹ , aluminium crucible).....	154
Figure 6.10 DSC thermograms of HMX (blue line), NP13 (red line), and a 50/50 (w/w) mixture (black line) from 30 to 300 °C (1 mg, 2 °C min ⁻¹ , aluminium crucible).....	156
Figure 6.11 DSC thermograms of RDX (blue line), NP13 (red line), and a 50/50 (w/w) mixture (black line) from 30 to 300 °C (1 mg, 2 °C min ⁻¹ , aluminium crucible).....	157
Figure 6.12 DSC thermograms of PETN (blue line), NP13 (red line), and a 50/50 (w/w) mixture (black line) from 30 to 300 °C (1 mg, 2 °C min ⁻¹ , aluminium crucible).....	158
Figure 6.13 DSC thermograms of ADN (blue line), NP13 (red line), and a 50/50 (w/w) mixture (black line) from 30 to 300 °C (1 mg, 2 °C min ⁻¹ , aluminium crucible).....	159
Figure 6.14 DSC thermograms of KClO_3 (blue line), NP13 (red line), and a 50/50 (w/w) mixture (black line) from 30 to 400 °C (1 mg, 2 °C min ⁻¹ , aluminium crucible).....	159
Figure 6.15 DSC thermograms of KNO_3 (blue line), NP13 (red line), and a 50/50 (w/w) mixture (black line) from 30 to 400 °C (1 mg, 2 °C min ⁻¹ , aluminium crucible).....	160
Figure 6.16 DSC thermograms of NH_4ClO_4 (blue line), NP13 (red line), and a 50/50 (w/w) mixture (black line) from 30 to 500 °C (1 mg, 2 °C min ⁻¹ , aluminium crucible).....	160
Figure 6.17 DSC thermograms of NH_4NO_3 (blue line), NP13 (red line), and a 50/50 (w/w) mixture (black line) from 30 to 300 °C (1 mg, 2 °C min ⁻¹ , aluminium crucible).....	161
Figure 6.18 DSC thermograms of RedP (blue line), NP13 (red line), and a 50/50 (w/w) mixture (black line) from 30 to 550 °C (1 mg, 2 °C min ⁻¹ , aluminium crucible).....	162
Figure 6.19 DSC thermograms of DPA (blue line), NP1 (red line), and a 50/50 (w/w) mixture (black line) from 30 to 300 °C (1 mg, 2 °C min ⁻¹ , aluminium crucible).....	163

Figure 6.20 DSC thermograms of 2,4-NDPA (blue line), NP1 (red line), and a 50/50 (w/w) mixture (black line) from 30 to 300 °C (1 mg, 2 °C min⁻¹, aluminium crucible)..... 163

Figure 6.21 DSC thermograms of Centralite (blue line), NP1 (red line), and a 50/50 (w/w) mixture (black line) from 30 to 550 °C (1 mg, 2 °C min⁻¹, aluminium crucible)..... 164

Figure 6.22 Thermal stability of pure NP1 and the same compound in the presence of three different stabilisers (1% w/w). 172

LIST OF TABLES

Table 2.1 List of binders in energetic formulations [23].	13
Table 2.2 Example of polymers used in energetic applications [20].	15
Table 2.3 Examples of energetic polymers used as binders [20].	17
Table 2.4 The physical properties of α , β and γ CDs [38].	22
Table 2.5 Thermal properties of α , β and γ CDs.	23
Table 2.6 The ^1H -NMR chemical shifts of CD protons in D_2O and DMSO-d_6 [63].	29
Table 2.7 The ^{13}C NMR chemical shifts of CDs in D_2O [63].	29
Table 2.8 Applications of cross-linked CDs	31
Table 2.9 Applications of CDs functionalised with energetic molecules.	34
Table 2.10 Summary of βCD nitration conditions [114].	36
Table 2.11 Performance of TEMTN: βNCD propellant formulations [114].	37
Table 2.12 Sensitivity of nitrated cross-linked βCCD and RDX complexes [109]	38
Table 4.1 Effect of NaOH concentration on the yield of βCPCDs at a PEGDGE: βCD ratio of 9:1.	53
Table 4.2 Effect of the reaction time (Step 2) on the yield of βCPCDs .	54
Table 4.3 Effect of the temperature on the yield of βCPCDs , when the PEGDGE: βCD ratio is 5:1.	55
Table 4.4 Effect of the time allowed for βCD alkoxide formation (Step 1) on the yield of βCPCDs .	56
Table 4.5 Effect of PEGDGE: βCD ratio on the yield of βCPCDs .	57
Table 4.6 Effect of cross-linker addition time.	60
Table 4.7 Synthesis of βCXCDs : summary of the most successful water-soluble products.	63
Table 4.8 Combined DSC/TGA data for the cross-linkers.	84
Table 4.9 Summary of the thermal properties of the βCXCDs .	95
Table 4.10 Comparison of DMA and DSC results for βCXCD samples and their precursors.	101
Table 5.1 Nitrogen content of the βNCXCDs .	128

Table 5.2 Thermal properties of the energetic derivatives of gel-like insoluble β CPCDs and insoluble β CTCD powders.	136
Table 5.3 Thermal properties of β NCXCDs prepared from water-soluble β CXCDs.	138
Table 6.1 Compatibility of inert β CPCD (sample IP19, PEG: β CD ratio = 4.0:1) with various energetics.	148
Table 6.2 Compatibility of nitrated β NCPCD (samples NP13 and NP1, PEG: β CD ratio = 3.8:1) with various energetics and stabilisers.	155
Table 6.3 Preliminary small-scale compatibility tests performed on β NCTCDs and β NCTCDs containing TEG and PEG units, respectively.	166
Table 6.4 EMTAP test data for sample NP17 based on Rotter impact and ESD values.	170
Table 6.5 DSC analysis of the decomposition temperatures of sample NP1 before and after HFC tests.	173

LIST OF EQUATIONS

Equation 1 Number of β CD anomeric protons determined by $^1\text{H-NMR}$	70
Equation 2 Number of all XEG: β CD protons in β CXCDs	70
Equation 3 Correction factor: Determination of nitrogen content.....	127
Equation 4 Nitrogen content (percentage)	127
Equation 5 Oxygen balance of explosives (percentage)	143

LIST OF ABBREVIATIONS

2,4-NDPA	2,4-Dinitrodiphenylamine
AP	Ammonium perchlorate
CD	Cyclodextrin
CEF	Trichloroethyl phosphate
CL-20	Hexanitrohexaazaisowurtzitane
CTPB	Carboxyl-terminated polybutadiene
D ₂ O	Deuterated water
DMA	Dynamic mechanical analysis
DMSO-d ₆	Deuterated dimethylsulfoxide
DNAN	2,4-Dinitroanisole
DPA	Diphenylamine
DS	Degree of substitution
DSC	Differential scanning calorimetry
E'	Storage modulus
EMTAP	Energetic Materials Testing Assessment Policy
ESD	Electrostatic discharge
Fol	Figure of insensitiveness
FTIR	Fourier transformed infrared
GPC	Gel permeation chromatography
HEG	Hexaethylene glycol unit
HEGDGE	Hexaethylene glycol diglycidyl ether
HFC	Heat flow calorimetry
HTPB	Hydroxyl-terminated polybutadiene
IH	Inert cross-linked β CD containing HEG units
IM	Insensitive munition
IP	Inert cross-linked β CD containing PEG units
IR	Infrared
IT	Inert cross-linked β CD containing TEG units
Kel-F 800	Poly(chlorotrifluoroethylene-co-vinylidene fluoride)
MIL-STD	Military standard
MWCO	Molecular weight cut-off

NC	Nitrocellulose
NCD	Nitrated cyclodextrin
NH	Nitrated cross-linked β CD containing HEG units
NMR	Nuclear magnetic resonance
NP	Nitrated cross-linked β CD containing PEG segments
NT	Nitrated cross-linked β CD containing TEG segments
PBAA	Polybutadiene-acrylic acid copolymer
PBAN	Polybutadiene-co-acrylonitrile
PEG	Polyethylene glycol unit
PEGDGE	Polyethylene glycol diglycidyl ether (500 Da)
PTFE	Polytetrafluoroethylene
RT	Room temperature
SEM	Scanning electron microscopy
STANAG	Standardisation agreement
$\tan\delta$	Damping factor
TBAB	Tetrabutyl ammonium bromide
TEG	Triethylene glycol unit
TEGDGE	Triethylene glycol diglycidyl ether
T_g	Glass transition temperature
TGA	Thermal gravimetric analysis
THF	Tetrahydrofuran
TIVS	Thermal initiated venting system
TMETN	Trimethylolethane trinitrate
TNAZ	1,3,3-Trinitroazetidine
TNT	Trinitrotoluene
TPE	Thermoplastic elastomer
XEG	Generic polyethylene glycol unit, used as a collective term for TEG, HEG and PEG units
β CD	β -Cyclodextrin
β CHCD	Cross-linked β CD containing HEG units
β CPCD	Cross-linked β CD containing PEG units
β CTCD	Cross-linked β CD containing TEG units
β CXCD	Generic cross-linked β CD system containing X segments, where

	X=TEG, HEG or PEG
β NCD	Nitrated β CD
β NCHCD	Nitrated cross-linked β CD containing HEG units
β NCPCD	Nitrated cross-linked β CD containing PEG units
β NCTCD	Nitrated cross-linked β CD containing TEG units
β NCXCD	Generic nitrated cross-linked β CD system containing X units, where X=TEG, HEG or PEG
Ω	Oxygen balance

1 Overview

The development of new binders is fundamental to the design of more advanced insensitive munitions (IMs). The function of the binder is to support the constituents of a formulation and create a cohesive mass. Binders also improve the properties of formulations, increasing their mechanical strength and/or the processability of the formulated energetics.

Binders used in the defence industry must enable the production of safe formulations with low vulnerability to stimuli such as impact, heat and electrostatic discharge (ESD) without compromising the energetic performance of the formulations.

Most traditional binders are unsustainably derived from crude oil and do not make an energetic contribution to the formulation. One exception is nitrocellulose (NC), which is sustainably derived from cotton cellulose and has been used extensively through history as a filler and energetic binder. However, NC has inconsistent batch-to-batch physicochemical properties due to structural differences caused by the origin of the cotton and the conditions of cultivation, harvesting and storage. These differences affect the properties of the biomass (lignocellulose) and ultimately those of the nitrated derivatives and the resulting energetic formulations. The selection and certification of cotton batches suitable for NC production is therefore a long and expensive process.

This PhD project focused on the development of reliable, sustainable binders that contribute to the energetic content of a formulation. With insight from the pharmaceutical industry, β -cyclodextrin (β CD) was considered as one of the most promising building blocks for future binders. This compound can be synthesised inexpensively from a renewable resource (starch) using a robust, enzymatic process. Natural β CD can be used to entrap small molecules such as drugs in pharmaceutical formulations.

The functionalisation of the hydroxyl groups in β CD is a simple and convenient method to produce new oligomeric and polymeric derivatives. The multiple hydroxyl groups in β CD macrocycles allow the creation of three-dimensional

(3D) macrostructures with enhanced inclusion ability. The main constituents of energetic formulations such as explosives, oxidisers and pyrotechnic fillers would be less susceptible to external stimuli when embedded in a β CD-based binder, making the formulation safer and easier to handle.

1.1 Objectives

The overall aim of this PhD project was to synthesise a series of energetic cross-linked β CD derivatives and characterise them to determine their suitability as novel binders. Pure β CD and its nitrated derivatives are unsuitable for the processing of energetics due to the high crystallinity of these molecules. Flexible polyethylene glycol segments of various lengths (XEG) were therefore chosen to cross-link β CD and improve its processability.

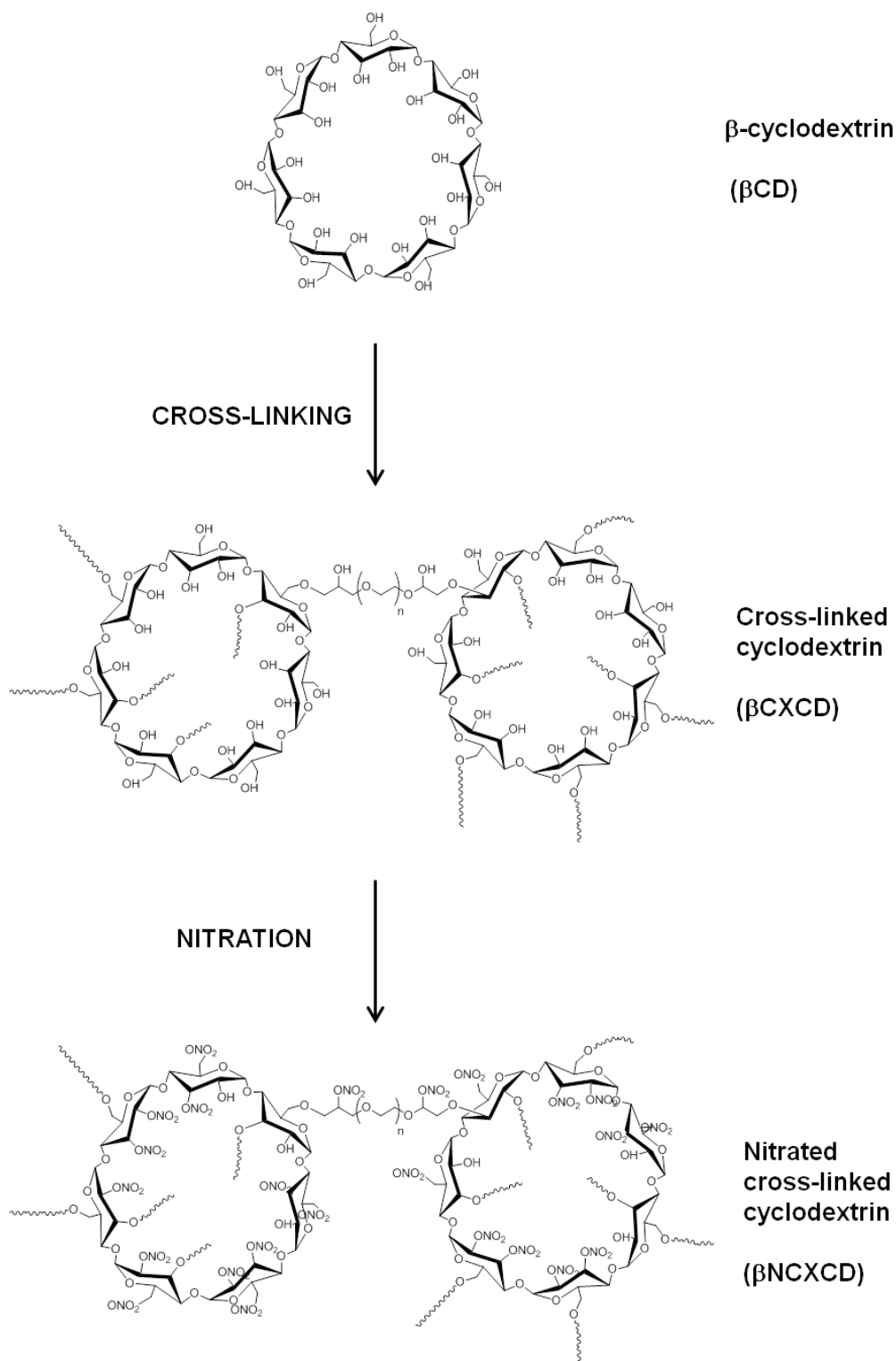
The synthesis route selected for the production of energetic cross-linked β CDs (β NCXCDs) comprises two steps, as summarised in Scheme 1.1:

1. Cross-linking of β CD using polyethylene glycol diglycidyl ethers of various lengths to form β CXCDs.
2. Nitration of the β CXCDs.

The solubility of β CXCDs in common polar solvents such as water, methanol or ethanol would facilitate formulation development. Therefore the studies focused on finding optimal reaction parameters to obtain water-soluble compounds for easy purification and processability. The properties of the prepared compounds were investigated using the following analytical techniques:

1. Nuclear magnetic resonance (NMR) and Fourier transform infrared (FTIR) spectroscopy for the chemical characterisation of the cross-linked and nitrated products.
2. Iron sulfate titration to measure the nitrogen content of the nitrated cross-linked products
3. Differential scanning calorimetry (DSC), thermal gravimetric analysis (TGA) and dynamic mechanical analysis (DMA) for the thermo-mechanical characterisation of the cross-linked and nitrated cross-linked products to determine their compatibility with energetic fillers.

4. Hazard tests to assess the vulnerability of the compounds.



Scheme 1.1 Schematic representation of the synthesis of β CXCD and β NCXCD binders.

1.2 Academic contributions

The work described in this thesis has thus far resulted in two peer-reviewed publications (one in *Propellants, Explosives, and Pyrotechnics*, and another in *Polymer Testing*) as well as two posters presented at one domestic conference (Defence and Security Doctoral Symposium 2015–2016, Cranfield University, UK) and one international conference (Macro 2018, 47th IUPAC World Polymer Congress, Cairns, Australia). The work also contributed to the Cranfield WSTC0037 Progress Internal Reports for the “Binders by Design Project” and was presented in progress meetings with the PhD sponsor.

1.3 Thesis structure

Following this overview, Chapter 2 (*Introduction*) guides the reader through the concept of binders and their use in energetic formulations, followed by a summary of current knowledge about the chemical properties of cyclodextrins, particularly their use in the energetics industry. Chapter 3 (*Experimental*) describes the materials, reactions and methods used to synthesise and characterise the compounds, as well as test conditions for hazard assessment.

Chapter 4 (*Synthesis and characterisation of inert β CXCDs*) explains the rationale behind the optimisation of the first synthesis reaction, and also describes the physicochemical and thermomechanical characterisation of the inert compounds. Chapter 5 (*Synthesis and chemical characterisation of energetic cross-linked β NCXCDs*) mirrors the structure of Chapter 4 but describes the production and characterisation of the energetic cross-linked systems. Chapter 6 (*Compatibility, hazard and stability studies*) provides the data needed for the reader to understand the contribution and limitations of the novel inert β CXCDs and energetic β NCXCDs in the development of new energetic formulations.

Finally, Chapter 7 (*Conclusions and recommendations*) provides a summary of the findings reported in the thesis and suggests additional work required to develop this cross-linked system into a successful binder for energetic applications.

The appendices contain additional experimental details that will help the reader to understand the research, as well as the published articles based on the work described in the thesis:

- Luppi F, Cavaye H, Dossi E (2018) Nitrated cross-linked β -cyclodextrin binders exhibiting low glass transition temperatures. *Prop Expl Pyrotech* 43 (10) 1023–1031.
- Luppi F, Kister G, Carpenter M, Dossi E (2019) Thermomechanical characterisation of cross-linked β -cyclodextrin polyether binders. *Polym Test* 73, 338–345.

2 Introduction

2.1 Insensitive munitions

Energetic formulations used in the defence industry must withstand unintended stimuli to prevent unwanted violent events, and manufacturing is therefore moving towards improved safety during phases of life. The development of insensitive munitions (IMs) is a direct response to the several accidents that caused the involuntary initiation of explosives [1]. A definition developed in the American Navy stands [1]:

“Insensitive munitions are those that reliably fulfil their performance, readiness, and operational requirements on demand, but are designed to minimize the violence of a reaction and subsequent collateral damage when subjected to unplanned heat, shock, fragment or bullet impact, electromagnetic pulse (EMP), or other unplanned stimuli.”

The development of IMs is guided by the handbooks STANAG 4439 and the American standard MIL-STD-2105 “Hazard Assessment Tests for Non-Nuclear Munitions”, which can be summarised in the following three strategies [2–4]:

1. The development of external packaging that improves the protection of the munitions.
2. The development of mitigation devices for uncontrolled events in the munitions.
3. The development of energetic materials with an intrinsic low vulnerability.

The first strategy relies on the design of new transport tools such as containers better insulated from thermal and kinetic shock, or coated with intumescent paint.

The second strategy is the development of passive or active devices to mitigate the effects of uncontrolled events. Passive devices do not provoke a response in the energetic materials, and examples include vent plugs, thread adaptors, mitigation sleeves and intumescent paint [5–7]. Not as widely used, active devices such as the thermal initiated venting system (TIVS) cause a controlled

thermal response to external stimuli in the IM, and thus reduce the severity of unplanned events [8].

Energetic materials with low vulnerability intrinsically prevent undesired consequences. The two global conflicts in the first half of the twentieth century increased the development of novel energetic materials. Polymers were introduced in energetic formulations as a medium to bind the explosive ingredients, thus increasing the compactness of the munitions and reducing their vulnerability [9]. In this role, polymers were used and defined as binders.

Polymers have a wide range of physicochemical properties that define their efficiency in energetic applications [10].

2.2 Polymers and their properties

Polymers are macromolecules comprising repeat units of one or more monomers, and they offer unique benefits when used as binders, including [11]:

- Wide variety of molecular architectures, e.g. linear, branched, homopolymer, copolymer, random, alternating, star, block copolymer, cross-linked;
- Dimensional stability (linear dimensional change in response to temperature changes);
- Durability (lifetime, ageing, degradation, stabilisation);
- Easy processing (flow, forming, solidification by moulding, extrusion).

The chemical identity of a polymer defines its morphology and the physical properties of the system. The synthesis route determines the molecular structure and is designed to avoid side-reactions, thus favouring the recovery of pure products. By controlling the reaction mechanism, the system can be defined in terms of the regularity of the backbone (stereochemistry, sequencing in copolymers), the molecular weight and polydispersity, and the polymer architecture. Most of these molecular structures offer numerous opportunities for functionalisation, process control and thus new applications.

Polymer morphology describes the arrangement and macroscale ordering of polymer chains in space, which affects properties such as strength, toughness and flexibility [12]. Crystallinity is often used to describe the morphology of a polymer compound. Crystalline polymers are rigid and melt at higher temperatures than amorphous polymers. Crystallinity increases mechanical strength at the cost of low impact resistance. Amorphous polymers are softer, with lower melting points than crystalline polymers, and there is a transition point at which the polymer reversibly changes from glassy to rubbery behaviour [13]. This is known as the glass transition temperature (T_g) [12]. The glassy state is hard, rigid and brittle like a crystalline solid, but retains the molecular disorder of a liquid. When the material is heated the polymer will reach a temperature at which segments of the entangled chains can move and the behaviour will change to rubbery [11].

There are two general classes of polymers based on their behaviour when exposed to heat: thermoplastics and thermosets [14]. Thermoplastic polymers have relatively weak forces of attraction between the macrochains (electrostatic forces, few cross-links), which are overcome when the material is heated [14]. Thermoplastics are permanently fusible and can always be softened, melted down and recycled. When frozen, a thermoplastic becomes glassy and more sensitive to fracture [14]. Thermoplastics have a distinctive stress–strain curve (elongation to break). Thermosets comprise molecules that are cross-linked by strong bonds during curing due to chemical reactions or the effects of heat or radiation [14]. Effectively, the thermoset is one large molecule, with no crystalline structure. Cured thermoset polymers do not soften and will char and break down at high temperatures. Thermosets are generally harder than the thermoplastics, more rigid and more brittle, and their mechanical properties are not heat sensitive. They are also less soluble in organic solvents [15].

Thermoplastic elastomer (TPE) materials combine the functional performance and properties of thermoset rubbers with the processability of thermoplastics. TPEs are generally low-modulus, flexible materials that can be stretched repeatedly to at least twice their original length at room temperature with an

ability to return to their approximate original length when stress is released [16]. TPEs are widely used to modify the properties of rigid thermoplastics, improving impact strength. This is quite common for sheet goods and general moulding TPEs [16]. Their soft texture, ease of manufacture and ability to absorb shocks are preferred for energetic applications. Several classes of polymers can be cross-linked in the defence industry to produce TPEs, including copolyesters, styrenes, polyurethanes, polyamides and polyolefin blends [17]

2.3 Polymers as binders in energetic formulations

The binder is an important component of munition fillings because it holds the explosive crystals together, allows the formulation to be safely casted or machined into complex shapes, and reduces its vulnerability to accidental stimuli during storage. Table 2.1 lists some examples of energetic formulations.

The properties of the binder strongly influence the physical properties of the formulation and its applications. The plastic behaviour of certain polymers allows the formulation of plastic explosives, which are malleable and can be hand-moulded [18]. In contrast, viscoelastic behaviour reduces vulnerability to mechanical stress by facilitating energy dissipation in large-calibre munitions and nuclear warheads [19].

The chemical properties of the binder influence the stability of the formulations. For example, the low chemical reactivity of fluoropolymers can protect the formulations from harsh chemicals. For this reason, fluoropolymers are compatible with many energetic ingredients and reduce the likelihood of unpredicted chemical reactions [20]. The nitro-ester groups of NC undergo autocatalytic decomposition, so stabilisers are required to ensure a sufficient shelf-life [21]. Furthermore, epoxy-amines are incompatible with nitramines such as 1,3,5-trinitro-1,3,5-triazinane (RDX) and 1,3,5,7-tetranitro-1,3,5,7-tetrazocane (HMX) [22].

Table 2.1 List of binders in energetic formulations [23].

Binder ¹		Energetic		Application	Energetic formulation
Name	%	Name	%		
Polyisobutene	2.1	RDX	91	Plastic explosives	C4
Wax	1	RDX TNT	63 36	Gun shells	Comp. B
Nitrocellulose elastomer	8 29	PETN	63	Engineer charges	Detasheet C
Hydroxyl-terminated polybutadiene (HTPB)	5	HMX	29	Nuclear warheads	EDC-29
2,4-Dinitroanisole (DNAN)	43.5	NTO NQ	19.7 36.8	Gun shells	IMX-101
DNAN	31.7	NTO RDX	53 15.3	Mortars	IMX-104
Viton-A	10	HMX	90	Nuclear warheads	LX-07-2
Polyurethane rubber	< 4.5	HMX	95.5	Nuclear warheads	LX-14-0
Kel-F 800	7.5	TATB	92.5	Nuclear warheads	LX-17-0
Nitrocellulose chloroethylphosphate (CEF)	3 3	HMX	94	Nuclear warheads	PBX 9404
Kel-F 800 ³	5	TATB	95	Nuclear warheads	PBX 9502
Nylon	n.a.	RDX	85	Missiles Warheads	PBXN-3
Fluoro-elastomer	5	HMX	95	Gun shells	PBXN-5
HYTEMP 4454 ²	2	HMX	92	Various	PBXN-9
HTPB	11	RDX	88	Plastic explosives	PE7
NC	n.a.	NC,NQ, NG	/	Solid rocket propellant	Single, Double or Triple base
HTPB	n.a.	AP	/	Solid rocket propellant	AP/HTPB propellant
Styrene butadiene rubber	9	PETN RDX	40.9 41.2	Plastic explosives	Semtex H

1 The percentage of binder varies according to the application.

2 Trade name of polyacrylate binder.

3 Trade name of fluoro-elastomers.

The constituents of energetic formulations must be compatible to avoid side reactions. The introduction of polymers used for other applications in the development of new energetic formulations can be slow, hence the rather small number of polymers used successfully in energetic applications (Table 2.2).

NC was the first compound to be used in energetic formulations following the invention of black powder. It was first synthesised in the nineteenth century, as recorded by Christian Friedrich Schonbein in Basel and Rudolf Christian Bottger in Frankfurt-am-Main [20]. A significant milestone in the defence applications of NC was the production of the smokeless propellant Poudre B, by Paul Vieille in 1884 [24], where it was used as binder. A thick jelly was produced by kneading NC in a mixture of ether and alcohol to produce thin films. The NC gave solidity to the processed propellant and improved the control of its burning velocity. However the compound shows limited elongation below room temperature [25].

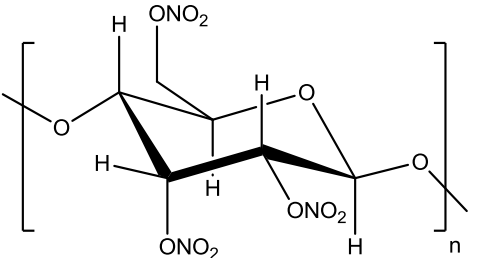

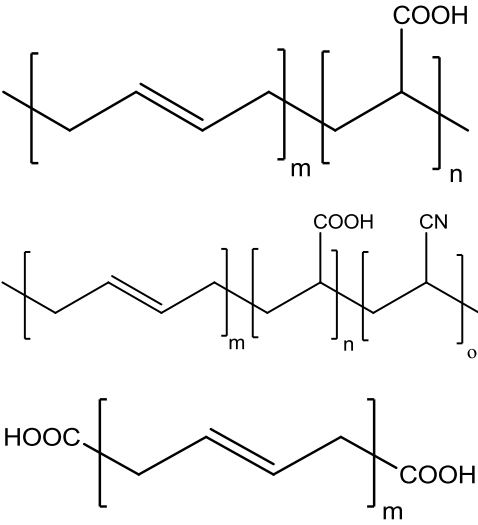
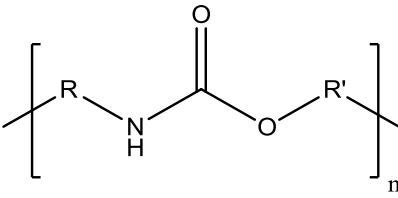
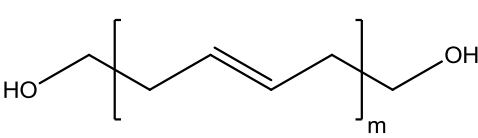
The moderate cost of NC makes it difficult to replace in defence applications even though the geographic and seasonal variations of raw cellulose mean that expensive selection processes are needed every few years to comply with military standards such as MIL-DTL-244 [26]. Special considerations are required to ensure batch-to-batch consistency in the polymer architecture [27]. In addition, it is difficult to prevent the degradation of this compound [28].

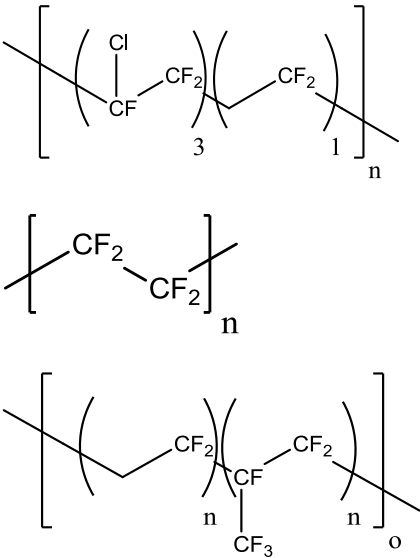
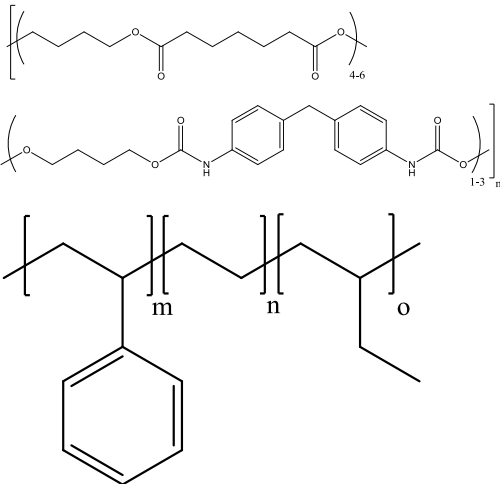
The escalation of European conflicts in the second half of the twentieth century stimulated the development of new binders. Polysulfides (PS) were the first synthetic polymers used as binders for propellants by the Thiokol Chemical Company in 1942 [29], although they are incompatible with the strong oxidisers used in many propellants and pyrotechnics [30].

Polybutadienes were developed in the 1950s to replace PS, and are more compatible with oxidisers in propellants. However, polybutadiene-acrylic acid copolymer (PBAA) showed low reproducibility during propellant manufacturing due to the synthetic nature of the radical polymerisation used to produce the binder [30]. Polybutadiene was copolymerised with acrylonitrile and acrylic acid

(PBAN) to achieve better pulse from the rockets, but a high curing temperature was needed for these binders [31].

Table 2.2 Example of polymers used in energetic applications [20].

Polymeric binder	Chemical structure	Applications
Nitrocellulose		Propellants, high explosives, 1888
Polysulfide		Propellants, 1945
Polybutadienes Poly butadiene-acrylic acid copolymer (PBAA) Poly butadiene-co-acrylonitrile (PBAN) Carboxyl-terminated polybutadiene (CTPB)		Propellants 1954 1954 Late 1950s
Polyurethane		Propellants, mid 1950s
Hydroxyl-terminated polybutadiene (HTPB)		Propellants and high explosives, 1972

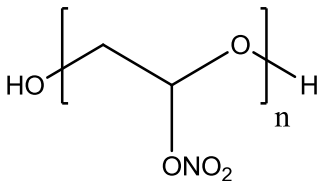
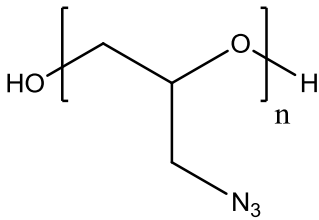
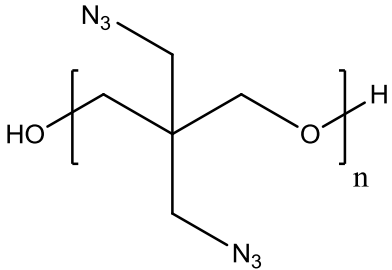
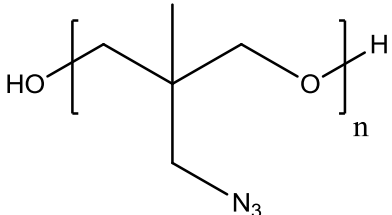
<p>Fluoropolymers</p> <p>Kel-F 3700</p> <p>Teflon</p> <p>Viton</p>		<p>High explosives, pyrotechnics, propellants</p> <p>Early 1960s</p> <p>Early 1960s</p> <p>Early 1960s</p>
<p>Thermoplastic elastomers (TPEs)</p> <p>Estane 5703 [32]</p> <p>Kraton</p>		<p>Propellants</p> <p>Early 1980s</p> <p>Early 1980s</p>

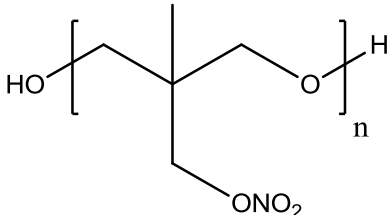
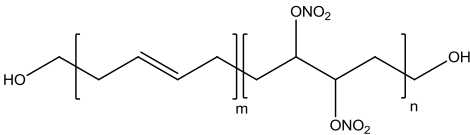
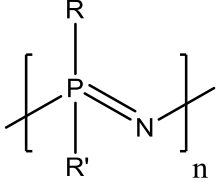
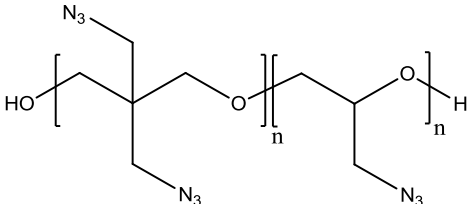
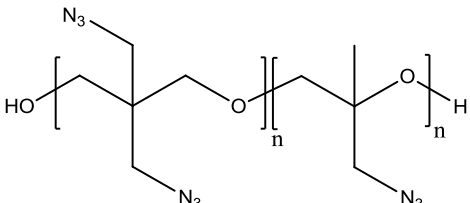
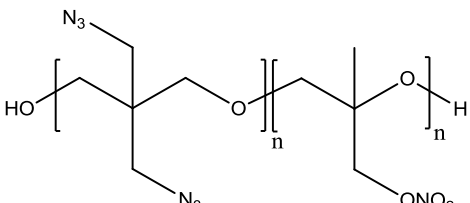
The development of new binders has been slow but continuous, although many end up in non-defence applications.

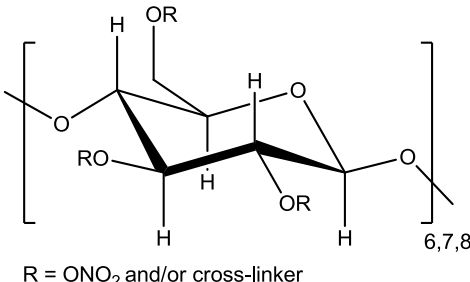
Cross-linked binders are manufactured by reacting bifunctional or multifunctional molecules such as isocyanates or polyols with these polymers to create a toughened three-dimensional (3D) network, a process defined as curing.

Hydroxyl-terminated polybutadiene (HTPB) is currently the most widely-used polymer for the preparation of polyurethane elastomer binders with unique properties such as low-temperature flexibility, hydrophobicity and resistance to hydrolysis [20,33,34]. However, with the exception of NC, the polymers listed in Table 2.2 do not contribute any energy to the formulation and negatively affect its energetic output. Energetic polymers, in which the binder contributes to the energy of the formulation, were developed to mitigate this major drawback (Table 2.3). The energetic contribution is provided by functional groups that decompose exothermically such as nitro, azido or nitro esters [35]

Table 2.3 Examples of energetic polymers used as binders [20].

Polymeric binder	Chemical structure	Applications
Polyglycidyl nitrate (PGN)		Propellants, 1953
Glycidyl azide polymer (GAP)		Propellants, 1976
Polyoxetanes		Propellants, high explosives, 1984
3,3-Bis(azidomethyl) oxetane polymer Poly(BAMO)		
3-Azidomethyl-3-methyloxetane polymer Poly(AMMO)		

Polymeric binder	Chemical structure	Applications
Poly(3-nitratomethyl-3-methyloxetane) Poly(NIMMO)		
Nitrated hydroxyl-terminated polybutadiene (NHTPB)		Propellants, 1980
Polyphosphazenes (PPZ)		Propellants, 2005
Energetic thermoplastic elastomers (ETPEs)		
BAMO-GAP		Propellants, 1984
BAMO-AMMO		
BAMO-NIMMO		

Polymeric binder	Chemical structure	Applications
<p>Nitrated cyclodextrin polymers</p>	 <p>R = ONO₂ and/or cross-linker</p>	<p>High explosives, propellants, early 1990s</p>

Most recent studies have focused on polyphosphazenes and energetic cyclodextrin (CD) derivatives, both of which produce feasible energetic binders. Polyphosphazenes are non-isocyanate curable energetic polymers which are less toxic than current binders [36,37]. A successful synthetic curing process for HTPB and polyphosphazenes using a non-toxic cross-linker was developed at Cranfield University, based on the in-house diepoxide triethylene glycol diglycidyl ether (TEGDGE), as shown in Figure 2.1 [12,18,28].

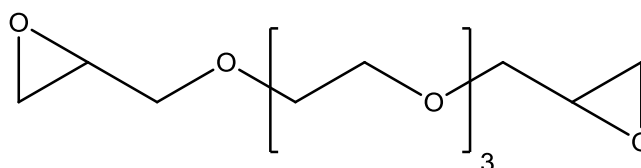


Figure 2.1 Chemical structure of triethylene glycol diglycidyl ether

The potential of CDs and their derivatives for energetic formulations is discussed in the next section. The physicochemical properties and the ability of CDs to envelop molecules is highlighted as means to reduce the vulnerability of energetic formulations.

2.4 Cyclodextrins

CDs are cyclic organic molecules characterised by the ability to envelop smaller molecules in their inner cavity. The three best-known CDs are α -cyclodextrin (α CD), β -cyclodextrin (β CD), and γ -cyclodextrin (γ CD), which are toroidal macrocycles of six, seven and eight glucopyranose units, respectively (Figure

2.2) [38]. CDs with larger rings have been isolated but they are not used in the defence industry [39].

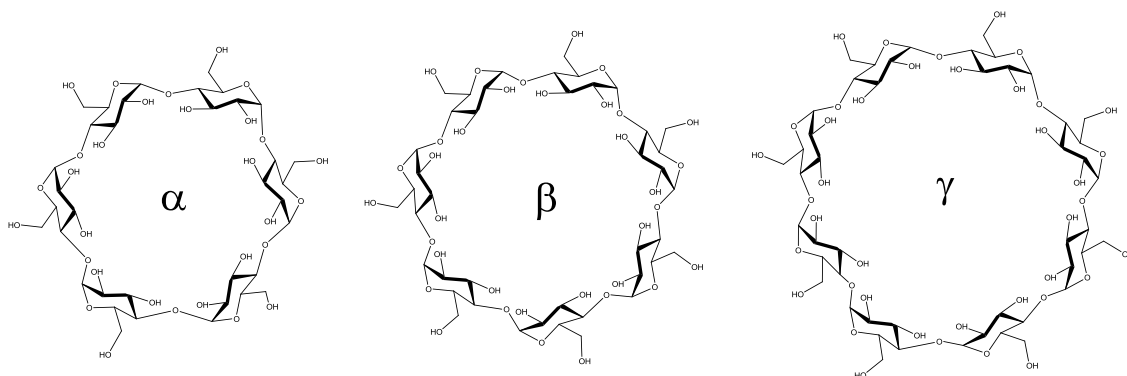


Figure 2.2 Chemical structure of α , β and γ CDs [40].

CDs were first synthesised in 1891 by Villiers and Schardinger. The work was then picked up by Pringsheim and colleagues, who discovered that CDs had the tendency to envelop organic molecules, leading to a burgeoning body of research literature during the 1970s [38].

This early research showed that α , β and γ CDs were suitable for pharmaceutical applications due to their enveloping properties [40]. However misleading information about their toxicity was publicised, reducing interest in these macrocycles. Modern toxicological tests show that CDs lack oral toxicity because they are not absorbed in the intestine [41]. Most publications concerning CDs focus on pharmaceutical applications and different functionalised variants are commercially available, including randomly methylated β CD (RAMEB), hydroxyalkylated derivatives (hydroxypropyl- β CD and hydroxypropyl- γ CD), acetylated- γ CD, reactive derivatives such as chlorotriazinyl- β CD, and branched versions such as glucosyl- β CD and maltosyl- β CD [38,40,42,43]. Figure 2.3 shows in the distribution of CD publications by application field over the last 20 years.

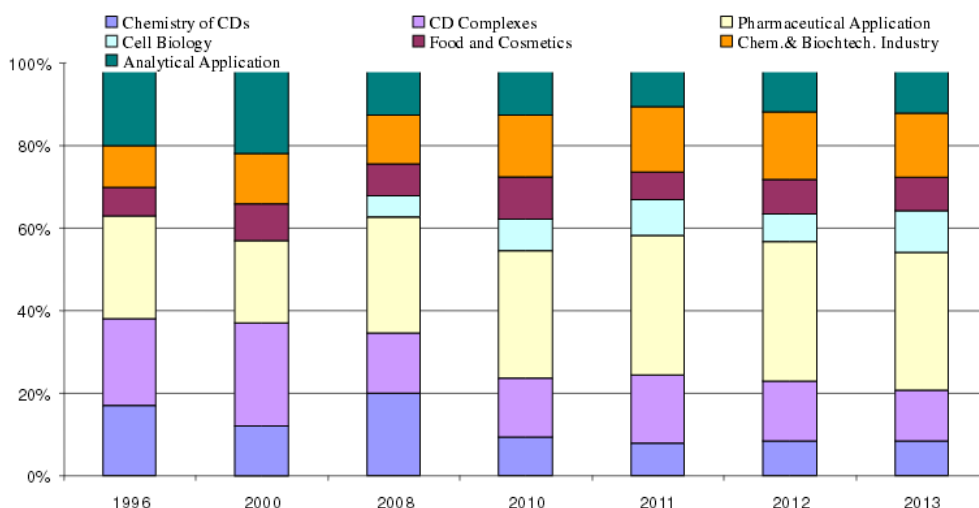


Figure 2.3 Distribution of the CD publications by application (1996–2013) according to *CD News* [38].

Most publications have considered pharmaceutical applications, where modified or unmodified CDs are used for drug delivery. The pharmaceuticals sector consumes several tons of medical-grade CD per year, with high purity and high development costs. There are smaller numbers of publications concerning applications in the food, cosmetics and detergent industries, which require a greater quantity of CDs but with less-stringent purity requirements and minimum prices of 6–7 US\$ per kg in the US and European markets [38], and 2–3 US\$ in the Chinese market. In Europe, Merck holds the bigger share of the CD market.

2.4.1 Properties of CDs

In the 1940s, the structures of CDs were defined by X-ray crystallography, revealing their ability to trap small molecules and to form inclusion complexes. The structural data obtained in these early studies showed how the primary hydroxyl groups cluster at one end of the toroidal molecules, whereas the secondary hydroxyl groups lie at the other end, as shown in Figure 2.4 (coloured in blue). The non-polar hydrogen atoms attached to C2 and C3 fill the inner side of the cavity along with the ether group. This leads to hydrophilic behaviour outside the toroid lipophilic cavity [40]. The physical properties of CDs are summarised in Table 2.4.

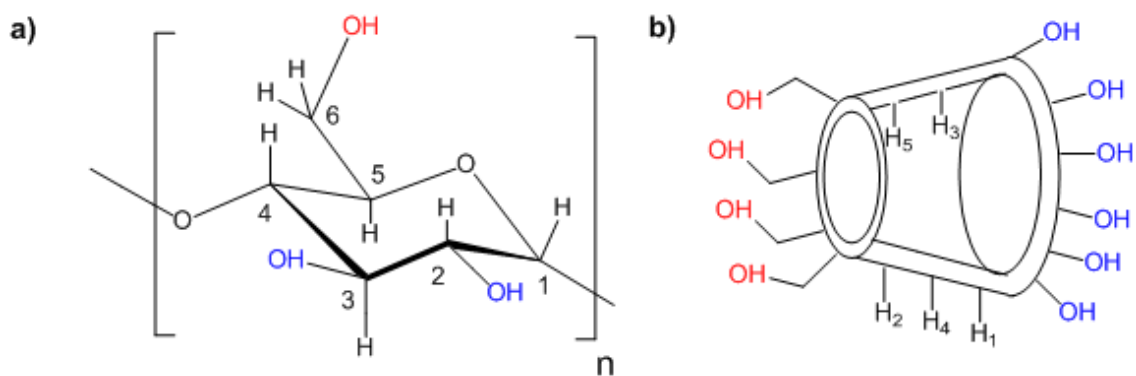


Figure 2.4 Structures of (a) α -D-glucopyranoside, the repeating unit of CD, and (b) the toroid representation of CDs, with primary and secondary hydroxyl groups in red and blue, respectively. H1, H2 and H4 are external to the toroid, whereas H3 and H5 are internal

Table 2.4 The physical properties of α , β and γ CDs [38].

CD	α	β	γ
Number of glucose units	6	7	8
Molecular weight	972	1135	1297
Solubility in water, g 100 mL ⁻¹ at room temperature	14.5	1.85	23.2
Cavity diameter, Å	4.7–5.3	6–6.5	7.5–8.3
$[\alpha]_D$ 25 °C	150 ± 5	162 ± 0.5	177.4 ± 5
Height of torus, Å	7.9 ± 0.1	7.9 ± 0.1	7.9 ± 0.1
Diameter of outer periphery, Å	14.6 ± 0.4	15.4 ± 0.4	17.5 ± 0.4
Approx. volume of cavity, Å ³	174	262	427
Approx. cavity volume in 1 mol CD (ml)	104	157	256
Crystal forms (from water)	Hexagonal plates	Monoclinic parallelograms	Quadratic prisms
Crystal water (% w/w)	10.2	13.2–14.5	8.13–17.7
Diffusion constant at 40 °C	3.443	3.224	3.000
pK (by potentiometry) at 25 °C	12.332	12.202	12.081

The thermal properties of CDs, such as phase transitions or mass changes during chemical reactions, have been studied by thermal analysis using techniques such as differential scanning calorimetry (DSC) and thermal gravimetric analysis (TGA). The literature reports slightly different thermal behaviours among the three cyclodextrins [44]. The main phase transitions and thermal events for the three CDs are summarised in Table 2.5.

Table 2.5 Thermal properties of α , β and γ CDs.

Cyclodextrin	Water loss (°C)	Phase transition (°C)	Degradation (°C)
α CD	74–121	224	319–304
β CD	87–110	221	328–330
γ CD	63–81	-	321–324

CDs are generally stable up to 300 °C, and degradation occurs at higher temperatures. CDs are hygroscopic and can entrap water molecules in their cavity, which is described as crystal water in Table 2.4. The high temperatures cause phase transitions in the structures of α and β CDs at 224 and 221 °C, respectively. The first part of the CD thermal profile is dominated by the loss of hydration water and phase transitions in the crystal structure due to this loss [45]. Among the three CDs, the water of hydration has the highest mobility in γ CD and is released earlier compared to the others [44], even though γ CD is the most soluble (Table 2.4).

The solubility of all CDs in water increases at higher temperatures, although β CD is less soluble than the others [42]. The differences in solubility reflect the different hydrogen bond interactions that occur between the hydroxyl groups of each glucopyranose unit and the flexibility of the corresponding CD rings [46]. The inner cavity of α CDs cannot accommodate very large molecules due to its small size (Table 2.4), but this is not the case for β and γ CDs, which are large enough to incorporate various chemical compounds, including linear polymers and aromatic rings [41]. In the less common and non-commercialised CDs (10,

14, 26, 32 repeat units) the spatial distortion causes cavity collapse, reducing the inner volume to less than the value observed for γ CDs, making them less suitable for encapsulation [47].

The enveloping structures formed by CDs in solution are influenced by the presence of solutes that could act as guest molecules. There is great interest in these compounds, reflecting their ability to form different supramolecular threads, allowing CDs to be used like polyrotaxanes (Figure 2.5) [48,49]. The interest in developing these supramolecular structures has led to more specific studies focusing on forces that control guest–host molecule interactions.

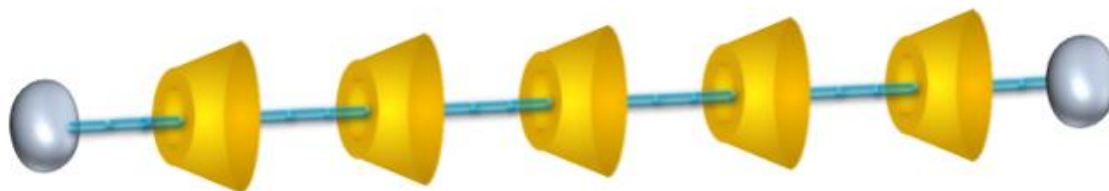


Figure 2.5 Schematic representation of a polyrotaxane formed by several CDs threaded on a polymer chain with ending caps.

2.4.1.1 Cyclodextrin inclusion complexes

CD inclusion complexes are affected by two main parameters:

- Steric hindrance;
- Replacement of solvent molecules with guest molecules.

Steric hindrance depends on the relative sizes of the guest molecule and the cavity, whereas the likelihood of replacement is based on thermodynamics. The inclusion of guest molecules by CDs involves an enthalpy-dependent driving force, i.e. water molecules inside the cavity have fewer interactions with the hydroxyl groups than water molecules in the bulk solution [50]. The replacement of water molecules with an organic molecule can therefore increase the stability, resulting in the dissolution of a sparingly soluble or insoluble organic molecule

in water. The organic molecule/CD complex is often less soluble than the CD alone [38].

Encapsulation tends to reduce the volatility, diffusion and reactivity of guest molecules [38,42,51,52]. The thermal properties of guest compounds are also affected, leading to increases in the glass transition and/or melting temperatures when embedded in CD [53]. The encapsulation ability of CDs has also been used to study their interactions with energetic molecules, as discussed later in this section.

Complexes may form in the solid state or in solution, following processes such as kneading, co-precipitation, dry mixing, sealing, slurry complexation, neutralisation, spray drying, freeze-drying, and solvent evaporation. This usually leads to an inclusion ratio of 1:1 for host and guest molecules [42,54,55]. The temperature affects the solubility of the complex as well as the stability of the interaction [52]. The solubility of the complex is often inferior to the pure CD, causing a fraction of the complex to precipitate when formed [56–60].

Most of these processes have only been tested at the laboratory scale, and they have been claimed in various patents covering the manufacture of CD polymers or derivatives. Many of the patents covering the manufacture of natural CDs and modified variants such as hydroxypropyl- β CD have now expired, although existing and novel CD polymer derivatives are still manufactured [41,61,62].

2.4.1.2 Chemical stability and characterisation of CDs

CDs are chemically stable compounds, hence their use as drug carriers. They are relatively resistant to oxidation, with only strong oxidising environments leading to ring-breaking reactions. CDs are more acid resistant than linear or branched polysaccharides, but treatment with strong acids causes ring opening and the formation of oligosaccharides. The magnitude of the ring opening rate is influenced by the size of the CD molecule, so the process is slower for α CDs than γ CDs [40].

In alkaline environments, the CD ether bond is stable towards nucleophilic or acid-base reactions and requires very strong conditions to react [40,42,59]. This low reactivity is also conferred to guest molecules within the CD ring.

Nuclear magnetic resonance (NMR) spectroscopy is widely used to characterise CDs because it determines their chemical structure in a complex. Figure 2.6 shows the proton assignments typical in deuterated water (D_2O) and the assignment in deuterated dimethylsulfoxide ($DMSO-d_6$).

Table 2.6 and Table 2.7 summarise the chemical shifts at 400 MHz reported for ^1H and ^{13}C NMR, respectively [63]. The signals attributed to the protons are split into two main regions. The region from 3.8 to 3.2 ppm includes most of the signals due to the chemical shifts of the aliphatic protons of the CD H-2 to H-6_{a,b}, whereas the region from 5.8 to 4.4 ppm includes the chemical shifts of the anomeric proton H-1 (Figure 2.6a). When DMSO- d_6 is used, the chemical shifts of the hydroxyl groups of the CD are also visible (Figure 2.6b). This region can be integrated and compared with the integration of H-1 to determine the degree of substitution (DS) that has occurred with the hydroxyl groups. The DS can also be determined by titration of the hydroxyl groups following standard methods [64–66].

Infrared (IR) spectroscopy is also widely used to characterise CDs [57,59,67–70]. The IR spectrum and the main adsorption bands for β CD are shown in Figure 2.7. A strong adsorption band at 3400–3300 cm^{-1} is due to the stretching of hydroxyl groups. The peak at 2926 cm^{-1} is assigned to the stretching of the C-H bond in CH and CH_2 groups. The peaks at 1200–1400 cm^{-1} are assigned to the bending of C-H in the primary and secondary hydroxyl groups of β CD (1411, 1368, 1335, 1301 and 1246 cm^{-1}) [71]. The strong adsorption at 1030–1200 cm^{-1} is attributed to the stretching of the C-O-C bonds in the ether and hydroxyl groups. Finally, the absorption bands at 700–950 cm^{-1} show the bending vibrations of the C-H bonds and the stretching vibrations in the glucopyranose ring [72]. The peak at 1626 cm^{-1} is actually due the water absorption included in the CD molecule as reported for the spectrum of water elsewhere [57,73].

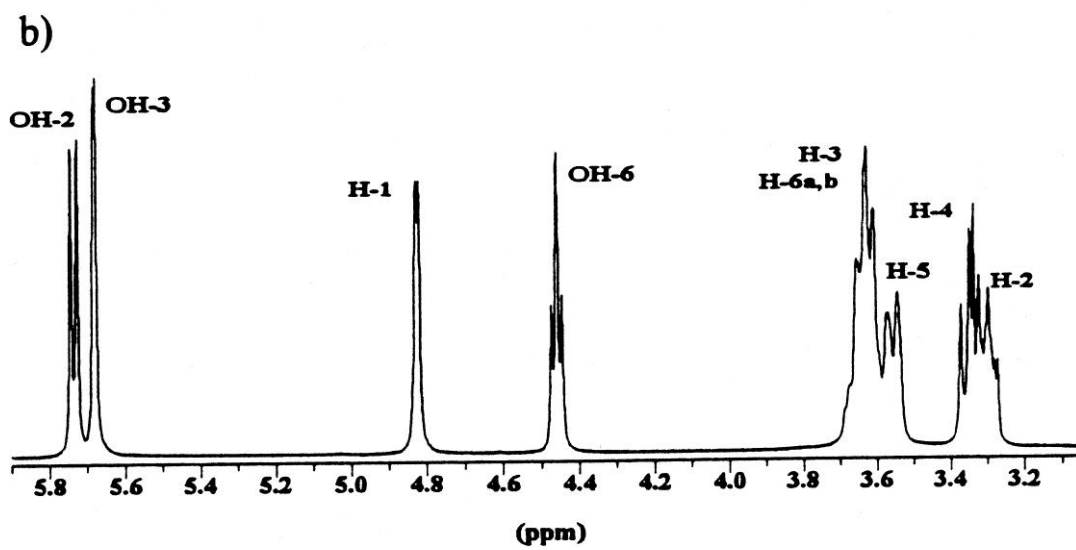
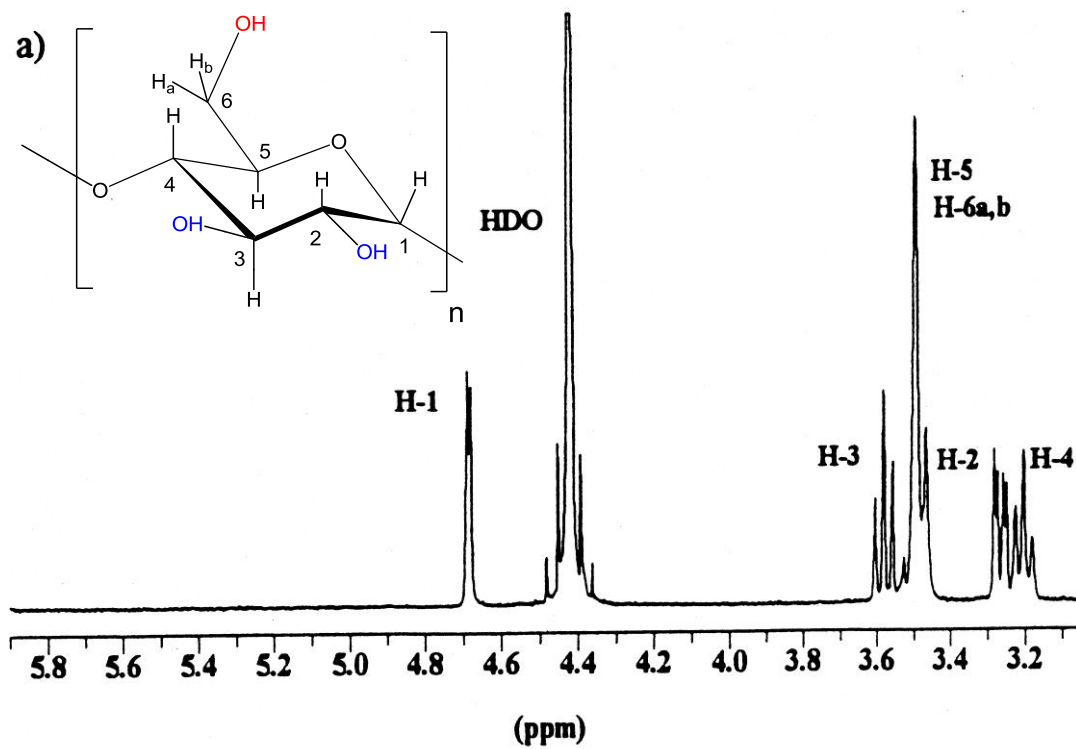


Figure 2.6 The ^1H -NMR spectra of CD (a) in D_2O and (b) in DMSO-d_6 [63].

Table 2.6 The ^1H -NMR chemical shifts of CD protons in D_2O and DMSO-d_6 [63].

Cyclodextrin	δ H-1	δ H-2	δ H-3	δ H-4	δ H-5	δ H-6a,b
D_2O						
α CD	4.60	3.19	3.57	3.08	3.39	3.44
β CD	4.68	3.26	3.58	3.19	3.47	3.49
γ CD	4.53	3.08	3.35	3.00	3.26	3.30
DMSO-d_6						
α CD	4.79	3.29	3.78	3.40	3.59	3.65
β CD	4.82	3.29	3.64	3.34	3.59	3.64
γ CD	4.89	3.32	3.65	3.36	3.56	3.65

Table 2.7 The ^{13}C NMR chemical shifts of CDs in D_2O [63].

Cyclodextrin	δ C-1	δ C-2	δ C-3	δ C-4	δ C-5	δ C-6
α CD	102.19	72.61	74.21	82.07	72.91	61.37
β CD	102.58	72.67	73.89	81.94	72.89	61.17
γ CD	102.42	73.19	73.82	81.33	72.69	61.21

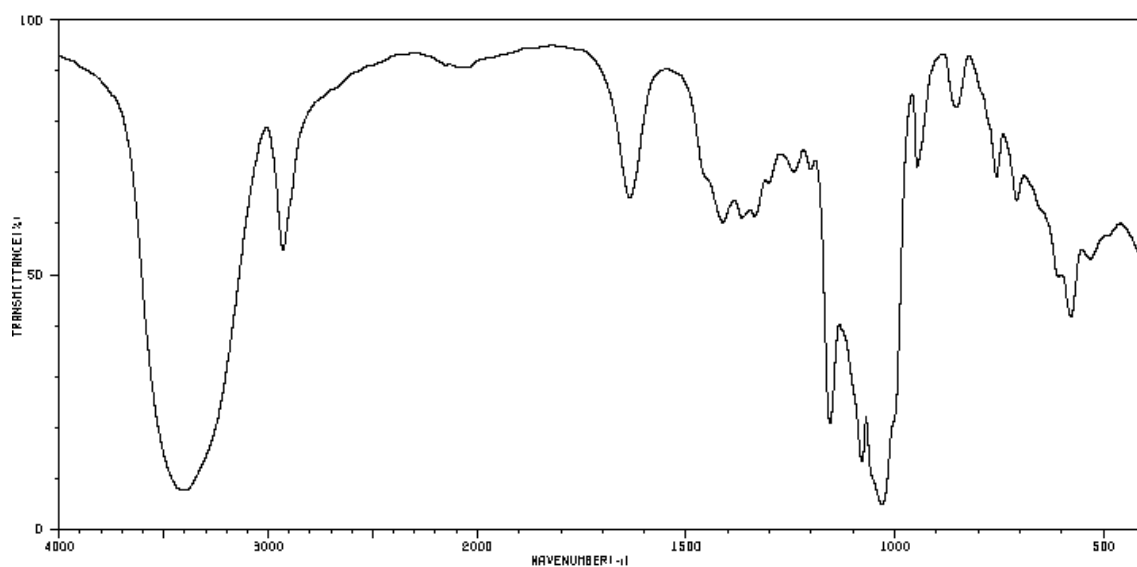


Figure 2.7 The infrared spectrum of β CD.

2.4.2 Synthesis of cyclodextrins

The enzyme CD glucosyltransferase (CGTase) converts starch into CDs. It is expressed by bacteria such as *Paenibacillus macerans*, *Klebsiella oxytoca*, *Bacillus circulans*, and alkalophilic *Bacillus* species [38,42,74]. CD synthesis begins with the liquefaction of starch by heating and hydrolysis to reduce the viscosity of the raw material. The enzyme is then mixed with the starch and different solvents are used as complexants to obtain the three CDs: toluene is used for β CD, 1-decanol for α CD, and cyclohexadecanol for γ CD. The CDs are separated from the mixture by filtration, washed with water, and the organic solvent is removed by distillation or extraction in water. The resulting aqueous solution is treated with active carbon to remove trace impurities and filtered. The cost of production depends on how easy it is to remove the CDs from the organic solvent [38].

2.4.3 Cross-linking of cyclodextrins

CDs can be grafted to polymer chains, can form complexes with the branches of an existing polymer, or can be entrapped in a polymer lattice such as the polyrotaxane configuration (Figure 2.5). Polymeric CDs are formed primarily due to a reaction between the primary and/or secondary hydroxyl groups with functional groups of other molecules, or due to guest–host interactions. CD is often cross-linked using a variety of cross-linkers to form 3D structures that are usually insoluble in common solvents (Table 2.8).

The first cross-linked CDs were formed by reacting monomers with epichlorohydrin under basic conditions. Changing the reaction parameters (pH, solvent, temperature and time) led to different degrees of cross-linking [38]. The solubility of the resulting products varies depending on the cross-linker and reaction parameters [59,75,76]. The ability of polymers to swell depends on whether the polymer is linear [77] or branched [71]. The synthesis of different 3D networks leads to different degrees of swelling and chiral properties [75]. Many cross-linked CDs are insoluble due to their high molecular weight (Mw), so characterisation is restricted to methods such as solid-state NMR or Fourier transform infrared (FTIR) spectroscopy [71,78]. Other synthesis routes include

the living polymerisation of CDs to form the core of thermosensitive polymers [79].

Table 2.8 Applications of cross-linked CDs

Studies	Cross-linker used	Ref.
Removal of bisphenol A from water	1,2,3,4-butanetetracarboxylic dianhydride	[71]
Removal of pollutants such as 2-methylisoborneol and chlorinated disinfection by-products from water	4,4' - methylenebis(cyclohexyl isocyanate), toluene diisocyanate	[80]
Absorption of phenol, methylene blue and aniline	Citric acid	[68,70]
Absorption of methylene blue and phenylalanine	Citric acid	[81]
Inclusion of aromatic compounds	Epichlorohydrin	[59]
Removal of urea from water	Epichlorohydrin	[51]
Manufacture of chromatographic stationary phase	Epichlorohydrin	[75] [77]
Removal of bisphenol A from water	Ethylene glycol diglycidyl ether	[78]
Solubility studies of the synthesised polymers	Poly(carboxylic acids)	[76]
Removal of bisphenol A from water	Poly(ethylene glycol diglycidyl) ether	[78]
Synthesis of thermosensitive star copolymers	Poly(N-isopropylacrylamide) and poly(N,N-dimethylacrylamide)	[79]
Manufacturing of antimicrobial packaging	Poly(vinyl alcohol) citric acid	[82]
Increasing the mechanical resistance of microneedles for drug injection	Poly(vinylpyrrolidone)	[83]
Control of drug release	Polyethelene glycol	[84–88]

Cross-linked CD polymers have been extensively used to remove chemicals from solution as reported in Table 2.8. The advent of green chemistry led to the production of different water-insoluble CD polymers using citric or polycarboxylic acids as environmentally friendly cross-linkers for wastewater treatment [68,70,76,81]. The same cross-linking technique has been used to manufacture antimicrobial packaging [82]. The thermal characterisation of these compounds indicated that the presence of CDs increases the T_g of any polymers to which they are grafted. The glass transition is defined by IUPAC as the “*Process in which a polymer melt changes on cooling to a polymer glass or a polymer glass changes on heating to a polymer melt*” [89]. Long-chained cross-linkers are necessary to reduce the T_g of cross-linked CDs [82].

The synthesis of non-toxic materials is necessary when cross-linked CDs are used for drug delivery [40]. Many reactants produce non-toxic compounds when combined with CDs, expanding research into the synthesis of hydrogels for drug delivery. The solubility, pH response and membrane permeability of these systems can be tuned by adjusting the reaction conditions, making them ideal carriers to bind specific drug molecules in pharmaceutical applications [90]. Hydrogels are insoluble matrices of polymers that can adsorb large amounts of water, which cause them to swell [90]. This specific ability is valuable in other fields such as wastewater treatment, to trap pollutants [91].

One of the most widely-used hydrogels is based on CDs cross-linked with polyethylene glycol based cross-linkers [68,78,84–88,92]. The mechanical properties of hydrogels are also beneficial in pharmaceutical applications. The hydrogel must maintain its integrity to deliver the drug cargo to a specific target in the human body. Several hydrogels based on CDs can self-heal, which means they can at least completely or partially regenerate their mechanical strength after damage [93–95], and many of these are CD/PEG systems [92,96,97].

Self-healing is a characteristic possessed by many polymeric systems, in which a material can restore its structural integrity in a damaged area [98]. Different

polymers rely on different self-healing mechanisms that involve three different processes:

- Irreversible covalent bonds;
- Reversible covalent bonds;
- Reversible intermolecular interactions.

The first two processes require the presence of an encapsulated monomer reservoir in the polymer bulk. When damage occurs, the capsules break and release the healing agent into the fracture, followed by cross-linking to repair the damage. This relies on the formation of reversible or irreversible covalent bonds at sites where stress has caused the cleavage of bonds in the polymer network. Examples of irreversible mechanisms include ring-opening metathesis polymerisation (ROMP) and click chemistry [99], whereas reversible mechanisms include cross-linked poly(dimethylsiloxane), retro Diels-Alder reactions, and deformable/reformable disulfide and alkoxyamine bonds in response to stimuli such as temperature or irradiation [100].

The healing behaviour of CD/PEG systems is based on reversible supramolecular interactions, where various intermolecular forces can drive the self-healing process:

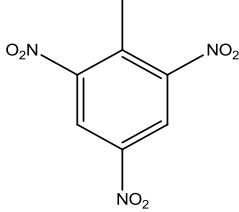
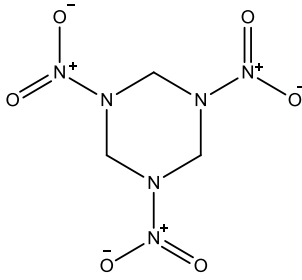
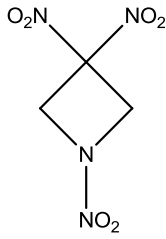
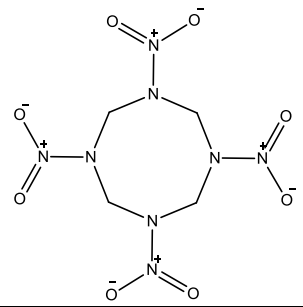
- Inclusion complexes form between the cross-linker and CD [95,96,101];
- Electrostatic interactions and intermolecular hydrogen bonding [50,94,102];
- Mobility of the polymeric chains in the bulk (reptation) [92,103,104];
- Mobility of the polymeric chains in the water of the hydrogel [105,106].

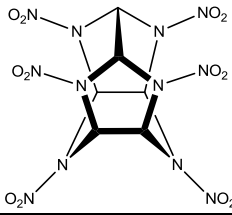
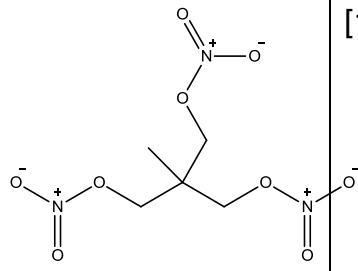
The combined effect of these driving forces allows the CD/PEG systems to heal, which is useful in applications that subject the materials to mechanical stress. In addition, the self-repairing ability of CD/PEG systems is enhanced when the compounds are exposed to heat due to the increased mobility of the polymer chains in water. Compounds that heal in response to external stimuli such as temperature or mechanical pressure are defined as healable or amendable [98,106].

2.4.4 Energetic applications of unlinked/cross-linked cyclodextrins

The ability of CDs to trap energetic molecules has been investigated in the past for the treatment of military waste streams [67,107]. A list of studies involving the energetic applications of CD is provided in Table 2.9.

Table 2.9 Applications of CDs functionalised with energetic molecules.

Application	CD type	Energetic	Ref
Removal of TNT from soil	β CD	Trinitrotoluene (TNT) 	[67]
Removal of RDX from soil	β CD	Cyclotrimethylene-trinitramine (RDX) 	[108,109]
Inclusion studies ¹	β CD		
High explosive manufacturing	β CD, γ CD		
Inclusion studies ²	α CD, β CD, γ CD	1,3,3-Trinitroazetidine (TNAZ) 	[110,111]
Inclusion studies ¹	β CD, γ CD	Cyclotetramethylene-tetranitramine (HMX) 	[110]

Application	CD type	Energetic	Ref
Inclusion studies ³	γ CD	Hexanitrohexaazaisowurtzitane (CL-20) 	[112,113]
Manufacturing of gun propellants with nitrated β CDs (β NCDs)	β CD	Trimethylolethane trinitrate (TMETN) 	[114]

1 ¹H-NMR solution studies.

2 Characterisation by IR spectroscopy and DSC.

3 Characterisation by IR spectroscopy.

CDs can be used as molecular sieves to remove nitroaromatic compounds such as TNT and RDX from soil. Dilute aqueous solutions of hydroxypropyl- β CD and methylated- β CD were used to absorb TNT from soil, achieving the removal of at least 25% of the pollutant. These studies directly demonstrated that β CDs can interact with and envelop aromatic explosive compounds [67,108].

The encapsulation of TNAZ, RDX and HMX has been attempted using α , β and γ CDs. Interactions were characterised by ¹H-NMR spectroscopy and showed that the degree of interaction was relative to the size of the macrocycle and its cavity, and the size of the molecule to be encapsulated. HMX only interacted with γ CD (having the larger cavity), whereas RDX interacted with both β CD and γ CD. In contrast, α CD did not interact with any of the energetics due to its relatively smaller cavity size. TNAZ formed a solid complex with β CD, that was also characterised by DSC, solid-state NMR, and Raman spectroscopy [111]. The physicochemical properties of this complex differed from those of the physical mixture: the volatility of TNAZ was reduced and the CD thermal decomposition profile was less exothermic, but the thermal stability of TNAZ was not affected by the complexation [111]. Other attempts to encapsulate

larger molecules such as CL-20 have been successful with the larger γ CD, but not with β CD [112]. A more recent study showed that complexation also occurs between CL-20 and the nitrated derivative of γ CD [113]. The inclusion studies offered insight into the ability of CDs to trap energetic molecules.

In addition, β NCD and β NCD cross-linked with epichlorohydrin and isocyanate have been used to develop energetic formulations that are less vulnerable to accidental stimuli [109,114]. These patents led to the registration of a warhead featuring nitrated cross-linked CDs as part of the main charge [115]. The first patent [109,114] claimed the use of β NCD to encapsulate trimethylolethane trinitrate (TMETN). Different nitration levels are possible because not all of the 21 β CD hydroxyl groups need to be nitrated. The level of nitration affects the energetic performance and physicochemical properties of the β NCD. When more than three hydroxyl groups are nitrated to form nitro groups, the β NCD becomes insoluble in water but remains soluble in organic solvents such as acetone, methylene chloride or tetrahydrofuran (THF) [116]. Consequently the β NCDs can be processed as acetone lacquers. The inventors tested different reaction conditions to obtain β NCDs that are listed in Table 2.10.

Table 2.10 Summary of β CD nitration conditions [114].

CD ¹ (g)	90% HNO ₃ Mass (g)	98% H ₂ SO ₄ (g)	Time (min)	Extent of nitration (%)
200	1296	-	15	_ ²
50	291	480 ³	_ ²	_ ²
750	2650	550	120-180	12.96

1 Reaction temperature < 30 °C.

2 Values not reported.

3 Oleum.

The β NCD/TMETN formulations were then used in hazard tests to determine their sensitivity towards accidental stimuli. Hazard tests are systematic studies to quantify the accidental initiation of energetic compounds using standardised methods [117]. Such methods were developed independently by several countries in the nineteenth century and the results differ in the way the

magnitude of the sensitivity is reported, which makes it difficult to compare studies carried out in different countries [117]. The formulated products were compared to pure TMETN and β NCD (Table 2.11), but no information on the methodology was reported, although the compounds were likely to have been tested under American standards.

The tests demonstrated that the addition of β NCD to TMETN reduced the vulnerability of almost all the all formulations to shock, with only the 6:1 ratio TMETN/ β NCD formulation becoming more susceptible to impact than the single ingredients. The addition of β NCD as a binder to TMETN did not improve the thermal stability of the mixtures. The temperature of decomposition (T_{dec}) of the single ingredients was not reported, but the T_{dec} of the formulations was 4 °C lower than the T_{dec} of TMETN and 20 °C lower than the T_{dec} of β NCD as reported elsewhere. The sensitivity of β NCD to electrostatic discharge (ESD) was mitigated by the formulation with TMETN up to the safe value of 12.5 J. The TMETN/ β NCD 2:1 propellant cured with R45M isocyanate was described as a flexible gum, but its characterisation was not reported in the patent [114].

The nitration of β CDs featuring different cross-linkers (such as epichlorohydrin, urethane and amines) was attempted to obtain softer binders less susceptible to impact and ESD, but still able to contribute to the energy of the system [109]. A cross-linked CD sample, obtained by cross-linking β CD with a large excess of epichlorohydrin (1:12 ratio) was nitrated with 98% HNO_3 and then formulated with RDX in different ratios. The sensitivity towards accidental stimuli was then determined in impact and ESD tests (Table 2.12).

Table 2.11 Performance of TEMTN: β NCD propellant formulations [114].

Sample	Hazard tests			DTA ¹ (Onset°C/ Exotherm°C)	Card gap
	5 kg Impact (mm)	Friction (lb)	ESD (J)		
TMETN	≥ 600	≥ 980	≥ 12.5	182 ²	15–20
β NCD	≥ 600	≥ 980	0.0125	200–208 ³	0
TMETN: β NCD	≥ 600	≥ 980	≥ 12.5	140/178	0

Sample	Hazard tests			DTA ¹ (Onset°C/ Exotherm°C)	Card gap
	5 kg Impact (mm)	Friction (lb)	ESD (J)		
2:1					
TMETN/ β NCD 4:1	≥ 600	≥ 980	≥ 12.5	140/178	0
TMETN/ β NCD 5:1	≥ 600	≥ 980	≥ 12.5	140/178	0
TMETN/ β NCD 6:1	225	≥ 980	≥ 12.5	110/172	0

1 Values obtained from data thermal analysis (DTA): onset temperature of the decomposition and exotherm peak temperature.

2 Exotherm peak value from [118].

3 This work.

The nitrated cross-linked β CD (β NCCD) reduced the sensitiveness of RDX against impact depending on the amount of β NCCD used as the binder. The presence of the binder slightly reduced the susceptibility of the formulation to friction compared to pure RDX. Although the formulations also remained vulnerable to ESD, the energy input required for ignition increased to that of the binder (0.1288 J), which is much higher than the value for pure RDX (0.0585 J) and significantly lower than the 0.02 J that can potentially be accumulated by an operator [119] (Table 2.12).

Table 2.12 Sensitivity of nitrated cross-linked β CCD and RDX complexes [109]

Sample	RDX : β NCCD ratio	Hazard Tests		
		Impact Bruceton (cm)	Friction (kg)	ESD (joule)
RDX	-	19	9.6	0.0595
β NCCD	-	47	28.8	0.1288
RDX: β NCCD	1:1	42	12.8	0.1288
RDX: β NCCD	5:1	27	10.8	0.1288
RDX: β NCCD	10:1	30	10.8	0.1288

The CD derivatives used thus far still need design improvements before they are considered suitable as binders for energetic applications. There is a need to develop new systems that are more resistant to impact and ESD stimuli. To the best of our knowledge, β CD systems cross-linked with XEG segments and nitrated derivatives thereof have not yet been synthesised and characterised as potential binders for energetic applications. The research described in Chapters 4–6 therefore focuses on the development and testing of these novel formulations.

3 Experimental

3.1 Materials

The β CD used in this project (97%, Sigma-Aldrich) was used from stock with a 11–13% water content, based on TGA data. Polyethylene glycol diglycidyl ether (PEGDGE 500 Mw, Sigma-Aldrich), sodium hydroxide (Fisher Chemicals), benzylated dialysis membranes with a molecular weight cut-off (MWCO) of 2000 (Sigma-Aldrich), epichlorohydrin (Sigma-Aldrich), tetrabutyl ammonium bromide (Sigma-Aldrich), hexaethylene glycol (Sigma-Aldrich) and triethylene glycol (Sigma-Aldrich) were used without further purification. Triethylene glycol diglycidyl ether (TEGDGE, 262 g mol⁻¹) and hexaethylene glycol diglycidyl ether (HEGDGE, 394 g mol⁻¹) were synthesised as described in Section 3.3.

3.2 Methods

3.2.1 NMR spectroscopy

The ¹H NMR spectra were recorded on a Bruker Ascend (400 MHz) with a broad band fluorine observation (BBFO) probe in deuterated dimethyl sulfoxide (DMSO-d₆) and deuterium oxide (D₂O) solutions. Signals representing the solvents served as internal standards. The solvent peaks were referenced to 2.5 ppm (DMSO-d₆) and 4.7 ppm (HDO, D₂O). Peak multiplicities were described as follows: singlet (s), multiplet (m), and broad (br).

3.2.2 FTIR spectroscopy

FTIR spectra were collected using a Bruker Alpha in attenuated total reflection (ATR) mode, allowing the immediate characterisation of undiluted samples. The spectra were collected in the region between 400 and 4000 cm⁻¹.

3.2.3 Gel permeation chromatography

Gel permeation chromatography (GPC) was used to determine the Mw of the products on a Waters size-exclusion chromatography system equipped with a 2410 refractive index detector. The samples in water (1–0 mg mL⁻¹) were passed through two columns (PL aquagel-OH MIXED-M 1000–500,000 Da, 8

μm , 300 x 7.5 mm). The buffer was a solution of 0.01 M LiNO_3 and 0.5% (w/w) NaN_3 in distilled water. Nitrated samples in anhydrous THF (1.5 mg mL^{-1}) were passed through the column (10 μm PL-gel, Polymer Laboratories) at a flow rate of 1.0 mL min^{-1} . Calibration curves were created using polyethylene oxide/polyethylene glycol standards for aqueous buffers, and polystyrene standards for anhydrous THF.

3.2.4 Differential scanning calorimetry and thermal gravimetric analysis

Thermal analysis of the βCXCD samples and their precursors was carried out using a Mettler Toledo DSC3+ instrument for low-temperature profile studies and a combination of Mettler Toledo TGA/DSC3+ and DSC30 instruments for decomposition and compatibility studies. The temperature was cycled three times for the low-temperature regime: the first heating run was set from -100 to $130 \text{ }^\circ\text{C}$ to eliminate the water present in the samples, whereas the second and third runs were set from -100 to $120 \text{ }^\circ\text{C}$, a higher temperature considered sufficient to dry the sample. The degradation of the samples was characterised in the temperature range $30\text{--}500 \text{ }^\circ\text{C}$. A mass of 10 mg was placed in a 40- μL aluminium pan with a pierced lid to analyse the degradation of the inert materials, and low-temperature profiles of energetic and inert samples were also assessed with 10-mg samples. The decomposition of the energetic products was characterised using 1-mg samples. The DSC chamber was continuously purged with N_2 at a flow rate of 50 mL min^{-1} . The variation of the heat flow in the samples was recorded as a function of temperature and time.

3.2.5 Dynamic mechanical analysis

The thermo-mechanical properties of the βCXCDs were determined by dynamic mechanical analysis (DMA) using a Perkin Elmer DMA8000 device. The samples were subjected to a controlled sinusoidal displacement of 0.05 mm at frequencies of 1, 5 and 10 Hz in the single cantilever clamped bending configuration. The storage modulus (E'), loss modulus (E'') and damping factor ($\tan\delta$) were monitored as a function of temperature and time. The free sample length between the vibrating and fixed cantilever clamps was $\sim 15 \text{ mm}$. The

testing temperature was cycled three times between -100 and 140 °C at a rate of either 2 or 10 °C min^{-1} . Each material was tested in triplicate under each condition. The samples were tested in aluminium pockets, a stainless steel mesh or aluminium pockets with polytetrafluoroethylene (PTFE) tape because the cross-linked CD samples were not capable of self-support. The aluminium pockets consisted of rectangular shims (30×14 mm) cut from a 0.1 mm thick aluminium strip (supplied by RS) and then folded lengthwise to form the pockets. About 25 mg of the cross-linked CD sample was placed in the centre of the pockets. This sample support was recommended by the DMA manufacturer when testing powders, gels and liquids. PTFE tape (30×15 mm) was used to fold the sample in the pocket and assess the bonding interaction between the sample and the metallic support during cooling. Rectangular strips of mesh (30×15 mm) were cut from a 0.65 mm thick sheet (supplied by RS). The wire forming the mesh had a diameter of 0.4 mm and the dimensions of the holes were 1×1 mm. About 30 mg of the crosslinked CD material was spread around and in the centre of the mesh strips.

3.2.6 Optical microscopy

The dynamic physical properties of the β CXCD materials under the influence of temperature were investigated by optical microscopy using a Leica DM microscope fitted with a temperature-controlled stage (Linkam THMS 600). The temperature was changed using a T95 controller and an automated LNP95 liquid N_2 pump (both from Linkam). The material was placed on a 0.5 mm thick quartz cover slip. The slide was placed in a carrier on the stage to allow visual scanning. The stage was cooled to -100 °C and then heated to 100 °C at either 2 or 10 °C min^{-1} . To prevent condensation forming on the windows of the cold stage, the interior was purged with dry N_2 gas prior to cooling. A digital Qicam Fast 1394 CCD camera (QImaging) was used to continuously record any changes in the samples during the temperature cycle. The sample was illuminated by a white light source set in transmission mode.

3.2.7 Scanning electron microscopy

Scanning electron microscopy (SEM) was conducted using a Hitachi SU3500 instrument which is a tungsten filament variable pressure device with an accelerating voltage of 20 kV at 80 Pa. Samples (5 mg) were pressed onto conductive carbon tabs and supported with specimen stubs.

3.3 Procedures

3.3.1 Triethylene glycol diglycidyl ether ^[120]

Sodium hydroxide (40.00 g, 1.00 mol) in water (50 mL), tetrabutylammonium bromide (1.19 g, 7.40 mmol) and epichlorohydrin (92.70 g, 1.00 mol) were placed in a three necked round bottomed flask. The reaction mixture was then stirred vigorously for 1 h at room temperature. Triethylene glycol (25.60 g, 0.17 mol) was added slowly over 3 h at room temperature with vigorous mechanical stirring. The reaction mixture was stirred at 40 °C for 1 h, allowed to cool and then filtered. The liquid phase was collected, dried overnight on sodium sulfate, and the excess epichlorohydrin was evaporated under high vacuum to leave a yellow-orange viscous liquid: ¹H-NMR (400 MHz, CDCl₃) : δ=4.00–3.40 (m, 16H, CH₂-O), 3.15 (m, 2H, CH-CH₂), 2.80 and 2.62 (2 m, 4H, CH₂-CH); ¹³C-NMR (CDCl₃): δ=72.0 (CH₂-O), 70.9, 70.7 and 70.6 (CH-CH₂-O), 50.8 (CH-CH₂) and 44.4 ppm (CH₂-CH); DSC (10 °C min⁻¹, N₂) 203 °C (T_{dec} onset); DSC (10 °C min⁻¹, N₂) T_g = 80 °C; yield 78%.

3.3.2 Hexaethylene glycol diglycidyl ether ^[120]

Sodium hydroxide (23.60 g, 0.59 mol) in water (29.5 mL), tetrabutylammonium bromide (0.70 g, 4.35 mmol) and epichlorohydrin (54.70 g, 0.59 mol) were placed in a three necked round bottomed flask. The reaction mixture was stirred vigorously for 1 h at room temperature. Hexaethylene glycol (28.50 g, 0.10 mol) was added slowly over 3 h at room temperature with vigorous mechanical stirring. The reaction mixture was stirred at 40 °C for 1 h, allowed to cool and then filtered. The liquid phase was collected and dissolved in dichloromethane (50 mL). The solution was washed with half-saturated brine three times and dried overnight on sodium sulfate. The excess epichlorohydrin was evaporated

under high vacuum to leave a yellow-orange viscous liquid: $^1\text{H-NMR}$ (400 MHz, CDCl_3) : $\delta=4.00\text{--}3.40$ (m, 26H, $\text{CH}_2\text{-O}$), 3.15 (m, 2H, CH-CH_2), 2.80 and 2.62 (2 m, 4H, $\text{CH}_2\text{-CH}$); $^{13}\text{C-NMR}$ (CDCl_3): $\delta=72.0$ ($\text{CH}_2\text{-O}$), 70.9, 70.7 and 70.6 ($\text{CH-CH}_2\text{-O}$), 50.8 (CH-CH_2) and 44.4 ppm ($\text{CH}_2\text{-CH}$); DSC ($10\text{ }^\circ\text{C min}^{-1}$, N_2) $273\text{ }^\circ\text{C}$ (T_{dec} onset); DSC ($10\text{ }^\circ\text{C min}^{-1}$, N_2) $T_g = 80\text{ }^\circ\text{C}$; yield 70%.

3.3.3 Cross-linked cyclodextrins (βCXCDs)

The reported procedure refers to the conditions optimised during this project. For the conditions tested, see the appendices (Table A 1, Table A 2 Table A 3). The βCD (5.00 g, 4.40 mmol) was dissolved in 5.6% w/w NaOH (21.0 mL) and stirred mechanically for 16 h. Diglycidyl ether (TEGDGE, HEGDGE or PEGDGE; 17.4–5.8 mL, 13.2–36.9 mmol) was then added dropwise over a period of 20 min with vigorous stirring. The reaction mixture was heated to $30\text{ }^\circ\text{C}$ for 6 h with vigorous stirring. After cooling to room temperature for 20 min, the mixture was neutralised with HCl (6 M). The volume of solvent was reduced and the reaction mixture was precipitated in acetone. The solid was dissolved in distilled water and dialysed against water using a benzylated cellulose membrane (2000 MWCO) for 5 days. The dialysis water was replaced every day. The dialysed white solid was collected and the water was evaporated under reduced pressure. The final product was characterised by $^1\text{H NMR}$ and DSC. $^1\text{H NMR}$ (400 MHz, DMSO-d_6 , ppm): $\delta=5.9\text{--}5.6$ (brm, $\text{C}_2\text{-OH}$, $\text{C}_3\text{-OH}$), 5.1–4.8 (m, H-C_1), 4.7–4.5 (br m, OH_A , OH_B), 4.4 (br m, $\text{C}_6\text{-OH}$), 4.0–3.2 (brm, $\beta\text{CDOCH}_2(\text{CHOH})\text{CH}_2\text{OCH}_2\text{CH}_2$). DSC $10\text{ }^\circ\text{C min}^{-1}$, N_2 : $240\text{--}250\text{ }^\circ\text{C}$ (T_{dec}); yield 45-72%.

3.3.4 Nitrated cross-linked cyclodextrins (βNCXCDs)

Nitric acid (100%, 2.1 mL) was poured into a round-bottomed flask and cooled below $10\text{ }^\circ\text{C}$ in ice water. The bath was removed and βCXCD (200 mg) was added in small fractions over 5 min, ensuring that the temperature remained below $10\text{ }^\circ\text{C}$. The crude slurry or solution was then left stirring at room temperature for 1 h. The reaction mixture was crushed into ice/water (10 mL). The solid was decanted and rinsed with distilled water. The solid was dissolved in acetone (5 mL) and re-precipitated in a solution of half saturated brine and

Na₂CO₃ (5% w/w, 100 mL) three times. The crude product was filtered and dissolved in 10 mL acetone. The solution was filtered through Na₂CO₃ and dried under vacuum. Small portions of products were characterised by ¹H NMR and DSC and stored under dichloromethane. Then ¹H NMR spectroscopy was performed in DMSO-d₆ and used for comparison with the precursors. DSC (10 °C min⁻¹, N₂): 197–210 °C (T_{dec}); yield 80%.

3.3.5 Hazard testing

A set of small-scale hazard tests were performed according to Cranfield internal procedures and following the Energetic Materials Testing Assessment Policy (EMTAP) Manual of Tests.

3.3.5.1 Small scale hazard tests

Direct impact: steel hammer on steel anvil

A small amount of the synthesised compound (20 mg) was placed on the steel anvil and struck 10 times with the steel hammer. Signs of decomposition, such as smell, colour change and material consumption, were evaluated after each blow.

Glancing blow: steel hammer on steel anvil

A small amount of synthesised compound (20 mg) was placed on the steel anvil and struck with a glancing blow using the curved edge of the steel hammer. Signs of decomposition were evaluated after each blow as above.

High temperature test

A small amount of compound (20 mg) was placed on a steel plate at 100 °C for 30 min. Signs of decomposition were evaluated as above.

Room temperature test

A small amount of compound (20 mg) was placed on a steel plate at 30 °C for 24 h. Signs of decomposition were evaluated as above.

Flame test

A small amount of compound (20 mg) was placed on a steel spoon and ignited using a blow torch. The nature of the combustion process was described by an expert member of the Cranfield University “Synthesis and Formulation” group.

3.3.5.2 Hazard tests based on the Energetic Materials Testing Assessment Policy Manual of Tests

Electrostatic discharge test

Nylon spark test strips were filled with the material and sealed with copper tape. Fifty samples were tested using a certified ESD testing apparatus and a spark of 4.5 J was discharged through the composition. The samples were inspected for perforation or signs of decomposition.

Rotter direct impact test

Samples (30–40 mg) were placed in a concavity at the centre of the supporting frame of the Rotter tester apparatus. A free-fall weight (5 kg) and striker were suspended above. The tests followed the Bruceon “up and down” testing technique with 50 replicates and the results were based on the height at which the compound was initiated 50% of the time, with the mean height reported as the figure of insensitiveness (Fol) [119]. Initiation was determined by the observation of parameters such as sound, smoke, flash and volume of gas released immediately after impact, and is therefore affected by operator judgment.

3.3.6 Compatibility tests

The tests were based on Test 4 of STANAG 4147 [121]. Approximately 0.5–1.0 mg of each material was analysed by DSC at a heating rate of 2 °C min⁻¹ under N₂ and then a mixture of the two materials was measured in the same manner. Any alteration in the shape, onset, or peak position of any measured thermal event can be indicative of incompatibility.

Under “Applicability” STANAG 4147 Test 4 states: *“This test is applicable to explosives likely to come into contact with plasticizers, fuels, additives,*

polymeric materials and other explosives.” It also states: “This test is not concerned with compatibility between ingredients in explosive compositions and the consequent stability of such compositions.” Even so, the method allows a large number of mixtures to be investigated rapidly. As such, the results from this tests are useful but not conclusive, and further experiments are required, such as vacuum stability testing [122].

Edition 2 of STANAG 4147 Test 4 states that shifts in thermal events that vary by less than 4°C indicate compatibility. For shifts between 4 and 20 °C, the test is inconclusive and, as above, further experiments are required [122]. Shifts greater than 20 °C are considered conclusive evidence that materials are incompatible.

3.3.7 Stability analysis

The stability of the nitrated products was determined by heat flow calorimetry (HFC). The samples (1.0 g) were placed in sealed vials (10 mL) with glass beads to fill the head space. The samples were characterised by isothermal calorimetry at 80 °C on a TAM IV device with a dedicated software package.

4 Synthesis and characterisation of inert β CXCDs

This chapter describes the cross-linking of β CD with the diglycidyl ethers TEGDGE, HEGDGE or PEGDGE as a first step towards the synthesis of a new, inert binder for energetic applications. The cross-linking reaction conditions discussed below were investigated and optimised to obtain products that exhibited the following properties, in alignment with the statement of requirements developed by the PhD sponsor organisation, the Weapons Science and Technology Centre (WSTC):

- Low T_g (possibly below 0 °C) to reduce vulnerability to shocks, ensuring the cross-linked binder remains soft in a wide operative temperature range, down to the T_g .
- Soluble in organic solvents and/or water, allowing the formulations to be processed by preparing a lacquer with the binder. The lacquer and the solid ingredients mixed with it can be extruded as a paste and granulated in pellets [2]. Low-molecular-weight cross-linked products with a low cross-linking ratio would guarantee the preparation of an extrudable paste.
- Easily converted to energetic derivatives by nitration. The new requirement for binders in energetic formulations is to contribute to the energetic output of the main filler. A simple and safe nitration procedure would produce a suitable replacement for NC.
- Good chemical and thermal stability to avoid uncontrolled events during the shelf life of the formulation.
- Good compatibility with energetic fillers such as high explosives, oxidisers, and pyrotechnics to avoid undesirable reactions and instability when the binder is mixed with the other ingredients of an energetic formulation.

4.1 Synthesis and chemical characterisation

The effect of the reaction conditions discussed in sections 4.1.1–4.1.7 and the chemical characterisation of some of the β CXCDs by $^1\text{H-NMR}$ and FTIR spectroscopy have been published in a peer-reviewed article: Luppi F, Cavaye H, Dossi E (2018) Nitrated cross-linked β -cyclodextrin binders exhibiting low

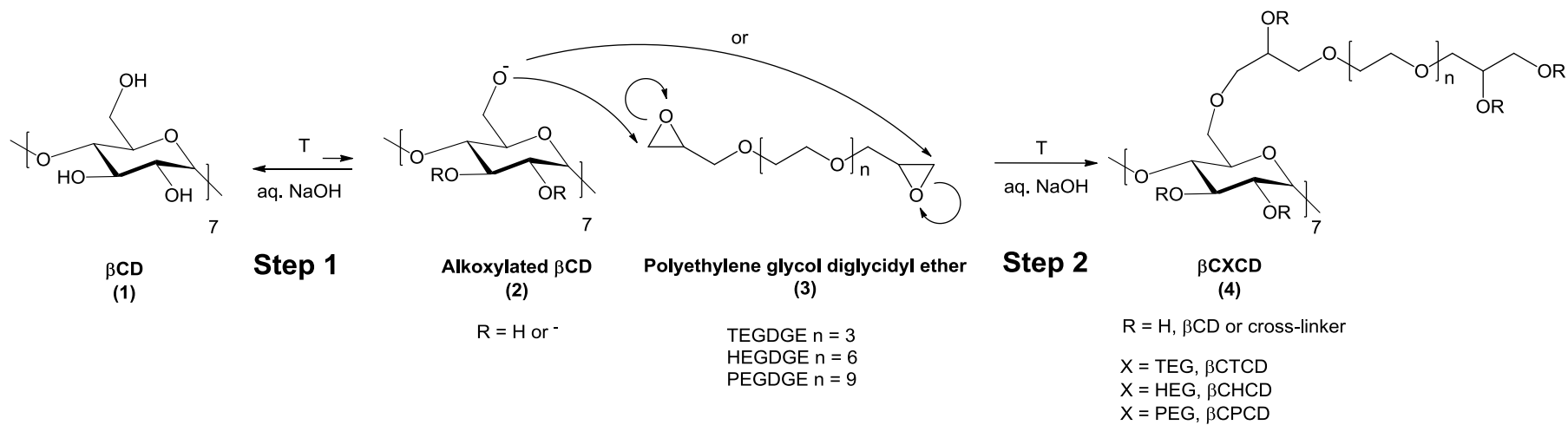
glass transition temperatures. *Prop Expl Pyrotech* 43 (10) 1023–1031. The paper is attached at the end of the annex to this thesis.

The synthesis of β CXCDs was based on the cross-linking of β CD with polyethylene glycol diglycidyl ethers containing ethylene glycol units, according to Scheme 4.1. Triethylene glycol diglycidyl ether (TEGDGE) contains three ethylene glycol units and was a synthetic sample. Hexaethylene glycol diglycidyl ether (HEGDGE) contains six ethylene glycol units and was also a synthetic sample. Polyethylene glycol diglycidyl ether (PEGDGE) was obtained from a commercial source and was a polydisperse 500 Da preparation with an average of nine ethylene glycol units. The abbreviation XEG is used to collectively refer to the ethylene glycol segments in the cross-linkers and the β CXCD products.

To note that, TEG: β CD ratio, HEG: β CD ratio, PEG: β CD ratio is used refer to the ratio of XEG units to β CD units in the reaction products β CXCDs

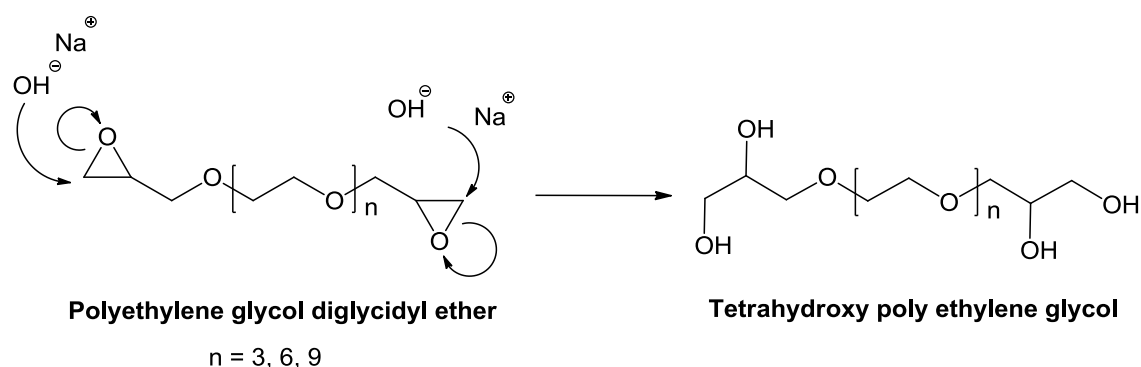
TEGDGE was prepared according to a published procedure [120] by reacting triethylene glycol with an excess of epichlorohydrin under basic conditions to produce the diglycidyl ether derivative. The same experimental conditions were then used for the synthesis of HEGDGE. The synthesis of HEGDGE from hexaethylene glycol has been described in the past following a similar route, but gave a lower yield (55%) [123]. The yield using the method followed in this PhD project was 70%.

As shown in Scheme 4.1, β CD (**1**) is dissolved in NaOH (5.6–50%) to give the corresponding alkoxyated β CD (**2**). The equilibrium is strongly shifted towards (**1**) (Step 1, Scheme 4.1) due to the pK_a values of the acid dissociation of the β CD hydroxyl groups. The pK_a values for the β CD secondary alcohols in the literature vary from 12.1 to 13.5 [124]. There is no information about the pK_a values of the primary hydroxyl groups because this is difficult to measure directly [124]. The alcohol-alkoxide equilibrium (Step 1, Scheme 4.1) therefore cannot be evaluated accurately. When a solution of 1.5 M NaOH (5.6% w/w) is used, the amount of (**1**) is six orders of magnitude higher than the alkoxyated derivative (**2**). It can be inferred that the alkoxylation of **1** is the rate-limiting step in the cross-linking process.



Scheme 4.1 The synthesis of cross-linked βCXCDs .

The reaction can be accelerated by modifying certain conditions, such as the temperature or concentration of NaOH or cross-linker, but a secondary reaction competes with the main reaction and its outcome is the loss of cross-linker. The competitive reaction is the opening of the diglycidyl rings of the cross-linker under basic conditions yielding the corresponding tetrahydroxyl derivative (Scheme 4.2).



Scheme 4.2 Competitive hydrolysis of diglycidyl rings under basic reaction conditions.

Both the cross-linking and competitive hydrolysis reaction kinetics are strongly affected by:

- NaOH concentration
- Reaction time
- Temperature
- Effect of the β CD alkoxide formation
- Volume of NaOH aqueous solution
- Cross-linker: β CD ratio
- Addition rate of the cross-linker

Because all of these parameters affect the efficiency of cross-linking, it was necessary to optimise them in order to avoid the competitive reaction as far as possible and increase the yield of the desired product. PEGDGE is a commercially available chemical and was used for most of the cross-linking experiments, but a few tests were carried out using the TEGDGE produced in-house.

4.1.1 Effect of the NaOH concentration

The effect of the concentration of NaOH was tested to determine which conditions favoured the primary cross-linking reaction rather than the side reaction in which the cross-linker is degraded. The effect of the NaOH concentration was investigated at a high temperature (70 °C) for short reaction times (Step 2, 1 h) to enable rapid screening. All the NaOH concentrations that were tested resulted in a strongly alkaline environment, which can deprotonate the β CD hydroxyl groups. Four β CXCD samples (IP1–IP4) were prepared using 50%, 40%, 36% and 5.6% w/w NaOH solutions and a PEGDGE: β CD ratio of 9:1 (Table 4.1) [78]. Higher concentrations of NaOH were used for the synthesis of epichlorohydrin/ β CD cross-linked systems [59,69,75], so these conditions were tested to determine their effect on the balance between cross-linking and PEGDGE degradation and also their effect on the solubility of the compounds. The results are summarised in Table 4.1.

Table 4.1 Effect of NaOH concentration on the yield of β CPCDs at a PEGDGE: β CD ratio of 9:1.

Sample ID ¹	NaOH ² (% w/w)	Reaction Time (Step 2) (h)	Yield ³ (%)	Water solubility
IP1	50	1	<1	Y
IP2	40	1	<1	Y
IP3	36	1	<1	Y
IP4	5.6	0.66	88%	N

¹ PEGDGE: β CD ratio = 9:1.

² Reaction temperature = 70 °C.

³ Yield measured as mass of products/mass of both reactants.

At 70 °C, the most dilute NaOH solution (5.6% w/w) promoted cross-linking whereas all the stronger NaOH solutions (36%, 40% and 50% w/w) favoured the rapid degradation of the cross-linker compared to the formation of the β CD alkoxide. When the NaOH concentration was low, the reaction reached the gelation point, thus causing a consistent change in viscosity of the reaction mixture accompanied by the appearance of an insoluble hydrogel. The speed of

gelation indicated that cross-linking with 5.6% NaOH at 70 °C is extremely fast and would make it difficult to recover soluble products. Accordingly, the studies proceeded by investigating the effect of the reaction time in the presence of 40% NaOH. However the optimisation of the temperature and the amount of cross-linker discussed in the following sections proved that this assumption was incorrect, and that 5.6% NaOH was a more effective choice at lower temperatures.

4.1.2 Effect of the reaction time

The slow step in the cross-linking mechanism is the formation of the alkoxide (Step 1, Scheme 4.1), only small amounts of which are available to react with the cross-linker. In order to increase the yield of β CPCDs, it appeared important to increase the reaction time to reform the alkoxides that reacted with the cross-linker and make more of these groups available for the cross-linking reaction. Two samples were synthesised, maintaining the earlier reaction conditions (40% NaOH, 70 °C) but extending the reaction time (Step 2) from 1 h (sample IP2, Table 4.2) to 5 h (sample IP5, Table 4.2).

Table 4.2 Effect of the reaction time (Step 2) on the yield of β CPCDs.

Sample ID ¹	NaOH ² (% w/w)	Reaction Time (Step 2) (h)	Yield ³ (%)	Water solubility
IP2	40	1	<1	Y
IP5	40	5	12	Y

1 PEGDGE: β CD ratio = 9:1.

2 Reaction temperature = 70 °C.

3 Yield measured as mass of products/mass of reactants.

The product yield increased from negligible amounts to 12% when the reaction time was extended to 5 h (Step 2). This suggested that longer times are necessary to replenish the consumed alkoxide, allowing the cross-linking reaction to proceed. Although 12% was a significant improvement, it was not considered ideal and the reaction conditions were investigated in further detail. Accordingly, extending the time from 5 to 6 h improved the yield even further.

4.1.3 Effect of the temperature

Higher temperatures often accelerate endothermic reactions [125]. However, both the cross-linking reaction and the degradation of the cross-linker are likely to be accelerated by temperature. A trial was therefore carried out using the following conditions:

- The temperature was reduced from 70 °C to 50 °C
- A low concentration of NaOH (5.6% w/w)
- A time of 5 h for the cross-linking reaction (Step 2, Scheme 4.1)
- The amount of cross-linker was reduced to a 5:1 ratio, to avoid the gelation observed when the ratio was 9:1

The cross-linker appeared more stable at 50 °C when the reaction proceeded for 5 h in the presence of 5.6% NaOH (sample IP6, Table 4.3). The lower yield at 70 °C (sample IP7, Table 4.3) reflected the loss of cross-linker in the competing degradation reaction, which is favoured by the higher temperature, whereas lower temperatures favour cross-linking. Water-soluble polymers were produced in the tests, confirming that a lower PEGDGE:βCD ratio was necessary to generate soluble cross-linked βCPCDs.

Table 4.3 Effect of the temperature on the yield of βCPCDs, when the PEGDGE:βCD ratio is 5:1.

Sample ID ¹	T (°C)	Yield ² (%)	Water solubility
IP6	70	1	Y
IP7	50	13	Y

¹ PEGDGE:βCD ratio = 5:1, 5 h reaction time (Step 2), aq. NaOH 5.6% w/w.

² Yield measured as mass of products/mass of reactants.

4.1.4 Effect of β CD alkoxide formation

The time allowed for the system to reach alcohol/alkoxide equilibrium (Step 1, Scheme 4.1) was extended by leaving the β CD stirring in 5.6% NaOH for 16 h, thus increasing the amount of alkoxide available to react with the cross-linker.

Table 4.4 Effect of the time allowed for β CD alkoxide formation (Step 1) on the yield of β CPCDs.

Sample ID ¹	Alcohol/alkoxide time (Step 1)	T (°C)	Yield ² (%)	Water solubility
IP6	0 h	70	1	Y
IP7		50	13	Y
IP8	16 h	50	30	Y
IP9		30	33	Y

1 PEGDGE: β CD ratio = 5:1, 5 h reaction time (Step 2), aq. NaOH 5.6% w/w.

2 Yield measured as mass of products/mass of reactants.

The difference between samples IP6 and IP7, where no time was allowed for the system to reach alcohol/alkoxide equilibrium (Step 1, Scheme 4.1), and samples IP8 and IP9 (where Step 1 in Scheme 4.1 involved stirring for 16 h), revealed that the cross-linking process requires more time to increase the availability of alkoxide groups for the reaction (Step 2, Scheme 4.1). Samples IP8 and IP9 were obtained at higher yields (30% and 33%, respectively), with the best results achieved at 30 °C. The malleability of the products prompted thermal characterisation studies, revealing that the T_g of compounds IP8 and IP9 were -18 and -22 °C, respectively. This confirmed that the processability of crystalline β CD could be improved by the incorporation of soft polyethylene glycol segments.

4.1.5 Effect of the volume of NaOH solution

When the concentration of β CD was higher than $0.23 \text{ g}_{\beta\text{CD}} \text{ mL}^{-1}_{\text{aq.NaOH}}$ in the reaction mixture, the solubility of the cross-linked β CPCDs was reduced,

causing their gelation (sample IP9, Table 4.4). In all subsequent experiments, the safe value of $0.21 \text{ g}_{\beta\text{CD}} \text{ mL}^{-1}_{\text{aq.NaOH}}$ was used.

4.1.6 Effect of cross-linker: β CD ratio

The next set of trials (Table 4.5) tested the effect of the PEGDGE: β CD ratio on the yield and physical properties of the products, with the other parameters maintained at the optimal values established above:

- 5.6% w/w NaOH
- 30 °C
- 16 h for the formation of the alkoxide (Step 1, Scheme 4.1)
- 5 h for the completed cross-linking reaction (Step 2, Scheme 4.1)
- PEGDGE as the cross-linker

The PEGDGE: β CD ratio influenced the final thermal properties of the β CPCD products. As expected, increasing the amount of cross-linker from 2 to 5 molar equivalents increased the cross-linking ratio in the product (Table 4.5). The cross-linker consumed in the competitive degradation reaction negatively affected the mass economy of the reaction, with the difference attributed to the degradation of the PEGDGE. Thermal analysis of the cross-linked products confirmed that lower amounts of cross-linker generated β CPCD products with greater crystallinity and higher T_g values. The synthesis of sample IP11 achieved a higher yield than the other compounds, and led to a further investigation of the purification method, which generally involved dialysis against water.

Table 4.5 Effect of PEGDGE: β CD ratio on the yield of β CPCDs.

Sample ID ¹	PEGDGE: β CD feed ratio	Yield ² (%)	Water solubility
IP9	5 : 1	34 ³	Y
IP10	4 : 1	36 ³	Y
IP11	3 : 1	68	Y
IP12	2 : 1	44 ³	Y

1 5.6% (w/w) NaOH, 30 °C, 16 h for alkoxide formation (Step 1), 5 h reaction time (Step 2).

2 Yield measured as mass of products/mass of reactants.

3 Estimated value due to the leaking of the product from the purification equipment.

4.1.6.1 Purification of β CXCDs

A typical work up for the cross-linked compounds started with the recovery of the crude product from the reaction mixture after neutralising the excess NaOH with 6 M HCl. Most of the water was removed under vacuum and the product was reprecipitated in acetone to eliminate unreacted and degraded cross-linkers. The compound was dissolved again in a small amount of water and dialysed against water to remove:

- NaCl formed during the neutralisation step
- Unreacted starting compounds (β CD and cross-linker)
- Any residual degraded cross-linker
- Low-molecular-weight oligomers

Dialysis was carried out using a cellulose membrane with a MWCO of 2000 Da for 5 days at room temperature (Figure 4.1). The dialysate was changed daily. At the end of the process, the retentate containing the desired cross-linked product was NaCl-free, as assessed by AgNO_3 qualitative analysis. When characterised by $^1\text{H-NMR}$ in DMSO-d_6 , the compounds were found to be free of impurities. The NMR characterisation of the product is discussed in detail in Section 4.2.



Figure 4.1 Dialysis apparatus for the purification of β CXCDs.

The dialysate residues were dried and weighed, revealing that 80–70% w/w of the expected impurities on the first day were dialysate, reaching 85–90% w/w on the second day. No residual NaCl was detected after replacing the water four times, leaving only the degraded cross-linker and oligomeric products with a $M_w < 2000$ Da. These were absent after 5 days of dialysis.

4.1.7 Effect of the duration of cross-linker addition

The duration of cross-linker addition to the reaction mixture containing the β CD alkoxide was tested, initially with prolonged exposure times of up to 7 h to determine whether generally lower amounts of cross-linker would react preferentially with the β CD alkoxide rather than undergoing degradation. The earlier results suggested that β CPCDs obtained with a PEGDGE: β CD ratio of 5:1 reflected the maximum ratio that still produced soluble compounds (Table 4.6). Considering a potential increase in the efficiency of the cross-linking reaction, the first test involved 16 h for the alkoxide formation (Step 1, Scheme 4.1) and 7 h for the addition of the cross-linker (Step 2, Scheme 4.1). The product obtained using the new reaction parameters (sample IP14) had a higher PEG: β CD ratio than a similar setup with a brief exposure time (sample IP13) reflecting an 8% higher cross-linking efficiency. No significant change in the

yield was observed, possibly due to losses of product during the purification dialysis (Table 4.6).

Table 4.6 Effect of cross-linker addition time.

Sample ID	PEGDGE:βCD ratio feed	PEG:βCD ratio by ¹ H NMR	Addition time (h)	Yield ¹ (%)	Cross-linker yield efficiency ²	Water solubility
IP13	5 : 1	3.8 : 1	20 min	68	75	Y
IP14	3.8 : 1	3.2 : 1	7 h	71	83	Y

1 Yield measured as mass of products/mass of PEGDGE and βCD.

2 Cross-linker yield is measured as the molar ratio between the feed of cross-linker and the amount of polyethylene glycol units present in the product.

The longer cross-linker addition time improved the mass economy of the reaction, but it seemed to have a negligible effect on the reaction yield and the product solubility. A cross-linker addition time of 20 min was therefore used for subsequent tests.

4.2 The synthesis of βCXCDs

The screening tests discussed in Sections 4.1.1–4.1.7 revealed the optimal conditions for the cross-linking of βCD with diglycidyl ethers. The reaction time was duly increased to 6 h to ensure that more unreacted cross-linker was consumed. The optimised parameters are shown below:

- Low NaOH concentration (5.6% w/w) to reduce the competitive side reaction (degradation of the cross-linker)
- Concentration of βCD in NaOH = 0.21 g_{βCD} mL⁻¹_{aq.NaOH} to avoid gelation
- A 16 h (overnight) reaction for βCD alkoxide formation (Step 1, Scheme 4.1)
- Cross-linker:βCD feed ratio < 5:1 to avoid gelation
- Addition of the cross-linker in 20 min
- Low temperature (30 °C) to favour cross-linking over the degradation of the cross-linker
- A 6-h reaction time (Step 2, Scheme 4.1)

Three sets of β CXCDs were synthesised using TEGDGE, HEGDGE and PEGDGE cross-linkers, varying the feed cross-linker: β CD ratio from 2:1 to 5:1. The water content of β CD can reach (13–14% w/w) [38]. The water content was determined by TGA prior to each cross-linking reaction to maintain the β CD concentration at $0.21 \text{ g}_{\beta\text{CD}} \text{ mL}^{-1}_{\text{aq.NaOH}}$, as discussed above. In a typical synthesis reaction, 5 g of wet β CD was dissolved in 20.5 mL 5.6% NaOH_{aq} w/w and left to react at 30 °C overnight to form the β CD alkoxide. The cross-linker was then added in 20 min and the reaction mixture was left for 6 h at 30 °C as shown in Figure 4.2.



Figure 4.2 Cross-linking apparatus for the synthesis of β CXCDs.

The reaction mixture was then neutralised with 6 M HCl to remove excess NaOH, reduced in volume and reprecipitated in acetone to eliminate organic impurities such as degraded and unreacted cross-linker (Scheme 4.2). The products were then purified by dialysis against water using a 2000 Da MWCO benzoylated cellulose membrane. The retentate was collected and dried under high vacuum for 48 h. The cross-linking of β CD with PEGDGE was replicated to produce enough sample mass for the tests discussed in the following chapters. No significant differences in the yield or properties of the synthesised products were observed when comparing the replicates (Table A 1).

The desired β CXCD products were obtained with yields of up to 68% when HEGDGE and PEGDGE cross-linkers were used, whereas slightly lower yields (63%) were achieved when TEGDGE was used. This may reflect the outcome of the dialysis step, with smaller β CTCD molecules not retained by the membrane. Table 4.7 summarises the results of representative cross-linking reactions with the best results in terms of yield and β CXCD properties. The remaining synthesis reactions are reported in Table A 1.

Table 4.7 Synthesis of β CXCDs: summary of the most successful water-soluble products.

Sample ID ^{1,2}	Cross-linker	Cross-linker : β CD ratio feed	XEG: β CD ratio by ¹ H NMR	Yield ³ (%)	Physical appearance
IT1	TEGDGE	5 : 1	3.6 : 1	63	Friable solid
IT2		4 : 1	3.1 : 1	52	Brittle solid
IT3		3 : 1	2.4 : 1	56	Brittle solid
IT4		2 : 1	1.9 : 1	45	Brittle solid
IH1	HEGDGE	5 : 1	4.0 : 1	68	Soft gum
IH2		4 : 1	3.2 : 1	72	Soft gum
IH3		3 : 1	2.6 : 1	67	Brittle solid
IH4		2 : 1	1.8 : 1	65	Brittle solid
IP13	PEGDGE	5 : 1	3.8 : 1	68	Soft gum
IP15		4 : 1	3.0 : 1	65	Soft gum
IP16		3 : 1	2.3 : 1	68	Brittle solid
IP17		2 : 1	1.6 : 1	68	Brittle solid

1 5.6% (w/w) NaOH, 30°C, 16 h for the formation of β CD alkoxide, 6 h reaction time, 20 min for cross-linker addition.

2 Sample ID: I = inert (not nitrated), T/H/P = cross-link segment, numeral = unique sample reference.

3 Yield measured as mass of products/mass of cross-linker and β CD.

The off-white β CXCDs were soft and malleable at cross-linker ratios of 4:1 and 5:1, but powdery and fragile at cross-linker ratios of 3:1 and 2:1 (Figure 4.3).

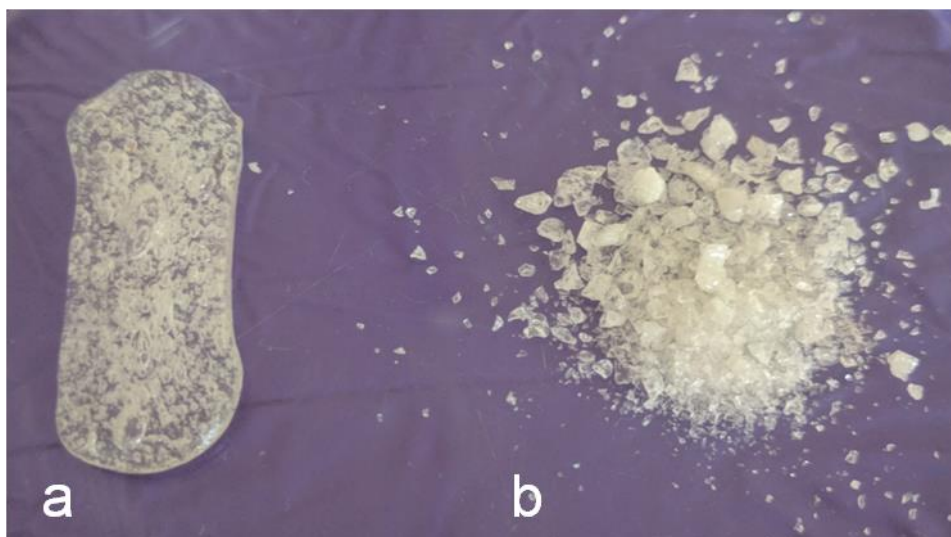


Figure 4.3 Physical characteristics of β CPCD. (a) Malleable IP13. (b) Powdery IP17.

Attempts to cross-link β CD using a greater ratio of cross-linker: β CD than 5:1 generated highly cross-linked β CXCD products that were insoluble in water. The β CXCDs produced with lower cross-link ratios were more soluble, and among the three sets of products those synthesised with TEGDGE were easier to dissolve than those synthesised with HEGDGE or PEGDGE. This is likely to reflect the lower Mw, generating a less intricate cross-linked network.

All the products were characterised by ^1H NMR:

- The NMR spectra were recorded in both DMSO- d_6 and D_2O solvents without a reference because β CD can encapsulate these reference compounds
- DMSO- d_6 was used as a solvent to investigate whether the hydroxyl groups of the β CDs at 4.4–5.5 ppm reacted with the cross-linker: a decrease in signal intensity would confirm this.
- D_2O was used as a solvent to determine the cross-linking ratio (this was not possible in DMSO- d_6 due to the overlapping water and product signals).

¹H-NMR analysis in DMSO-d₆

The ¹H-NMR analysis in DMSO-d₆ of the βCPCD sample IP13 and its precursors PEGDGE and βCD led to the proposed βCXCD general chemical structure shown in Figure 4.4. The corresponding ¹H-NMR spectra are shown in Figure 4.5.

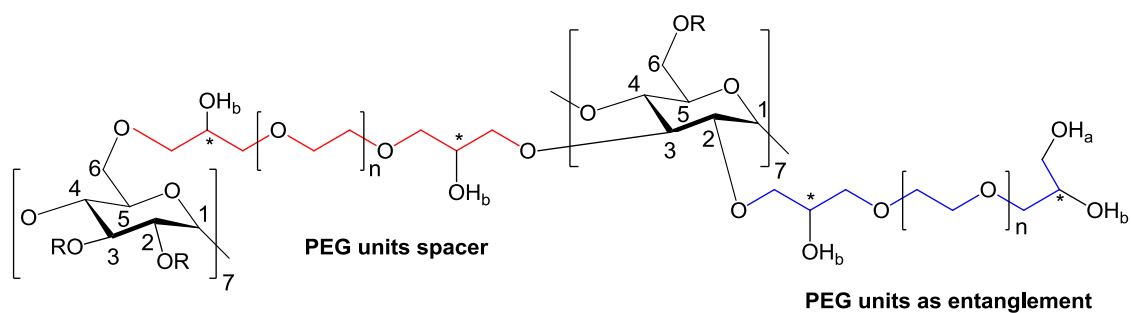


Figure 4.4 Proposed chemical structure of the βCXCD products based on IP13 incorporating PEG segments, underlining the co-existence of PEG units as spacers and as entanglements.

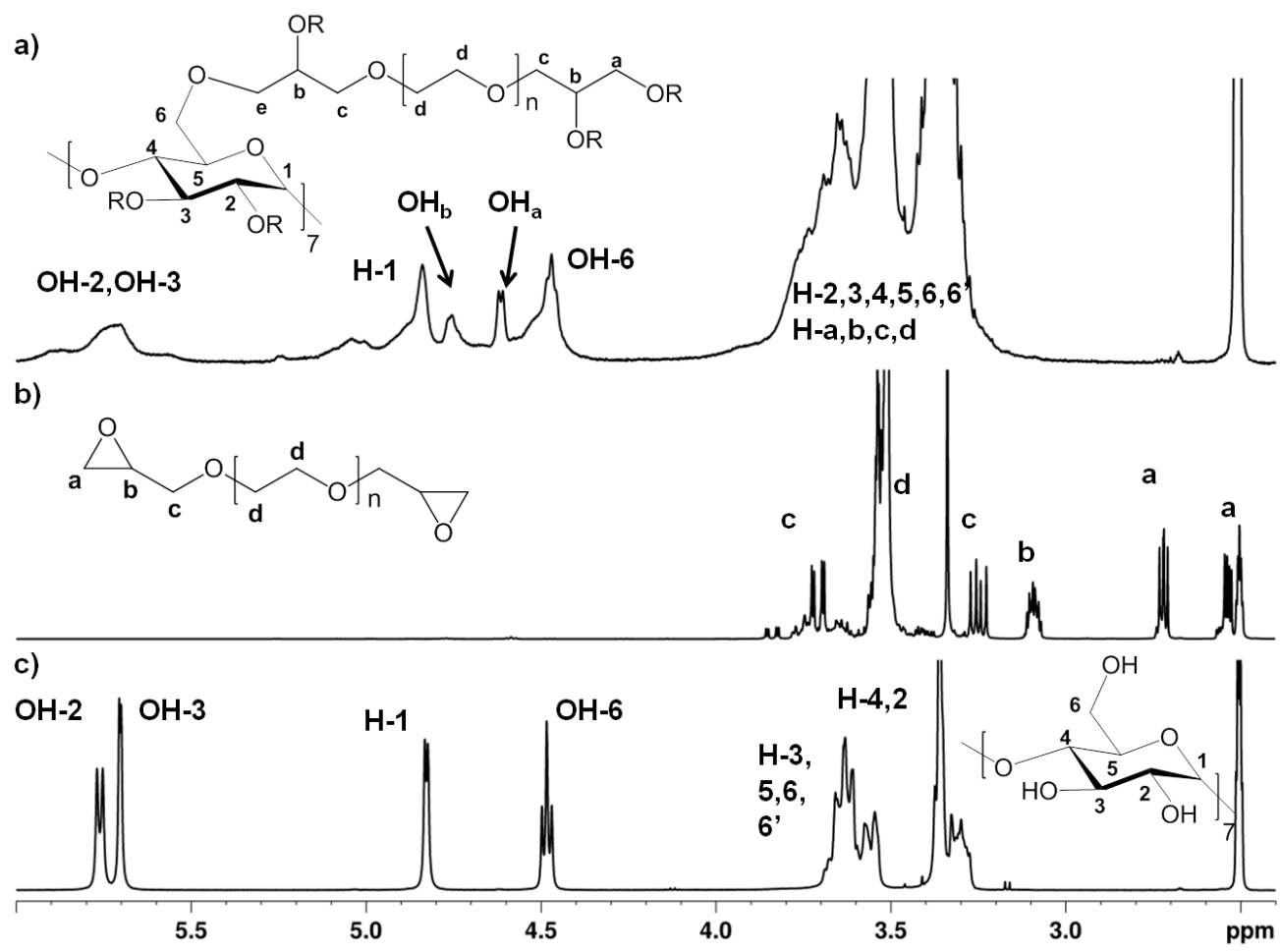


Figure 4.5 Comparative ^1H NMR spectra of (a) sample IP13 (PEG: β CD ratio = 3.8:1), (b) PEGDGE, and (c) β CD in DMSO-d_6 with assignments of signals. The DMSO reference peak is at 2.5 ppm. R= H, cross-linker $\text{C}_a\text{-OR}$ = H or β CD.

The NMR spectra of β CD and PEGDGE match the values reported in the literature and discussed in Section 2.4.1 [63]. The spectrum of sample IP13 in DMSO- d_6 shows broadened peaks due to the macromolecular structure of the cross-linked product, given the complex chemical environment of protons in larger cross-linked molecules compared to the smaller β CD and cross-linkers. This is a general observation valid for all the synthesised β CXCD systems, confirming their polymeric nature. The integration of the NMR signals gave reliable indications for the chemical structure of the products, including the reduction of the integrals from OH groups at 5.9 ppm. The consumption of the OH-6 groups cannot be confirmed because they overlap with new signals between 5.0 and 4.6 ppm, which were attributed to the OH_b on the PEG spacer units after the opening of the diglycidyl ring of the PEGDGE (Scheme 4.2). The anomeric proton H-1 was found at 4.7 ppm broadened by the macromolecular structure and by its overlap with signals from OH_a and OH_b. The remaining proton signals from β CD and methylene protons from the PEG units were found between 3.9 and 3.2 ppm. Many signals overlap and peak attribution is therefore difficult. The absence of the characteristic diglycidyl group signals between 3.2 and 2.6 ppm excludes the presence of the cross-linker in the purified product (Figure 4.6a-c).

It was difficult to confirm the absence of degraded cross-linker (Figure 4.5b) in the final cross-linked products. In order to help with the assignment of the peaks, a sample of PEGDGE was left to react under the cross-linking reaction conditions, resulting in partial degradation and the formation of a blend of unreacted and degraded PEGDGE (Figure 4.6). During the synthesis of all β CXCDs, the by-products were removed during purification by reprecipitation in acetone followed by dialysis.

In addition, when only one of the glycidyl groups of PEGDGE reacts with β CD, a new pendant PEG unit is formed which contains two new hydroxyl groups (OH_b and OH_a) at the end of each entanglement. The NMR signals of the new OHs appear as a broad peak between 4.9 and 4.55 ppm (Figure 4.6).

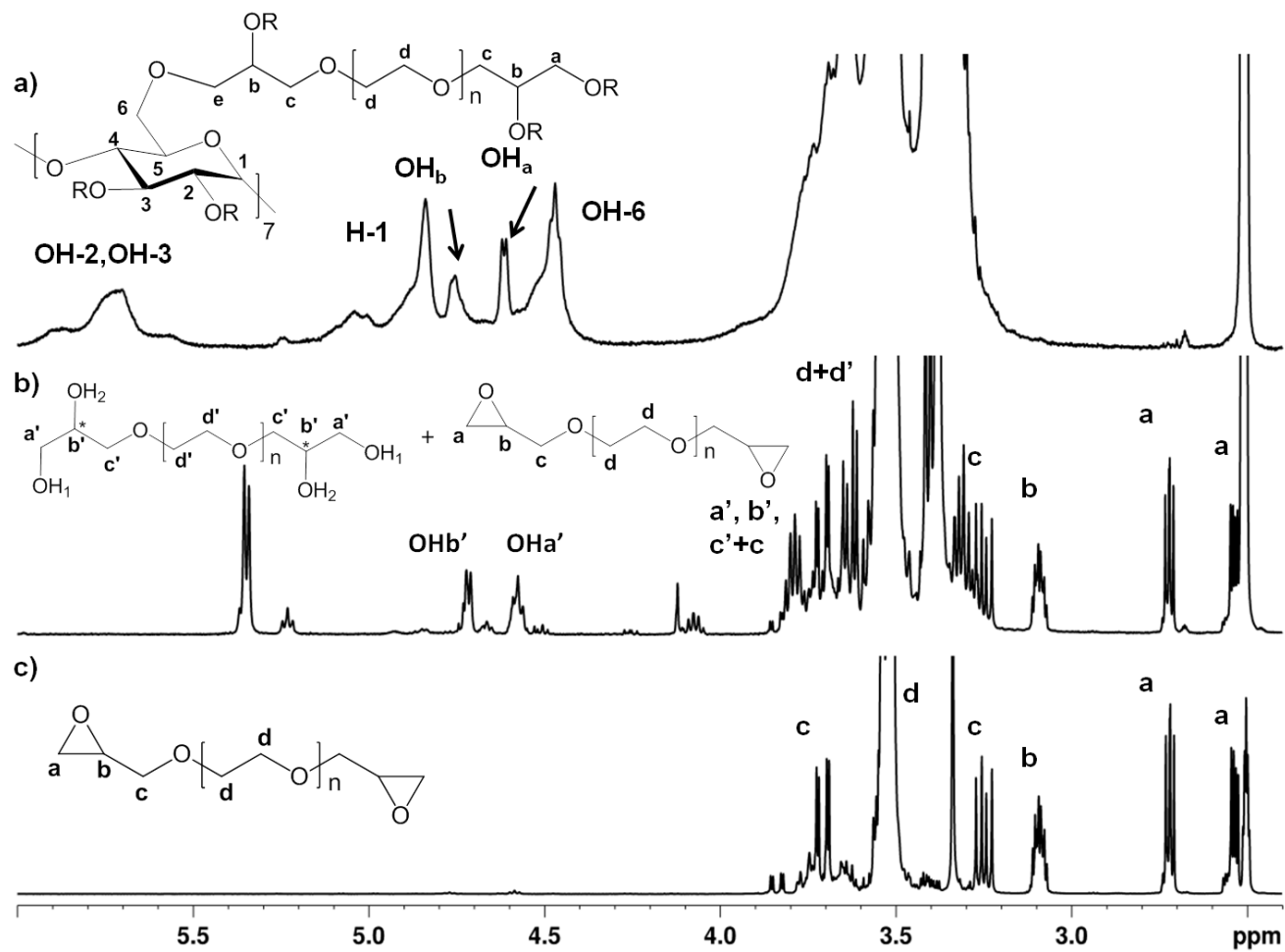


Figure 4.6 Comparative ^1H NMR spectra of (a) IP13 (PEG: β CD ratio = 3.8:1), (b) mixture of degraded/non degraded PEGDGE, and (c) PEGDGE in $\text{DMSO}-d_6$.

¹H-NMR analysis in D₂O

The ¹H-NMR spectra of the βCXCDs were then recorded in D₂O to determine the degree of cross-linking. The spectrum of the representative sample IP13 in Figure 4.7 is divided in two distinct regions: 5.2–4.6 ppm attributed to the chemical shift of the H-1 anomeric protons in two different situations as seen in Fig 4.7b and 4.1–3.4 ppm assigned to the chemical shift of the CH and CH₂ protons of both βCD and PEG units in the βCXCDs.

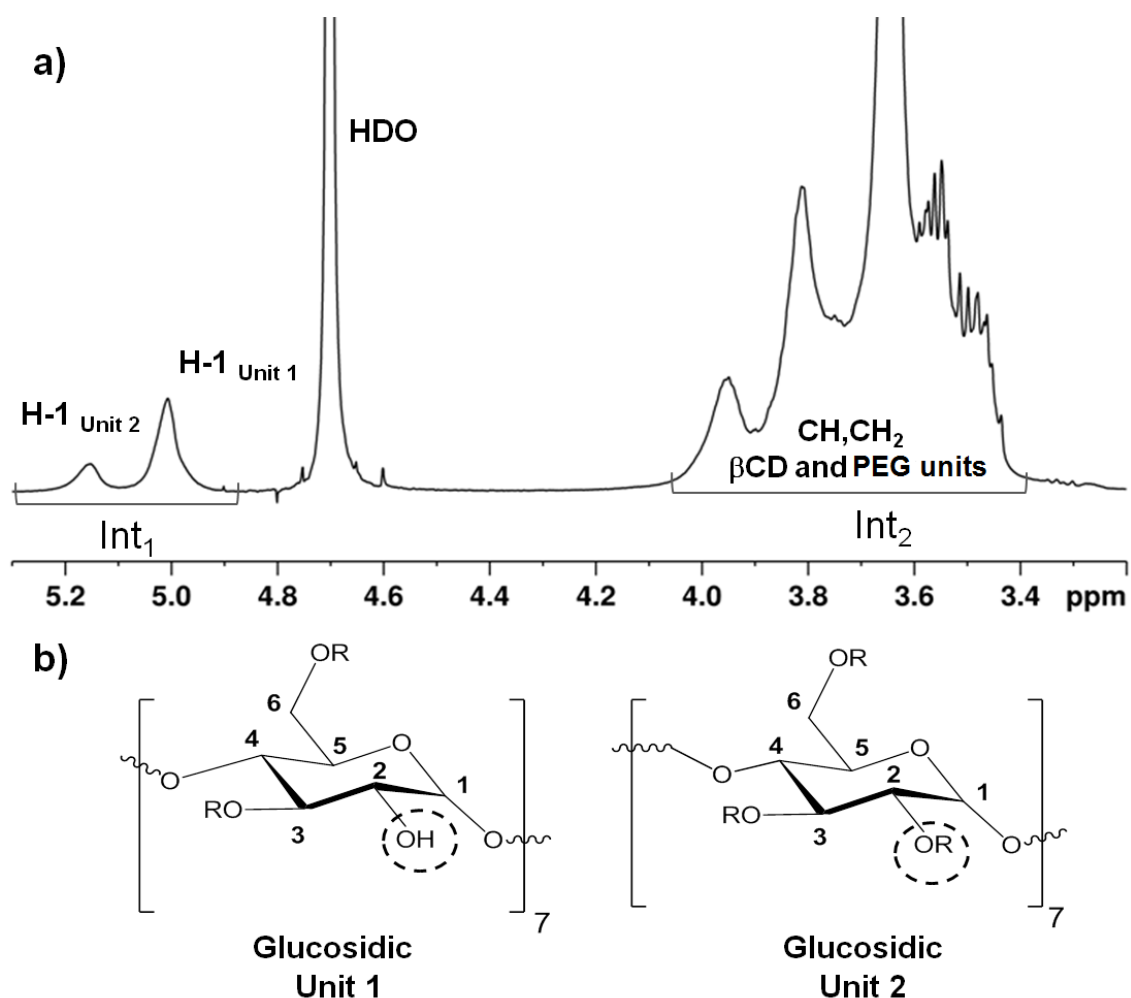


Figure 4.7 (a) The ¹H-NMR spectrum of IP13 (PEG:βCD ratio = 3.8:1) in D₂O and (b) the proposed chemical structure of βCXCDs highlighting the two different situations for the anomeric H-1, when in unit 1 or unit 2 of βCXCDs.

The broad signal centred at 5.00 ppm is assigned to the anomeric H-1 protons of the glucosidic unit 1 of βCD and represents the chemical environment of H-1

β CD when the protons of the OH-2 groups are not involved in the cross-linking. In contrast, when the protons of the OH-2 groups were substituted with PEG units (Figure 4.7, unit 2) the anomeric proton signal was shifted downfield at 5.18 ppm. The ratio between the two integrals in Figure 4.7 (Int_1 and Int_2) was used to determine the degree of cross-linking in β CXCDs (XEG: β CD molar ratio) [86]. Int_1 refers to the seven anomeric protons of β CD units, whereas Int_2 refers to all remaining protons in the β CXCD monomeric unit, specifically:

- 42 protons of β CD units
- Protons of the polyethylene glycol unit (X), namely
 - 22 protons when X = TEG
 - 34 when X = HEG
 - 44 when X = PEG

The following system of two equations was used

$$Int_1 = 7 H-1 \tag{1}$$

$$Int_2 = H\beta CD \text{ units} + nH_{PEG \text{ or } HEG \text{ or } TEG} \tag{2}$$

From the 1 H-NMR spectra, the calculated XEG: β CD ratios in the β CXCDs were 25% lower than the initial feed ratio of the reaction. Using sample IP13 as an example, the PEGDGE: β CD feed ratio was 5:1 but the PEG: β CD ratio in the product was 3.8:1 (Table 4.7) reflecting the degradation of the cross-linker as discussed in section 4.1.1. The PEG: β CD ratio was also confirmed by the integrals ratio of the H-1 signals in unit 2 and unit 1 (Figure 4.6b).

The calculation of the XEG: β CD ratio in the β CXCDs was also attempted by comparing Int_1 and Int_3 , where Int_3 between 3.7 and 3.6 ppm is the integral of the four ethylene glycol CH_2 protons present in the XEG repeat units in β CXCD (Figure 4.8).

However, the cross-linking ratios obtained when comparing Int_1 and Int_3 were 5–10% higher in value in relation to the cited method (Equations 1 and 2) which uses Int_1 and Int_2 [86], reflecting the partial overlap of the β CD protons and the

methylene groups of the XEG chains. The values obtained via the cited method were therefore used for subsequent evaluations.

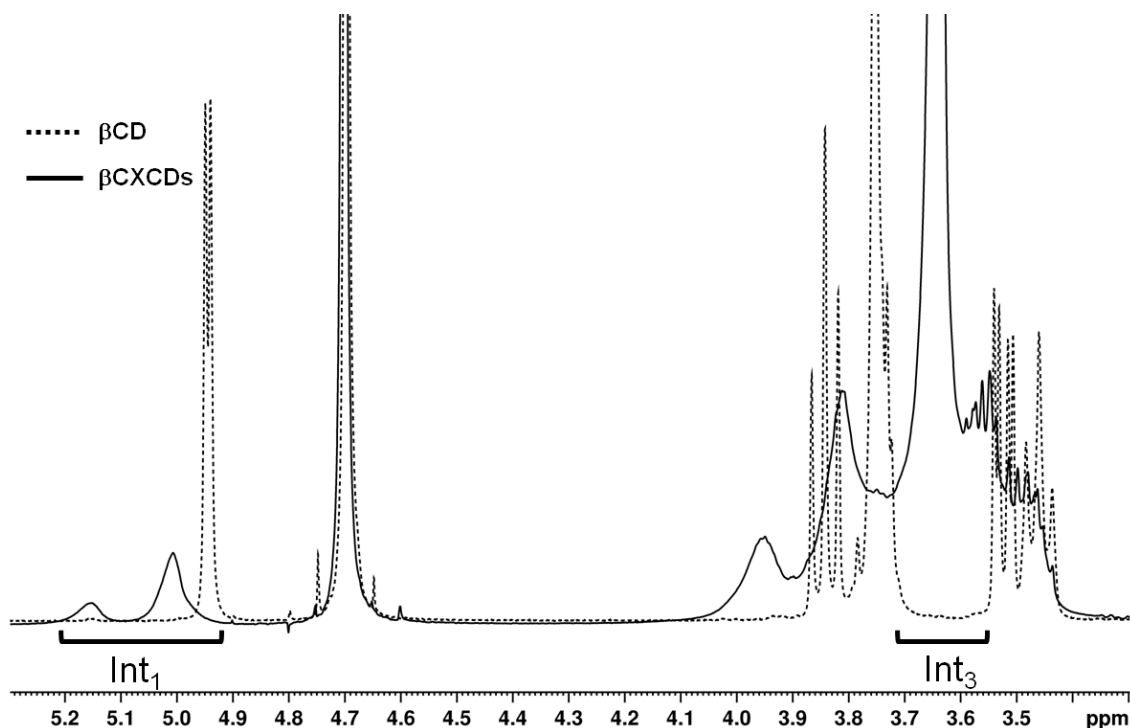


Figure 4.8 The ^1H -NMR spectrum of IP13 (PEG: β CD ratio = 3.8:1) in D_2O . Int_1 = anomeric H-1, Int_3 = CH_2 of PEG.

The NMR spectra of the three sets of β CXCDs prepared using PEGDGE were similar, as shown in Figure 4.9. However, the intensity of the signal between 5.2 and 4.9 ppm, attributed to unit 2 (the anomeric H next to cross-linking point), increased at higher PEG: β CD ratios. Three sharp signals attributed to the H-3 proton of β CD units appeared in the region between 3.6 and 3.4 ppm when the PEG: β CD ratio was lower than 2.6, due to the absence of the broad signals at high level of cross-linking (black arrows, Figure 4.9).

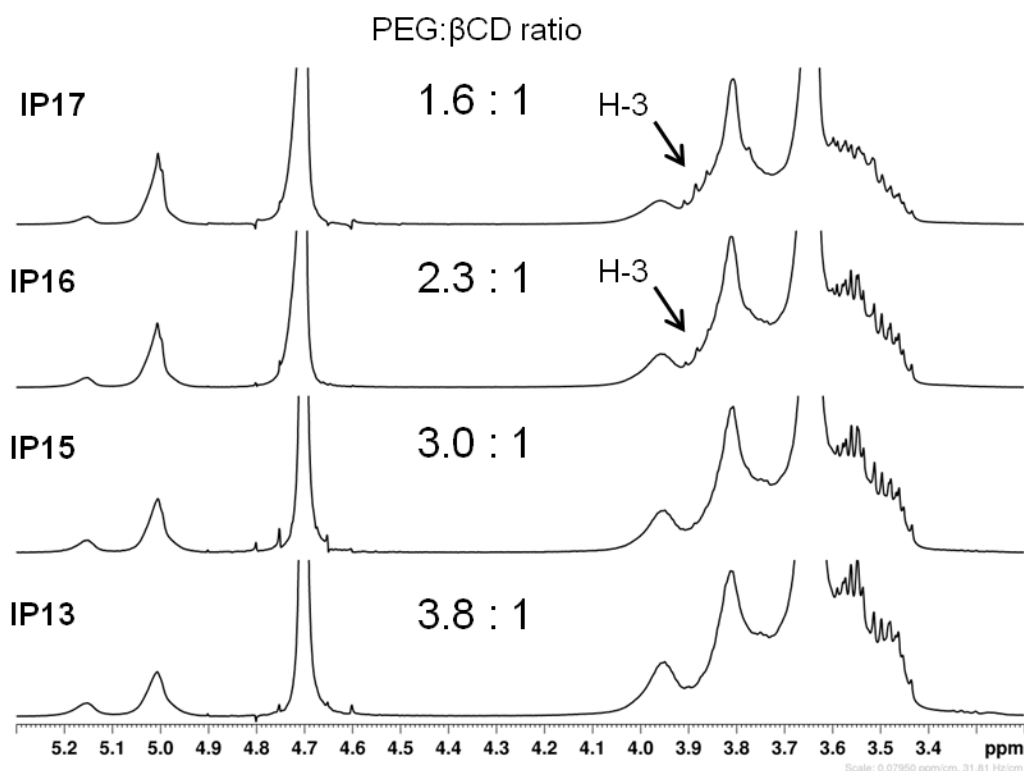


Figure 4.9 Comparative $^1\text{H-NMR}$ spectra of βCPCD samples (IP13, IP15–IP17) with different PEG: βCD ratios. Lower ratios enhance the visibility of the βCD proton (marked with the arrow).

All βCXCDs were characterised by FTIR spectroscopy and the spectrum of a representative sample (IP13) was compared to those of the precursors βCD and PEGDGE (Figure 4.10). The strong absorption at 1077 and 1023 cm^{-1} (Figure 4.10, red curve) was attributed to the stretching of C-O-C cross-linking bonds in βCXCDs . The absorption intensity at 2940 cm^{-1} (symmetric stretching of CH_2 and CH), 2871 cm^{-1} (asymmetric stretching of CH_2 and CH), 1453 cm^{-1} (scissoring of CH_2) and 1349 cm^{-1} (bending of CH) in the βCXCDs was higher than in the βCD precursor, confirming the presence of the cross-links. The signals in all the spectra at 1642 cm^{-1} represented the secondary vibration of adsorbed water [73].

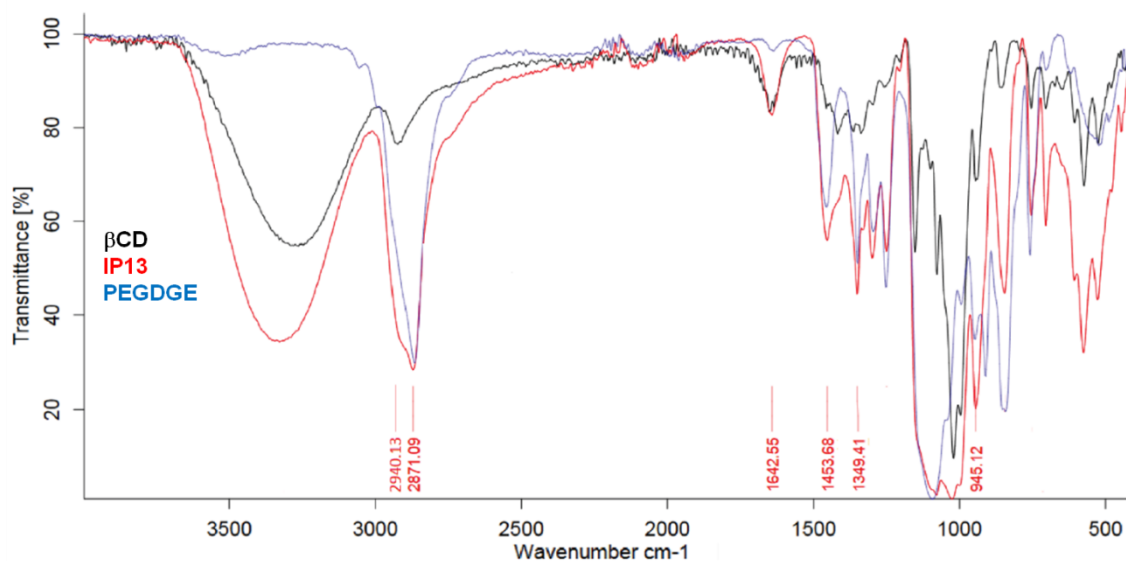


Figure 4.10 Comparative FTIR spectra of β CD (black curve), β CPCD sample IP13 (red curve), and PEGDGE (blue curve).

The M_w of water-soluble β CXCDs containing TEG, HEG or PEG units were determined by GPC. The samples were dissolved in aqueous 0.1 M LiNO_3 containing 0.05% w/w NaN_3 , with polyethylene glycol/polyethylene oxide standards for nine-point calibration in the range 106 Da to 1 MDa. Therefore, all M_w values reported are standards equivalents. These standards were the nearest available to the chemical composition of the β CXCDs.

GPC analysis of the precursors β CD and PEGDGE was carried out under the same experimental conditions. The β CD chromatogram showed a peak at retention time 13.7 min ($M_w=1134.98 \text{ g mol}^{-1}$, 200 Da standards equivalents) that fell outside the calibration curve of the standards (Figure 4.11). As expected, the standards eluted at different times compared to pure β CD. Their equivalents cannot be used to assess the M_w of the oligomers, but provide a useful qualitative estimate.

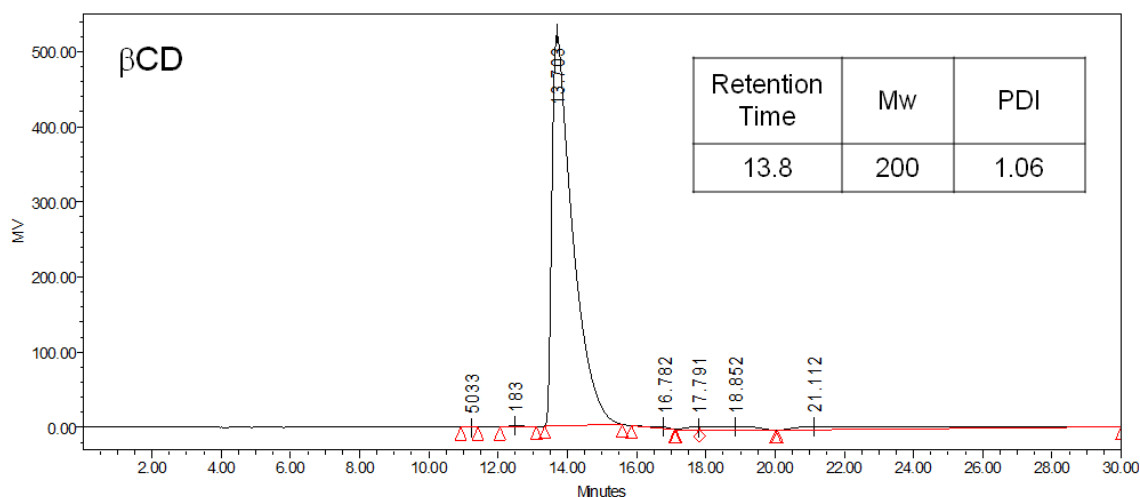


Figure 4.11 GPC analysis of β CD compared to polyethylene glycol/polyethylene oxide standards.

The chromatogram of PEGDGE (Figure 4.12) revealed the polydispersity of the compound as stated by the manufacturer (Sigma-Aldrich, average Mw=500). Two major fractions were detected, with retention times of 12.7 and 13.5 min, respectively (equivalent = 200 Da for the first fraction, with the other outside the calibration range). The TEGDGE and HEGDGE cross-linkers were not analysed by GPC because $^1\text{H-NMR}$ analysis confirmed their monodisperse nature (Mw = 262 and 394 Da, respectively; Figure A 2 and Figure A 3).

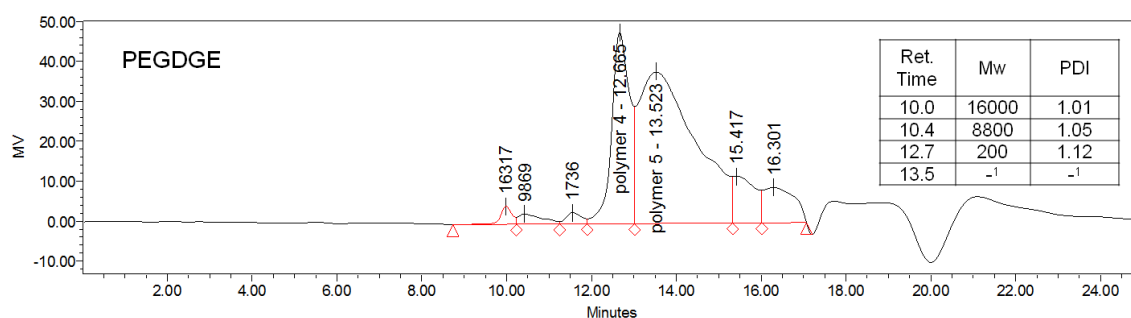


Figure 4.12 GPC analysis of PEGDGE compared to polyethylene glycol/polyethylene oxidestandards.

The β CXCD samples analysed by GPC (IT21, IH2 and IP22) were synthesised using TEGDGE, HEGDE and PEGDGE, respectively. Their chromatograms (Figure 4.13) were composed of two major elution peaks between 12 and 16 min. Sample IH2 presented a broader distribution of higher Mw, represented by

the onset of elution at 7.5 min corresponding to fractions with higher Mw (Figure 4.13b). The Mw of all β CXCDs, calculated using the elution times of the standards equivalents, were lower than expected. Again this reflected the different elution behaviour of the β CXCDs compared to the standards, due to the presence of β CD with a different hydrodynamic volume [125]. The peak at 13.7–14 min suggested the sample was contaminated with β CD and/or dimers that were not eliminated during the purification process.

GPC analysis of the β CXCDs confirmed that products with higher XEG: β CD ratios (3.6:1) eluted at lower retention times, corresponding to their higher Mw. Figure 4.14 shows the chromatograms of β CTCDs containing a decreasing ratio of TEG units.

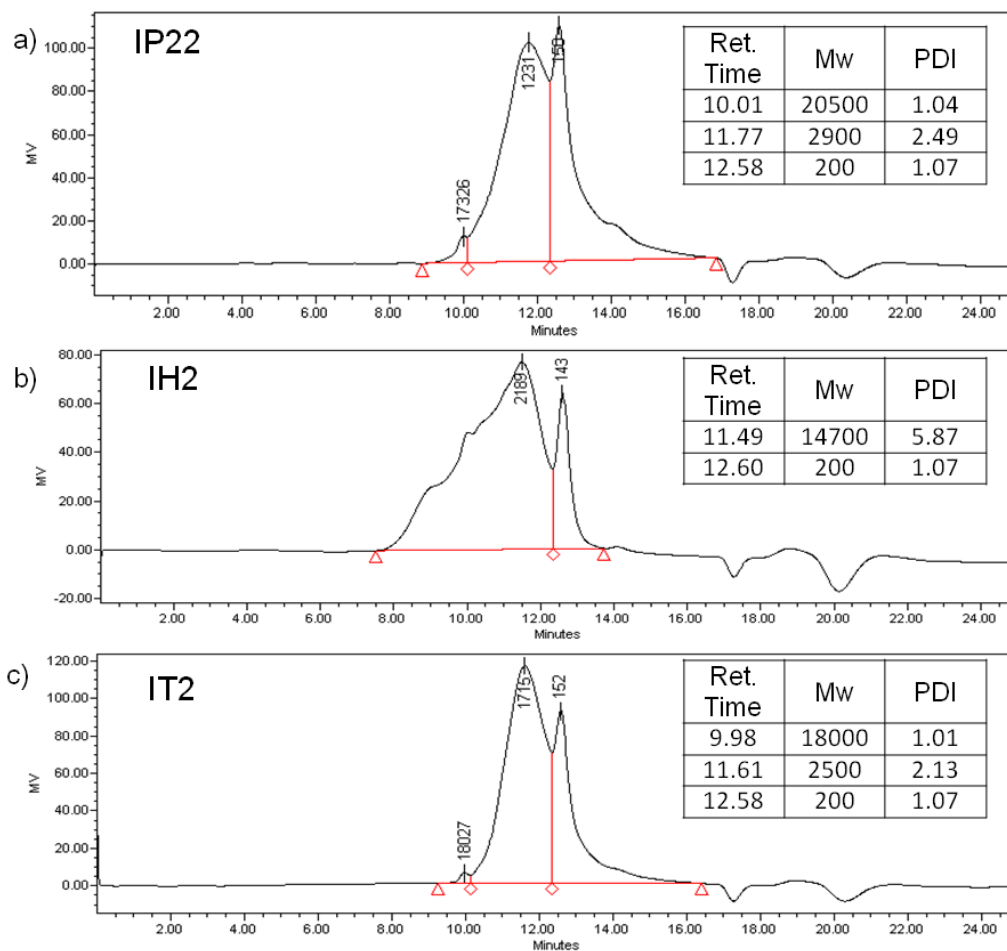


Figure 4.13 Analysis of β CXCDs by GPC compared to polyethylene glycol/polyethylene oxide standards. (a) Sample IP22 (PEG: β CD ratio = 2.9). (b) Sample IH2 (HEG: β CD ratio = 3.2). (c) Sample IT2 (TEG: β CD ratio = 3.1).

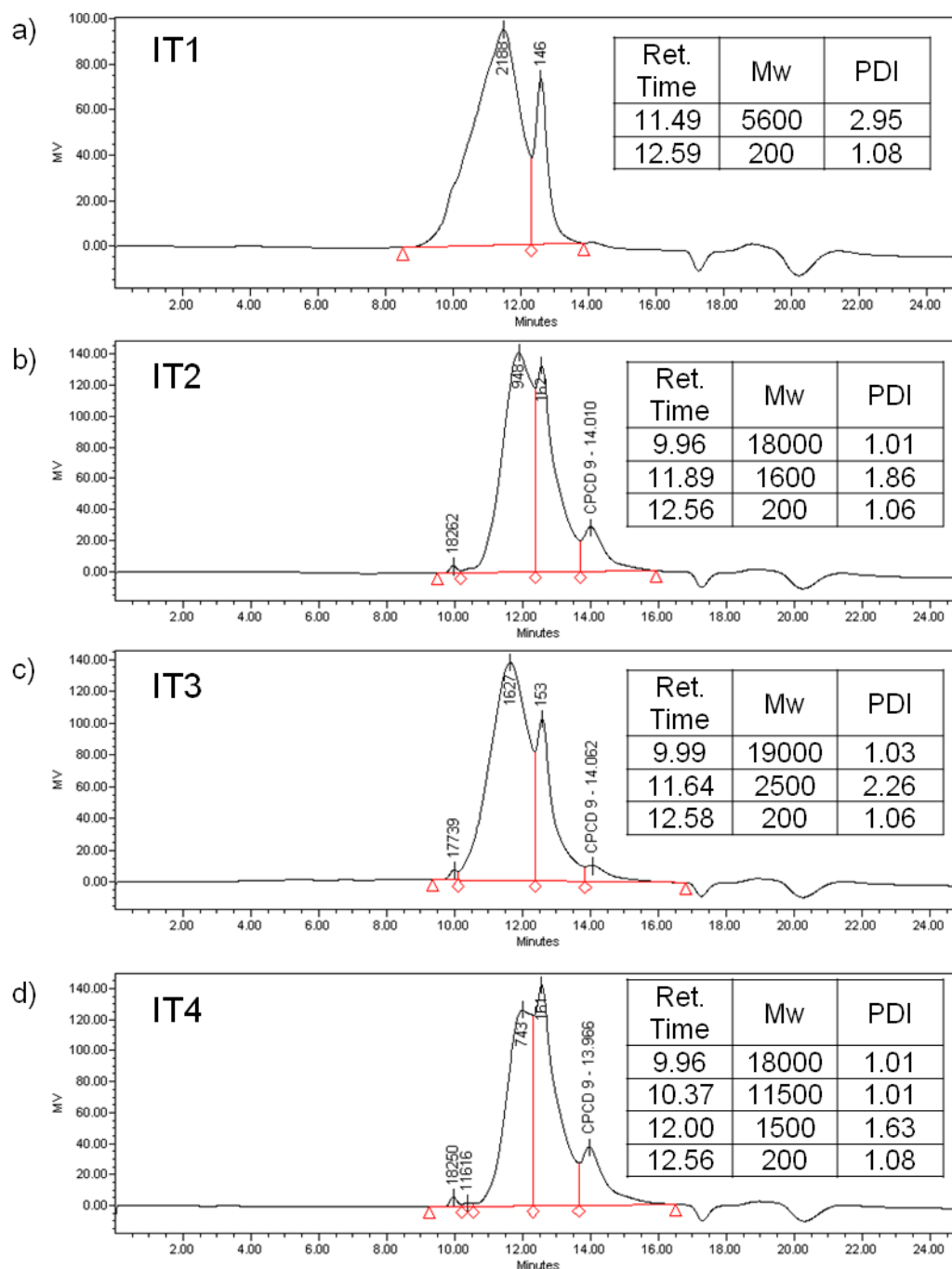


Figure 4.14 Analysis of β CTCDs by GPC compared to polyethylene glycol/polyethylene oxide standards. (a) Sample IT1 (TEG: β CD ratio = 3.6). (b) Sample IT2 (TEG: β CD ratio = 3.1). (c) Sample IT3 (TEG: β CD ratio = 2.4). (d) Sample IT4 (TEG: β CD ratio = 1.9).

4.3 Thermal and thermo-mechanical characterisation of β CXCDs

The thermo-mechanical characterisation of some of the β CPCDs synthesised using the PEGDGE cross-linker has been published as a peer-reviewed article: Luppi F, Kister G, Carpenter M, Dossi E (2019) Thermomechanical characterisation of cross-linked β -cyclodextrin polyether binders. *Polym Test* 73, 338–345 (see Appendix).

The thermo-mechanical properties of the β CXCDs were investigated to determine their suitability as binders for energetic formulations. Their thermal properties, specifically the decomposition temperature (T_{dec}), the enthalpy of decomposition and the glass transition temperature (T_g) were determined by DSC and DMA.

DSC was carried out using two temperature regimes: a low temperature range (–100 to 100 °C) to determine T_g and a high-temperature range (25–500 °C) to determine the T_{dec} . DMA was carried out solely in the low-temperature range.

The first task was the characterisation of the starting materials (β CD and the cross-linkers TEGDGE, HEGDGE, PEGDGE). The low-temperature heat flow changes were initially examined from –100 to 100 °C, but the upper temperature was later extended to 140 °C to detect thermal events attributed to β CD. The thermo-mechanical properties of β CD/ethylene glycol hydrogel systems have been investigated before, revealing their viscoelastic properties [86,87,92]. The β CXCDs were characterised to determine whether their viscoelasticity was sufficient to reduce their sensitivity to shocks and hence their vulnerability when used as binders.

In this chapter, the published data are combined with data for the β CTCDs and β CHCDs. This chapter also discusses the self-healing properties of the β CXCDs.

4.3.1 Thermo-mechanical characterisation of the starting materials

4.3.1.1 Thermal characterisation of β CD

The degradation of β CD under N_2 gas was observed in the temperature range 30–500 °C by the combined use of DSC and DSC + TGA techniques. The β CD thermogram is shown in Figure 4.15.

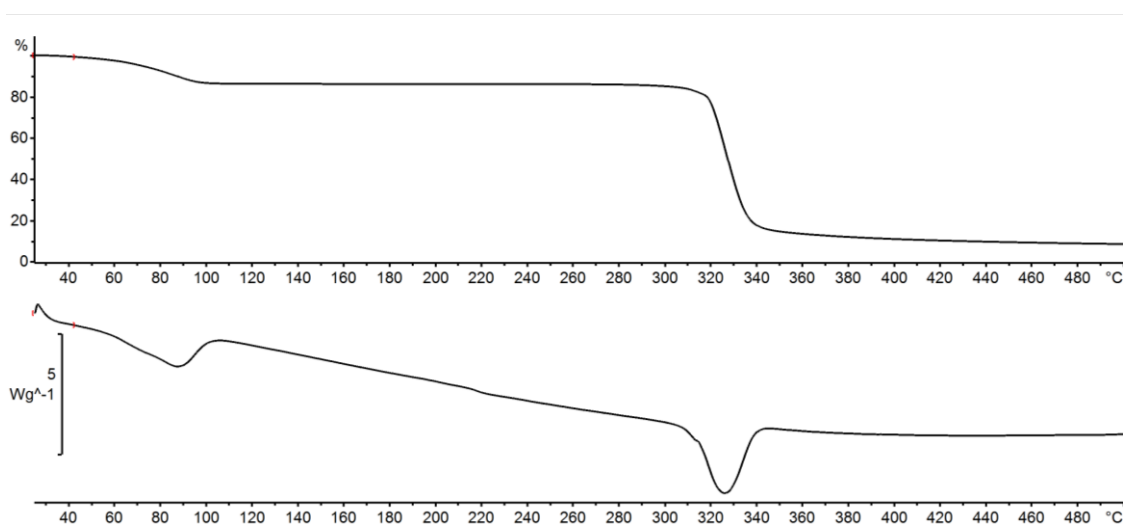


Figure 4.15 Combined TGA and DSC analysis of β CD (10 °C min⁻¹, 25–500 °C, aluminium crucible).

An endothermic event occurring before the temperature reached 110 °C was attributed to the presence of water in the β CD stock sample, confirming the precursor is hygroscopic. The mass loss percentage of 13.6% was similar to that reported in the literature [38,126]. This value varied by several percentage points depending on the moisture adsorbed daily by the β CD (13.1–13.7%). The major event indicated by DSC was an endothermic peak at 328 °C, which represented the degradation of β CD (Figure 4.15). Additional melting point analysis revealed that β CD degradation passes through a caramelisation phase, where the white β CD powder quickly undergoes three sequential stages of browning, melting and charring (Figure 4.16).

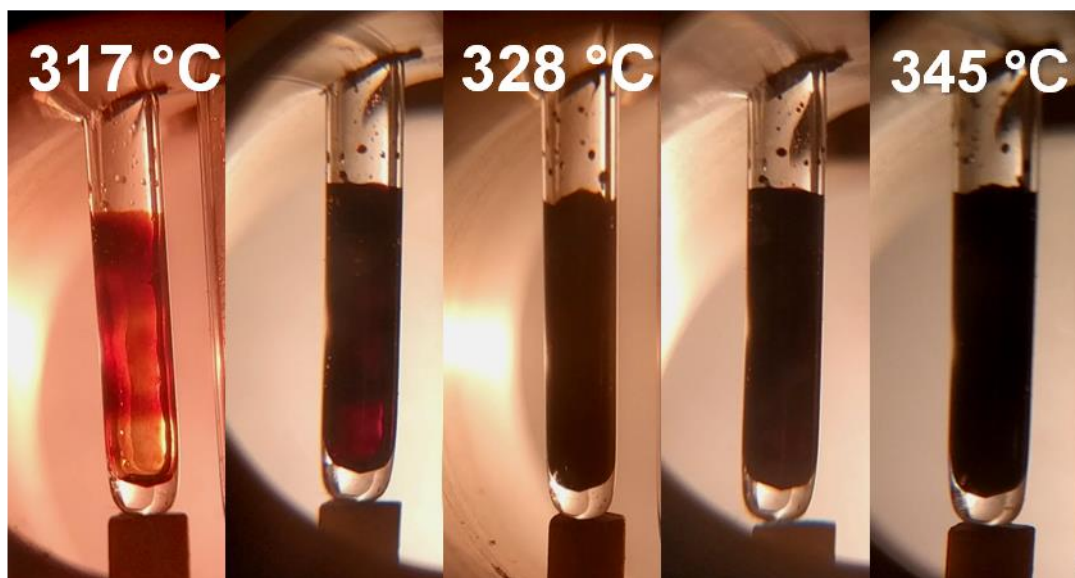


Figure 4.16 The decomposition of β CD observed by melting point analysis. At 317 °C, melting and caramelisation are dominant, but above 328 °C charring prevails.

The low-temperature scan to determine the T_g was initially cycled three times from -100 to 100 °C to eliminate effects caused by the presence of water in the thermogram (Figure 4.17). A second-order phase transition at 85 °C persisted during these temperature cycles. Earlier reports attributed this phenomenon to the dissolution of β CD crystals in water already present in the sample [45]. Molecular dynamics simulations predicted a T_g of 61 °C for β CD [127] whereas others determined an empirical T_g of 216 °C [128].

The temperature extreme was gradually increased by 10 °C up to a maximum of 140 °C (Figure 4.17). The phase transition stabilised at ~ 100 °C in all subsequent runs. The shifting of the transition to higher temperatures reflected the evaporation of water molecules within the β CD cavity, which requires more energy. This experiment suggested that the transition is not due to the dissolution of β CD in water, as previously suggested [45]. The second-order transition at 61 °C may represent the T_g of β CD predicted by modelling [127].

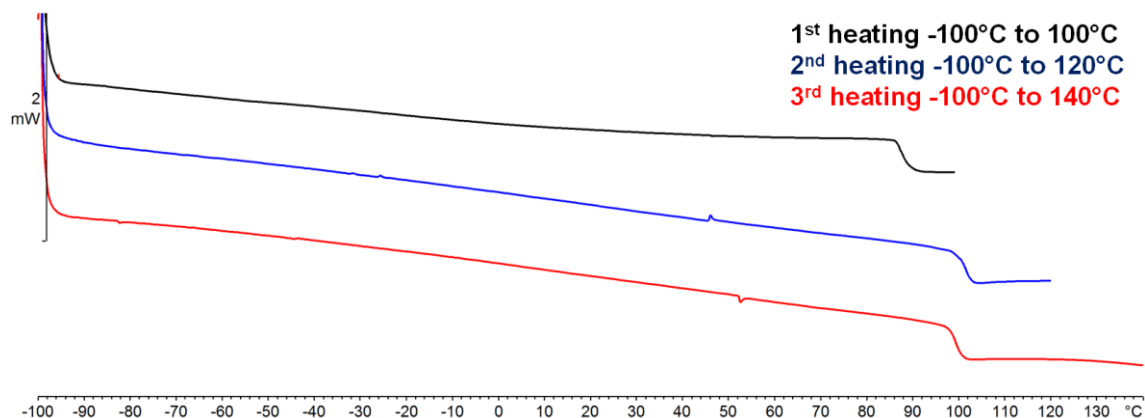


Figure 4.17 DSC heating curves of β CD ($10\text{ }^{\circ}\text{C min}^{-1}$) from -100 to $100\text{ }^{\circ}\text{C}$ in the first cycle (black), from -100 to $120\text{ }^{\circ}\text{C}$ in the second cycle (blue), and from -100 to $140\text{ }^{\circ}\text{C}$ in the third cycle (red).

4.3.1.2 Thermo-mechanical characterisation of β CD

DMA was used to determine the storage modulus (E') and damping factor ($\tan\delta$) of β CD over three heating/cooling cycles. One difference between DSC and DMA is the higher temperature at which transition occurs due to the effect of the sinusoidal stress frequency during mechanical analysis [129]. The temperature range was then set from -100 to $140\text{ }^{\circ}\text{C}$ at $10\text{ }^{\circ}\text{C min}^{-1}$ in order to investigate the second-order transition due to the presence of β CD in the cross-linked compounds. There were no significant differences between the second and third thermal cycles. The last thermal cycle is shown in Figure 4.18.

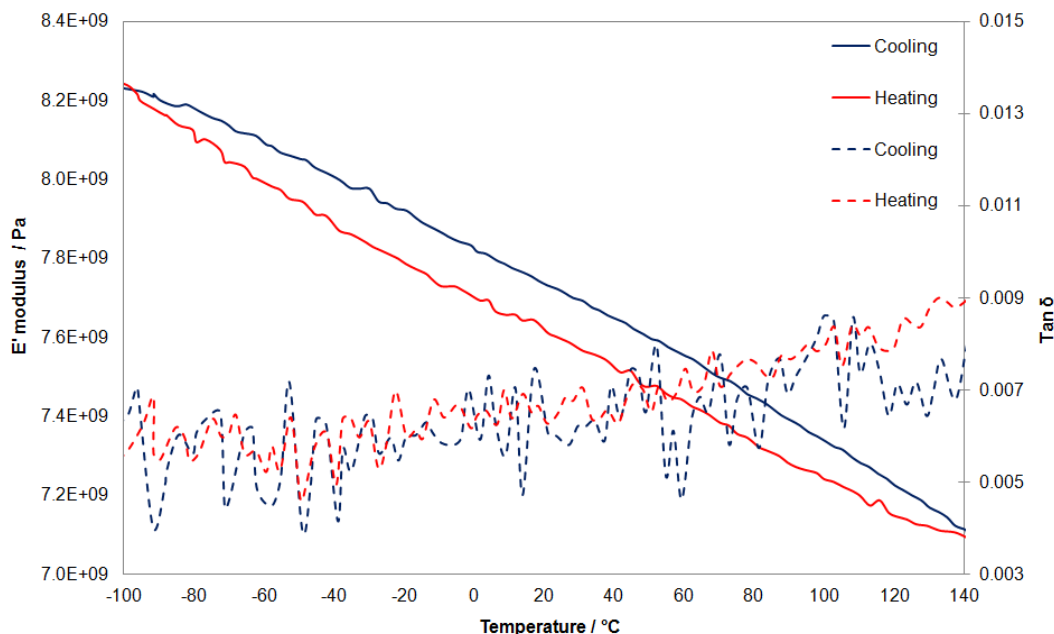


Figure 4.18 DMA showing variation in the storage modulus (E' , solid lines) and $\tan\delta$ (dashed lines) of β CD ($10\text{ }^\circ\text{C min}^{-1}$, 1 Hz, third temperature cycle, -100 to $140\text{ }^\circ\text{C}$, aluminium pocket).

The E' values of the pure β CD sample were inversely related to the temperature, whereas the $\tan\delta$ values remained relatively constant during each temperature cycle, showing there was no phase transition. This is consistent with earlier experiments that defined β CD as a crystalline compound [14]. A minor hysteresis was observed between cooling and heating. The lower E' value during heating reflects the higher degree of relaxation in the material at high temperatures. Therefore, the higher E' value during cooling is due to the stress generated by the high cooling rate.

The variation in E' and $\tan\delta$ was also investigated as a function of the oscillation frequency. The increase in frequency during the temperature cycle had no significant influence on either value. The corresponding thermogram is shown in Figure A 4.

4.3.1.3 Thermal characterisation of TEGDGE, HEGDGE, and PEGDGE

The cross-linkers were also characterised by DSC, and their degradation profiles (30–500 °C) and low-range temperature profiles (–100 to 140 °C) are compared below.

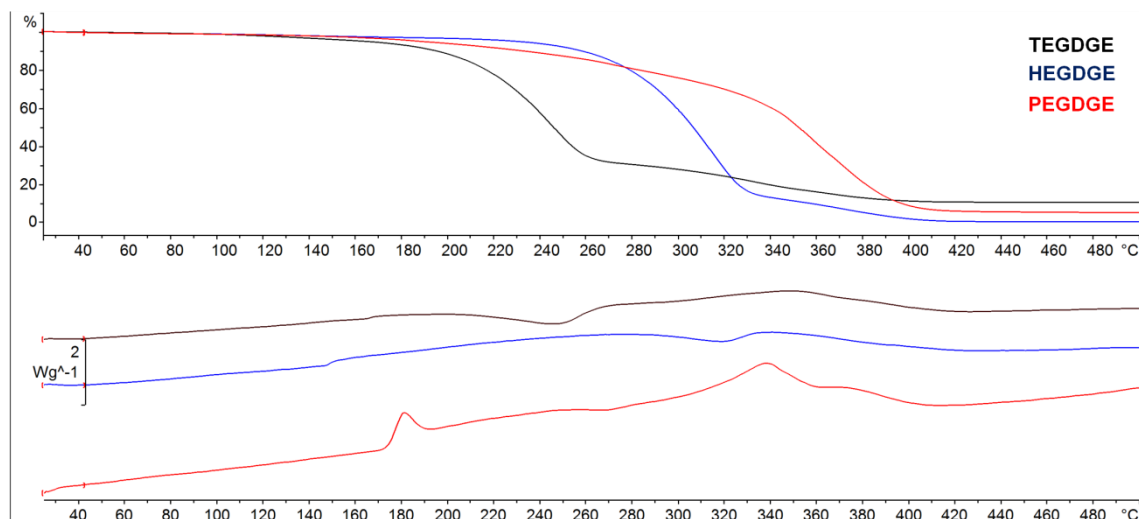


Figure 4.19 Combined DSC/TGA thermograms of the cross-linkers TEGDGE (black), HEGDGE (blue) and PEGDGE (red), from 30 to 500 °C (10 °C min⁻¹, third temperature cycle, aluminium crucible).

Heating the cross-linkers highlighted a continuous loss of substrate mass starting at 160 °C. Part of the mass of the cross-linkers was lost even before the onset of degradation (Table 4.8). The decomposition of TEGDGE was more endothermic than its longer analogues, but the degradation events cannot be analysed in detail using the available thermogram data. The TGA results (Table 4.8 and Figure 4.19) indicate that longer cross-linkers are more thermally stable, which reflects the degradation of PEGDGE at 312 °C compared to the shorter TEGDGE at 214 °C. The thermal stability of the longer chain can be attributed to the scission mechanism of the chain extremities that occurs before its complete decomposition. The PEGDGE cross-linker showed a mass loss of 27% before the main degradation event at 312 °C, which was greater than the 18–19% observed for the other cross-linkers. This can be attributed to the degradation of the shorter chains present in the blend, which degraded earlier

than the predominant long-chain fraction resulting in a higher initial loss compared to the two monodisperse cross-linkers (Table 4.8).

Table 4.8 Combined DSC/TGA data for the cross-linkers.

Cross-linker	Number of ethylene glycol units	Mw (g mol ⁻¹)	Mass loss before onset of degradation (% w/w)	Onset of degradation (°C)
TEGDGE	3	262	18	214
HEGDGE	6	394	19	278
PEGDGE	9	500	27	312

The T_g was initially characterised by three temperature cycles from -100 to 100 °C. Subsequently, the range was extended to 120 °C to completely remove any water in the samples. The increase in temperature did not change the T_g of the cross-linkers (Figure 4.20). There were no significant differences among the three runs and the third heating cycle of -100 to 120 °C is shown as an example in Figure 4.20.

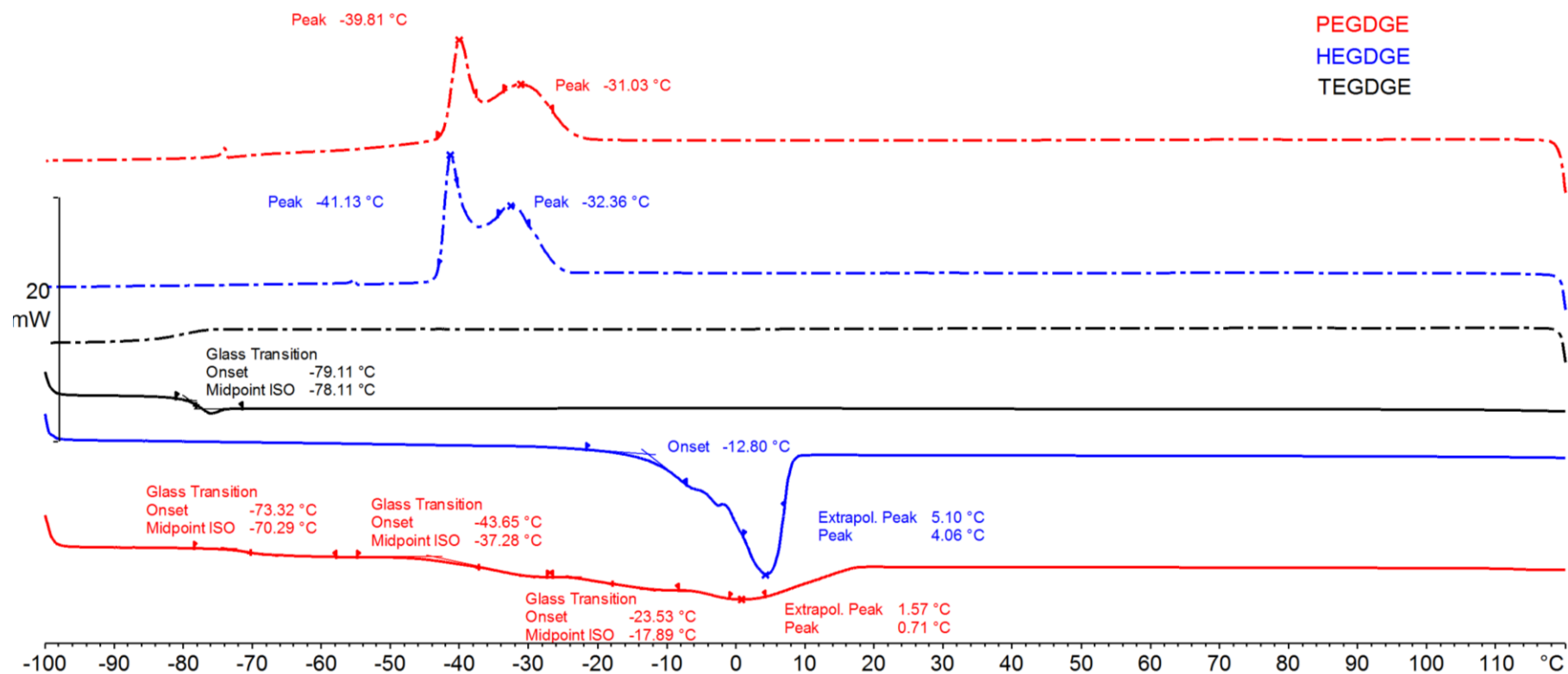


Figure 4.20 DSC thermogram of the cross-linkers: heating (solid) and cooling (dashed) of TEGDGE (black), HEGDGE (blue) and PEGDGE (red) from -100 to 120 °C (10 °C min⁻¹, third temperature cycle, aluminium crucible).

DSC analysis indicated the presence of a single, well-defined T_g for TEGDGE at -78°C due to the monodisperse and pure nature of the sample. For HEGDGE, the thermogram highlighted the presence of a first-order transition attributed to chain melting as well as the glass transition beginning at -13°C and peaking at 4°C . Indeed, the baseline of the thermogram changes when the thermal event concludes. The cooling curve for HEGDGE also reflected the sum of the two transitions, with two crystallisation peaks centred at -41°C and a lower baseline after the thermal transition.

During heating (-100 to 120°C), the heat flow adsorption of PEGDGE increased between -70 and 10°C in a multi-step transition that represented the polydispersity of the sample as described by the manufacturer, the combination of longer polymer chains melting (centred at 1°C) and the increased mobility of the shorter and middle-length chains after the glass transitions at -70 , -18°C and -37°C , respectively. The multiple changes in the baseline from -71°C reflected a series of glass transitions involving different middle-length and shorter polymer chains that can also act as plasticisers for the longer chains, as reported for polyethylene glycol based polymers [130].

During cooling, the longer chains of HEGDGE and PEGDGE crystallised within the temperature range from -23 to -50°C , whereas the T_g of TEGDGE is reiterated at -80°C . The cooling curves support the hypothesis that exotherms during the crystallisation of HEGDGE and PEGDGE mask a vitrification event that would explain the change in the baseline of the heat flow.

4.3.1.4 Thermo-mechanical characterisation of TEGDGE, HEGDGE, PEGDGE

DMA was also used to determine the thermo-mechanical properties of the cross-linkers, with three heating/cooling cycles from -100 to 100°C at $10^\circ\text{C min}^{-1}$. When PEGDGE was analysed, there were no significant differences among the thermal cycles so only the third cycle is shown in Figure 4.21. The E' value fell during heating, with two main transitions at -70 and -22°C corresponding to the glass transitions of the PEGDGE sample. The broad and laddered decline in E' reflects the specific properties of this commercial product,

a blend of PEG chains with an average molecular weight of 500 Da and a polydispersity index of 1.7.

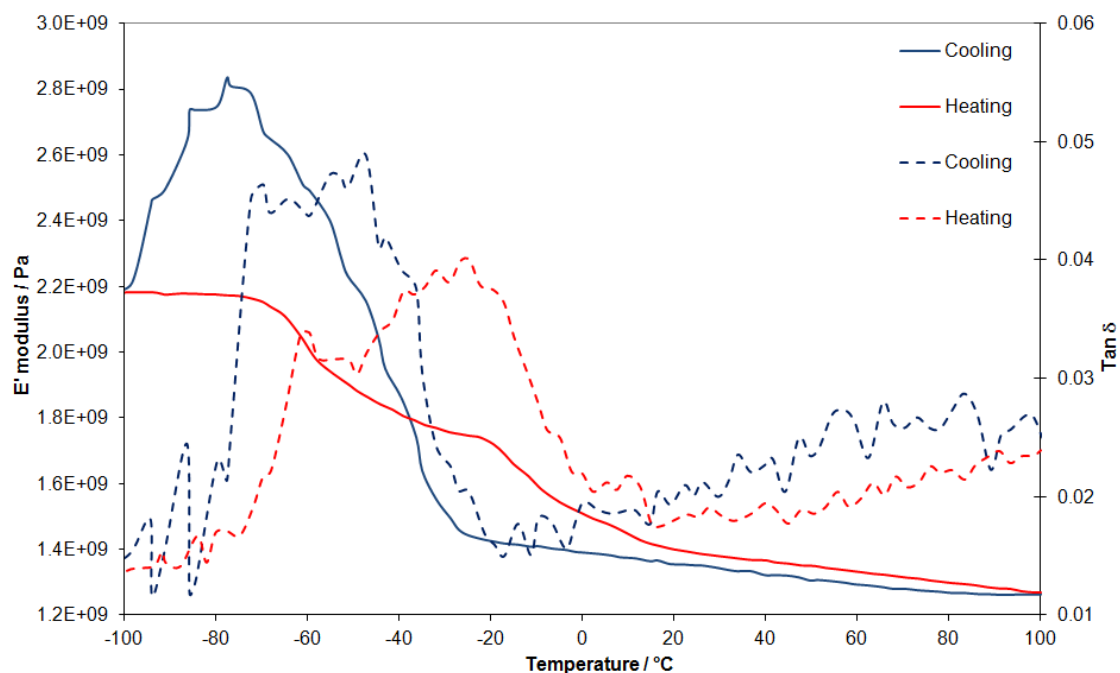


Figure 4.21 DMA showing variation in the storage modulus (E' , solid lines) and $\tan\delta$ (dashed lines) of PEGDGE ($10\text{ }^{\circ}\text{C min}^{-1}$, 1 Hz, third temperature cycle from -100 to $100\text{ }^{\circ}\text{C}$, aluminium pocket).

Previous studies have shown that the T_g of PEGDGE is inversely related to its polydispersity because the shortest polymer chains act as plasticisers, reducing the brittleness and tensile strength while increasing the overall impact strength of the material [46,47]. During cooling, PEGDGE underwent a single glass transition event, increasing its stiffness. However, the rapid increase in E' from about $-30\text{ }^{\circ}\text{C}$ was followed by a sudden drop at about $-75\text{ }^{\circ}\text{C}$, the latter corresponding to 28% of the maximum E' value. This phenomenon also occurred in tests conducted at the lower heating/cooling rate of $2\text{ }^{\circ}\text{C min}^{-1}$. DMA was used to test the aluminium support in order to eliminate artefacts caused by the machine and/or support matrix (Figure A 5). The E' value of the support showed linear variation within the experimental temperature range, suggesting that the observed phenomenon is caused by the viscoelastic behaviour of the PEGDGE and its strong interaction with the supporting pocket. Hydroxyl, epoxy and carboxyl groups in polymers allow the formation of

hydrogen bonds with metal and glass [48]. The strong adhesive interactions and the change in the stiffness of the PEGDGE sample during the glass transition promote internal stress which is suddenly released, initiating cracking and debonding of the sample from the support, recorded as a sudden drop in the E' value. The physical damage (such as cracking) that emerged during the cooling cycle provided an interesting initial assessment of the adhesive strength between the sample and different support matrices. The same thermal profile during the second and third cycles confirmed that PEGDGE recovers its initial mechanical properties when heated above the T_g in each cycle, and the process is therefore reversible.

The effect of the oscillation frequency on the mechanical properties of PEGDGE was tested at 1, 5 and 10 Hz. The E' curves at 1 and 10 Hz are shown in Figure 4.22. The cooling and heating curves at both frequencies diverge at the point of glass transition. During heating, the glass transition of the compound is complete at ~ 25 °C as confirmed by the small decrease in E' and the overlapping of the curves at different frequencies. The T_g is directly proportional to the frequency during both heating and cooling, and thus increases at higher frequencies [49,50]. The drop in E' value caused by cracking is also influenced by the oscillation frequency: the E' peak at 1 Hz occurs at -78 °C whereas the 10 Hz peak occurs at -70 °C.

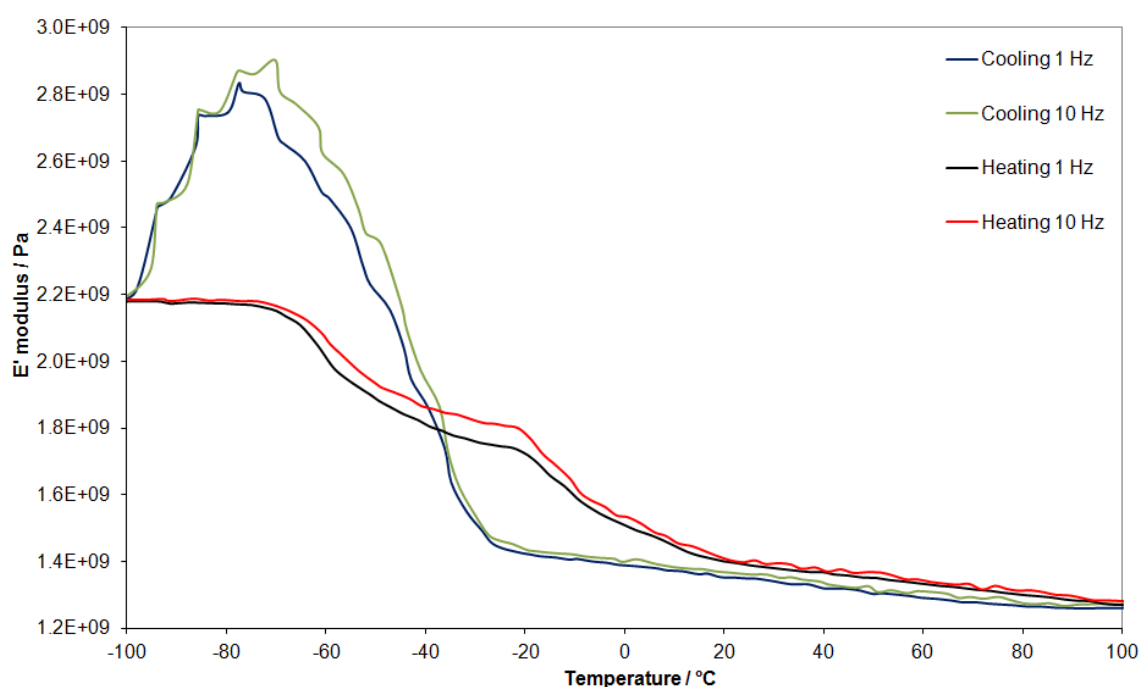


Figure 4.22 DMA showing variation in the storage modulus (E') of PEGDGE with frequency ($10\text{ }^\circ\text{C min}^{-1}$, 1 and 10 Hz, third temperature cycle from -100 to $100\text{ }^\circ\text{C}$, aluminium pocket).

DMA revealed that HEGDGE behaved similarly to PEGDGE (Figure 4.22). During cooling, HEGDGE underwent significant stiffening and the E' and $\tan\delta$ values increased below $-20\text{ }^\circ\text{C}$. The E' values dropped when HEGDGE passed the vitrification point, and it cracked due to adhesion with the support. When HEGDGE was heated, the rigidity decreased above $-78\text{ }^\circ\text{C}$ in a two-step transition that concluded at $20\text{ }^\circ\text{C}$. The $\tan\delta$ value gradually increased when the sample was heated, reaching its maximum at $1\text{ }^\circ\text{C}$. The cross-linker undergoes a broad transition representing the sum of its glass transition and melting as observed by DSC (Figure 4.20). In addition, the drastic fall in $\tan\delta$ at $1\text{ }^\circ\text{C}$ revealed the point at which the compound becomes a liquid.

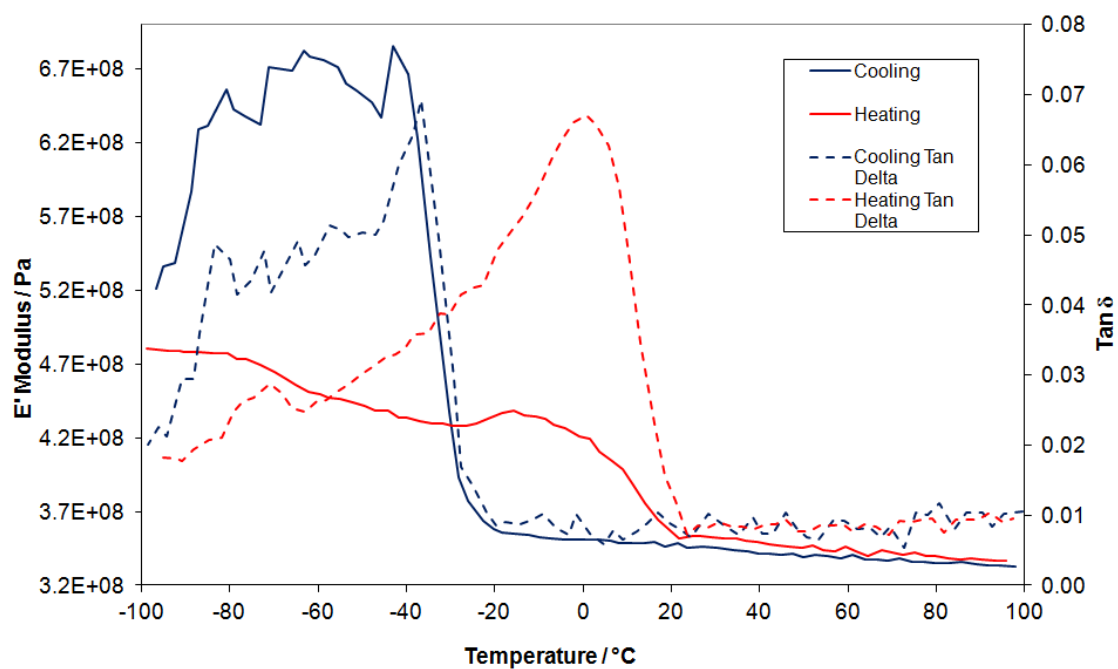


Figure 4.23 DMA showing variation in the storage modulus (E' , solid lines) and $\tan\delta$ (dashed lines) of HEGDGE ($10\text{ }^{\circ}\text{C min}^{-1}$, 1 Hz, third temperature cycle from -100 to $100\text{ }^{\circ}\text{C}$, aluminium pocket).

The transition was also affected by the frequency of oscillation: a higher frequency increased the E' value by 2% up to 20°C (Figure 4.24).

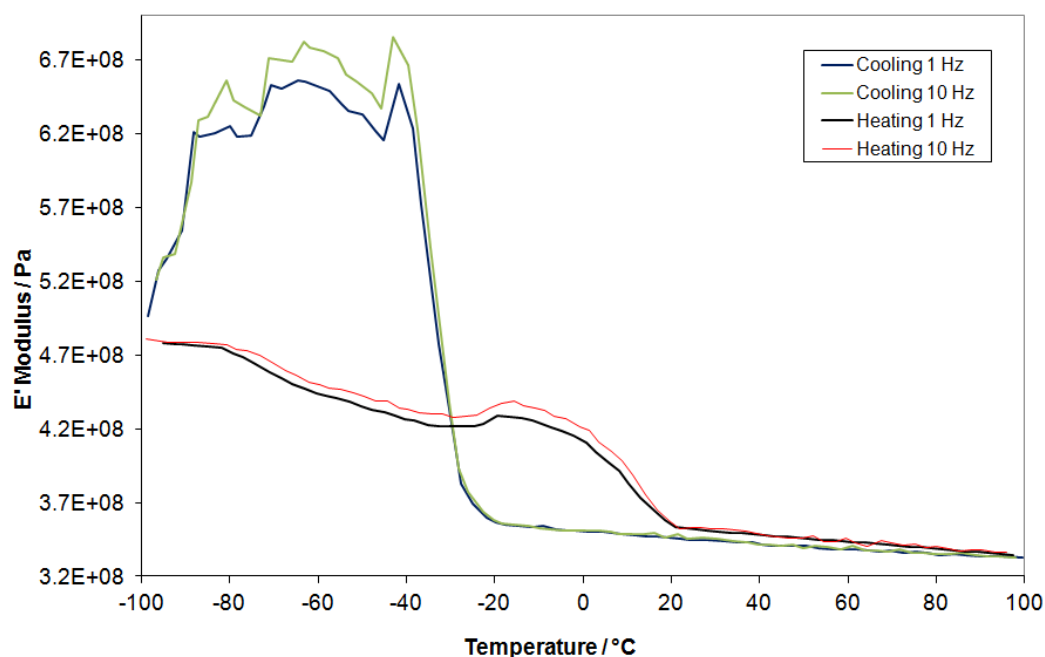


Figure 4.24 DMA showing variation in the storage modulus (E' , solid lines) of HEGDGE with the frequency ($10\text{ }^\circ\text{C min}^{-1}$, 1 and 10 Hz, third temperature cycle from -100 to $100\text{ }^\circ\text{C}$, aluminium pocket).

The DMA data for TEGDGE (Figure 4.25) was compared with the DSC results (Figure 4.15). The T_g of the cross-linker was indicated by the $\tan\delta$ peak at $-71\text{ }^\circ\text{C}$ and the transition was neat compared to the other cross-linkers, due to its monodispersity and the absence of crystallisation in this short-chained polymer.

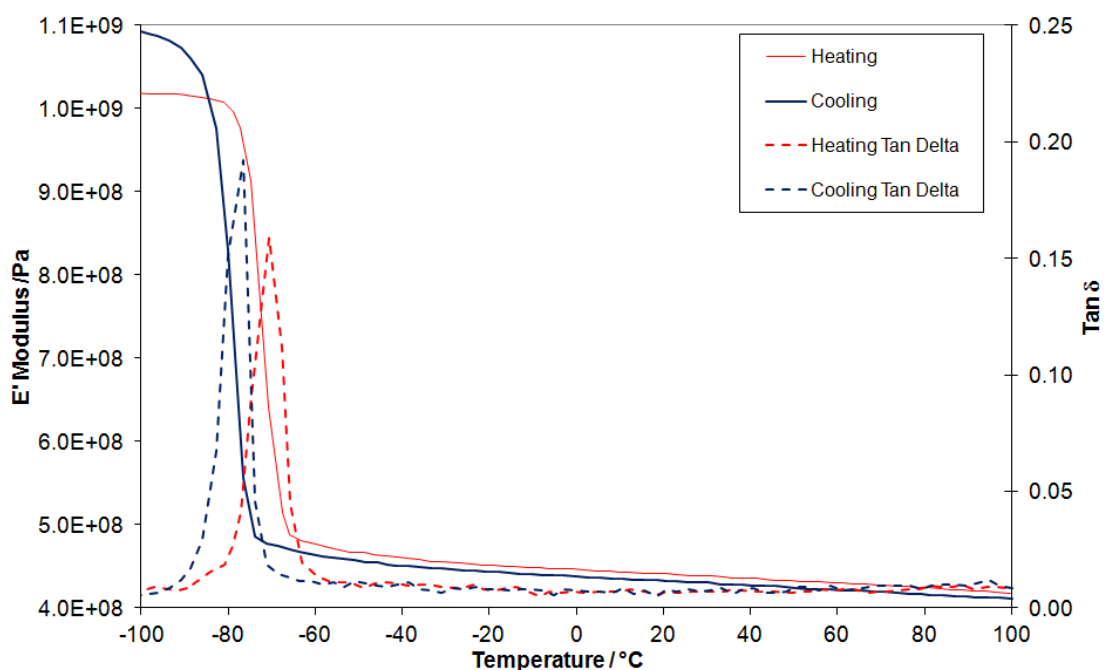


Figure 4.25 DMA showing variation in the storage modulus (E' , solid lines) and $\tan\delta$ (dashed lines) of TEGDGE ($10\text{ }^\circ\text{C min}^{-1}$, 1 Hz, third temperature cycle from -100 to $100\text{ }^\circ\text{C}$, aluminium pocket).

The T_g was found to be dependent on the frequency, as was the case for the other cross-linkers. Due to the extreme vicinity of the T_g to the lowest extreme, the temperature range was extended to the lower temperature of $-140\text{ }^\circ\text{C}$ to determine whether cracking occurred. Accordingly, TEGDGE began to crack at $-100\text{ }^\circ\text{C}$ (Figure 4.26).

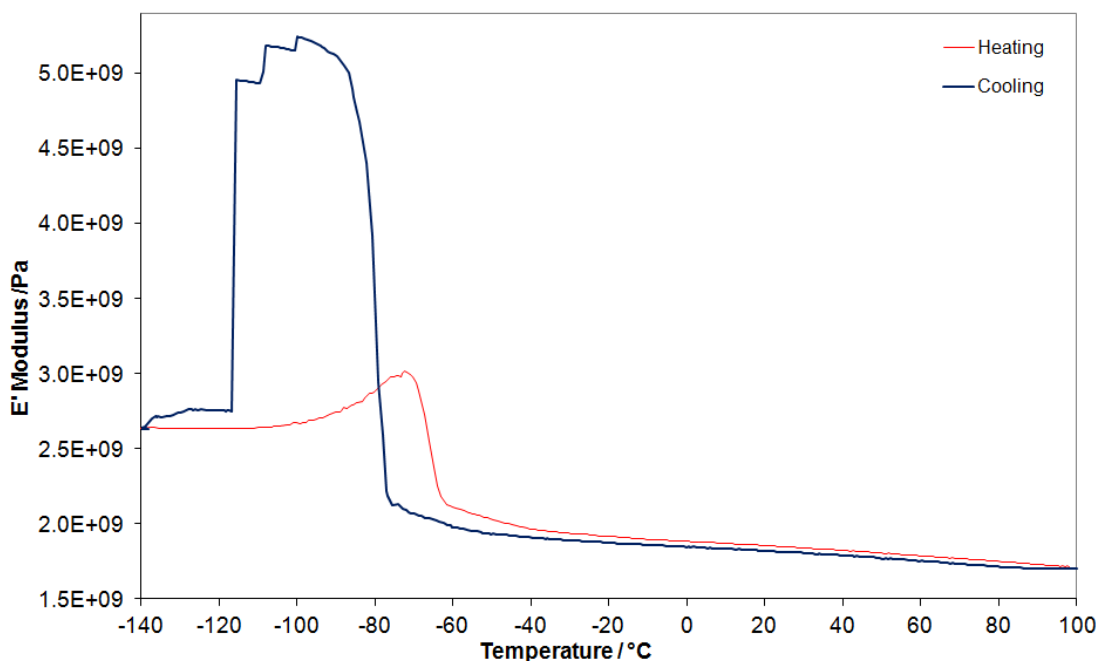


Figure 4.26 DMA showing variation in the storage modulus (E' , solid lines) and $\tan\delta$ (dashed lines) of TEGDGE in an extended temperature scan ($10\text{ }^{\circ}\text{C min}^{-1}$, 1 Hz, third temperature cycle from -140 to $100\text{ }^{\circ}\text{C}$, aluminium pocket).

4.3.2 Thermal and thermo-mechanical characterisation of inert β CXCDs

Thermal analysis using DSC, TGA and DMA as described above was also used to characterise the β CXCDs, to determine how the cross-linking conditions influenced the thermo-mechanical properties of each β CXCD system.

4.3.2.1 Thermal characterisation of inert β CXCDs

The thermal degradation of all β CXCDs revealed similar thermal properties. Table 4.9 summarises the T_{dec} , T_g and mass loss data. The cross-linking reaction increased the T_{dec} of β CXCDs compared to the single cross-linkers, reflecting the presence of β CD in the compounds, thus increasing the temperature at which thermolysis affected their stability. The effect was stronger in the β CTCD products (containing TEG units) due to their higher β CD content. The T_{dec} of the β CXCD products was linearly dependent on the length of the

cross-linker, as seen for the single cross-linkers (Section 4.3.1.3). Accordingly, the β CHCDs (containing HEG units) were associated with higher T_{dec} values than the β CTCDs (containing TEG units). However, the β CPCDs (containing PEG units) did not follow this trend, with T_{dec} values lower than the β CTCDs. This reflects the presence of short chains in the polydisperse PEGDGE reagent and subsequently in the cross-linked products, which set up decomposition hotspots in the blend earlier than expected for a pure compound. A pure compound with longer chains would have a higher T_{dec} than HEGDGE.

Replicate samples produced using the same reaction conditions differed slightly in terms of their mean cross-linker ratio due to the uncontrolled nature of the reaction and the uncontrolled selection of hydroxyl groups that react with the cross-linkers. However, products with the same feed ratio showed similar thermal profiles (Table 4.9).

The glass transition event attributed to β CD was difficult to assess in the β CXCDs. The T_g was inconsistent in the replicates and was only visible in β CTCDs, and in the β CPCDs and β CHCDs with cross-link ratios of 3.8:1 or 1.8:1. This trend suggests that the transition is registered by DSC only when the amount of β CD exceeds 51 % w/w. The mass lost during decomposition did not differ significantly among the β CXCDs indicating similar thermodynamic decomposition behaviours.

Table 4.9 Summary of the thermal properties of the β CXCDs.

Sample	Cross-linker	Cross-linker: β CD feed ratio	XEG: β CD ratio by ^1H NMR	T_{dec} onset ($^{\circ}\text{C}$) ¹	T_{dec} peak ($^{\circ}\text{C}$) ¹	T_g midpoint ($^{\circ}\text{C}$)	T_g β CD midpoint ($^{\circ}\text{C}$)	Mass loss decomposition (%)
β CD	-	-	-	318	328	-	101	-
TEGDGE	-	-	-	203 ¹	-	-79	-	-
HEGDGE	-	-	-	273 ¹	-	-13 ²	-	-
PEGDGE	-	-	-	339 ¹	-	-71 ³	-	-
IT1	TEGDGE	5 :1	3.6 :1	252	287	-	99	84
IT2		4 :1	3.1 :1	257	277	-	95	80
IT3		3 :1	2.4 :1	268	289	-	94	83
IT4		2 :1	1.9 :1	259	277	-	94	82
IH1	HEGDGE	5 :1	4.0 :1	278	308	-10	-	87
IH2		4 :1	3.2 :1	279	303	-6	-	84
IH3		3 :1	2.6 :1	276	307	-	-	80
IH4		2 :1	1.8 :1	274	301	-	101	74
IP18		5 :1	4.1 :1	248	257	-20	-	87
IP19		5 :1	4.0 :1	247	256	-18	-	88
IP13		5 :1	3.8 :1	252	261	-19	110	-

Sample	Cross-linker	Cross-linker:βCD feed ratio	XEG:βCD ratio by ¹ H NMR	T _{dec} onset (°C) ¹	T _{dec} peak (°C) ¹	T _g midpoint (°C)	T _g βCD midpoint (°C)	Mass loss decomposition (%)
IP20	PEGDGE	5 :1	3.7 :1	250	256	-19	-	84
IP21		5 :1	3.6 :1	247	256	-13	104	84
IP9		5 :1	3.5 :1	237	254	-14	106	81
IP14		4 :1	3.2 :1	242	252	-8	96	81
IP15		4 :1	3.0 :1	236	250	-7	90	-
IP22		4 :1	2.9 :1	239	250	-3	90	80
IP23		4 :1	2.6 :1	239	246	-6	108	88
IP24		3 :1	2.5 :1	228	248	+5	106	82
IP25		3 :1	2.1 :1	226	243	-	102	84
IP17		2 :1	1.6 :1	221	233	-	90	75

1 DSC onset was used instead of TGA to determine the mass loss during decomposition (Figure 4.19, p. 83).

2 Onset of the transition of HEGDGE (Figure 4.19, p. 83).

3 First glass transition of PEGDGE (Figure 4.19, p. 83).

All DSC experiments were conducted in duplicate and the values shown in Table 4.9 are averages. However, the replicates gave consistent results differing by only ± 1 °C from the average value.

The thermogram of product IP18 (PEG: β CD ratio = 4.1:1) compared to its precursors (PEGDGE and β CD) is shown as a representative of the other β CXCDs in Figure 4.27.

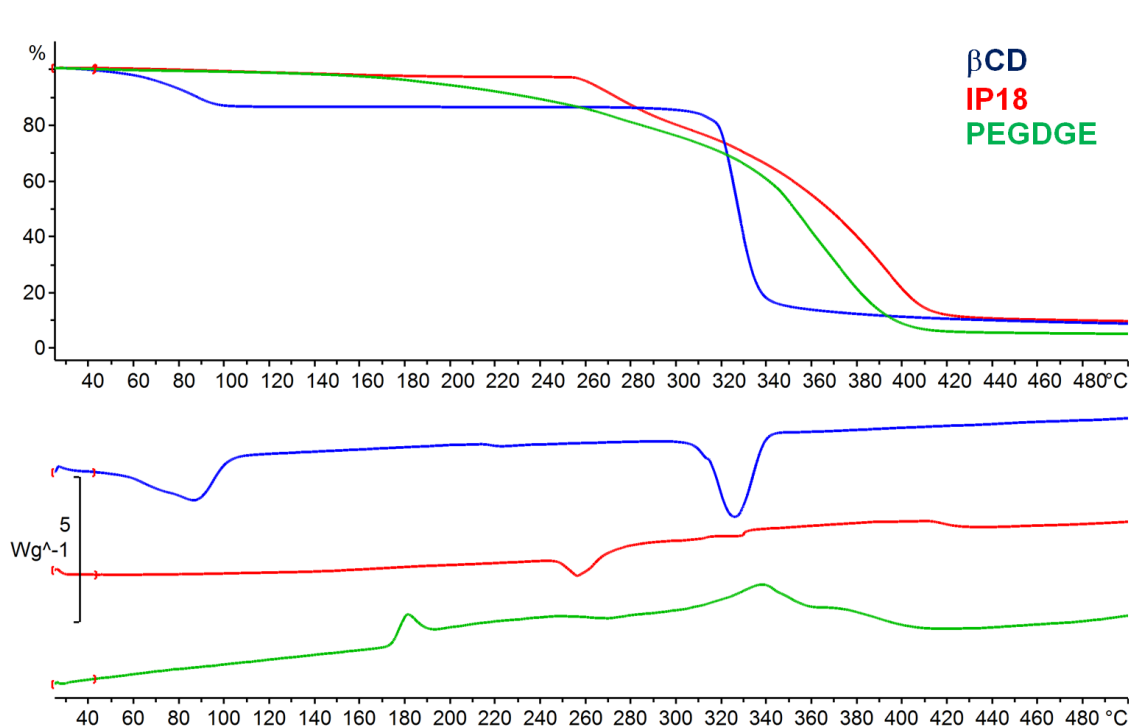


Figure 4.27 Combined DSC analysis and TGA of IP18 (PEG: β CD ratio = 4.1:1, red line) and its precursors β CD (blue) and PEGDGE (green) over the temperature range 30–500 °C (10 °C min⁻¹, aluminium crucible).

The thermogram of the product (red line) in each experiment indicates that degradation occurred at 257 °C, whereas β CD degraded at 328 °C (blue line) and PEGDGE initiated at 180 °C with a major drop at 338 °C (green line). The thermal stability of each β CXCD lies midway between that of its precursors (Table 4.9). Specifically, β CD improves the thermal stability of the short-chained cross-linked systems (β CTCDs and β CHCDs) but reduces the thermal stability of systems with longer cross-linkers (β CPCDs). The degradation of the compound resembled the β CD thermogram, with a major endothermic event at

257 °C suggesting that the cross-linked products undergo a degradation/caramelisation process.

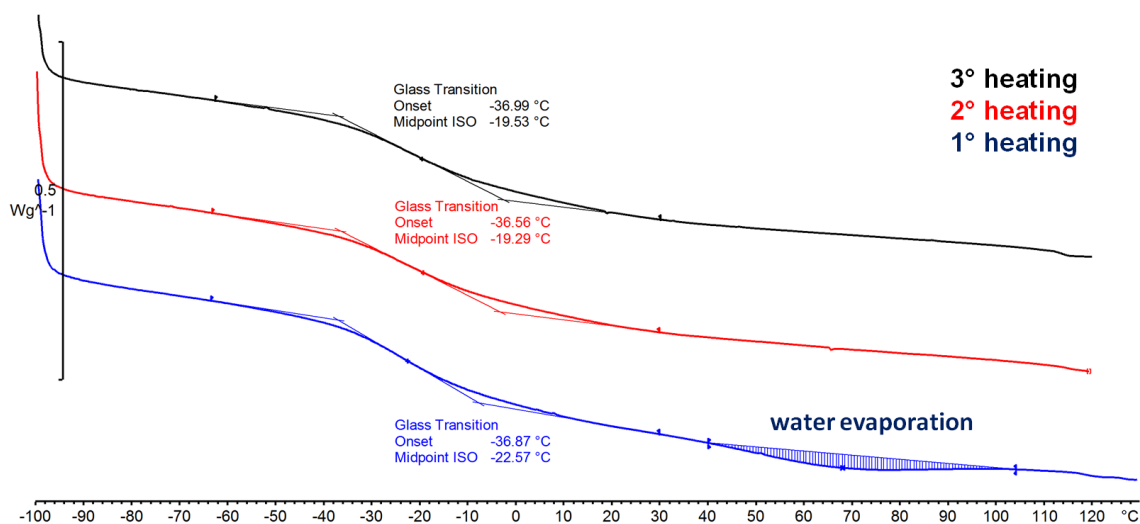


Figure 4.28 DSC analysis showing the plasticising effect of water in IP18 from -100 to 120 $^{\circ}C$ (10 $^{\circ}C$ min^{-1} , third temperature cycle, aluminium crucible).

The water entrapped by β CD affected the T_g of β CD and β CXCD (IP18) in a similar manner, hence the water was eliminated during a first heating cycle up to 130 $^{\circ}C$ to achieve the T_g of the pure compounds without the plasticising effect of the water. The iterative heating cycles eliminated the endotherm present in the first heating curve caused by the evaporation of water. The second and third heating runs were stopped at 120 $^{\circ}C$ to reduce the thermal shock on the β CXCDs. The absence of water therefore caused the T_g to increase from approximately -23 to -20 $^{\circ}C$, confirming its plasticising effect in the β CXCDs. The third heating of each compound was used to report the T_g of the dry product (Table 4.9). Comparison of the three cross-linked products IT1, IH1 and IP13, which feature high cross-link ratios of 3.6:1, 4.0:1 and 3.8:1, respectively (Table 4.9), indicated that the cross-linker type affects the thermal properties of the products. The T_g of the three different β CXCD products based on a temperature scan from -100 to 120 $^{\circ}C$ is shown in Figure 4.29.

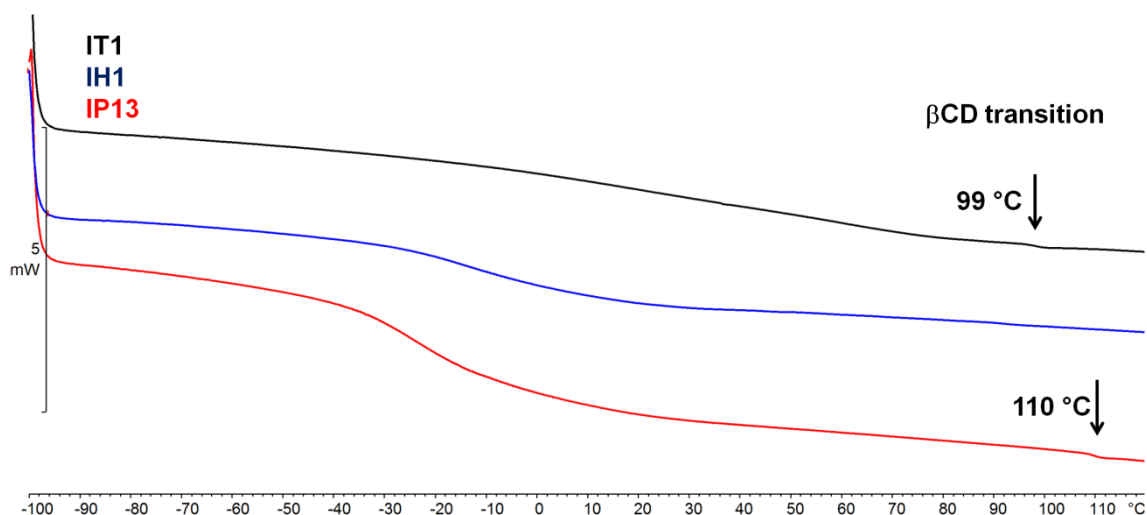


Figure 4.29 DSC analysis of β CXCD products with high XEG: β CD ratios, namely IT1 (3.6:1, black line), IH1 (4.0:1, blue line) and IP13 (3.8:1, red line) from -100 to 120 $^{\circ}\text{C}$ (10 $^{\circ}\text{C min}^{-1}$, third temperature cycle, aluminium crucible).

The cross-linker chains dominated the behaviour of the cross-linked samples at low temperatures. A glass transition occurred in at least part of the products with a notable shift towards positive temperatures compared to the cross-linkers alone (Table 4.9). However, softening was observed in all the tested products even when no evident glass transition occurred, as represented by the black curve in Figure 4.29 related to the β CTCDs. The T_g was absent from products cross-linked with TEGDGE, and general softening occurred in the entire thermal spectrum. The products synthesised with the longer cross-linkers retained the glass transition if the HEG: β CD ratio exceeded 3:1 or the PEG: β CD ratio exceeded 2.5:1 (Table 4.9). The heating curve revealed that the glass transition of the β CXCDs was broad and gradual, as seen in the PEGDGE cross-linkers. The broadness of the transition depended on the polydispersity of the products, as also highlighted by GPC experiments. The secondary transition attributed to β CD occurred at lower temperatures in the products cross-linked with TEGDGE and PEGDGE, with few exceptions (Table 4.9). The β CHCD curves showed no evidence of a secondary transition other than IH4 (HEG: β CD ratio = 1.8), which contains the least amount of cross-linker. This general trend suggests that the small secondary transition becomes visible by DSC only when a significant proportion of β CD is present in the system.

4.3.2.2 Thermo-mechanical characterisation of the inert β CXCDs

The cross-linked β CPCD samples were tested with three different supports to determine whether the adhesion of the material to the supports influenced the tendency to crack and/or affected the thermal transitions. The supports were aluminium pockets (Figure 4.30a), a stainless steel mesh (Figure 4.30b), or aluminium pockets with PTFE tape (Figure 4.30c).

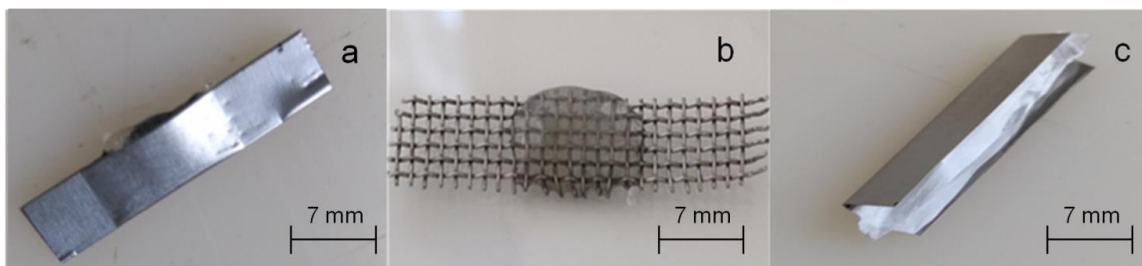


Figure 4.30 Photographs of β CPCD samples supported by (a) an aluminium pocket, (b) a stainless-steel mesh, and (c) an aluminium pocket wrapped in PTFE tape.

4.3.2.2.1 Analysis of the β CXCD product in aluminium pockets

DMA was used to determine if the type of cross-linker and amount (XEG: β CD ratios ranging from 4.3:1 to 1.6:1) affected the thermo-mechanical properties of β CXCD. Initially the tests were performed with the samples held in aluminium pockets as recommended by the DMA manufacturer for materials incapable of self-support. The temperature was extended from 100 to 140 °C at 10 °C min⁻¹ in order to cover the shift in temperatures for the minor second-order transition identified by DSC. The DMA and DSC data are compared in Table 4.10.

The change in heat flow of the T_g recorded by DMA reduced as the amount of β CD present in the β CXCDs increased. Furthermore, the secondary transition captured by DSC was not detected by DMA up to 140 °C. The temperature range was not extended any further to avoid the degradation of the β CXCDs. The thermogram of IP9 (PEG: β CD ratio = 3.5) is used as an example to discuss the significant changes in E' and $\tan\delta$ values at T_g (Figure 4.31).

Table 4.10 Comparison of DMA and DSC results for β CXCD samples and their precursors.

Sample	Cross-link ratio	T_g ($^{\circ}\text{C}$)		
		$\tan\delta$ DMA ¹	STD ²	DSC
IT1	3.6	-	-	-
IT2	3.1	-	-	-
IT3	2.4	-	-	-
IT4	1.9	-	-	-
IH1	4.0	31	6.4	-10
IH2	3.2	53	4.5	-6
IH3	2.6	72	4.0	Soft
IH4	1.8	104	7.0	Soft
IP18	4.1	16	1.2	-19
IP19	4.0	41	4.8	-18
IP13	3.8	44	3.6	-19
IP20	3.7	47	3.1	-19
IP9	3.5	27	3.9	-16
IP15	3.0	67	7.5	-7
IP22	2.9	48	3.6	-3
IP17	1.6	-	-	-

1 Third cooling cycle at 1 Hz, T_g determined as the $\tan\delta$ peak.

2 Standard deviation (STD) of three replicates.

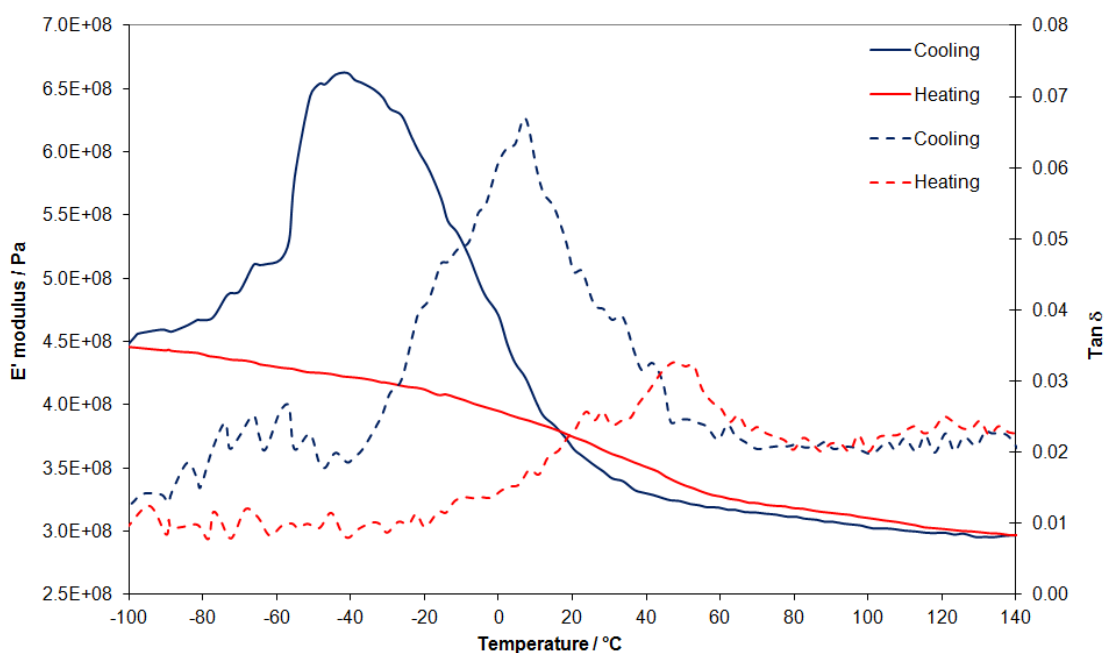


Figure 4.31 DMA showing variation in the storage modulus (E' , solid lines) and $\tan\delta$ (dashed lines) of sample IP9 ($10\text{ }^\circ\text{C min}^{-1}$, 1 Hz, third temperature cycle from -100 to $140\text{ }^\circ\text{C}$, aluminium pocket).

Figure 4.31 shows the E' and $\tan\delta$ values for sample IP9 (containing 67% w/w PEGDGE) during the third temperature cycle from -100 to $140\text{ }^\circ\text{C}$. There were minor differences in each value between the first cycle and the second and third cycles, suggesting that the cross-linked system retained water adsorbed from the air and during the purification process.

During heating, DMA revealed a gradual stepwise decrease in E' between the temperature extremes with a major step at $55\text{ }^\circ\text{C}$ coinciding with a $\tan\delta$ peak. This broad transition was frequency dependent, suggesting it represented a glass transition event for sample IP9 highlighted at $-10\text{ }^\circ\text{C}$ by DSC. The softening of the IP9 product was represented by a change in the slope of the E' curve at $-31\text{ }^\circ\text{C}$, matching the onset of the $\tan\delta$ peak, and this relates to the viscoelasticity of the PEG soft segments present in all the cross-linkers. The difference in T_g determined by DSC and DMA was much larger than the typical shift of $10\text{--}20\text{ }^\circ\text{C}$ often reported in the literature at 10 Hz [131,132].

With an aluminium support in place, the DMA thermogram for IP9 showed a similar profile to PEGDGE during the cooling phase, which can be attributed to the cracking of the sample. This was shown by the sudden drop in E' from its maximum value to 31% at around $-30\text{ }^{\circ}\text{C}$. The temperature at which cracks begin to appear in the IP9 sample was not significantly dependent on the oscillation frequency, whereas cracking of the PEG chains in PEGDGE shifted from $-78\text{ }^{\circ}\text{C}$ at 1 Hz to $-70\text{ }^{\circ}\text{C}$ at 10 Hz. The cracking temperature was not dependent on the material used, but was dependent on overall changes in the sample preparation method and differences in stress dissipation within the bulk compound. The lower mobility of the cross-linked samples reflects the existence of a cross-linked matrix compared to the viscous PEGDGE liquid, which has a higher adhesive surface area.

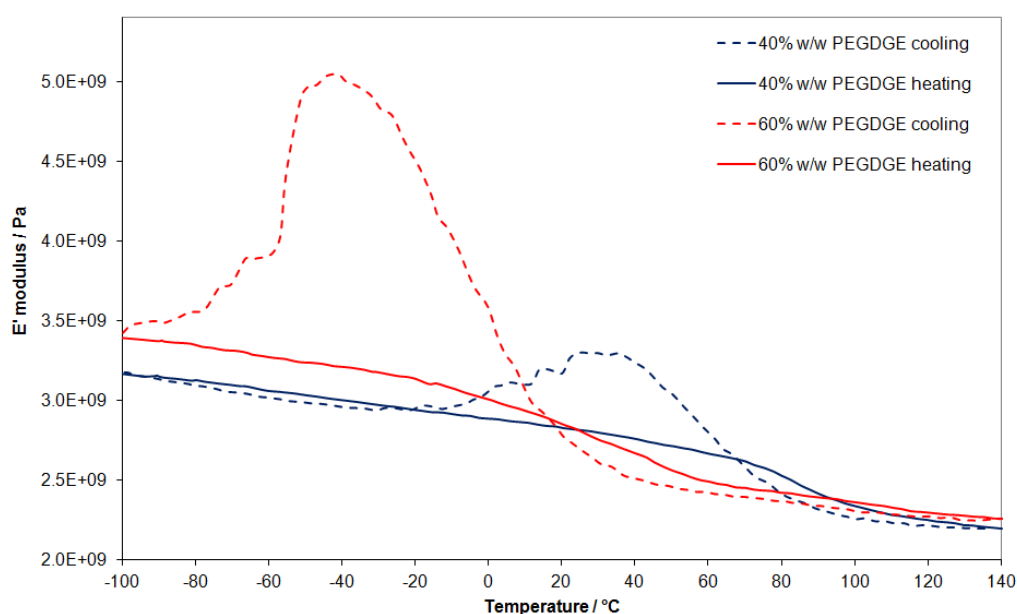


Figure 4.32 DMA showing variation in the storage modulus (E') and $\tan\delta$ of sample IP9 (PEG: β CD ratio = 3.5, solid and dotted red lines) and IP17 (PEG: β CD ratio = 1.6, solid and dotted blue lines) ($10\text{ }^{\circ}\text{C min}^{-1}$, 1 Hz, third temperature cycle from -100 to $140\text{ }^{\circ}\text{C}$, aluminium pocket).

The DMA curves of samples IP9 (PEG: β CD ratio = 3.5) and IP17 (PEG: β CD ratio = 1.6) are compared in Figure 4.32. The lower PEG content of IP17 resulted in cracks appearing at a much higher temperature ($35\text{ }^{\circ}\text{C}$) and the E'

value dropped to 10% of its maximum value. In comparison, the E' value of IP9 with the higher PEG content fell to only 30% of its maximum. The relatively low cross-linker content of sample IP17 therefore appears to cause earlier cracking compared to sample IP9 and reduces its viscoelastic behaviour, also limiting its binding strength given that the low E' value is related to the strength of adhesion to the metallic support. The glass transitions determined from the peak $\tan\delta$ values shift to higher temperatures when the PEG content is low. The absence of first-order transitions in the β CPCD samples during cooling was confirmed by DSC (Figure A 6) suggesting that β CPCD products are completely amorphous at temperatures between -100 and 140 °C.

4.3.2.2.2 Analysis of the β CXCD product on a steel mesh support

The interaction between the β CXCDs and the support had a noticeable effect in the cooling thermogram. Sample IP9 (PEG: β CD ratio = 3.5) was analysed with a stainless-steel mesh in lieu of the aluminium pocket. The sample was spread over the mesh prior to analysis (Figure 4.30). The glass transition of IP9 as determined by DMA was interrupted by stress relaxation at 15 °C (Figure 4.33). Cracking was still observed during cooling, but the phenomenon was less severe compared to the sample held in an aluminium pocket (Figure 4.33). The cracking manifested itself over a wider temperature range (-14 to -70 °C) compared to the sudden drop observed with the aluminium pocket. The characteristic drop in E' began at about -17 °C and reached 3% of the maximum value. The drop was visible during each cycle, confirming the stress relaxation effect that occurs with each round of heating. The metallic mesh changed the manner in which the stress introduced during each cooling cycle was dissipated. The mesh had a greater surface area to which IP9 could bind (362 mm²) compared to the aluminium pocket (180 mm²) but nevertheless allowed effective stress dissipation within the bulk sample.

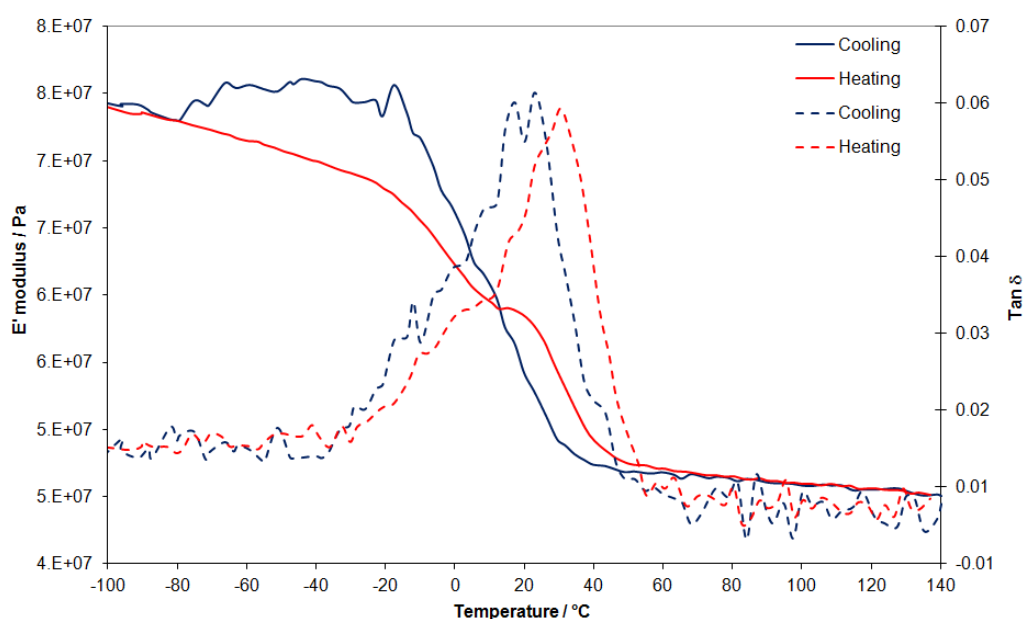


Figure 4.33 DMA showing variation in the storage modulus (E' , solid lines) and $\tan\delta$ (dashed lines) of IP9 ($10\text{ }^\circ\text{C min}^{-1}$, 1 Hz, third temperature cycle, -100 to $140\text{ }^\circ\text{C}$, stainless-steel mesh).

4.3.2.2.3 Analysis of the βCXCD product in aluminium pockets with PTFE tape

In order to confirm that the drop in the E' values during cooling was due to the de-bonding of the sample from its support, PTFE tape was used to hold βCPCD1 samples within an aluminium pocket, thus allowing the samples to contract freely as the temperature declined. Preliminary DMA characterisation of the PTFE tape (blank) showed a softening at the onset temperature of $18\text{ }^\circ\text{C}$ (Figure A 7). The absence of adhesion between sample IP9 and the support when the sample was enfolded by PTFE tape was confirmed by the drop in E' during cooling (Figure 4.34).

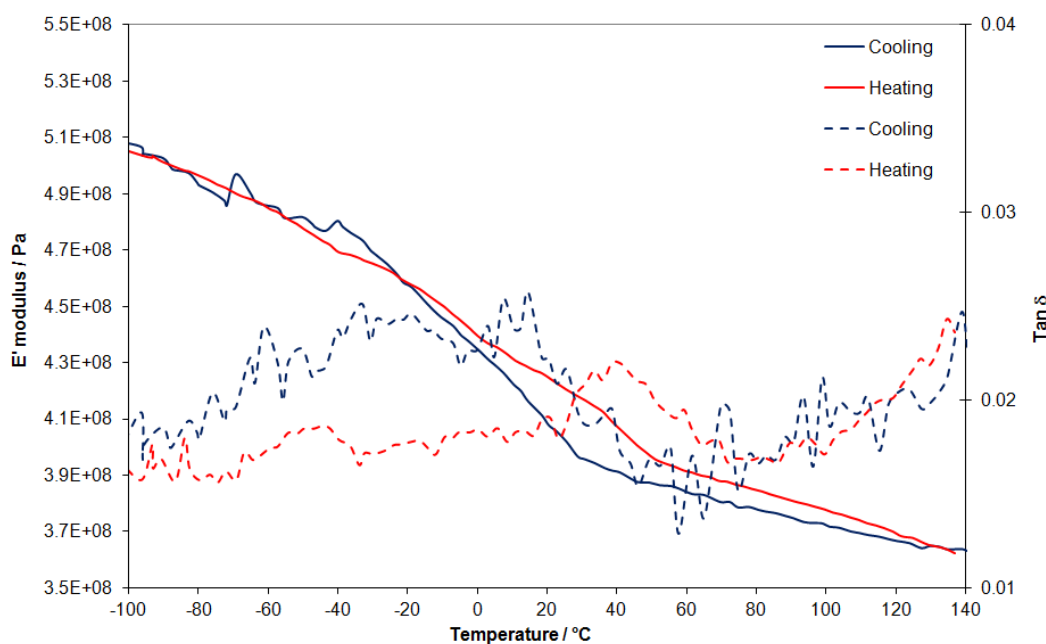


Figure 4.34 DMA showing variation in the storage modulus (E' , solid lines) and $\tan\delta$ (dashed lines) of IP9 ($10\text{ }^{\circ}\text{C min}^{-1}$, 1 Hz, third temperature cycle, -100 to $140\text{ }^{\circ}\text{C}$, aluminium pocket and PTFE tape).

The hysteresis between the heating and cooling curves during the same temperature cycle diminished with each cycle. Therefore, the PTFE tape almost completely eliminated the de-bonding phenomenon and the thermal stress in the sample during the cooling phase. The T_g of IP9 under these conditions was 41°C , identical to the value recorded in the aluminium pocket without tape, confirming that the experimental setup does not affect the T_g .

4.3.2.3 Analysis of the βCXCDs by optical microscopy

Optical microscopy was used to characterise the cracking of the IP9 product (PEG: βCD ratio = 3.5) in more detail during cooling (Figure 4.35). A glass support was considered adequate as a transparent substitute for the metallic support we used to investigate the adhesion of the compound. The sample was cooled from $25\text{ }^{\circ}\text{C}$ (Figure 4.35a) and began to crack at about $-55\text{ }^{\circ}\text{C}$ (Figure 4.35b), with the cracks propagating further as the temperatures was reduced to $-100\text{ }^{\circ}\text{C}$ (Figure 4.35c,d). The same sample was then heated to $100\text{ }^{\circ}\text{C}$ and the cracks began to self-repair, starting at $0\text{ }^{\circ}\text{C}$ (Figure 4.35e) until healing was complete at $\sim 80\text{ }^{\circ}\text{C}$ (Figure 4.35h).

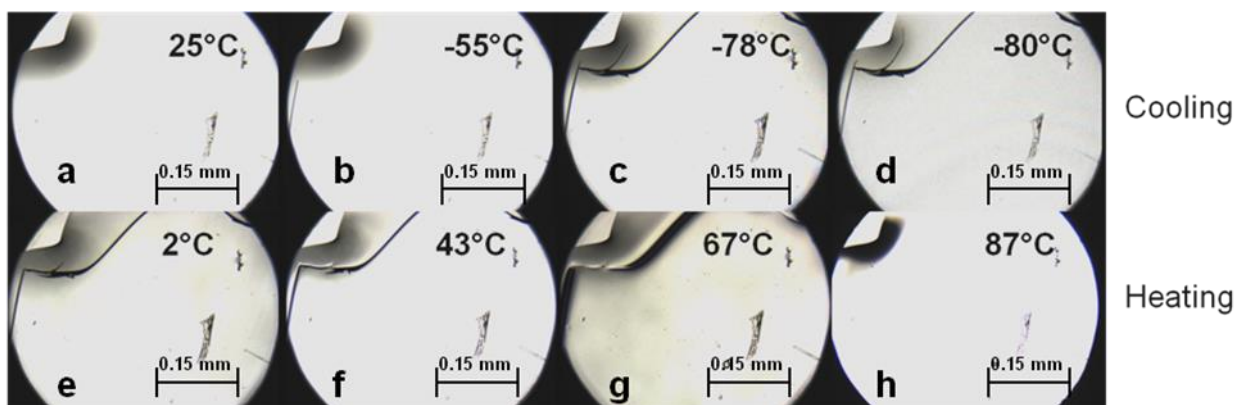


Figure 4.35 Optical microscope images of IP9 (PEG:βCD ratio = 3.5) during the first temperature cycle from -100 to 100 °C. The top row (a-d) shows the cooling phase captured at 25 °C, -55 °C, -78 °C and -80 °C and the bottom row (e-h) shows the heating phase captured at 2 °C, 43 °C, 67 °C and 87 °C .

During the second thermal cycle in the same sample, cracking began at -58 °C and initiated at a different location (Figure 4.36c). This confirms the evidence provided by the similar E' values in each thermal cycle, i.e. the thermal history is erased by heating as previously reported for a hydrogel CD/PEG system [33]. During the second cycle, sample healing occurred at ~ 80 °C as in the first cycle (Figure 4.36h). Furthermore, IP9 placed on PTFE tape showed no evidence of cracking during the cooling phase, confirming that stress relief by cracking was due to the bonding of IP9 to the glass support (Figure A 8).

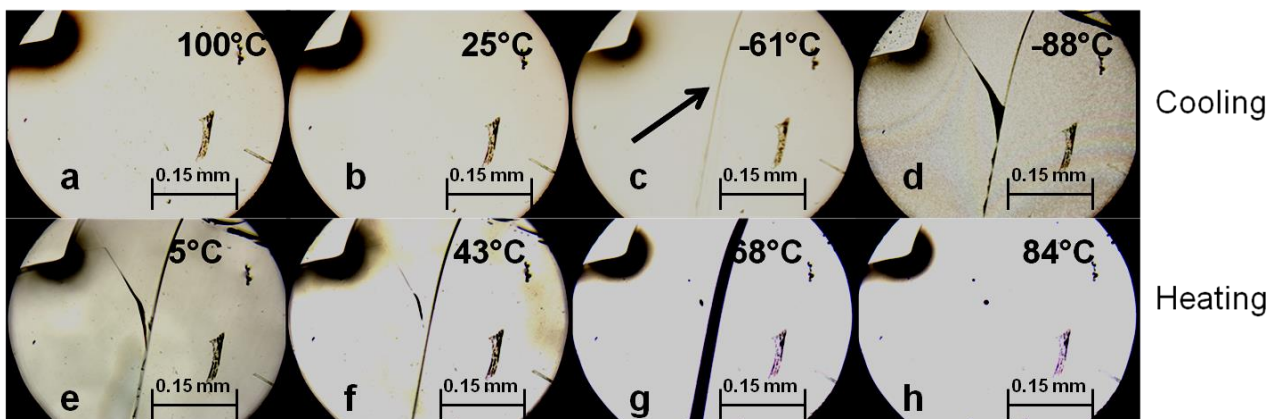


Figure 4.36 Optical microscope images of IP9 (PEG:βCD ratio = 3.5) during the second temperature cycle from -100 to 100 °C. The top row (a-d) shows the cooling phase captured at 100 °C, 25 °C, -61 °C and -88 °C and the bottom row (e-h) shows the heating phase captured at 5 °C, 43 °C, 68 °C and 84 °C.

This experiment confirmed the self-healing of the compound and explained why the E' curves are identical during multiple temperature cycles. The self-healing behaviour is thought to reflect the reformation of hydrogen bonds and host-guest interactions as seen in CD hydrogel systems due to the lower viscosity of the cross-linked system when heated above the T_g [33,52–54]. The physical transformation occurs at the onset of material flow behaviour, allowing the crack to be filled in, and probably involves a rheological model involving the snake-like displacement of the polymeric chains, described as reptation [55].

4.3.2.4 Qualitative assessment of the self-healing properties

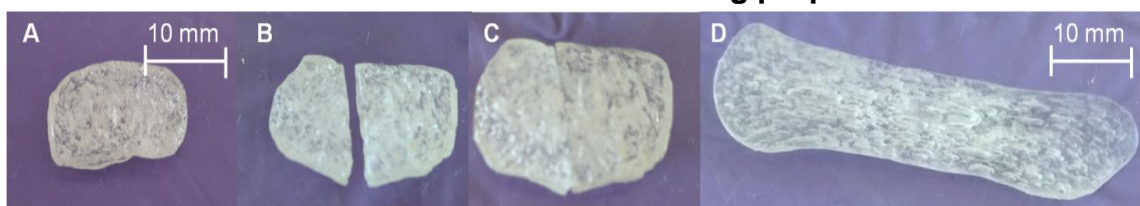


Figure 4.37 Self-healing of IP13 (PEG: β CD ratio = 3.8). (a) Sample after solvent evaporation. (b) Sample after cutting. (c) The parts are placed in contact. (d) The sample is heated to 70 °C for 30 min and pulled by the extremities.

The rupture strength of sample IP13 was qualitatively assessed by intentionally cutting the sample (Figure 4.37b). The parts were subsequently rejoined and annealed in the oven at 70 °C for 30 min (Figure 4.37c). The joined parts were found to be cohesive after this qualitative test (Figure 4.37d). The sample was gripped at its extremities and pulled gently at room temperature. The sample showed considerable elongation. Diffusion of the polymeric chains by reptation and the reforming of hydrogen bonds in the fracture allowed the material to qualitatively self-repair and self-heal.

4.3.2.5 Scanning electron microscopy

The surface morphology of the β CXCDs was explored by scanning electron microscopy (SEM) and compared to the precursor β CD, which is a crystalline material with roughly square particles of different sizes (Figure 4.38).



Figure 4.38 Scanning electron micrograph of β CD crystals.

In contrast to the precursor, the surface of the β CXCDs was more amorphous due to the cross-linking reaction. The foamy appearance of the surface was due to the evaporation of water during the drying process. The β CTCD samples with various TEG: β CD ratios showed significant differences when analysed by SEM (Figure 4.39). The surface of IT1 (TEG: β CD ratio = 3.6) was amorphous with large aggregates, whereas the higher TEG content of samples IT2 (TEG: β CD ratio = 3.2), IT3 (TEG: β CD ratio = 2.4) and IT4 (TEG: β CD ratio = 1.8) caused the particles to appear progressively less amorphous and to resemble the crystalline morphology of native β CD.

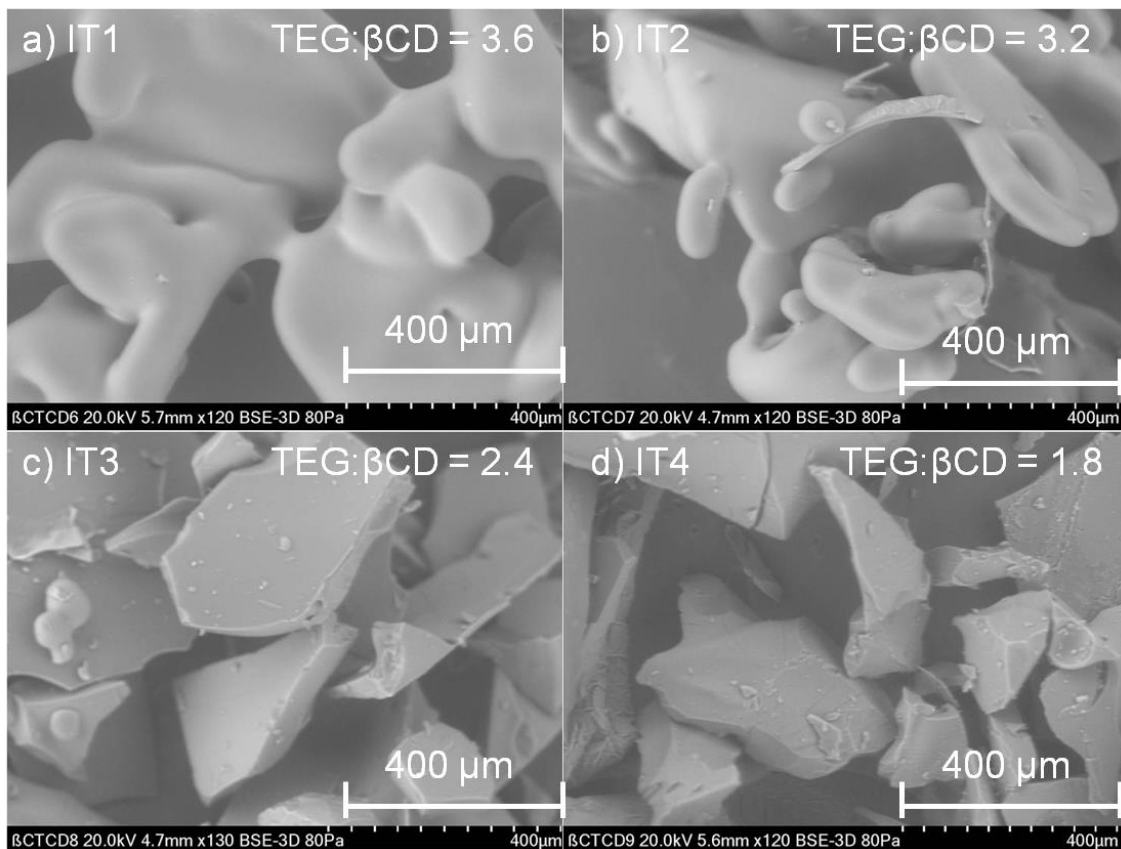


Figure 4.39 Scanning electron micrographs of the β CTCDs (a) IT1 (b) IT2 (c) IT3 and (d) IT4.

The β CXCDs containing HEG and PEG units were not significantly affected by the degree of cross-linking and were characterised by a homogeneous smooth surface (Figure 4.40). Crystalline domains were observed in the β CPCDs with fewer cross-links (Figure 4.40d).

The upper part of Figure 4.40 compares the surface morphology of sample IH1 (HEG: β CD ratio = 4.0) and IH4 (HEG: β CD ratio = 1.8), whereas the lower part compares samples IP19 (PEG: β CD ratio = 4.0) and IP17 (PEG: β CD ratio = 1.6). The crystalline domains in the less cross-linked sample IP17 may have a higher β CD content given their similarity to native β CD. The exposure of these regions to the electron beam for a few minutes in the vacuum chamber generated a honeycomb structure, due to the evaporation of water and/or the degradation of these regions.

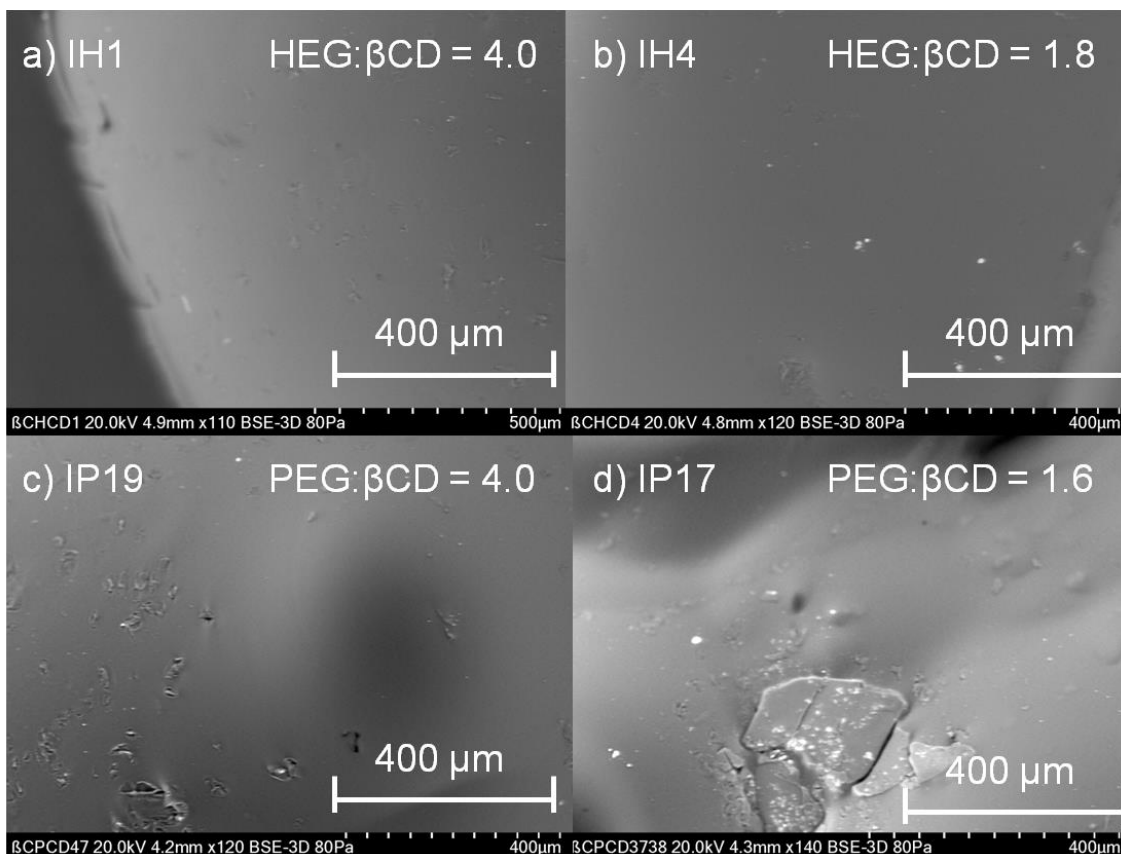


Figure 4.40 Scanning electron micrographs of the β CHCDs (a) IH1 and (b) IH4, and the β CPCDs (c) IP19 and (d) IP17.

4.3.2.6 The β CXCD product in an early-stage formulation

A basic formulation was prepared to study the effect of the inert binder on the formulation's mechanical properties. Sample IP17 (10% w/w) was mixed with melamine in water. The melamine was used as inert substitute for RDX given the similarities in their particle sizes. The mixture was left stirring for 1 h at room temperature before drying under vacuum. The dry mixture contained aggregates rather than finely-dispersed melamine. DMA experiments were conducted, resulting in the thermogram shown in Figure 4.41.

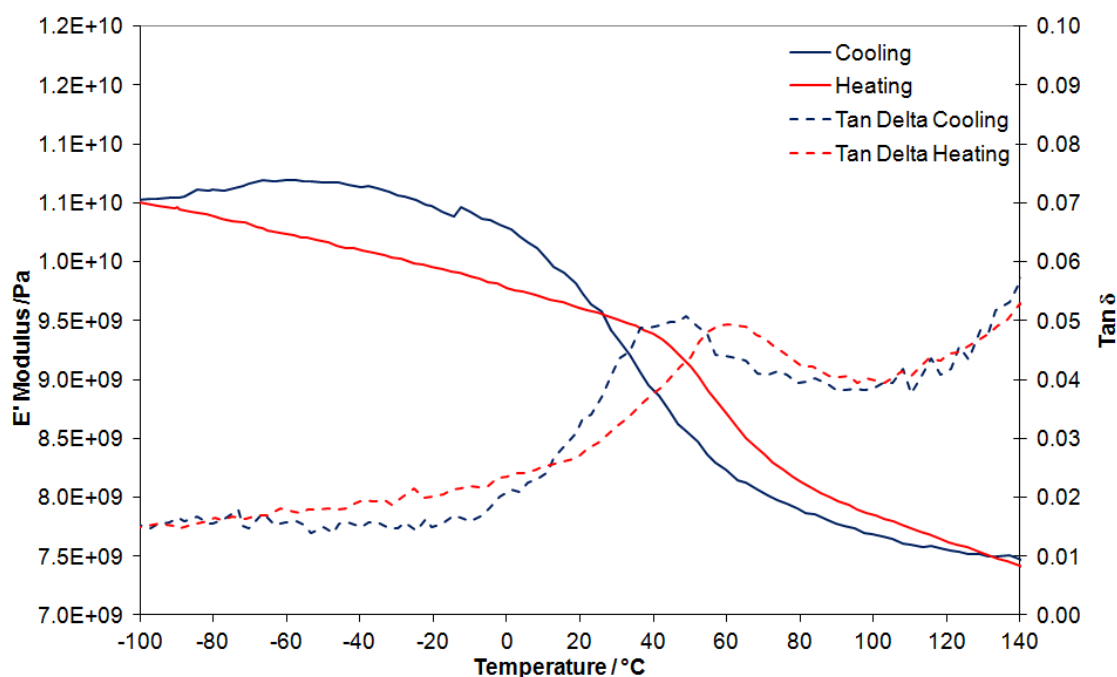


Figure 4.41 DMA showing variation in the storage modulus (E' , solid lines) and $\tan\delta$ (dashed lines) of sample IP17 (10% w/w) formulated with 90% w/w melamine ($10\text{ }^{\circ}\text{C min}^{-1}$, 1 Hz, third temperature cycle from -100 to $140\text{ }^{\circ}\text{C}$, aluminium pocket).

The formulation inherited some of the mechanical properties of the binder given the T_g highlighted by the $\tan\delta$ peak at $60\text{ }^{\circ}\text{C}$ and the drop in E' at $-45\text{ }^{\circ}\text{C}$, matching the values of the binder alone (Figure 4.31). The cracking attributed to IP17 was not abolished in the formulation and a small drop in E' was observed at $-12\text{ }^{\circ}\text{C}$. The drop in E' was lower than the equivalent drop for the pure cross-linker.

4.4 Conclusions

This chapter summarised the outcome of cross-linking βCD with polyethylene glycol diglycidyl ethers containing three, six and nine repeat units, as a first step towards the synthesis of a new inert semi-synthetic binder for energetic applications. The investigation focused on the optimisation of the cross-linking reaction, which was strongly affected by several factors including NaOH concentration and volume, reaction time, temperature, βCD alkoxide formation, cross-linker: βCD ratio, and the addition rate of the cross-linker in the βCD alkoxide solution. The optimal conditions for the reaction were 5.6% NaOH,

0.21 g $_{\beta\text{CD}}$ mL $^{-1}_{\text{aq.NaOH}}$, 30 °C, 16 h to form the βCD alkoxide, 20 min for the addition of the cross-linker, a cross-linker: βCD feed ratio < 5:1, and 6 h for the cross-linking. A unique synthesis procedure was adopted for all βCXCDs . Samples with different cross-linker: βCD feed ratios (5:1, 4:1, 3:1 and 2:1) were synthesised using the three different cross-linkers. Up to 25% of the cross-linker was consumed in a parallel degradation reaction. Characterisation by $^1\text{H-NMR}$ and FTIR spectroscopy confirmed the formation of βCXCDs containing units of βCD and XEG chains. Characterisation by $^1\text{H-NMR}$ in D_2O allowed the XEG: βCD ratio in the repeat unit of the macromolecule to be calculated. Samples with XEG: βCD ratios between 4:1 and 3:1 were malleable whereas compounds with lower ratios were friable.

The compounds synthesised using the shorter cross-linker TEGDGE were friable and easy to dissolve in water regardless of the TEG: βCD ratio. The βCXCDs synthesised using longer cross-linkers (HEGDGE and PEGDGE) took longer to dissolve when the XEG: βCD ratio defined by $^1\text{H-NMR}$ was > 3.4:1.

The thermal and mechanical properties of the precursor βCD were tuned by the cross-linking, giving βCXCDs with low T_g values (from -20 to 5 °C). The softness of the βCXCD samples was dependent on the quantity and length of the polyethylene glycol units. In products with a XEG: βCD ratio > 3.7:1, the T_g was as low as -20 °C, whereas the glass transition was absent in the βCXCDs with the lowest number of cross-links. No glass transition was observed in βCTCDs , which contained the shorter TEG units.

The βCXCD samples were found to crack when cooled during DMA due to the formation of strong hydrogen bonds with the metallic support. The βCXCDs also healed rapidly when heated, retaining some of the healing properties of hydrogels synthesised with βCD and polyethylene glycol reported in pharmaceutical research projects. The characterisation of βCHCDs and βCPCDs by SEM confirmed their amorphous nature, but the βCTCDs increasingly resembled the crystalline morphology of native βCD when the TEG: βCD ratio was < 2.4:1.

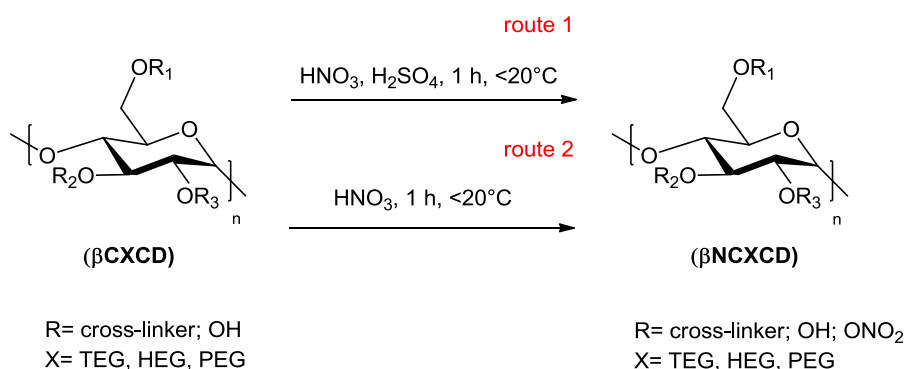
Having established a robust synthesis route for β CXCDs and investigated the properties of the water-soluble products, the project moved on to the synthesis and characterisation of nitrated derivatives, as described in Chapter 5.

5 Synthesis and characterisation of energetic cross-linked β NCXCDs

In order to produce new binders that provide energy to energetic formulations, the cross-linked β CXCDs systems described in Chapter 4 were nitrated using conventional protocols. The nitration procedure was initially developed at a scale of 200 mg. The energetic properties of the nitrated products were assessed by Cranfield Defence and Security experts before synthesis was scaled up to 1 g.

The number of β CD hydroxyl groups that can be nitrated, i.e. converted to nitrate groups (ONO_2), can vary from 1–3 per glucosidic unit of β CD and 1–21 per β CD molecule (Scheme 5.1). The available hydroxyl groups could become sterically hindered when the precursor molecules are cross-linked to form β CXCDs. Therefore, to ensure a high degree of nitration, a large excess of the nitrating mixture was used as discussed below.

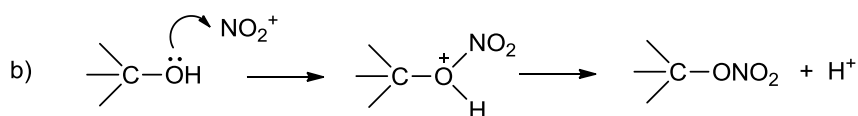
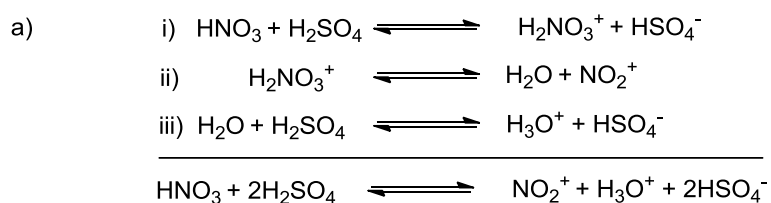
Two conventional synthesis routes used for the preparation of other nitro-esters were tested [21]. Route 1 used a mixture of concentrated sulfuric acid (98%) and nitric acid (95%) whereas route 2 used fuming nitric acid (Scheme 5.1).



Scheme 5.1 Synthesis routes selected to achieve the nitration of β CXCDs.

Route 1 is typically used for the synthesis of NC [27]. The sulfuric acid catalyses the formation of the nitronium ion, resulting in an electrophilic attack on the organic substrate, and its desiccant power removes the water generated during nitration as shown in Scheme 5.2. The removal of water is a highly exothermic

process and has the potential to degrade β CD if not properly controlled. During the synthesis of NC, sulfuric acid can also promote the formation of sulfate esters during the nitration process, which affect the yield and stability of the nitrated product. The presence of sulfate esters, which are sensitive to moisture and temperature, could reverse the nitration reaction thus degrading the nitroesters. This negatively affects the physicochemical properties and stability of the products, as reported for NC [27].



Scheme 5.2 Nitration of β CD units: (a) the sulfuric acid catalyses the formation of nitronium ions, and (b) the formation of nitroesters.

In route 2, fuming nitric acid was used as the nitrating mixture. This procedure has already been used for the synthesis of nitrated β CD and the experimental data from this PhD project can therefore be compared with data reported in the literature [109,114,116].

Two-phase nitration was also attempted for the nitration of β CXCDs using the halogenated solvent dichloromethane, which can act as a heat sink, removing the nitrated product from the nitrating medium and increasing the yield. This approach is commonly used in the synthesis of polymeric nitroesters such as polyNIMMO and polyGLYN [133]. Two-phase nitration is also used to extract nitrated organic substrates such as nitroglycerine from the nitrating mixture [133]. However, dichloromethane was found to be inefficient for the nitration of β CXCDs because neither the cross-linked precursors nor the nitrated products dissolved in this solvent. Therefore, two-phase nitration was considered unsuitable as method to produce nitrated β CD derivatives.

The β CXCD systems containing TEG, HEG and PEG were nitrated using fuming HNO_3 . The conditions and work-up were optimised primarily using the water-soluble β CPCD products, given the commercial availability of PEGDGE. However, the insoluble products generated by cross-linking with TEGDGE and PEGDGE were initially used to assess the efficiency of nitration of insoluble precursors, as described in Section 5.1.

5.1 Attempts to nitrate the insoluble β CXCD precursors

The first nitration attempts targeted the insoluble products synthesised during the optimisation of the cross-linking reaction conditions. The nitration of the cross-linked products was influenced by three parameters:

- The physical properties of the starting material;
- The strength of the nitrating medium;
- The duration of the nitration reaction.

Four insoluble β CXCDs were chosen, namely samples IP26 and IT5–IT7 containing PEG and TEG units, respectively (Appendix, Table A 4) and nitrated using the sulfuric and nitric acid mixture (Route 1, Scheme 5.1) or fuming nitric acid (Route 2, Scheme 5.1). The degree of cross-linking reflected on the swelling power of the two precursors in water. The optimisation of the synthesis parameters was guided by the data collected during the characterisation of the thermal properties of the β NXCXCD products, as discussed below.



Figure 5.1 Physical appearance of the insoluble IP26 and IT5–IT7 precursors.

The insoluble β CXCDs were mixed with a large excess of the nitrating mixture or fuming nitric acid (~1 mL) relative to the mass of cross-linked substrate (200 mg). The samples were crushed into small pieces before nitration to increase the available surface area for the nitration. The nitration mixtures were stirred at 200–900 rpm during the trials to grind the largest particles and guarantee good contact with the acids. The starting materials physically disintegrated under these conditions to give a cloudy suspension, indicating that the insoluble compounds were not efficiently converted to soluble nitrated derivatives. The nitration reaction was interrupted after 1 h at room temperature by quenching the mixture in excess water and ice. The crude slurry was rinsed with large amounts of water to dilute and eliminate the acids and the solids were partially extracted with acetone. The insoluble solid products were rinsed with water and then acetone. Small fractions were recovered when rinsing with acetone and these were dried. Both fractions were characterised by $^1\text{H-NMR}$ spectroscopy and DSC.

Several replicates of the nitration of β CTCDs containing TEG units (samples IT5–IT7) led only to insoluble β NCTCDs, whereas the β NCPCD mixtures generated small amounts of acetone-soluble material comprising highly-nitrated derivatives. The nitrated samples were not soluble in acetone (Appendix, Table A 5) and they showed good thermal stability with a decomposition peak at ~200 °C. The energy content of the samples was relatively low for energetic binders,

at 450–800 J g⁻¹ (Table 5.2), and seemed to be independent of the nitration conditions. Generally, the yields of the nitration reactions of β CTCDs were high (450–1400 J g⁻¹, Table 5.2). In contrast, the synthesis of β CPCDs from insoluble precursors was more difficult given the physical properties of the starting material, which was less gummy and friable. Nitration thus produced a variety of nitrated insoluble compounds with different thermal properties, as well as some acetone-soluble fractions.

In conclusion, the properties of the nitrated products were strongly dependent on the method used to disperse the insoluble particles of the inert β CXCD precursors in the nitration medium. The β CTCD precursors were well-dispersed fine powders whereas the β CPCD precursors were hydrogels that were difficult to penetrate and wet by the acids. The traces of β NCPCD soluble in acetone consisted of highly nitrated oligomers with crystalline properties, similar to the nitrated β CD (Table 5.1) and were not pursued further.

5.2 Attempts to nitrate the soluble β CXCD precursors

Initial tests revealed that the solubility of the β CXCD precursors in the nitrating media was inversely proportional to the degree of cross-linking. The dissolution of β CXCD substrates took up to 1 h at room temperature for derivatives with a XEG: β CD ratio of 3:1, and less than 20 min when the XEG: β CD ratio was < 3:1. (As stated in Chapter 4, the abbreviation XEG is used here to refer collectively to the TEG, HEG and PEG segments in the cross-linked products.) The volume of nitric acid used per 200 mg of β CXCD was therefore increased to 2.1 mL, and most precursors took less than 40 min to fully dissolve. Subsequently, all reaction mixtures were left to stir at room temperature for 1 h before quenching in excess ice-water. The liquid was decanted and the solid residue was washed several times with water, dissolved in a minimum amount of acetone, and re-precipitated in water (450 mL). The product was dispersed in the water, making it difficult to recover, so a half-saturated solution of brine was used instead of distilled water in order to change the zeta potential of the solution and promote the flocculation of product particles. The precipitate was subsequently re-dissolved in acetone, the inorganic components were filtered off and the

β NCXCDs were dried under high vacuum. Small portions were then used for chemical and thermal characterisation. The β NCXCD samples obtained from soluble β CXCD precursors showed a high thermal stability ($T_{\text{dec}} \sim 200^\circ\text{C}$, $E_{\text{dec}} \sim 1700 \text{ J g}^{-1}$; Table 5.3). These values were also consistent when compared to the nitrated products of the insoluble precursors, as discussed above.

The compounds emitted a smell consistent with traces of acid (NO_x) when briefly stored (hours) in a vial, indicating the purification method was inefficient. Subsequent tests were therefore carried out to assess the efficiency of three variations of the purification method for β NCXCDs:

- Multiple re-precipitations from acetone in water;
- Re-precipitation from acetone in boiling water;
- Re-precipitation from acetone in an aqueous CaCO_3 suspension (100 or 25 $^\circ\text{C}$).

When the compounds were purified by multiple re-precipitations in boiling water, they retained the characteristic smell of NO_x albeit less pungent compared to the original purification method. The use of a boiling water/ CaCO_3 mixture was adopted from the NC manufacturing process and was considered an unnecessary extreme choice at this initial stage of research, where the stability of the β NCXCDs was not fully understood. The crude nitrated products from the initial ice-water wash were rinsed several times with water, re-dissolved in small amounts of acetone and re-precipitated in an excess of water containing 1% (w/w) CaCO_3 . The resulting products lacked the NO_x smell suggesting that the latter purification method was the most efficient.

A side experiment using a strong base (NaOH) at room temperature as a neutralising agent resulted in the degradation of the product, with the release of NO_x from the nitrated product and absorption onto its surface (Figure 5.2).

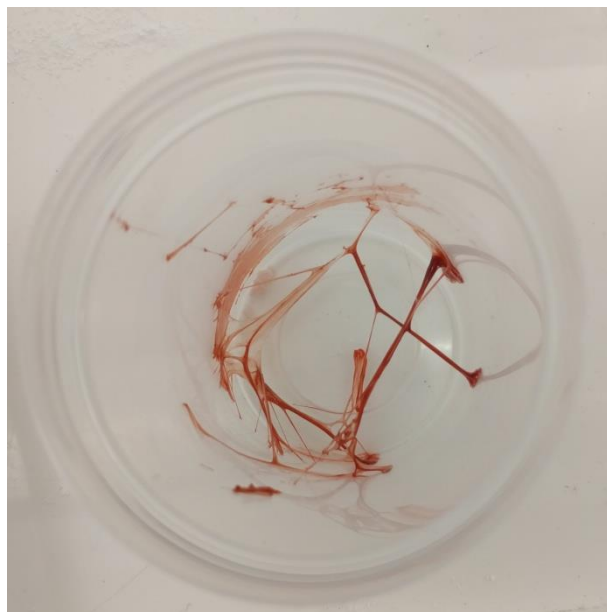


Figure 5.2 Nitrated product degraded by the use of NaOH during purification.

A number of replicates confirmed that re-precipitation from acetone in 0.5% w/w CaCO_3 in water at room temperature gave consistent results with clean, acid-free βNCXCDs , and this purification method was adopted for their preparation.

5.3 Synthesis and chemical characterisation of βNCXCDs

Based on the pilot studies described above, several βCXCD samples were nitrated and extracted in acetone using the following general procedure. Nitric acid (2.1 mL, 100%) was cooled below 10 °C in an ice-water bath, and 200 mg of βCXCD was added in small portions over 5 min, ensuring that the temperature remained below 10 °C. The crude slurry was then stirred at room temperature for 1 h and the nitration mixture changed from the slurry to a clear solution, indicating complete dissolution of the βNCXCD products. To quench the reaction, the nitrating mixture was poured into excess ice-water and the solid compounds were collected and washed with distilled water to eliminate acid residues. The products were then re-dissolved in a small amount of acetone and precipitated in an excess of half-saturated brine. Subsequent re-precipitation from acetone in a 0.5% w/w aqueous CaCO_3 suspension at room temperature gave a crude precipitate which was dissolved in a small amount of acetone and filtered to remove the inorganic salts. The βNCXCDs

were then chemically characterised by ^1H -NMR spectroscopy. The nitrated products were soluble in acetone- d_6 and DMSO- d_6 allowing the nitrogen content to be determined (Table 5.1). The NMR spectra of the βNCXCDs were compared with those of the βCXCD precursors, revealing similar profiles although lower chemical shifts for the nitrated derivatives due to the presence of the nitro groups.

An attempt was made to attribute the signals to specific protons or groups of protons in the βNCXCD molecules. The literature provides a number of assignments for the parent nitrated βCD molecule (βNCD), and the corresponding ^1H NMR and FTIR spectra were used as references. However, the chemical characterisation of similar cross-linked systems has not been published [116,134]. In order to facilitate the assignment of peaks, a sample of βCD precursor was nitrated as an internal comparison using the method described above for the nitration of βCXCDs . Figure 5.3 compares the ^1H NMR spectra of βNCD and sample NP1, prepared from the inert precursor IP18 with a PEG: βCD ratio of 4.0:1. The similarities between the spectra confirmed the formation of βNCPCDs .

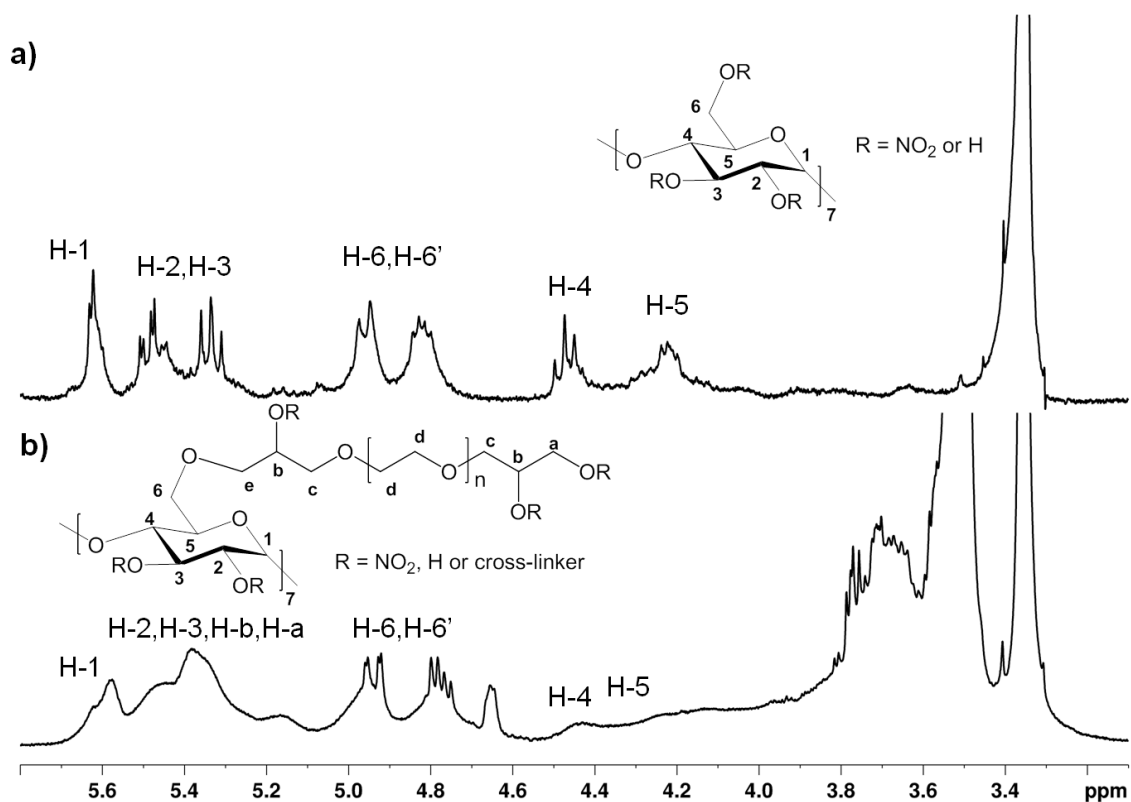


Figure 5.3 The ^1H NMR spectra of (a) βNCD [116] and (b) NP1 in DMSO-d_6 .

Figure 5.4 compares the ^1H -NMR spectra of the inert precursor IP18 and a representative nitrated sample NP1. The detailed properties of both samples are summarised in Appendix A (Table A 1 and Table A 6).

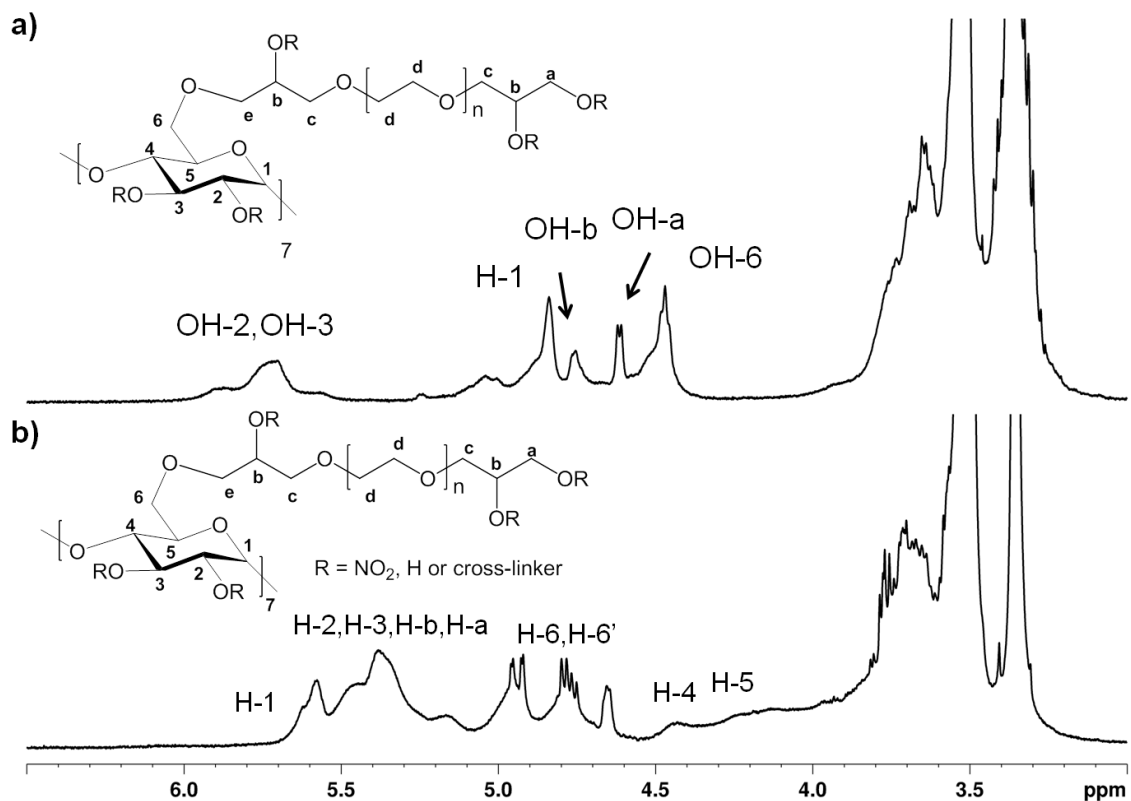


Figure 5.4 Comparative $^1\text{H-NMR}$ spectra of (a) inert precursor IP18 (PEG: β CD ratio = 2.5:1) and (b) its nitrated product NP1, both in DMSO-d_6 .

The assignment of $^1\text{H-NMR}$ signals in the βNCXCD spectra was complex. The spectrum of the nitrated sample is characterised by three sets of broad signals at 5.70–5.20 ppm, 5.10–4.00 ppm and 3.80–3.40 ppm. The first set of peaks at 5.70–5.20 ppm indicated different chemical environments in the nitrated macromolecule due to the presence of the stronger electro-withdrawing nitrate groups. The anomeric proton H-1 of sample IP18 with a chemical shift centred at 4.8 ppm was shifted at 5.60 ppm in the NP1 spectrum. The shoulder at 5.60 ppm is possibly the H-1 signal when the cross-link was added at position OH-2 of unit 2, as described in Scheme 5.1. The broad signals centred at 5.45 and 5.35 ppm can be assigned to protons H-2 and H-3 of the β CD units and H-b, next to a chiral centre in the PEG chain. The region 5.10–4.00 ppm represents the modified chemical shift of all the β CD and PEG units protons situated close to the nitrate groups. The two broad signals between 5.15 and 4.65 ppm can be assigned to Ha and H6 protons. The set of small, broad signals at 4.60–3.80 ppm can be assigned to all CH_2 protons belonging to β CD and PEG units that

are not adjacent to a nitrate group, but are close enough to be influenced by them. The complex environment between 3.80 and 3.40 ppm can be assigned to the remaining β CD protons which are situated far enough away from the nitrate groups to maintain the chemical shifts of their precursors.

No significant differences were observed among the spectra for β CTCDs, β CHCDs and β CPCDs, containing TEG, HEG and PEG units, respectively, and with similar XEG: β CD ratios (Figure 5.5).

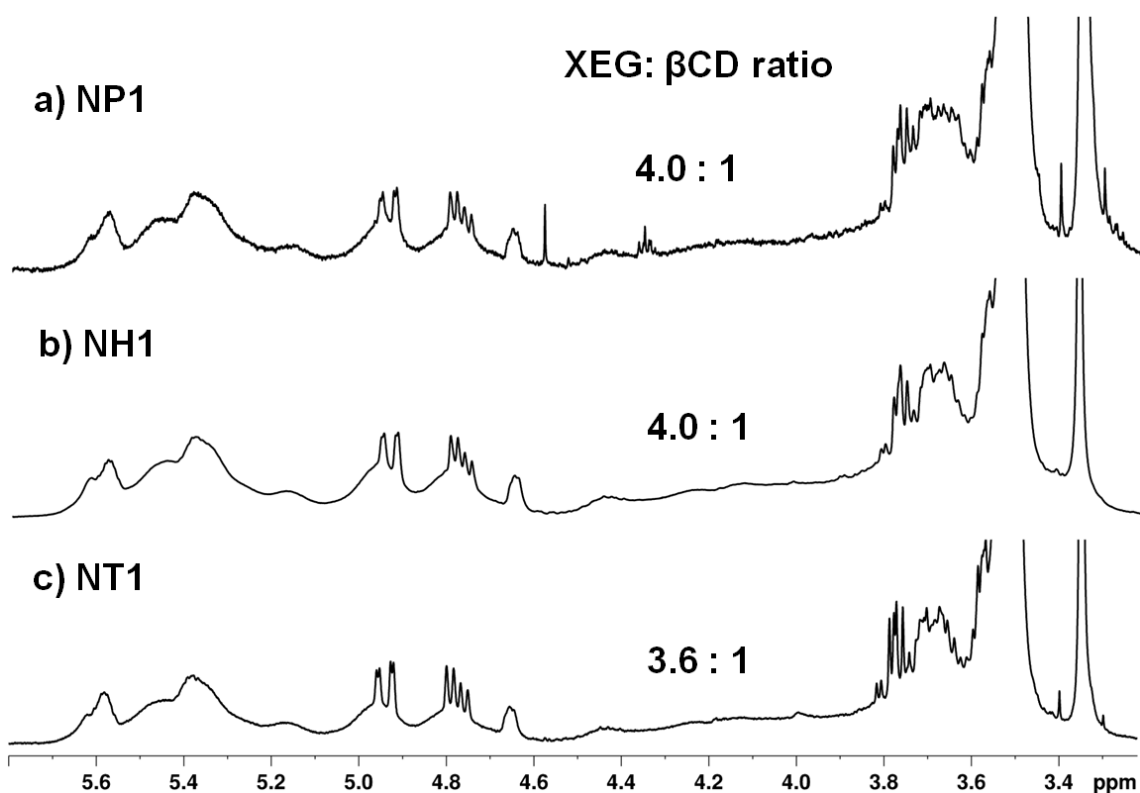


Figure 5.5 The ^1H NMR spectra of products (a) NP1, (b) NH1 and (c) NT1 in DMSO-d_6 . The XEG: β CD ratios were previously determined by NMR spectroscopy.

The compounds with fewer cross-links featured a sharper H-1 anomeric signal at 5.7–5.5 ppm (Figure 5.6). Fewer cross-links promote the comparable conversion of all three available hydroxyl groups in the β CD unit into ONO_2 groups (Figure 5.6d), whereas the conversion of OH-2 was more frequent in the highly cross-linked products as highlighted by the presence of the shoulder at 5.7–5.6 ppm (Figure 5.6a).

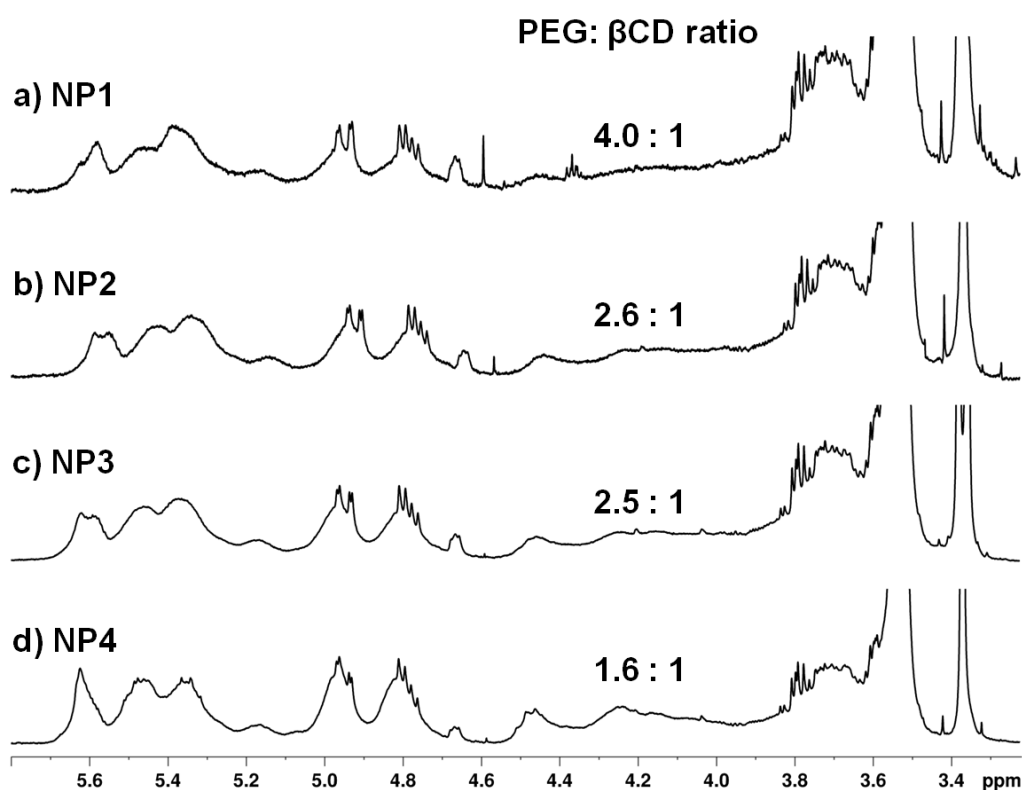


Figure 5.6 The ^1H NMR spectra of products (a) NP1, (b) NP2, (c) NP3 and (d) NP4, which show a gradually decreasing PEG: β CD ratio.

The degree of substitution (DS) of the hydroxyl groups in β NCD was determined by NMR spectroscopy as described in the literature [116], revealing that 2.6 of the 3 hydroxyl groups available per β CD repeat unit were nitrated under the adopted reaction conditions. The technique has an error of $\pm 2.5\%$ in terms of the nitrogen content [116] and the values were assessed also by iron sulfate titration (Table 5.1) [135]. The nitrogen content of β NCD was also determined by titration to confirm the consistency of the results.

The iron sulfate titration method is based on the hydrolysis of nitrate groups in excess 98% sulfuric acid while stirring for 1 h at room temperature. The nitric acid generated in this reaction forms NO_x complexes with the iron titrant and turns the solution pink, allowing quantification by colour change [135]. KNO_3 is used as a standard to determine the correction factor (F) from ideal to real titration conditions using (3):

$$F = \frac{A \times 13.833}{B} \quad (3)$$

where 13.833 is the nitrogen content of KNO_3 (g mol^{-1}), A is the weight of NT or NH or NP (g), and B is the amount of titrant used to reach the endpoint (mL).

Several βNCXCDs were subsequently titrated and the nitrogen content then determined using (44):

$$N\% = \frac{V \times F}{m_{\text{NC}}} \quad (4)$$

where N% is the nitrogen content, m_{NC} is the weight of the NT, NH or NP samples (g), V is the amount of titrant required to reach equivalency (mL), and F is the correction factor from Equation 3.

The nitrogen content was inversely dependent on two factors:

- The XEG: βCD ratio (degree of cross-linking);
- The length of the polyethylene glycol repeat unit in the βNCXCDs .

The TEG, HEG and PEG units increase the overall mass of carbon atoms in the βNCXCDs and therefore reduce the percentage of nitrogen in the total mass of the macromolecule. The only exception was NT4, which diverged from the trend in all three triplicates and further investigation is therefore needed. The DS in the βNCXCDs was generally greater than 2.1/3. The lower DS in the βNCPCDs can be attributed to the lower efficiency of nitration in the less-soluble βNCXCDs , which take longer to dissolve in the nitrating medium.

Table 5.1 Nitrogen content of the β NCXCDs.

Sample ID	Inert precursor		Nitrogen content		DS per β CD unit (ideal max = 3)
	Name	XEG: β CD ratio	(% w/w) ¹	Error (%)	
β NCDD	-	-	11.6	11	2.1
NT1	IT1	3.6	8.2	2	2.4
NT2	IT2	3.1	9.4	8	2.7
NT3	IT3	2.4	9.5	8	2.4
NT4	IT4	1.9	6.3	15	1.3
NH1	IH1	4.0	5.6	20	3.1
NH2	IH2	3.2	7.2	5	2.2
NH3	IH3	2.6	9.0	4	2.8
NH4	IH4	1.8	9.4	13	2.5
NP1	IP18	4.0	6.3	3	2.4
NP5	IP13/20	3.7	6.2	2	2.4
NP6	IP13/20	3.7	6.8	25	2.5
NP2	IP23	2.6	7.0	5	2.2
NP3	IP33	2.5	6.9	12	2.2
NP4	IP32	1.6	8.8	28	2.4

¹ Values are means of three replicate experiments with a variance of $\pm 0.2\%$.

The nitrated products were then characterised by FTIR spectroscopy in attenuated total reflectance (ATR) mode for the rapid analysis of solid-phase samples. A representative sample NP1 is compared with its precursor in Figure 5.7.

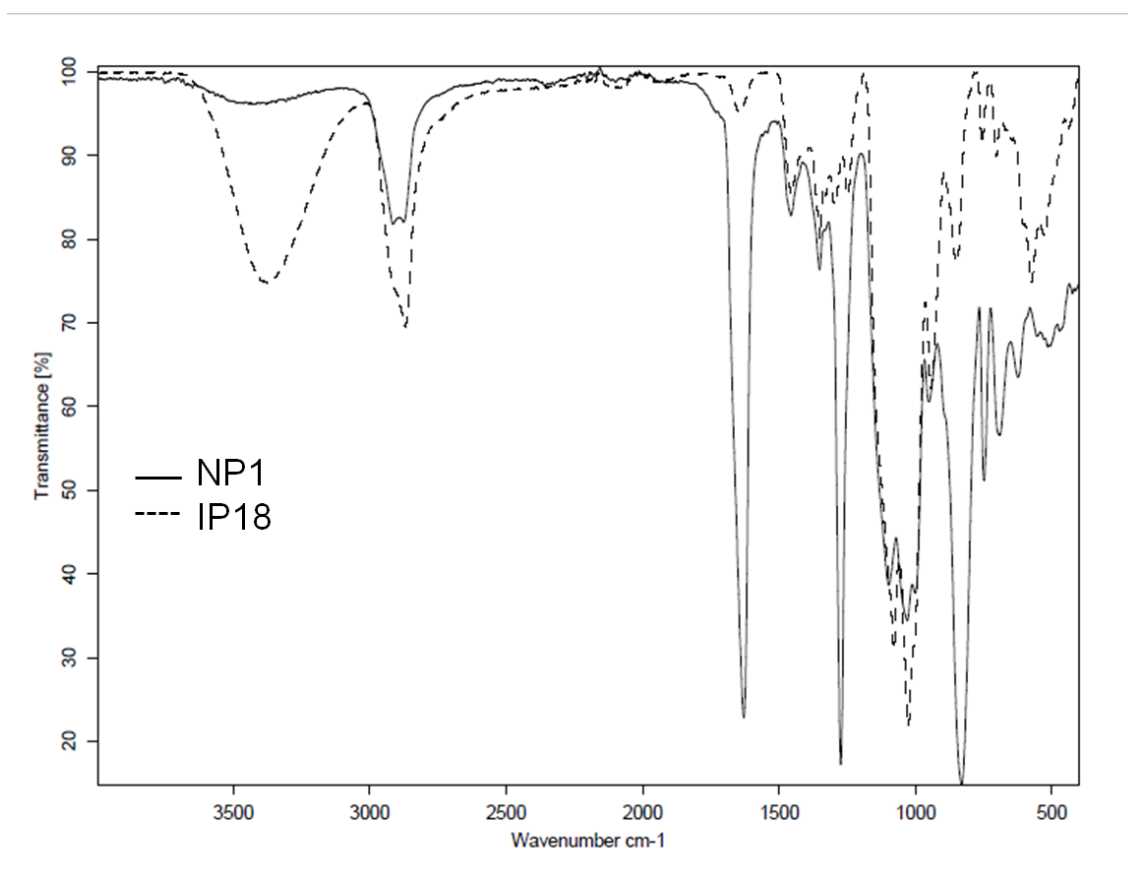


Figure 5.7 Comparative FTIR spectra of sample NP1 (solid line) and its inert precursor IP18 (dashed line).

The absorption peak at 3440 cm^{-1} was assigned to the O-H stretching vibration of the remaining hydroxyl groups in the cross-linked system, and the peak at 2900 cm^{-1} was assigned to the C-H stretching vibration. The absorbance was significantly reduced at 3440 cm^{-1} and strong absorption peaks, attributed to the introduction of nitrate groups, appeared at 1646 , 1274 and 831 cm^{-1} . Sample NP8 was also compared with β NCD to identify any differences in the absorption spectrum (Figure 5.8).

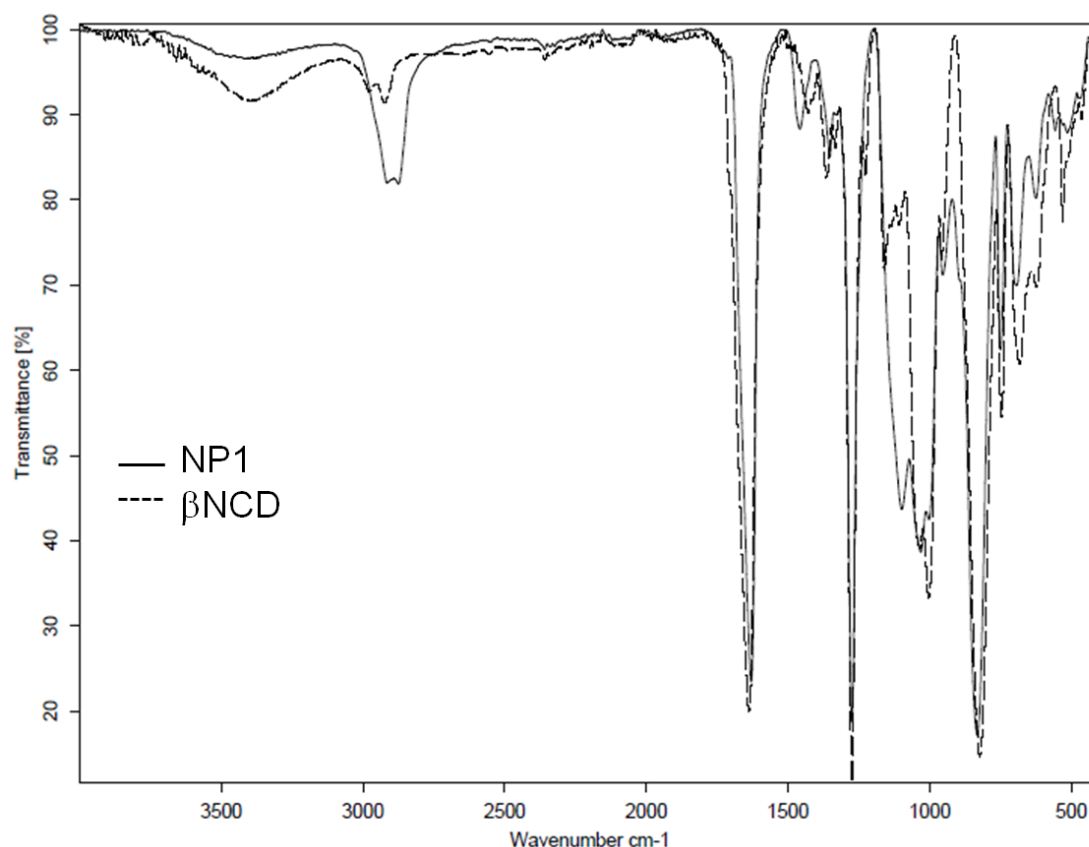


Figure 5.8 Comparative FTIR spectra of sample NP1 (solid line) and β NCD (dashed line).

The NP1 spectrum revealed stronger absorption peaks at 2900 and 2800 cm^{-1} due to the vibration of the C-H bond of the methylene groups (symmetric and asymmetric stretching) and weaker absorption by the OH groups (bending) at 3400 cm^{-1} . This last difference in the OH bond vibration can be attributed to the Mw of the two materials: free OH groups in β CD have a greater mass than the same groups in the macromolecule.

The peaks at 1460 cm^{-1} and 1100 cm^{-1} were more intense in NP1 than β NCD and were assigned to the bending vibrations of the C-H bond of the methylene groups in the PEG units of NP1. There were no significant differences between the nitrated systems with different XEG: β CD ratios (Appendix, Figure A 9).

The molecular weights of the β NCXCD derivatives were determined by GPC in the solvent THF. Polystyrene standards were used for a nine-point calibration

(600 Da to 1.7 MDa) and all Mw values are reported as polystyrene equivalents.

The broad chromatograms of the β NCXCDs were similar to their precursors and confirmed the polymeric structure of the nitrated products (Figure 5.9). The Mw distribution in the three β NCXCD systems is compared in Figure 5.9. The systems have similar XEG: β CD ratios (~3.8) but contain different repeat units, namely PEG (Figure 5.9a), HEG (Figure 5.9b) or TEG (Figure 5.9c). All samples had a broad Mw distribution with the elution of high-Mw fractions beginning at 12 min. Sample NP1 displayed a broader profile, whereas NH1 and NT1 differed slightly due to the presence of two major elution peaks as observed following the GPC analysis of β CXCD.

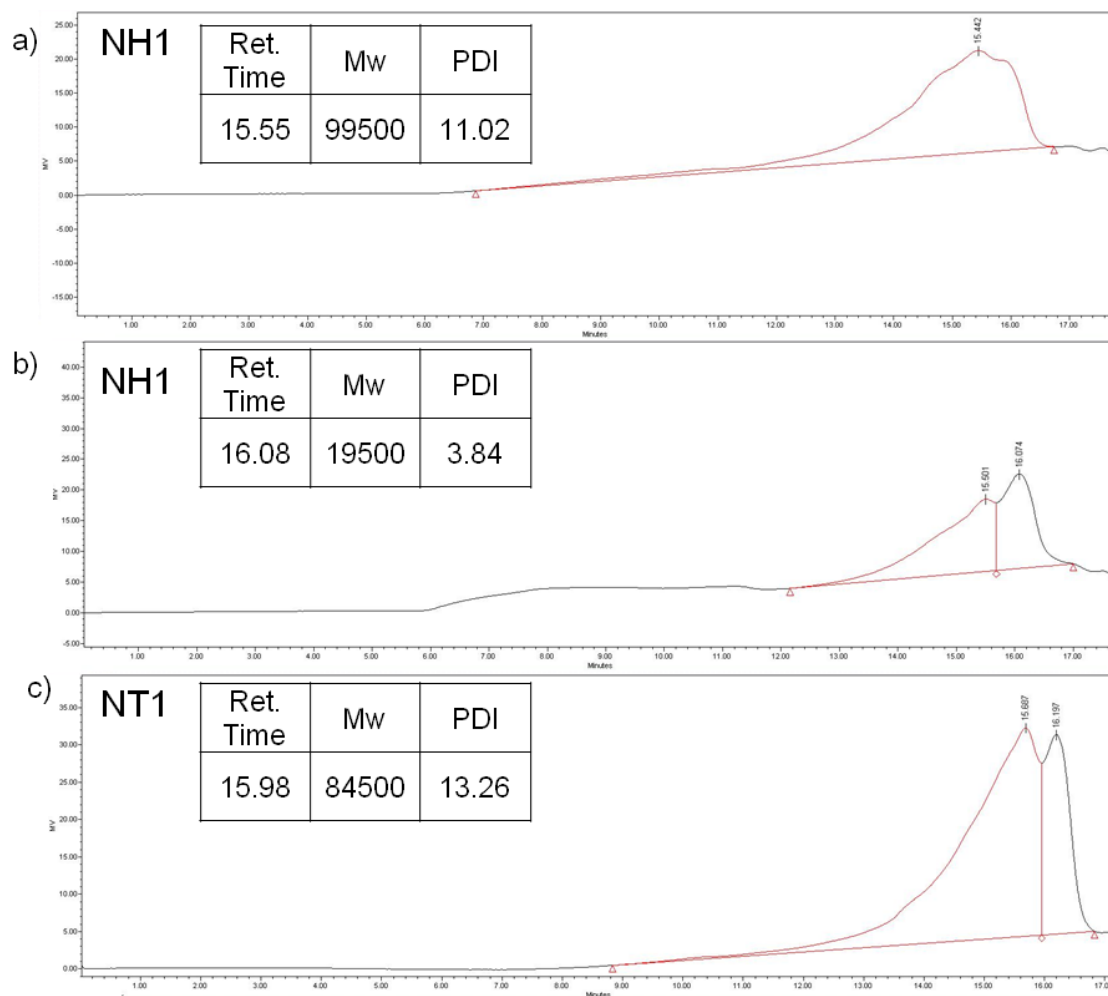


Figure 5.9 Comparative GPC analysis of β NXCDs: (a) NP1 (PEG: β CD ratio = 3.8), (b) NH1 (HEG: β CD ratio = 4.0), and (c) NT1 (TEG: β CD ratio = 3.8).

As expected, both the Mw distribution and polydispersity index of the samples were dependent on the XEG: β CD ratio. As observed for the inert β CXCDs, the GPC analysis of β NCXCDs confirmed that products with higher XEG: β CD ratios (3.8:1) eluted at lower retention times corresponding to their higher Mw (Figure 5.10).

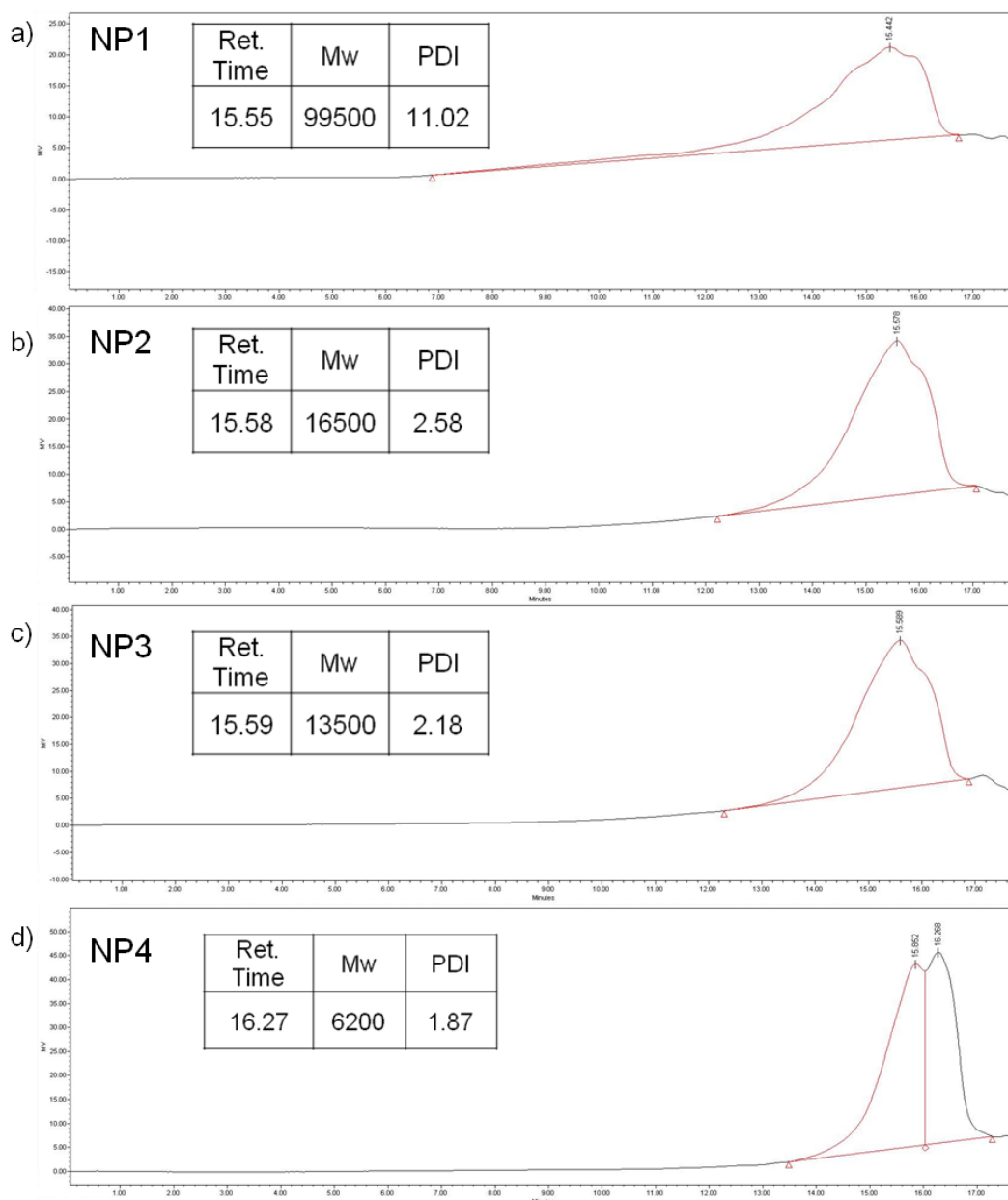


Figure 5.10 Comparative GPC chromatograms of β NPCDs with decreasing PEG: β CD ratios: (a) NP1 (PEG: β CD ratio = 3.8), (b) NP2 (PEG: β CD ratio = 2.6), (c) NP3 (PEG: β CD ratio = 2.1), and (d) NP4 (PEG: β CD ratio = 1.6).

5.4 Thermal and thermo-mechanical characterisation of energetic β NCXCDs

As discussed above, two sets of β NCXCDs were synthesised from inert precursors having differing in terms of their solubility in water. The thermo-

mechanical characterisation of the inert β CXCDs by DSC, TGA and DMA (Chapter 4) was therefore extended to the nitrated derivatives, the β NCXCDs.

5.4.1 Thermal characterisation of β NCXCDs prepared from insoluble precursors

The thermal behaviour of β NCXCDs obtained by nitrating the insoluble β CXCDs was variable. The thermal stability of the nitrated products was affected by a combination of four different factors:

- Strength of the nitrating medium;
- Cross-link ratio of the inert precursor;
- Nitration reaction time;
- Physicochemical properties of the inert precursors.

The conditions used for the synthesis of the β NCPCDs (samples NP7–NP11) and β NCTCDs (samples NT5–NT15) from inert precursors containing PEG and TEG units, respectively, are summarised in Appendix A (Table A 4 and Table A 5, respectively). The nitration of the insoluble β CTCDs released similar amounts of energy in every trial, but this was variable and random in the β NCPCDs.

The thermal profiles of samples NP7–NP11 synthesised from the same precursor (IP26) were found to be inconsistent during decomposition due to the insolubility of the precursor in the nitrating medium. However, longer nitration times promoted higher degrees of nitration and higher decomposition enthalpies compared to analogues NT1–NT10 containing TEG units (Appendix A, Table A 5). The reaction conditions were changed in each trial to increase the efficiency of the reaction, but the nitration was strongly affected by the gel-like physical properties of the β CPCD precursors. Increasing the nitration time to 2 h (NP7–NP12) and the stirring speed (900 rpm), facilitated the dispersion of the hydrogel. The products demonstrated greater thermal stability up to T_{dec} (peak = 200 °C) which were attributed to the more efficient purification. However, the thermal properties of the compounds still appeared to be random, with NP8 and NP9 exceeding 1000 J g⁻¹ (Figure 5.11), but NP7 and NP10–NP12 falling within the range 400–600 J g⁻¹ (Table 5.2).

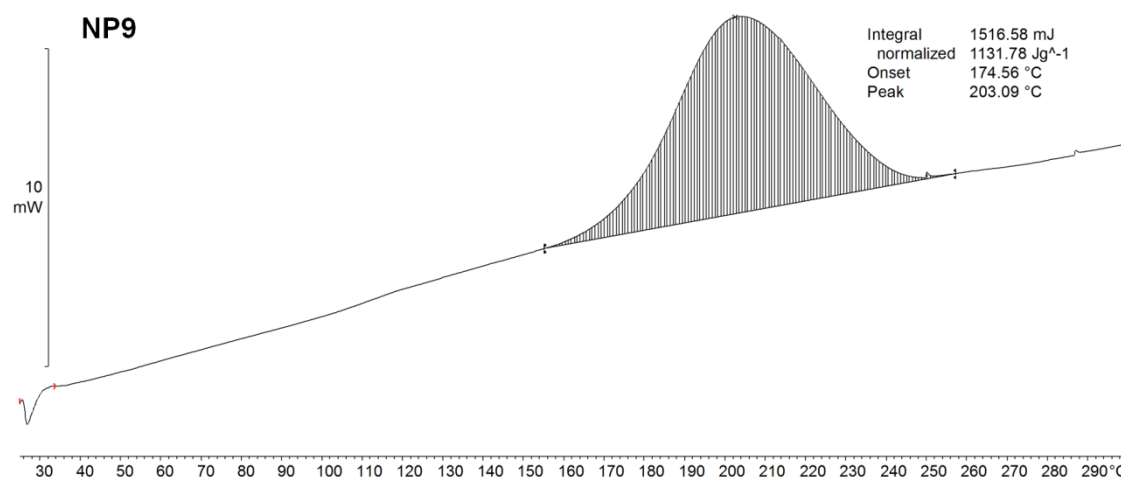


Figure 5.11 DSC thermogram of NP9, from 30 to 300 °C (10 °C min⁻¹, aluminium crucible).

All the β NCTCDs containing TEG segments showed similar thermal stabilities, with a decomposition peak centred at ~200 °C (Figure 5.12).

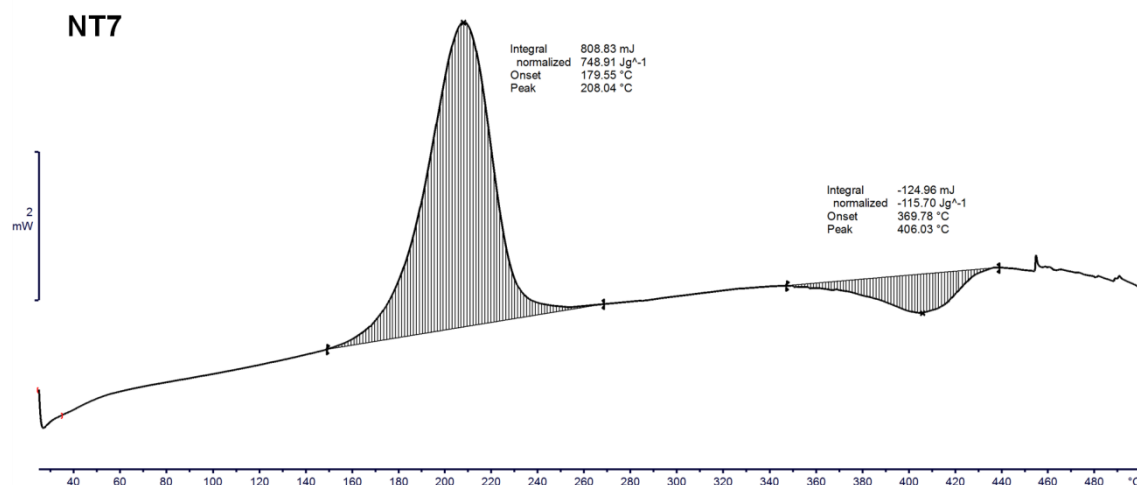


Figure 5.12 DSC thermogram of NT7, from 30 to 500 °C (10 °C min⁻¹, aluminium crucible).

The energy associated with the decomposition of NT5–NT14 was always in the range 430–810 J g⁻¹ regardless of the nitration conditions (Table 5.2) and the thermal profiles were quite similar when characterised by DSC. The decomposition energy was low compared to the values for NC (~2000 J g⁻¹

when measured under the same conditions [28]), indicating a low degree of nitration in the samples. The residue began to char at 370 °C.

Table 5.2 Thermal properties of the energetic derivatives of gel-like insoluble β CPCDs and insoluble β CTCD powders.

Sample ID	Inert Precursor		Product			
	ID	Cross-linker: β CD feed ratio ¹	T_{dec} (°C)		ΔH_{dec} (J g ⁻¹)	T_g (°C)
			Onset	Peak		
NP7	IP26	9:1	100	108	690	-
NP8	IP26	9:1	129	135, 139 ²	1400	-
NP9	IP26	9:1	174	203	1132	-8
NP10	IP26	9:1	181	208	460	-8
NP11	IP26	9:1	109	208	460	-28
NT5	IT5	9:1	183	210	530	-24
NT6	IT5	9:1	183	208	650	-19
NT7 ³	IT5	9:1	179	208	760	-19
NT8 ³	IT5	9:1	179	208	810	-18
NT9 ³	IT5	9:1	179	208	760	-22
NT10 ³	IT6	3:1	182	209	430	-22
NT11 ³	IT7	6:1	175	206	570	-22
NT12 ³	IT5	9:1	175	208	590	-21
NT13	IT6	3:1	181	208	570	-22
NT14	IT7	6:1	176	207	510	-21
NT15	IT5	9:1	183	210	530	-24

1 Double spiked decomposition.

2 Compounds are insoluble. The cross-linker: β CD feed ratio is reported.

3 Nitration time = 2 h.

The low-temperature characterisation of the compounds was achieved by cycling the temperature from -100 to 100 °C three times. The β NCXCDs derived from insoluble precursors appeared to be hygroscopic, retaining water in their structures. This affected the T_g of the product which fell to -26 °C

(Figure 5.13). By heating the sample, the water evaporated allowing the real T_g to be determined in the second heating cycle, revealing a value of $-22\text{ }^\circ\text{C}$. The transition at $80\text{ }^\circ\text{C}$ attributed to the β CD units in β NCXCDs was also recorded in several nitrated samples (Figure 5.10).

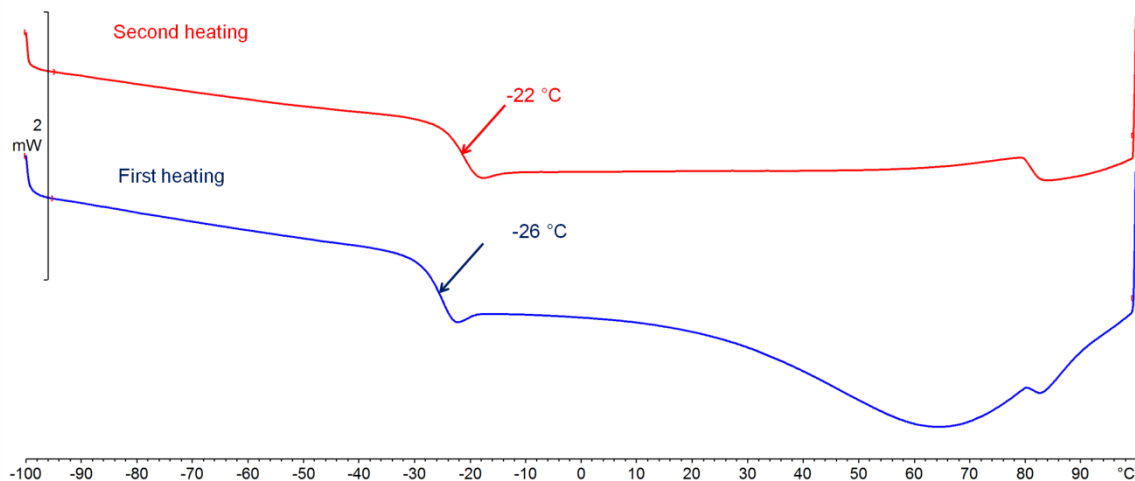


Figure 5.13 DSC thermogram of NT9 from -100 to $100\text{ }^\circ\text{C}$ ($10\text{ }^\circ\text{C min}^{-1}$, third temperature cycle, aluminium crucible).

In conclusion, the nitration of insoluble precursors generated sparsely nitrated products. It was not possible to control the degree of nitration and thus the thermal properties of the β NCXCDs so these products were not considered in the subsequent experiments.

5.4.2 Thermal characterisation of β NCXCDs prepared from soluble precursors

The β NCXCDs prepared from water-soluble β CXCDs were soluble in organic solvents such as acetone and THF. The thermal properties were duly investigated by DSC and TGA, and the nitrogen content was determined by titration (Table 5.3).

Table 5.3 Thermal properties of β NCXCDs prepared from water-soluble β CXCDs.

Sample ID	Inert precursor		Nitrated product					
	XEG: β CD ratio	T_g ($^{\circ}$ C)	T_{dec} ($^{\circ}$ C)		ΔH_{dec} ($J.g^{-1}$)	Nitrogen content %	Ω (%)	T_g ($^{\circ}$ C)
			Onset	Peak				
β NC	-	-	193	207	1990	11.6	-40	-
NT1	3.6	- ¹	180	196	2080	8.2	-81	- ¹
NT2	3.2	- ¹	180	203	1430	9.4	-71	- ¹
NT3	2.5	- ¹	179	200	1690	9.3	-69	- ¹
NT4	1.6	-	176	198	1850	6.2	-87	-
NH1	4	-10	179	191	1750	8.2	-87	+6
NH2	3.2	-6	174	198	1730	7.1	-93	+26
NH3	2.6	- ¹	178	199	1720	9.0	-76	+47
NH4	1.8	- ¹	174	196	1720	9.4	-70	+65
NP1	4.0	-20	176	198	1750	6.2	-109	-14
NP5	3.7	-19	178	190	1800	6.2	-101	+7
NP6	3.7	-19	175	190	1540	6.6	-105	+7
NP2	2.8	-6	172	196	1840	6.8	-97	+31
NP3	2.5	+5	174	197	1630	7.0	-94	+23
NP4	1.6	-	174	193	1730	8.7	-76	+45

¹ Change in heat flow due to the softening of the compound.

The offsets for β NCXCD decomposition fell within the range 172–193 °C (Table 5.3) whereas the degradation peaks were in the range 190–203 °C and were comparable to those of the corresponding products obtained from insoluble β CXCD precursors in water and also to NC (201–205 °C) [28]. The ΔH_{dec} values were 1360–2080 J g⁻¹, lower than the 2200–1800 J g⁻¹ released by the less fuel-rich NC [28]. Some general observations were made for the three sets of β NCXCDs and are reported below.

For samples NT1–NT4 containing TEG units, the decomposition temperatures were very close to 200 °C regardless of the TEG content whereas the decomposition enthalpies fell within the range 1430–2080 J g⁻¹. No glass transition was observed, confirming that the length of TEG units was insufficient to make the β NCTCD products soft and rubbery.

For samples NH1–NH4 containing HEG units, the decomposition temperatures were variable (191–199 °C) whereas the decomposition enthalpies were stable at 1700 J g⁻¹. A glass transition occurred between 6 and 65 °C confirming that the length of the HEG units was sufficient to influence the thermo-mechanical properties of the β NCHCD products.

For samples NP1–NP6 containing PEG units, the decomposition temperatures were again variable (190–197 °C) and the decomposition enthalpies varied in the range 1360–1840 J g⁻¹. A glass transition occurred between 7 and 45 °C confirming that the length of PEG units was also sufficient to influence the thermo-mechanical properties of the β NCPCD products. Exceptionally, NP1 was found to undergo a glass transition at –14°C.

Finally, the T_g of the β NCXCDs appeared to be linearly dependant on the HEG/PEG content, as shown in Figure 5.16.

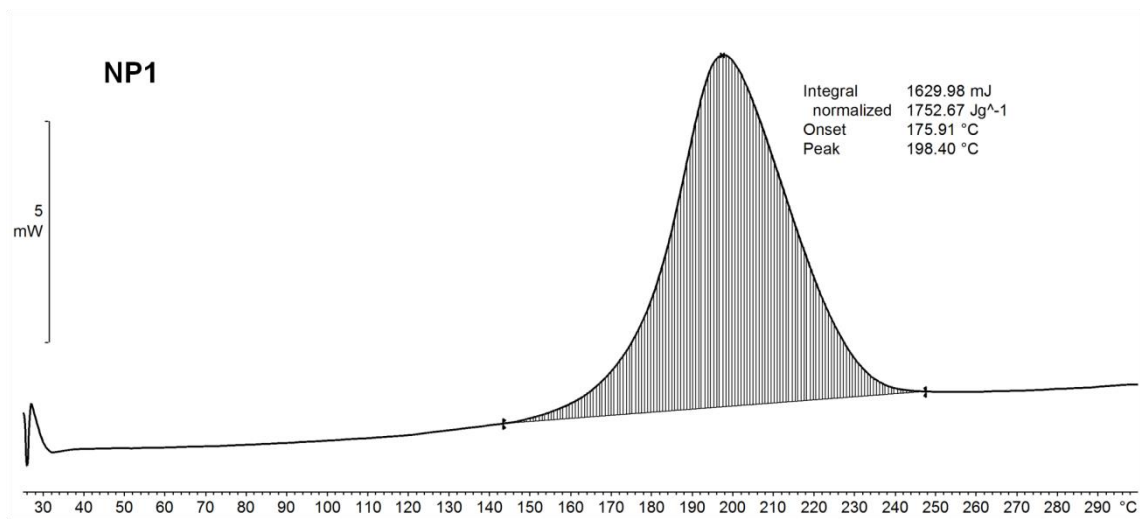


Figure 5.14 DSC thermogram of NP1 from 25 to 300 °C (10 °C min⁻¹, aluminium crucible).

The T_g of the β NCXCDs was 20–30 °C higher than that of the precursors (Table 5.3). The presence of hydrogen bonds increases the T_g [136]. The replacement of hydroxyl groups with nitrate groups in the β NCXCDs should reduce the number of hydrogen bonds but the T_g nevertheless increased. One potential explanation is that the nitrate groups expanded the polar surface area of the compounds, therefore increasing their cohesive energy and limiting chain mobility to an even greater extent than hydrogen bonds [137]. The cohesive energy is the increase in internal energy when all intermolecular forces are eliminated [137]. The trend in T_g values could be evaluated by Hildebrand or Hansen solubility parameter modelling to assess the effect of hydroxyl and nitrate groups on the cohesive energy of the β NCXCDs [138].

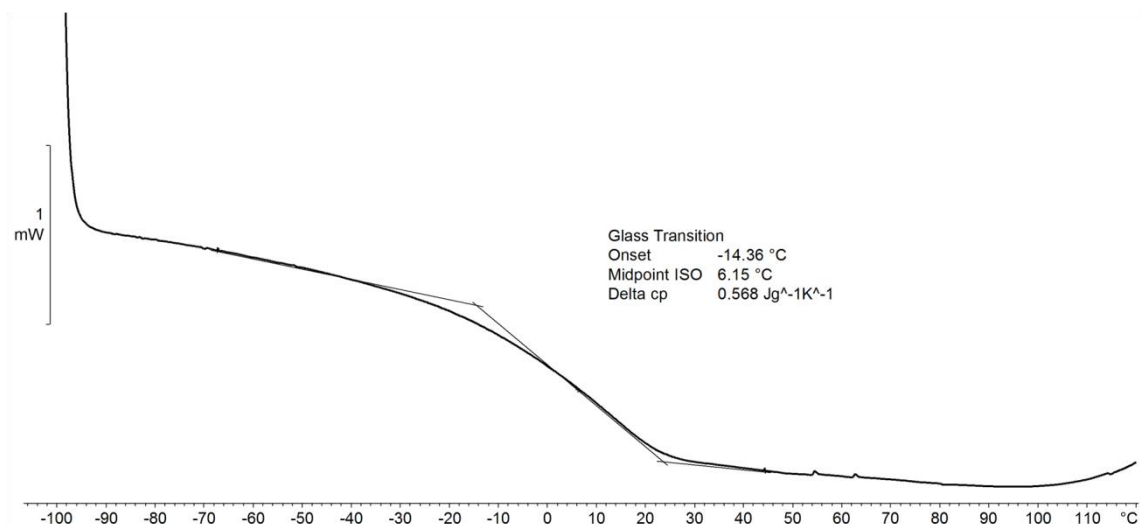


Figure 5.15 DSC thermogram of NP1 from –100 to 100 °C showing the pronounced glass transition of the highly cross-linked products (10 °C min⁻¹, aluminium crucible).

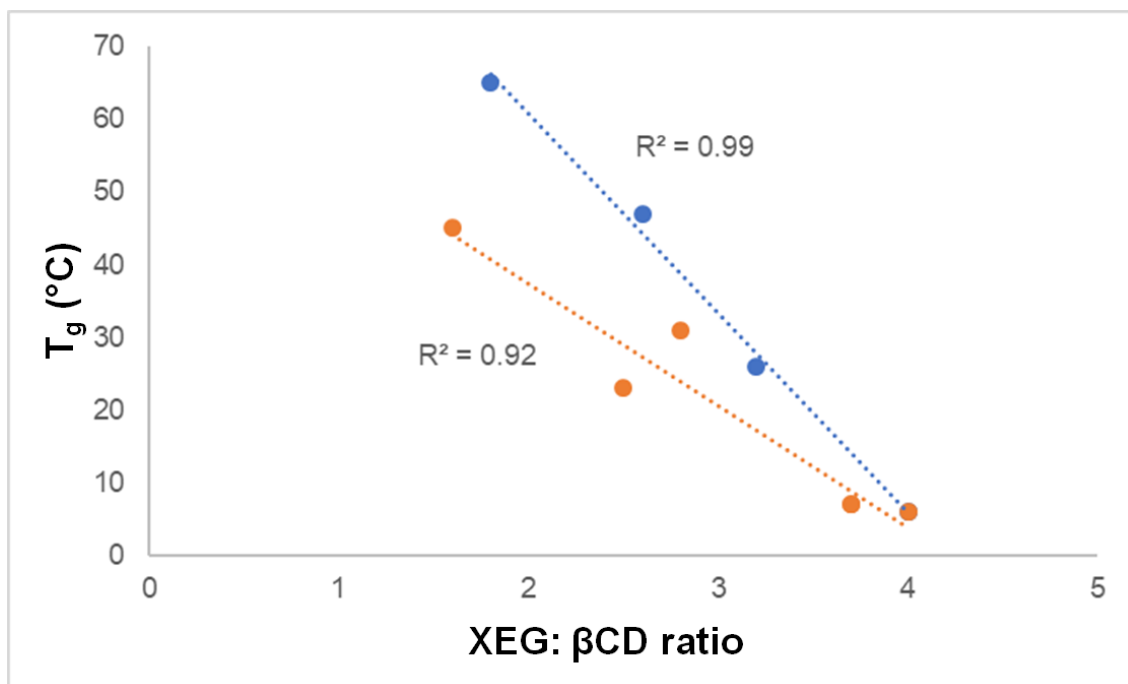


Figure 5.16 Plot of T_g against XEG:βCD ratio for βCHCDs (blue line) and βCPCDs (orange line).

The nitrogen content of the βNCXCDs was determined by titration as discussed above and was found to be inversely proportional to the length of the PEG segment. The βNCPCDs contained less nitrogen (6.5%) than the βNCTCDs and βNCHCDs (8–9%). The longer polyethylene glycol chains reduced the nitrogen content because the spacer increases the proportion of C, H and O relative to N. Furthermore, the βCPCDs are less soluble than the analogous molecules synthesised with the HEGDGE and TEGDGE cross-linkers, reducing the efficiency of the nitration reaction.

The nitrogen content of the βNCXCDs was needed to determine the chemical formula of each compound and thus its contribution to the combustion of energetic formulations. The difference between inert and energetic binders is the contribution to the overall energetic output of the formulation. The power of an explosive is proportional to the amount of molecular oxygen it contains, which determines the gaseous products produced during detonation. This is expressed as the oxygen balance (Ω), as shown in Equation 5:

$$\Omega = \frac{(d - 2a - \frac{b}{2}) \times 1600}{Mw} \% \quad (5)$$

where d is the number of oxygen atoms in the compound, a is the number of carbon atoms, b is the number of hydrogen atoms and Mw is the molecular weight of the compound.

Equation 5 indicates the ability of the compound to produce gaseous products and release energy as heat [2]. Positive Ω values correspond to the complete oxidation of the compounds in the formulation and the production of large quantities of gases such as CO₂ and hence more energy, whereas negative Ω values indicate the compound is deficient in oxygen, does not achieve complete oxidation, and that there is a higher yield of gases such as CO and solid residues rich in carbon, and hence less energy.

The Ω values for all β NCXCDs were negative due to the high proportion of carbon compared to oxygen. Furthermore, the Ω value of β NCD is -40% , which is identical to NC with a nitrogen content of 11.6% . The XEG units in the β NCXCDs reduced Ω even further, yielding values of -69% to -109% .

5.4.3 Thermo-mechanical characterisation of β NCXCDs

Due to the energetic properties of β NCXCDs, only one sample containing PEG units (NP1) was characterised by DMA. Preliminary small-scale hazard tests were completed before the characterisation and sample NP1 was declared safe for testing under the induced stresses generated by the DMA measurement conditions. NP1 was not susceptible to ignition during the impact and friction mallet tests as described in Chapter 6. The T_g of NP1 was similar to that of its precursor IP18, with an onset at 15 °C and a $\tan\delta$ peak at 25 °C (Figure 5.17). The nitrated derivative interacted strongly with the support, just like its precursors (Section 4.3.2.2) and accordingly, cracking was observed at -51 °C during the cooling cycle at the onset of E' .

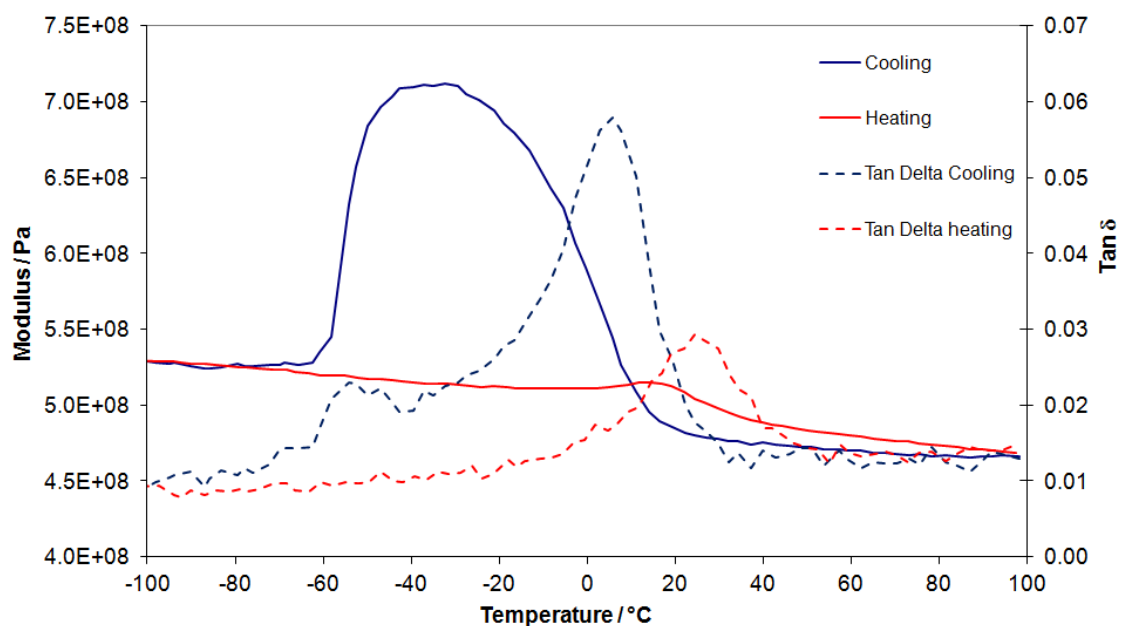


Figure 5.17 DMA showing variation in the storage modulus (E' , solid lines) and $\tan\delta$ (dashed lines) of NP1 (10 °C min^{-1} , 1 Hz, third temperature cycle from -100 to 140 °C, aluminium pocket).

5.4.4 Qualitative analysis of the self-healing properties of β NCPCD34

The self-healing ability of NP1 was qualitatively visible, as for the inert β CPCDs (Chapter 4). NP1 was assessed by first cutting the sample (Figure 5.18a,b) and then re-joining the parts by leaving it at rest for 4 h (Figure 5.18c). The sample was then pulled gently by its extremities, showing a high degree of elongation (Figure 5.18d).

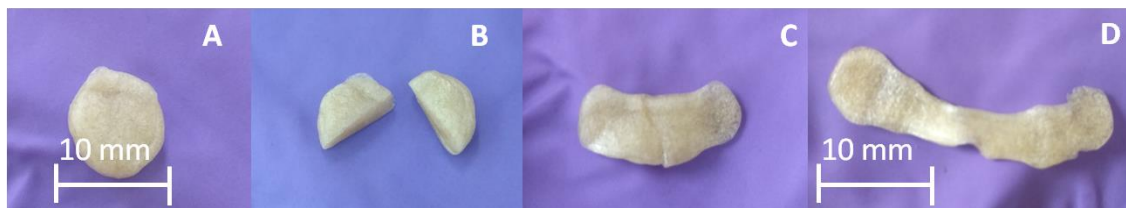


Figure 5.18 Self-healing ability of NP1 (PEG: β CD ratio = 4:1).

These experiments showed that the loss of some hydrogen bonds due to the replacement of hydroxyl groups with nitrate groups did not inhibit the mobility of the polymer chains in NP1 and did not eliminate its thermal healability. The healing of NP1 was driven by supramolecular interactions, such as hydrogen bonds and Van der Waals forces, as was the case for its precursor. The higher mobility of the dangling PEG chains accelerated the self-healing of these compounds.

5.5 Conclusions

The results presented in this chapter provide key data required for the nitration of β CXCDs, which are produced from β CD and diglycidyl ethers such as TEGDGE, HEGDGE and PEGDGE, and thus for the preparation of β NCXCDs as new energetic binders. The nitration reaction with fuming nitric acid led to two sets of β NCXCDs differing in terms of their solubility in water and other organic solvents, and their properties were strongly dependent on the physicochemical characteristics of the β CXCD precursors.

Insoluble β CXCD systems yielded cross-linked derivatives with various degrees of nitration that were insoluble in acetone, whereas water-soluble β CXCD precursors produced β NCXCDs that were soluble in acetone and easy to

characterise and process. The degree of nitration in these products was not only dependent on the properties of the precursor, but also the duration of the nitration reaction and the XEG:βCD ratio of the products. Better control of the properties of the βNCXCD products was achieved when soluble βCXCD precursors were used, and the workup was simpler compared to the insoluble precursors. A purification method based on the NC manufacturing process removed acid traces from the nitration reaction more efficiently, stabilising the compound during storage.

All of the synthesised products were characterised by ¹H-NMR and FTIR spectroscopy to confirm their effective nitration. No significant differences in the degree of nitration were observed for systems containing variable quantities of the linkers TEG, HEG and PEG. The nitrogen content of the βNCXCDs was determined by the titration of free hydroxyl groups in the molecules and was dependent on the degree of cross-linking and the length of the polyethylene glycol chains in the βNCXCDs. A lower degree of nitration was observed in derivatives containing PEG segments compared to those containing TEG or HEG segments due to the lower solubility of the βCPCD precursors in the nitration media.

The thermal stability of the βNCXCDs ($T_{\text{dec}} = 190\text{--}200\text{ }^{\circ}\text{C}$) was independent of the degree of cross-linking and type of linker segment in the macromolecule, whereas ΔH_{dec} was influenced by the type of linker segment and ranged from 1300 to 2100 J g⁻¹. The βNCXCDs retained much of the softness of their βCXCD precursors, with T_g values in the range 6–65 °C. The analysis of one βNCPCD sample showed that it retained the self-healing characteristics of its precursor after 4 h at room temperature.

6 Compatibility, hazard and stability studies

It is expected that the main constituents of munitions, such as explosives, oxidisers and pyrotechnic fillers, would be less susceptible to external stimuli when embedded in a β CD binder, making the formulation safer and easier to handle. Compatibility, hazard and stability testing help to ensure the safety of an energetic formulation during manufacturing and storage. Compatibility tests determine whether materials such as binders, plasticisers and other additives in energetic formulations have an adverse effect on stability when in contact with each other. The tests check for chemical compatibility between the constituents of a formulation and with the tools used during manufacturing and storage. The effect of ageing on the stability of the materials is determined by accelerated ageing at high temperatures. Hazard tests offer a comprehensive understanding of the sensitiveness of formulations and their components against thermal, mechanical and electrostatic stimuli, and help with the development of guidelines for safe manufacturing, storage, transport and use.

This chapter discusses the compatibility, hazard and stability testing of the inert β CXCDs and nitrated β NCPXCDs developed in Chapters 4 and 5, according to NATO STANAG 4147 Test 4 S [121] and EMTAP guidelines [119]. Any changes in the shape, onset, or peak position of any thermal event may be indicative of incompatibility.

6.1 Compatibility tests – β CXCDs

A set of preliminary compatibility tests was carried out by mixing sample IP19 (an inert β CPCD with a PEG: β CD ratio of 4:1) with a set of inert, oxidising and energetic materials following the procedure described in Chapter 3. The decomposition temperatures of the pure compounds and 50:50 w/w mixtures were determined by DSC, and the results are summarised in Table 6.1. All DSC tests for compatibility were carried out with a heating rate of 2 °C min⁻¹ rather than the 10 °C min⁻¹ used to record the thermal properties in Chapters 4 and 5. The differences in thermal behaviour between the pure compounds and mixtures were taken as indications of compatibility/incompatibility as per

STANAG 4147 (Ed.2) Test 4 (see Section 3.3.6). Specifically, shifts of less than 4 °C generally indicate compatibility, shifts of more than 20 °C generally indicate incompatibility, and values between are inconclusive and warrant further testing.

Table 6.1 Compatibility of inert β CPCD (sample IP19, PEG: β CD ratio = 4.0:1) with various energetics.

Formulation	T _{dec} (°C)		ΔT (°C)	Shape change
	Energetic	Mixture		
IP19/HMX	279	279	0	Significant
IP19/RDX	226	212	-14	Significant
IP19/PETN	185	184	-1	Minor
IP19/ADN	172	149	-23	Significant
IP19/KClO ₃	- ¹	- ¹	0	None
IP19/KNO ₃	- ¹	- ¹	0	None
IP19/NH ₄ ClO ₄	264	260	-4	Minor
IP19/NH ₄ NO ₃	- ¹	188	0	Significant
IP19/RedP	400/492	404/471	+4/-11	Significant

¹ No decomposition

Pure HMX decomposed at 279 °C (Figure 6.1) and there was no shift in the position of the decomposition peak when mixed with IP19. However, the shape and onset of the decomposition curve changed slightly in the mixture, with a broader degradation ramp starting at 10 °C, which is earlier than pure HMX. Further evaluation of the compatibility is therefore required according to NATO STANAG recommendations.

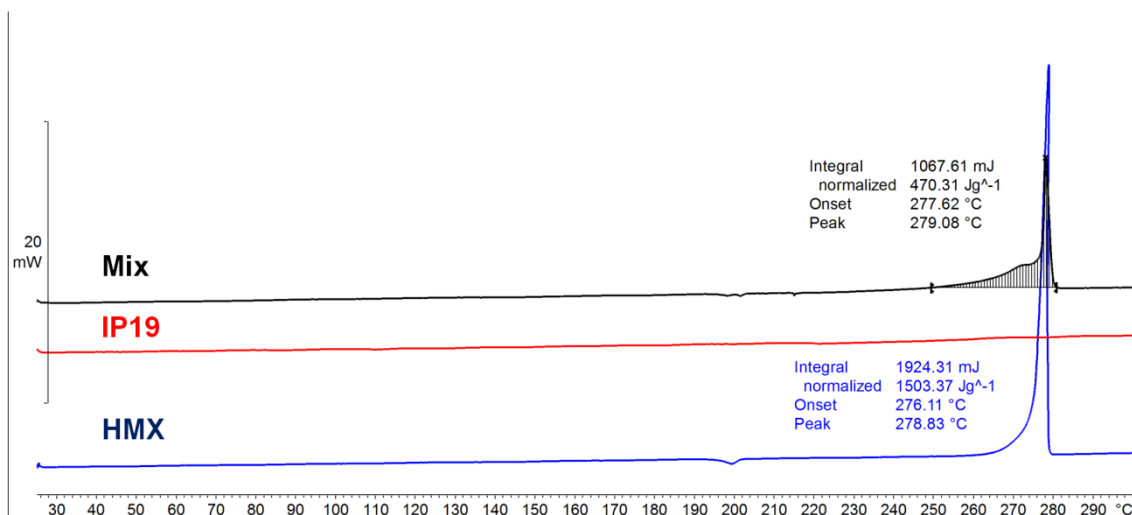


Figure 6.1 DSC thermogram of HMX (blue line), IP19 (red line), and a 50/50 (w/w) mixture (black line) from 30 to 300 °C (1 mg, 2 °C min⁻¹, aluminium crucible).

Pure RDX melted at 204 °C before decomposing at 226 °C (Figure 6.2, blue curve) whereas the mixture with IP19 decomposed directly at 212 °C with a lower onset of decomposition at 30 °C (Figure 6.1, black curve). The 14 °C shift in the decomposition temperature between pure RDX and the RDX/IP19 mixture suggests a degree of incompatibility and further investigation is needed. There was a significant difference in compatibility between the IP19 formulations with RDX and HMX, which may reflect the relative size of the two nitramines. RDX is the smallest (4–5 Å) and can be partially encapsulated by the βCD cavity (6–6.5 Å), which translates to the small hump in the degradation curve. In contrast, HMX remains free due to its larger size (5–8 Å). The βCD-based binder was therefore anticipated to encapsulate energetic fillers but no direct chemical reaction was expected.

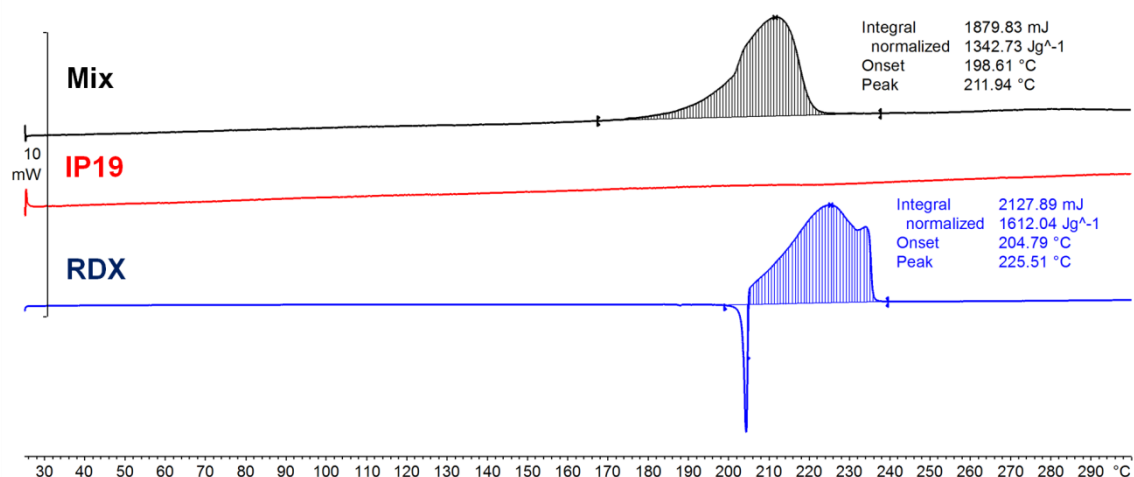


Figure 6.2 DSC thermogram of RDX (blue line), IP19 (red line), and a 50/50 (w/w) mixture (black line) from 30 to 300 °C (1 mg, 2 °C min⁻¹, aluminium crucible).

Pentaerythritol tetranitrate (PETN) melted at 142 °C and decomposed at 185 °C (Figure 6.3, blue curve) and these properties were not affected by mixing with IP19 (Figure 6.3, black curve). The energy of the mixture increased, suggesting that the binder had a synergistic effect on the energy output of the system during decomposition.

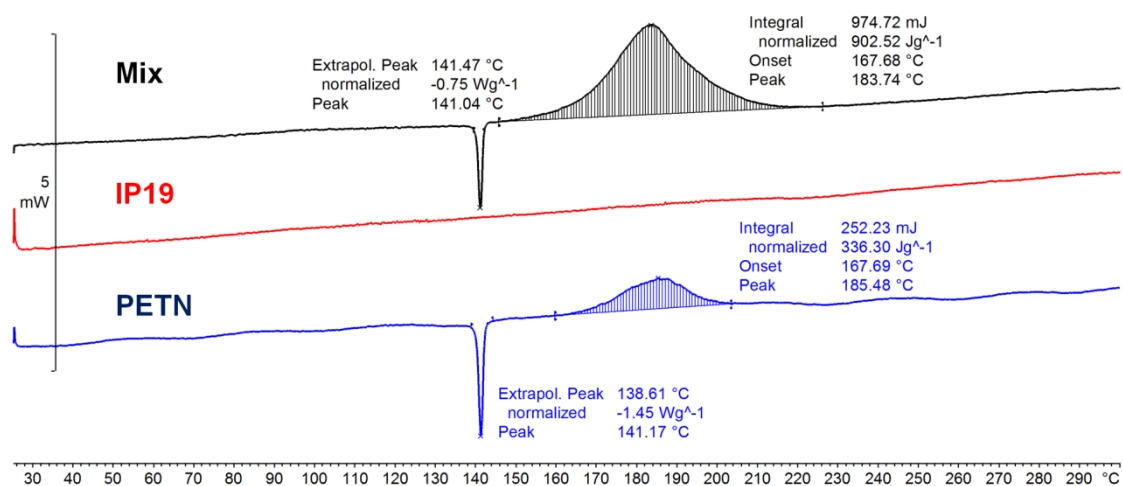


Figure 6.3 DSC thermogram of PETN (blue line), IP19 (red line), and a 50/50 (w/w) mixture (black line) from 30 to 300 °C (1 mg, 2 °C min⁻¹, aluminium crucible).

Neat ammonium dinitramide oxidiser (ADN) melted at 93 °C (Figure 6.4, blue curve), and this did not change in the mixture with IP19 (Figure 6.4, black curve). ADN decomposed at 172 °C, but the mixture showed a biphasic decomposition curve with major peaks at 149 and 172 °C. This indicated a degree of incompatibility between the two compounds, perhaps reflecting the encapsulation of some of the ADN molecules within the β CD cavity, as proposed for RDX.

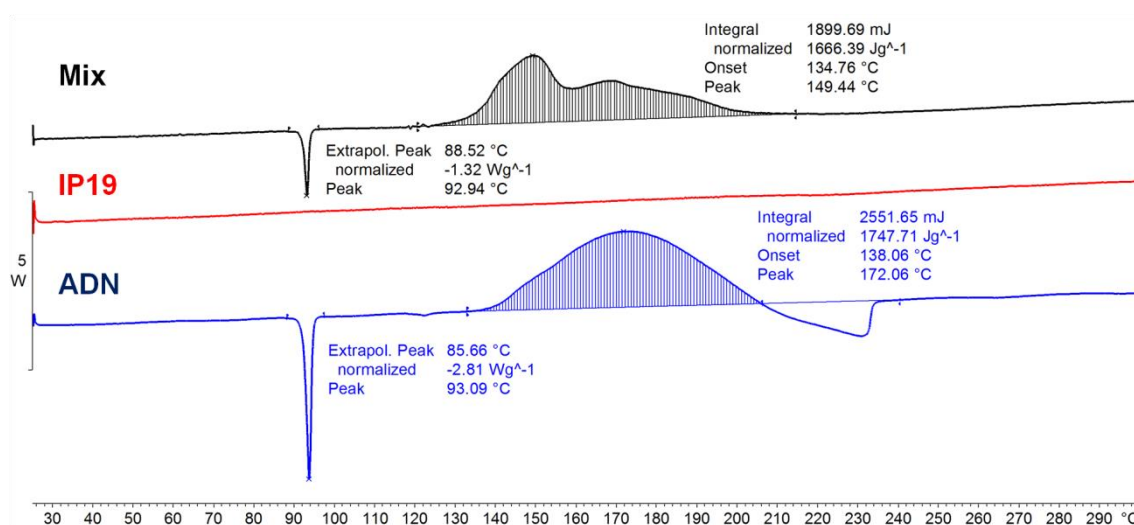


Figure 6.4 DSC thermogram of ADN (blue line), IP19 (red line), and a 50/50 (w/w) mixture (black line) from 30 to 300 °C (1 mg, 2 °C min⁻¹, aluminium crucible).

KClO₃ showed no exothermic peaks below 400 °C with a small endotherm visible at 303 °C (Figure 6.5, blue curve), possibly due to the compound melting. The mixture with IP19 exhibited the same endotherm and a tiny additional endotherm at 214 °C, suggesting good compatibility between these components (Figure 6.5, black curve).

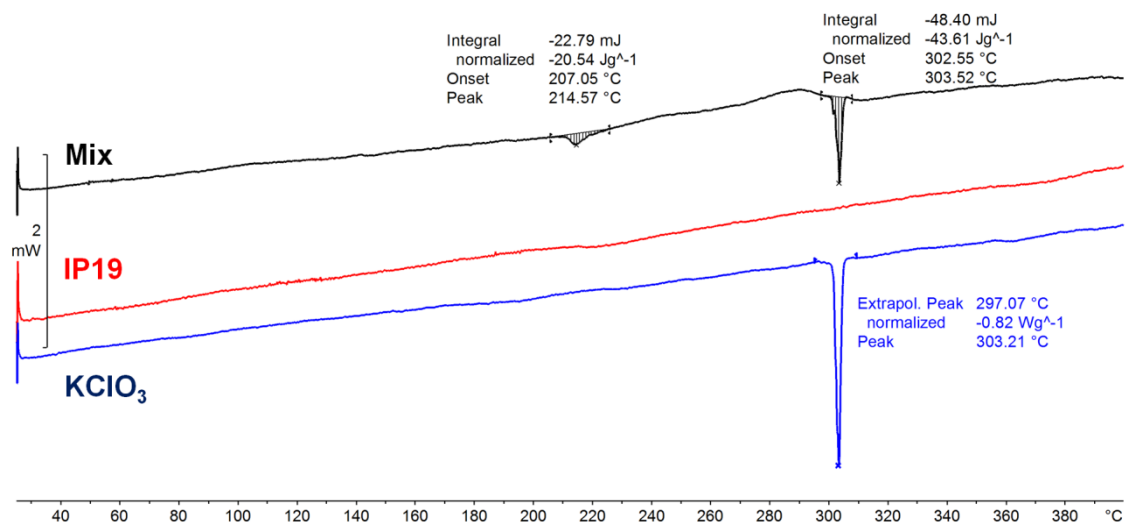


Figure 6.5 DSC thermogram of KClO₃ (blue line), IP19 (red line), and a 50/50 (w/w) mixture (black line) from 30 to 400 °C (1 mg, 2 °C min⁻¹, aluminium crucible).

KNO₃ melted at 335 °C (Figure 6.6, blue curve) and no changes were observed in the mixture with IP19 (Figure 6.6, black curve). These components were therefore considered to be compatible.

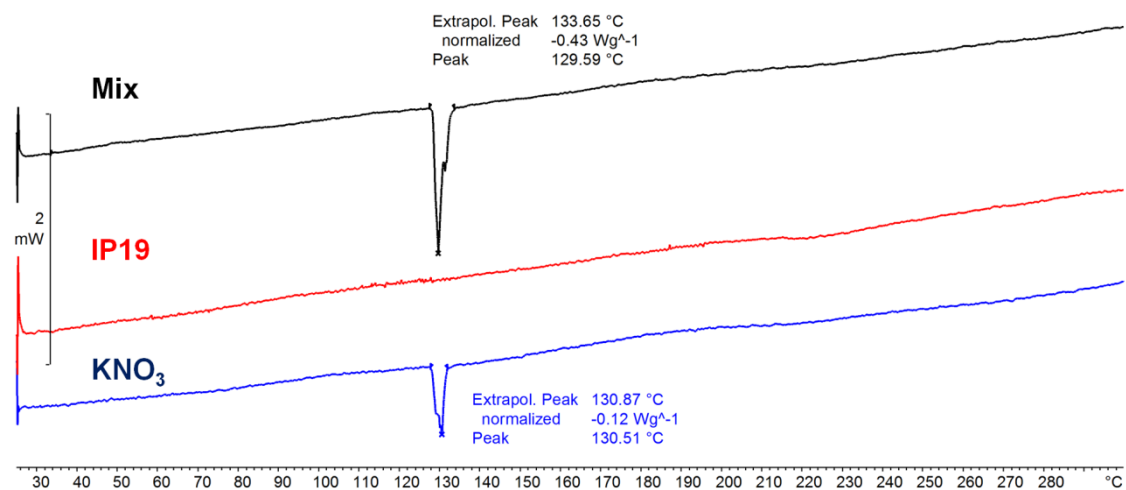


Figure 6.6 DSC thermogram of KNO₃ (blue line), IP19 (red line), and a 50/50 (w/w) mixture (black line) from 30 to 300 °C (1 mg, 2 °C min⁻¹, aluminium crucible).

The thermal profile of pure NH_4ClO_4 showed a melting point at 242 °C and decomposition at 264 °C (Figure 6.7, blue curve). These values were unchanged in the mixture with IP19 (Figure 6.7, black curve). Decomposition involved a principal event followed by two minor exothermic peaks. These results indicated that the two components were compatible.

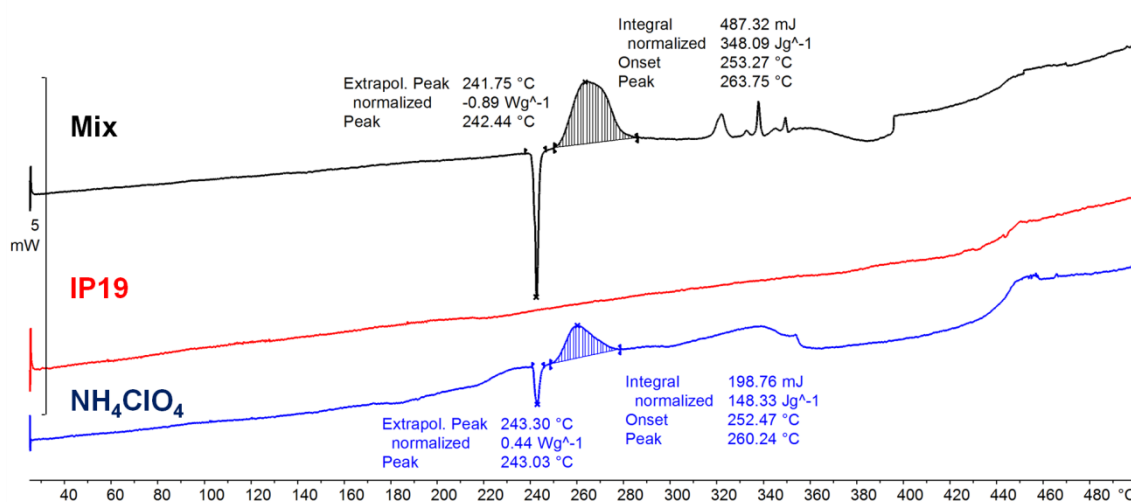


Figure 6.7 DSC thermogram of NH_4ClO_4 (blue line), IP19 (red line), and a 50/50 (w/w) mixture (black line) from 30 to 500 °C (1 mg, 2 °C min⁻¹, aluminium crucible).

Pure NH_4NO_3 showed a broad endotherm above ~200 °C caused by the volatile compound evaporating after melting (Figure 6.8, blue curve). When mixed with IP19, one endotherm became an exotherm with a peak at 188 °C (Figure 6.8, black curve), possibly indicating chemical reactivity between molten ammonium nitrate and the binder. This indicates the two ingredients are likely to be incompatible.

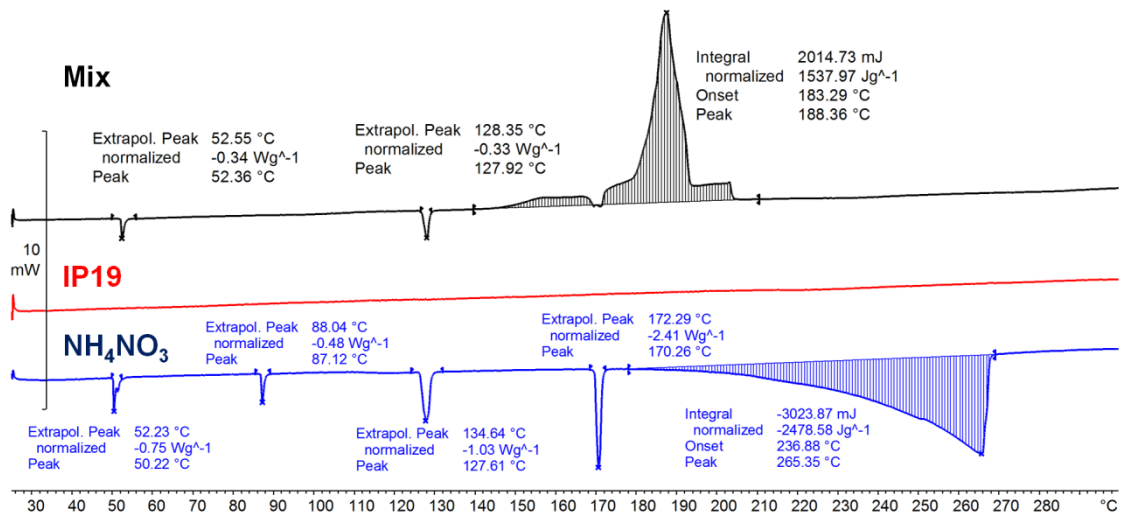


Figure 6.8 DSC thermogram of NH_4NO_3 (blue line), IP19 (red line), and a 50/50 (w/w) mixture (black line) from 30 to 300 °C (1 mg, 2 °C min⁻¹, aluminium crucible).

Two decompositions were observed for pure red phosphorous (RedP) at 400 and 492 °C (Figure 6.9, blue curve) but the mixture with IP19 showed a broader decomposition profile with maxima at 409 and 471 °C (Figure 6.9, black curve). Much more energy is released when RedP is mixed with the binder. The two ingredients could therefore be described as compatible, with reservations.

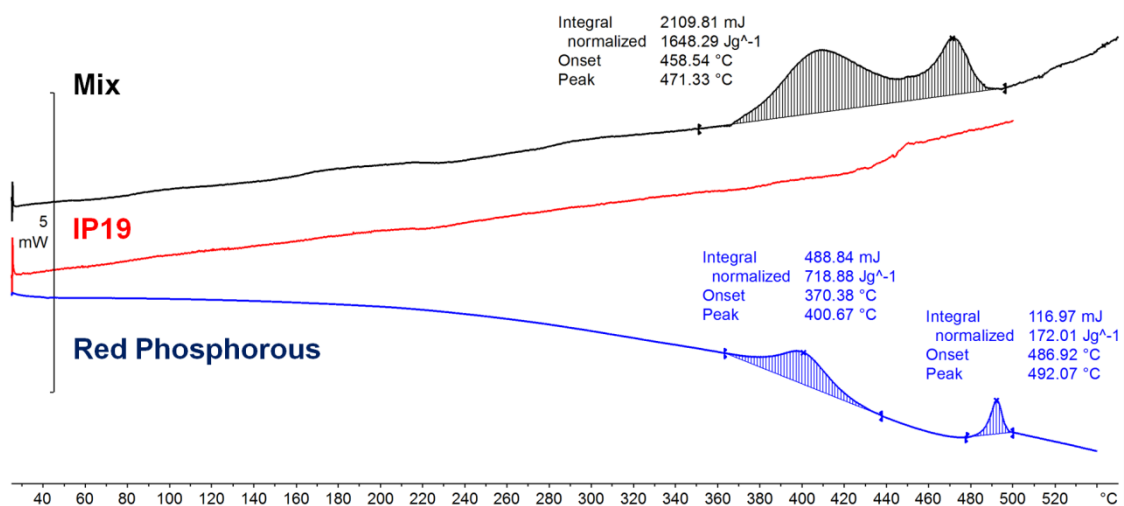


Figure 6.9 DSC thermogram of red phosphorus (blue line), IP19 (red line), and a 50/50 (w/w) mixture (black line) from 30 to 550 °C (1 mg, 2 °C min⁻¹, aluminium crucible).

6.2 Compatibility tests – β NCXCDs

In the next set of compatibility tests, sample NP13 (a nitrated β NCPCD with a PEG: β CD ratio of 3.8:1) was mixed with a set of inert, oxidising and energetic materials and analysed by DSC to determine their compatibility in accordance with STANAG 4147 guidelines as described above for the inert precursor IP10. Like NC, the β NCXCDs are nitroesters and need to be mixed with stabilisers to ensure an adequate shelf life [139,140]. Therefore, the widely-used stabilisers diphenylamine (DPA) and N,N'-diethyl-N,N'-diphenylurea (Centralite) were also tested in the compatibility tests, as well as 2,4-nitrodiphenylamine (2,4-NDPA), which is an intermediate product of DPA. Due to the small-scale synthesis (200 mg) of the β NCXCD compounds, the compatibility tests with the stabilisers were conducted using a different sample (NP1), although this has the same chemical composition as NP13. The decomposition temperatures of the pure compounds and mixtures were determined by DSC, and the results are summarised in Table 6.2.

Table 6.2 Compatibility of nitrated β NCPCD (samples NP13 and NP1, PEG: β CD ratio = 3.8:1) with various energetics and stabilisers.

Formulation	T_{dec}^2 (°C)		ΔT (°C)	Shape change
	Energetic	Mixture		
NP13/NP11	186	-	-	-
HMX	279	278	-1	Significant
RDX	226	210	-13	Significant
PETN	185	187	+2	Minor
ADN	172	161	-11	significant
KClO ₃	-3	-3	0	none
KNO ₃	-3	1853	-13	minor
NH ₄ ClO ₃	264	265	+1	minor
NH ₄ NO ₃		1893	+34	Significant
RedP	400/492	404/481	+4/-11	minor

NP1	184	-	-	-
DPA		140 ⁴	-44	
2,4-NDPA		190 ⁴	+6	
Centralite		185 ⁴	+1	

1 PEG:βCD ratio = 3.8:1

2 At 2 °C min⁻¹, N₂ atmosphere.

3 No decomposition.

4 Decomposition is related to the solely energetic binder.

The decomposition peaks of pure HMX at 279 °C (Figure 6.10, blue line) and the energetic binder NP13 at 186 °C (Figure 6.10, red line) were not affected when the two components were mixed (Figure 6.10, black line). As discussed for the inert precursor IP19, the onset of degradation remained the same, but a portion of the HMX started to degrade earlier, causing an initial step at 272 °C. This revealed a degree of incompatibility between NP13 and HMX that warrants further investigation.

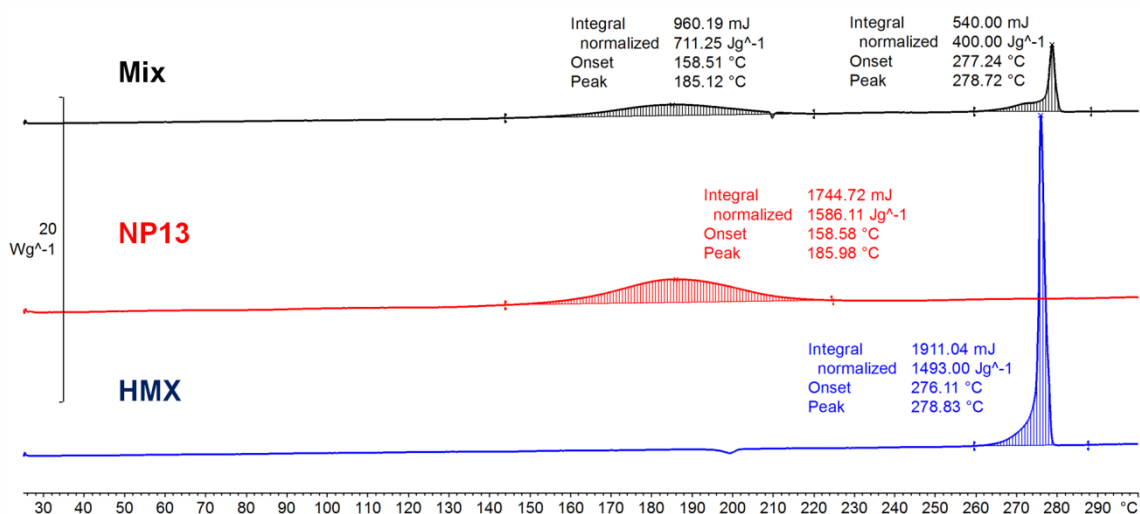


Figure 6.10 DSC thermograms of HMX (blue line), NP13 (red line), and a 50/50 (w/w) mixture (black line) from 30 to 300 °C (1 mg, 2 °C min⁻¹, aluminium crucible).

Pure RDX melted at 204 °C before decomposition with a major peak at 226 °C (Figure 6.11, blue line). When mixed, RDX and NP13 decomposed in the same temperature range between 140 and 230 °C. The RDX decomposition moved from 226 to 210 °C, with the shift of -16°C suggesting a degree of incompatibility which needs investigation. In contrast, the NP13 was 5 °C more

stable when mixed with RDX, with its T_{dec} shifted from 186 to 191 °C. As for the inert binder, there was a noticeable difference between NP13 formulations containing RDX and HMX, which likewise can be attributed to the different sizes of the nitramines and resulting differences in their degree of encapsulation by the β CD units of the energetic binder.

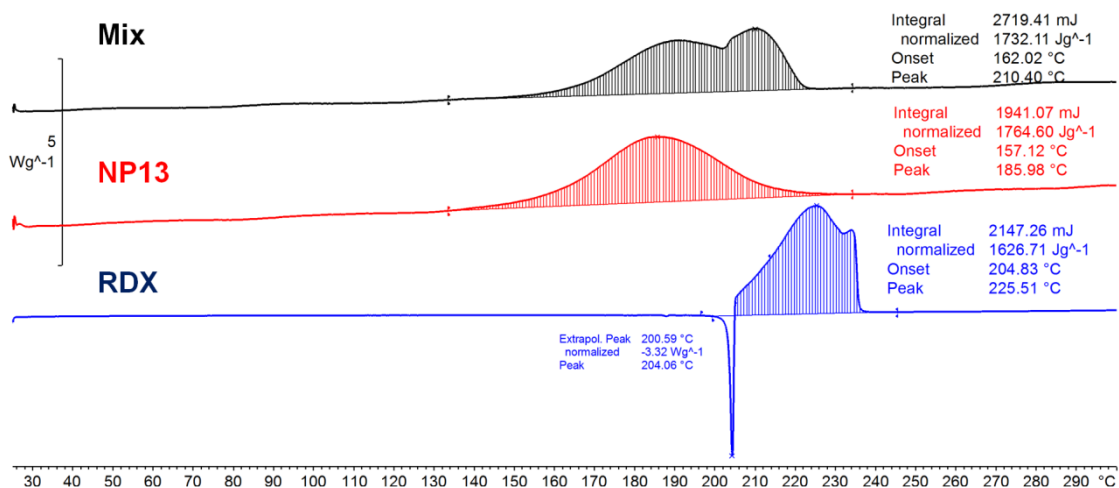


Figure 6.11 DSC thermograms of RDX (blue line), NP13 (red line), and a 50/50 (w/w) mixture (black line) from 30 to 300 °C (1 mg, 2 °C min⁻¹, aluminium crucible).

PETN and NP13 are both nitroesters containing nitrato groups and this is reflected in their very similar decomposition profiles (Figure 6.12, blue and red curves respectively). The melting of PETN at 141 °C was unchanged in the mixture. Furthermore, the mixture produced more energy than either of the components alone (Figure 6.12, black curve). The two components were therefore declared compatible.

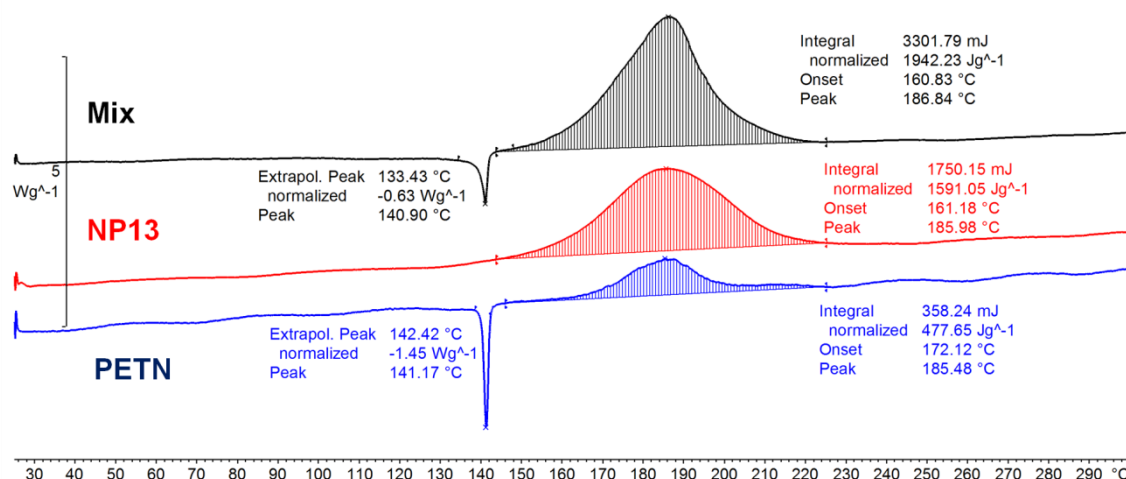


Figure 6.12 DSC thermograms of PETN (blue line), NP13 (red line), and a 50/50 (w/w) mixture (black line) from 30 to 300 °C (1 mg, 2 °C min⁻¹, aluminium crucible).

ADN melted at 93°C, a feature retained in the mixture with NP13 (Figure 6.13, blue and black curves). The ADN profile featured an exothermic decomposition with an onset at 137 °C and a peak at 172 °C, but in the mixture the onset shifted to 142 °C with a major peak at 161 °C, and a secondary peak at 157 °C matching the decomposition temperature of NP13 (Figure 6.13, red and black curves). The shape of the mixture's decomposition diverged from the profile of the pure compounds and became more indented, with a shift of +9 °C compared to ADN. This indicated a degree of incompatibility between the two components, and also suggested there was a ~20% increase in the amount of energy released by the mixture.

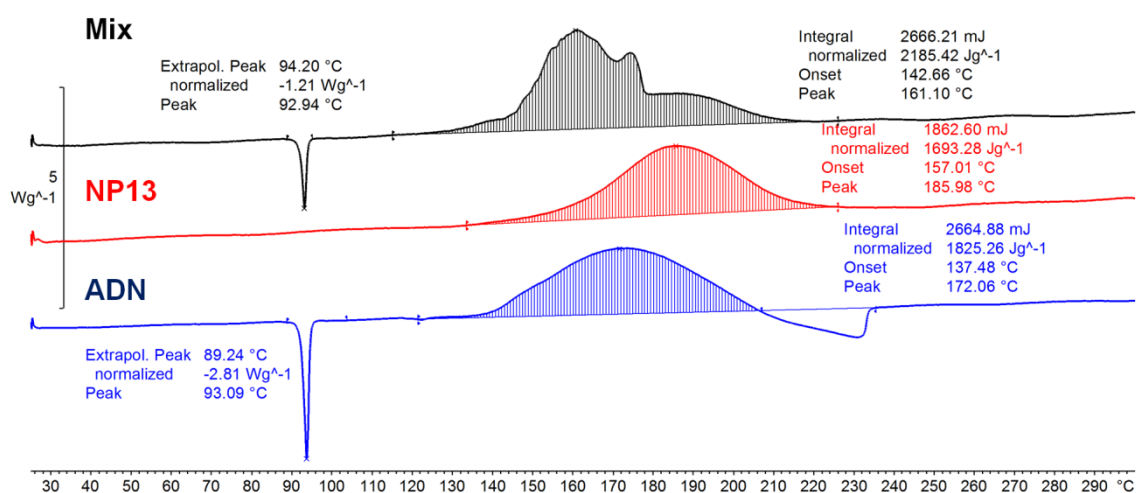


Figure 6.13 DSC thermograms of ADN (blue line), NP13 (red line), and a 50/50 (w/w) mixture (black line) from 30 to 300 °C (1 mg, 2 °C min⁻¹, aluminium crucible).

KClO₃ consistently melted at 303 °C (Figure 6.13, blue curve). The mixture displayed the same endotherm at 305 °C, as well as a shoulder in the very sharp exotherm (Figure 6.13, black curve). The data suggested these two compounds are highly compatible, as seen for the analogous experiments with IP19.

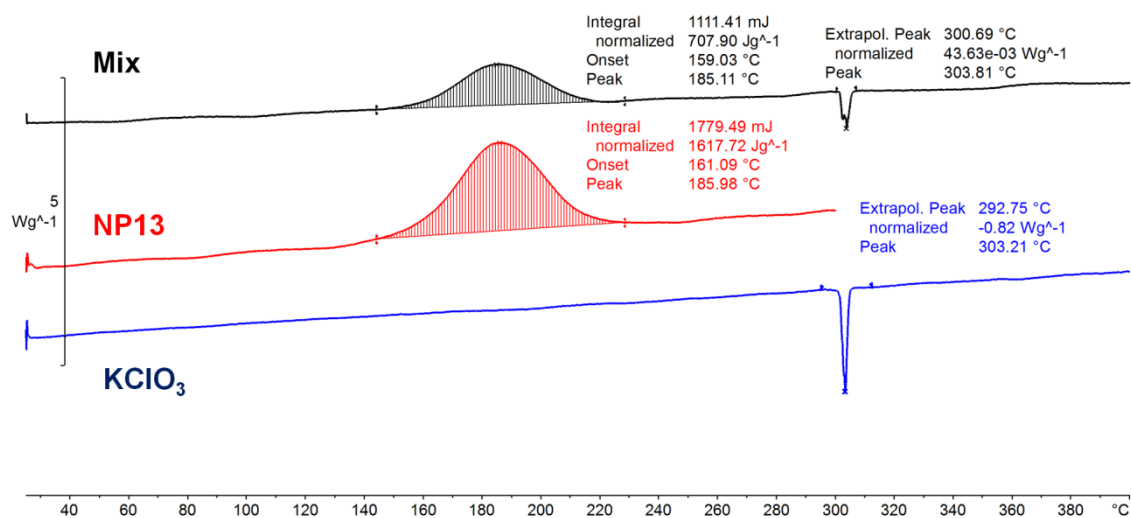


Figure 6.14 DSC thermograms of KClO₃ (blue line), NP13 (red line), and a 50/50 (w/w) mixture (black line) from 30 to 400 °C (1 mg, 2 °C min⁻¹, aluminium crucible).

KNO₃ showed no evidence of decomposition below 550 °C but melted at 335°C (Figure 6.15, blue curve). When the mixture was tested, there was no change in

the thermal profile (Figure 6.15, black curve). This indicated that the two components were compatible.

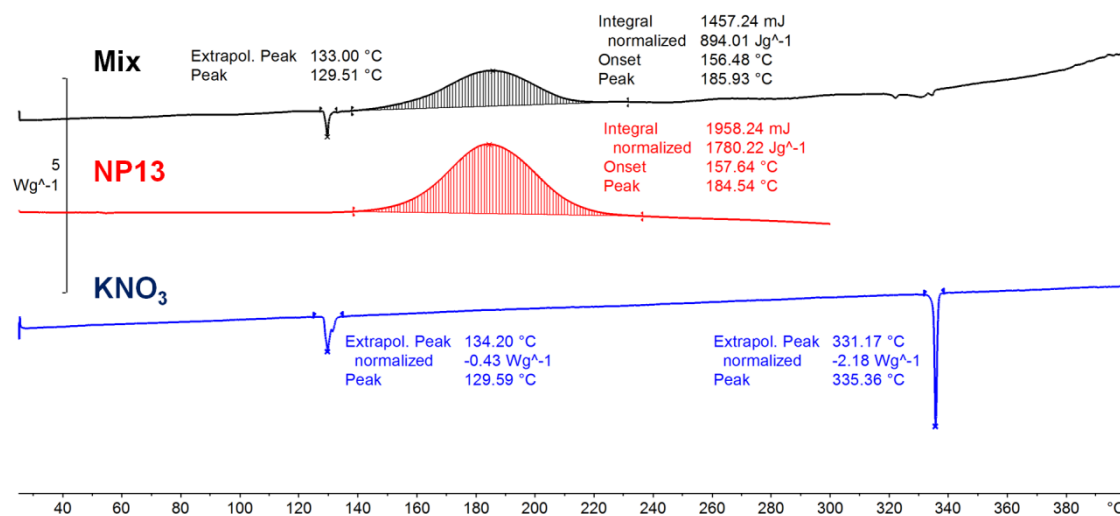


Figure 6.15 DSC thermograms of KNO₃ (blue line), NP13 (red line), and a 50/50 (w/w) mixture (black line) from 30 to 400 °C (1 mg, 2 °C min⁻¹, aluminium crucible).

NH₄ClO₄ melted at 242 °C and this property did not change in the mixture with NP13 (Figure 6.16, blue and black curves). The subsequent decomposition consisted of a main decomposition event at 264 °C followed by small exothermic peaks. The thermograms of the individual components and the mixture were comparable, suggesting the components were compatible.

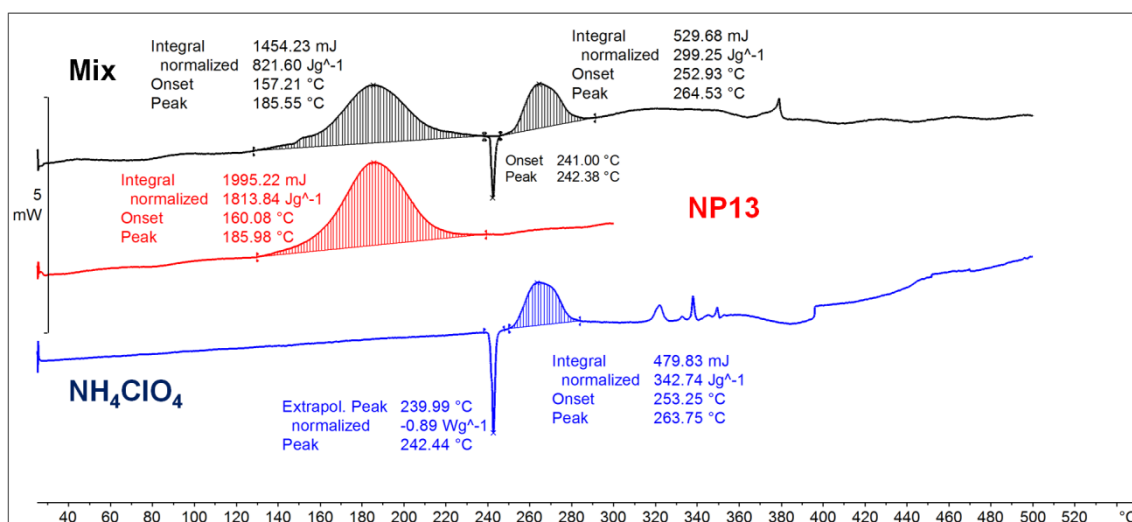


Figure 6.16 DSC thermograms of NH₄ClO₄ (blue line), NP13 (red line), and a 50/50 (w/w) mixture (black line) from 30 to 500 °C (1 mg, 2 °C min⁻¹, aluminium crucible).

NH_4NO_3 displayed an endothermic peak at 67 °C (Figure 6.15, blue curve) but this disappeared in the mixture (Figure 6.17, black curve). Furthermore, the endotherm at 265 °C (caused by the evaporation of NH_4NO_3) led to a strong exothermic event at 208 °C. This may have been caused by a reaction between the NH_4NO_3 vapour and the binder NP13, indicating that the two components are likely to be incompatible.

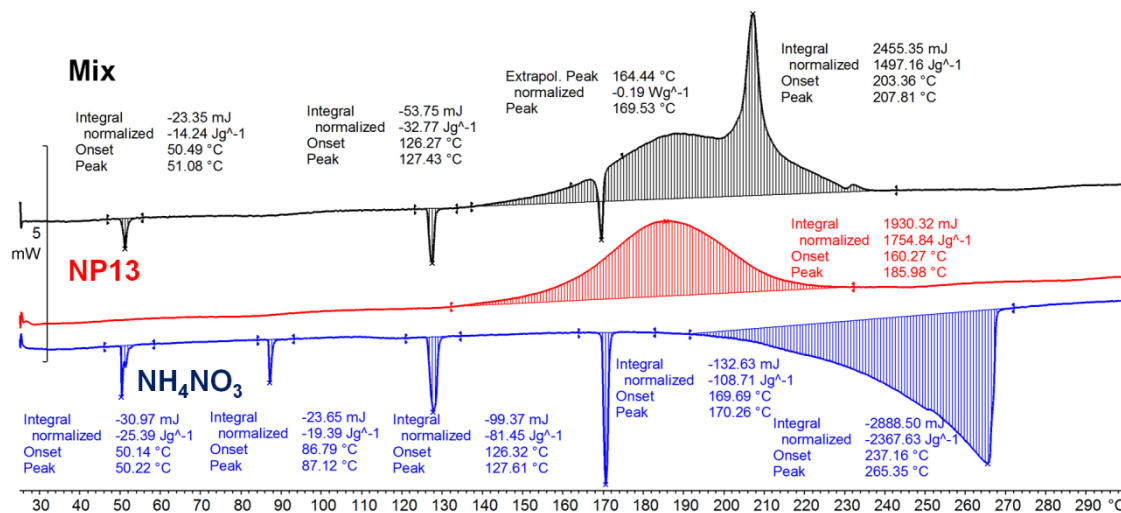


Figure 6.17 DSC thermograms of NH_4NO_3 (blue line), NP13 (red line), and a 50/50 (w/w) mixture (black line) from 30 to 300 °C (1 mg, 2 °C min⁻¹, aluminium crucible).

The decomposition of the mixture of RedP and NP13 differed very slightly from the individual components due to the drop in the baseline (Figure 6.18). The first RedP decomposition event shifted from 400 to 404 °C, whereas the second shifted from 492 to 481 °C. Despite the changes in the mixture, it is unlikely that any in-service munition containing these two components would reach such temperatures. Therefore, the components can be considered as compatible.

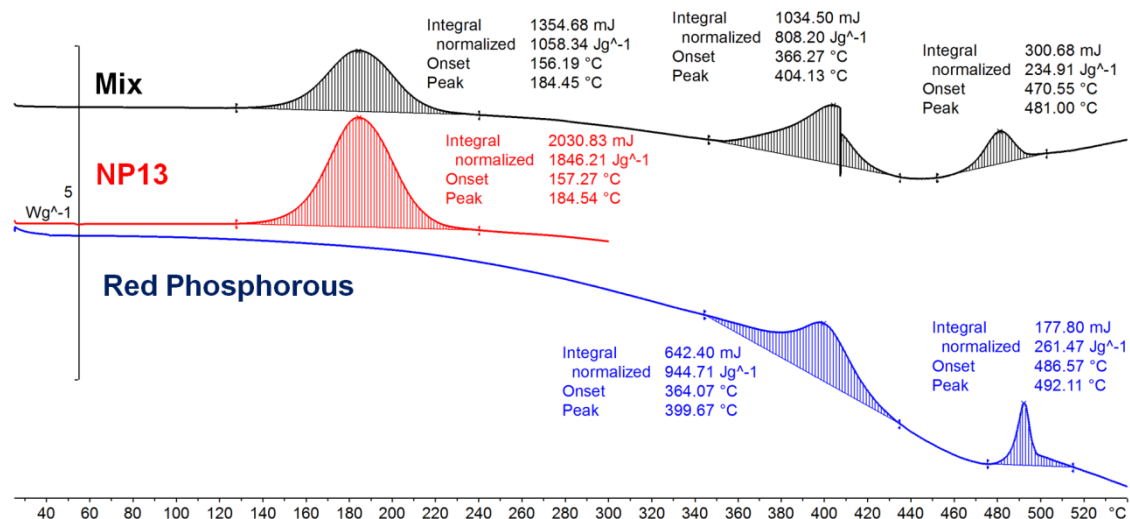


Figure 6.18 DSC thermograms of RedP (blue line), NP13 (red line), and a 50/50 (w/w) mixture (black line) from 30 to 550 °C (1 mg, 2 °C min⁻¹, aluminium crucible).

The pure DPA stabiliser melted at 54 °C (Figure 6.19, blue curve) and this did not change in the mixture (Figure 6.19, black curve). Evaporation of the DPA from the pin hole in the crucible commenced as soon as the sample was heated above 100 °C due to the flow of nitrogen in the experiment. The development of vapours caused the early decomposition of NP1, from 157 to 130 °C. The DPA was not gassed away from the nitrogen purge when the crucible was sealed. The mixture was tested with sealed and unsealed vessels and the thermograms were identical, confirming that the evaporation of DPA causes NP1 to decompose at a lower temperature. This means that the DPA vapour does not stabilise NP1 but actually accelerates its decomposition.

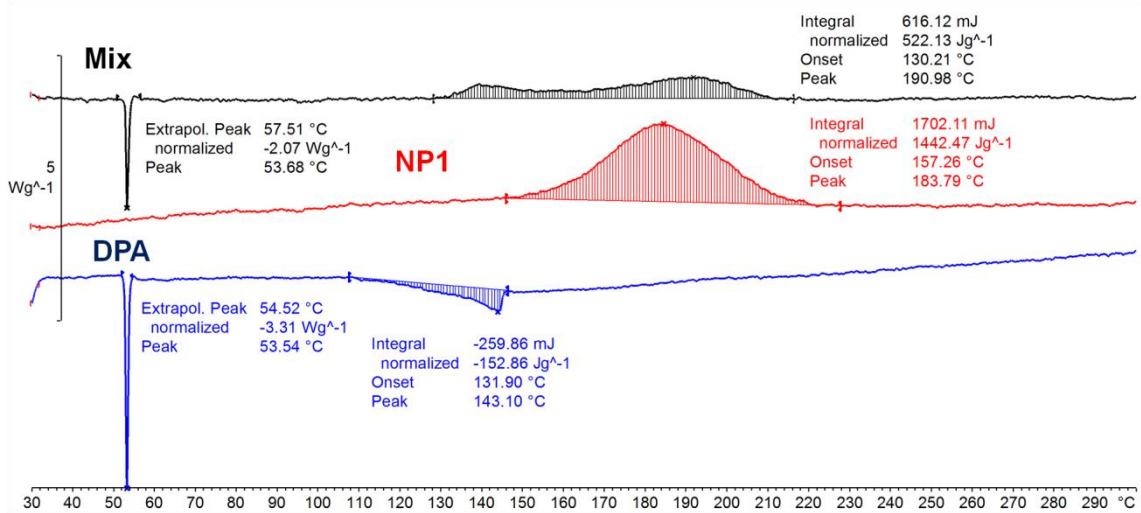


Figure 6.19 DSC thermograms of DPA (blue line), NP1 (red line), and a 50/50 (w/w) mixture (black line) from 30 to 300 °C (1 mg, 2 °C min⁻¹, aluminium crucible).

The 2,4-NDPA melted at 157 °C (Figure 6.20, blue curve) and the same melting peak was also present in the mixture (Figure 6.20, black curve). Unlike DPA, the 2,4-NDPA was found to stabilise NP1, shifting the degradation of the binder from 184 to 190 °C.

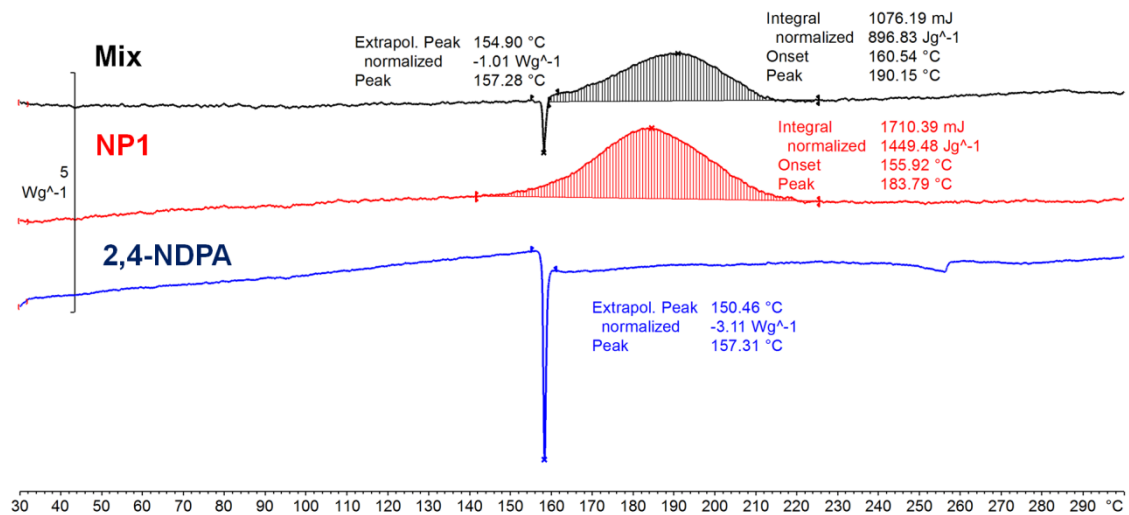


Figure 6.20 DSC thermograms of 2,4-NDPA (blue line), NP1 (red line), and a 50/50 (w/w) mixture (black line) from 30 to 300 °C (1 mg, 2 °C min⁻¹, aluminium crucible).

Centralite melted at 73 °C (Figure 6.21, blue curve) and this did not change when it was mixed with NP1 (Figure 6.21, black curve). Centralite also evaporated in the temperature range 130–154 °C, as observed above for DPA.

A second test with sealed crucibles showed no change in the thermogram of the mixture. Therefore, the degradation of the binder was not affected by the presence of Centralite, making it a suitable stabiliser.

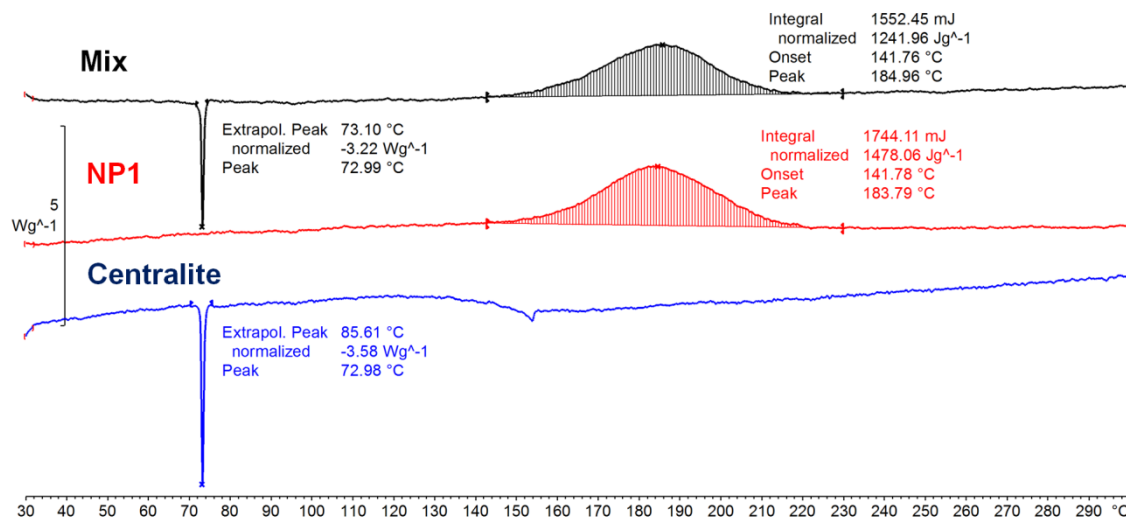


Figure 6.21 DSC thermograms of Centralite (blue line), NP1 (red line), and a 50/50 (w/w) mixture (black line) from 30 to 550 °C (1 mg, 2 °C min⁻¹, aluminium crucible).

6.3 Hazard tests – βNCXCDs

The new energetic βNCXCDs were characterised using internal hazard tests at Cranfield Defence and Security School to determine the conditions under which the energetic binders are likely to ignite. Two sets of small-scale (20 mg) hazard tests were performed using two different types of βNCXCDs.

The first set of tests was carried out on insoluble nitrated products synthesised from insoluble βCDTCD and βCDPCD precursors, containing TEG and PEG units respectively. These experiments are described in the appendix: samples NT1–NT5 (Table A 5) and samples NP13–NP15 (Table A 4).

The second set of tests was carried out on acetone-soluble βNCPCD samples NP1, NP5, NP6 and NP16–NP17 (Table 6.3). These were synthesised from βCPCDs with PEG:βCD ratios > 3.5:1, and their softness makes them promising in terms of processability. Sample NP16, with a low PEG:βCD ratio of 2.6:1 was characterised as well as βNCD to determine any increase in hazards

caused by the crystalline structure (Table A6). The following tests were performed:

- Impact and friction sensitivity test;
- Colour change tests to assess thermal stability;
- Temperature ignition test to assess combustion properties.

Materials which clearly failed these tests were considered too hazardous for manual handling and were not considered further. These tests were not standardised methods to characterise the energetic properties of a material, but were carried out to provide a degree of confidence in handling before full Energetic Materials Testing and Assessment Policy (EMTAP) tests on a larger scale. The test results are summarised in Table 6.3.

Table 6.3 Preliminary small-scale compatibility tests performed on β NCTCDs and β NCTCDs containing TEG and PEG units, respectively.

Sample	Polyethylene glycol: β CD feed ratio ¹	Colour change RT 24 h	Colour change 100 °C 30 min	Impact (GO)	Friction	Ignition ⁴	Evaluated ⁵
β NCD	-	No change	Browning	7/10	No response	HVB	Hazardous
NP13	6:1	No change	Browning	2/10	No response	HVB	Hazardous
NP15	9:1	No change	Browning	0/10 (smell)	No response	VB ⁴	Not hazardous
NP16	3:1	No change	Browning	3/10	No response	HVB ²	Hazardous
NP5	5:1	No change	Browning ²	0/10	No response	VB	Not hazardous
NP6	5:1	No change	Browning ²	0/10	No response	VB	Not hazardous
NP17	5:1	No change	Browning ²	0/10	No response	VB	Not hazardous
NP1	5:1	No change	Browning ²	0/10	No response	VB	Not hazardous
NT1	9:1	No change	Browning	0/10	No response	VB	Not hazardous
NT2	9:1	No change	Browning	0/10	No response	VB	Not hazardous
NT3	9:1	No change	Browning	0/10	No response	VB	Not hazardous
NT4	9:1	No change	Browning	0/10	No response	VB	Not hazardous
NT5	9:1	No change	Browning	0/10	No response	VB	Not hazardous

1. Feed ratio of cross-linker TEGDGE or PEGDGE, as appropriate to β CD.
2. The compound softened when heated.
3. HVB - Highly vigorous burning, similar to the ignition of a match.
4. VB - Vigorous burning, like the flame of a candle.

5. Assessed by CDS experts.

Colour change test

A colour change generally indicates that a decomposition reaction occurs (Table 6.3). The effect of temperature on the colour of each compound was assessed using two methods. In the first method, 20 mg of each sample was heated to 100 °C and maintained at this temperature for 30 min. In the second method, the samples were left at room temperature for 24 h. Samples NP1, NP5, NP6 and NP13–17 displayed a change in viscosity when heated to 100 °C, as anticipated from their thermal profiles. In contrast, the viscosity of the insoluble gels NT5–NT8 did not change as the temperature increased. All the samples became slightly brown during the test reflecting the decomposition of the nitroesters to form NO_x, which was adsorbed by the samples. The inert precursor IP19 (PEG:βCD ratio = 4.0) was also heated to exclude the possibility that browning reflected the caramelisation of the βCD or the ageing of the PEG segments in the cross-linked system. IP19 showed no signs of browning after 30 min, but browning was observed when this inert sample was kept at 100 °C for 24 h.

Impact and friction test

The impact and friction sensitivity of insoluble gels NT5–NT10 and NP15, and acetone-soluble samples NP1, NP5, NP6 and NP13–NP17 was assessed using the steel-on-steel mallet test (Table 6.3). The detection of smell, flash or sound was left to the judgment of an operator trained for the test. This determined whether the compound was recorded as *go* (decomposition detected) or *no-go* (no decomposition detected). The βNCD control was quite susceptible to impact (7/10 *go*) whereas almost all of the synthesised compounds showed no evidence of decomposition, the exceptions being samples NP13, NP15 and NP16. This was attributed to the purification method, which left traces of acid, and the low degree of cross-linking of these products. However, the three sensitive samples showed evidence of a localised initiation that did not consume the entire sample mass. The soft samples (NP1, NP5, NP6 and NP17) were not sensitive to impact but underwent deformation due to the

impact itself of the heat thus generated, confirming the softness of these compounds.

Ignition test

The samples were burnt over an open flame and the energy of the flame was qualitatively described to evaluate the susceptibility of the compound to burning. Fast burning refers to a type of combustion that is often compared to the ignition of a safety match, and vigorous burning is like the flame produced by wood burning. As expected from the earlier hazard tests, samples NP13, NP16 and β NCD burnt more vigorously than the others, with a sparking flame. The intensity of the ignition was directly dependent on the Ω value of the compound, with the less cross-linked compounds (less rich in carbon chains) burning more vigorously.

6.3.1 EMTAP tests

The EMTAP tests described below followed the certificated methods presented in the *EMTAP Manual of Tests*, which sets the British Standards relevant to the qualification of energetic materials and associated technical assessments [119]. Each test is based on the repetition of several forms of analysis to increase confidence in the result. The Rotter impact test (Test No. 1A) and electrostatic discharge (ESD) test (Test No. 4) were performed on sample NP17 (Table 6.4). Due to the large quantity of sample required and the safety restrictions applied at Cranfield University, the NP17 sample was obtained by dissolving and blending in acetone the products of four nitration reactions at the 2.5-g scale (Table A 6) using a precursor with a PEG: β CD ratio of 3.8:1. The resulting blend passed the small-scale tests described above and was considered safe for EMTAP testing. Given the properties of the sample, the material was soft and malleable, making it a promising candidate for future processing. Further work is needed to collect more data for the scaled-up manufacturing of this compound and to increase confidence in the assessment of its sensitivity.

Table 6.4 EMTAP test data for sample NP17 based on Rotter impact and ESD values.

Energetic sample	Impact by drop-weight input (cm)¹	ESD² 4.5 J
NP17	29.3	0/50

1 Impact value is the mean of 50 tests.

2 ESD value is the mean of 50 tests at 4.5 J.

The Rotter impact test indicated a figure of insensitiveness (Fol) of 29 for NP17 with a release of 1 mL gas per test. The initiated samples were not completely consumed, indicating a localised initiation as seen in the small-scale tests described above.

The Fol value indicated that the compound was highly sensitive to impact, given that sensitive compounds have values in the range $100 \geq \text{Fol} \geq 30$, and initiators have Fol values < 30 . Dry β NCD has an Fol value of 60 [114] but this value is not comparable to the Fol of NP17 described here because it was based on the results of an impact test conducted under American standards that differ from the British system. Furthermore, the Fol value reported for a similar epichlorohydrin: β CD cross-linked nitrated product was 47 [109]. The values determined in the Rotter impact test therefore provide an indication of the potential sensitivity of NP17 but should not be considered conclusive. The test is affected by several factors, including the homogeneity of the blend and the presence of impurities. Given that this was the first attempt to synthesise a significant quantity of the nitrated product, more tests are required to achieve a confident result.

The ESD test (spark sensitivity test) determines the sensitivity of a sample to initiation by electrostatic discharges. NP17 was not susceptible to ESD up to an energy input of 4.5 J, which is a significant improvement compared to β NCD, which initiates at 0.0125 J [114], and the epichlorohydrin: β CD cross-linked nitrated product discussed above, which initiates at 0.1288 J [109].

6.4 Stability of β NCXCDs determined by heat flow calorimetry

The single-temperature stability test is a standardised technique in STANAG 4582 that uses heat flow calorimetry (HFC) to determine the shelf life of energetic formulations [139]. The test was repurposed in this project as a method to obtain indicative data about the lifetime thermal stability of β NCXCDs.

Four lots (~1 g) of sample NP1 were prepared, with a PEG: β CD ratio of 4:1. One lot was kept pure, and the others were mixed with one of three stabilisers (DPA, 2,4-NDPA or Centralite) as a 1% w/w formulation. A sample of pure (non-stabilised) NC with a nitrogen content of 12.6% was used as benchmark.

The heat flow from of the samples was measured at a constant temperature of 80 °C. At this temperature, the STANAG criterion is that the sample should have a heat flow less than a tabulated value of 114 $\mu\text{W g}^{-1}$ (Figure 6.22, dashed line) for a time of 10.6 days, in order to be defined as stable. The heat flow is recorded after the release of the first 5 J of energy. Therefore, the thermograms do not present the initial stabilisation of the temperature when the samples are introduced in the machine. The results are summarised in Figure 6.22.

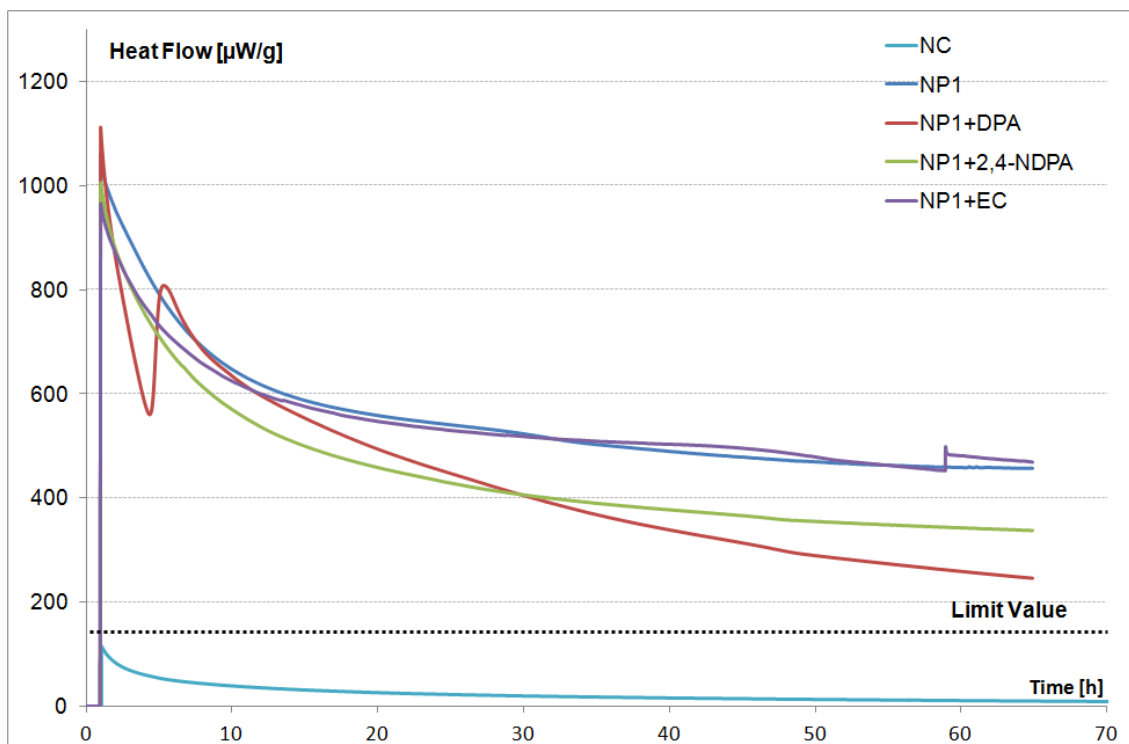


Figure 6.22 Thermal stability of pure NP1 and the same compound in the presence of three different stabilisers (1% w/w).

The experiment was automatically halted after 70 h by the safety control of the HFC instrument due to the high heat flow values that were registered. All samples containing the energetic binder NP1 were unstable throughout the recording (Figure 6.22). The heat flow from NC was lower than the limit value of $114 \mu\text{W g}^{-1}$ (light blue curve). The viscous consistency of the sample is thought to influence its stability because gaseous and liquid materials decompose more quickly than crystalline solids [141,142]. The air and moisture trapped in the spongy matrix of the samples, as well as that in the head space of the vials, probably accelerated the decomposition, as reported for other nitroesters [140].

The highest heat flow was recorded for the pure NP1 sample. The presence of a stabiliser reduced the heat flow during decomposition, indicating that NP1 can be stabilised. Interestingly, DPA reduced the heat flow particularly during the first 4 h, but this was followed by an increase at ~ 4.5 h probably reflecting the consumption of the stabiliser. Despite the consumption of the DPA, a residual stabilising effect was observed, probably conferred by DPA nitro-derivatives,

which include 2,4-NDPA in the latter stages of decomposition [143]. This explains why DPA has a greater stabilising effect than 2,4 NDPA alone.

The addition of Centralite did not influence the stability of the binder, as shown by the similar heat flow curves over time with and without this additive. It would be interesting to determine the quantity of stabiliser remaining throughout the experiment, but the specialised chromatography technique required for this type of experiment was not available [139]. However, the samples were analysed before and after testing by ¹H-NMR spectroscopy, which showed that the stabilisers decomposed during the experiment (Figure A 10, Figure A 11 and Figure A 12). The aged samples were also thermally characterised by DSC. The T_{dec} was not significantly changed following exposure to a constant temperature of 80 °C for 3 days under HFC testing conditions (Table 6.6). The presence of stabilisers slightly improved the stability of NP1, increasing the T_{dec} marginally compared to the pure sample, but the variations were small and within the range of experimental error.

Table 6.5 DSC analysis of the decomposition temperatures of sample NP1 before and after HFC tests.

Sample	T_{dec} before HFC tests (°C)	T_{dec} (after 3 days at 80 °C) (°C)
NP1	195	195
NP1/DPA	198	197
NP1/2,4-NDPA	198	196
NP1/Centralite	198	195

6.5 Conclusion

Energetic β NCXCDs were characterised by compatibility, hazard and stability tests to determine their suitability for energetic applications. Most of the studies were performed on the β NCPCD derivatives containing PEG segments because these had superior mechanical properties making them potentially suitable for

industrial exploitation. The compatibility studies determined whether the binder was likely to initiate unwanted reactions among the other constituents.

The β CPCDs and β NCPCDs behaved similarly in the tests. They were compatible with several pyrotechnic ingredients such as KClO_3 , KNO_3 and NH_4ClO_4 , as well as explosives such as HMX and PETN. A degree of incompatibility of both inert and nitrated compounds was observed with RDX, possibly due to the size of the nitramines, which were small enough to be encapsulated within the β CD macrocycles. Centralite was also compatible with the energetic β NCPCDs, but DPA reduced the T_{dec} of the binder by 44 °C (specifically when the DPA evaporated at 143 °C) suggesting that DPA vapours are incompatible with the binder.

Small-scale hazard tests were performed on a set of the new energetic binders differing in terms of their cross-linker ratio. The most malleable β NCPCD compounds (PEG: β CD ratio > 3.0) were insensitive to impact and friction with a mallet. In contrast, samples with PEG: β CD ratios < 3.0 were susceptible to impact due to the low cross-linker content and thus greater crystallinity. All the compounds underwent a colour change when left at 100 °C for 30 min. At this temperature, the nitroesters undergo rapid thermal cleavage to form NO_x molecules that are adsorbed into the matrix of the compound.

A highly cross-linked β NCPCD product (PEG: β CD ratio = 3.8:1) was subjected to EMTAP tests for impact and ESD resistance. The recorded Fol value of 29 indicated that the nitrated products can be sensitive to impact, but the same sample was insensitive to ESD stimuli up to 4.5 J, which is a considerable improvement.

HFC-based stability tests were performed on the soft nitrated compound NP1, either in pristine form or mixed with 1% (w/w) of one of three different stabilisers (DPA, 2,4-NDPA or Centralite). The results indicated that the softer compounds were unstable when incubated at 80 °C for 3 days even in the presence of stabiliser, with heat flow exceeding 200 $\mu\text{W g}^{-1}$. The inherent viscosity of these materials is thought to accelerate the degradation of the nitroester groups. The

T_{dec} of the samples did not change significantly after the HFC tests, although DPA showed a stronger stabilising effect on the β NCXCDs.

7 Conclusion and recommendations

Conclusions

This PhD project has contributed to the development of new inert and energetic binders for energetic applications. The function of the binder is to hold together the constituents of an energetic formulation, improving its response to external stimuli and, when possible, contributing to the energy of the system. The project focussed on the use of β CD, a cyclic polysaccharide that has been investigated as a drug delivery vehicle due to its ability to envelop guest molecules. The design and synthesis of a set of inert and nitrated cross-linked β CD systems was achieved by the cross-linking of β CD with diglycidyl ethers containing a variety of polyethylene glycol units followed by a nitration reaction.

Three polyethylene glycol diglycidyl ethers (TEGDGE, HEGDGE and PEGDGE, containing three, six and an average of nine ethylene glycol units, respectively) were used to generate β CXCD products containing TEG, HEG or PEG segments. The abbreviation XEG is used to describe these segments collectively.

The cross-linkers were used to tune the properties of β CD and generate malleable cross-linked β CXCD compounds suitable for processing. The investigation focused on the optimisation of the cross-linking reaction, which was strongly affected by several factors including NaOH concentration and volume, reaction time, temperature, β CD alkoxide formation, cross-linker: β CD feed ratio, and the addition rate of the cross-linker in the β CD alkoxide solution.

The optimal experimental conditions for the cross-linking of β CD were investigated extensively using PEGDGE as the cross-linker due to its low cost and commercial availability. Cross-linked β CPCD products that were insoluble in water and other common solvents were produced using PEGDGE: β CD feed ratios higher than 5:1. The optimal conditions were a PEGDGE: β CD ratio of up to 5:1, 5.6% NaOH aqueous solution, 16 h to form the β CD alkoxide, 20 min for the addition of the cross-linker, and 6 h reaction time at 30 °C. Under these conditions, several β CPCDs containing different quantities of PEG units were

synthesised. The same procedure was then adopted for the synthesis of the other β CXCD systems. The products were characterised by $^1\text{H-NMR}$ and FTIR spectroscopy, confirming the polymeric nature of the β CXCDs. In all trials, up to 25% of the cross-linker was consumed in a parallel degradation reaction resulting in a lower XEG: β CD ratio in the products compared to the feed ratio. The XEG: β CD ratio in the β CXCDs was determined by $^1\text{H-NMR}$ in D_2O . The length of the XEG segments and the degree of cross-linking influenced the physical appearance of the β CXCDs. Samples with PEG: β CD ratios between 4:1 and 3:1 were malleable whereas those with PEG: β CD ratios below 3:1 were friable. Samples containing TEG units were friable and easy to dissolve regardless of the TEG: β CD ratio. Also, β CXCDs containing HEG and PEG units took longer to dissolve if the XEG: β CD ratio was higher than 3.4:1, as determined by $^1\text{H-NMR}$ spectroscopy.

As expected from the design of the materials, the thermal and thermo-mechanical properties of β CD precursors were affected by the cross-linking reaction, yielding β CXCDs with low T_g values. The softness of the β CXCD samples was directly dependent on the length of the XEG unit and the XEG: β CD ratio. Therefore, β CXCDs containing HEG and PEG segments with a XEG: β CD ratio exceeding 3.7:1 were characterised by T_g values as low as -20 °C. No glass transition was observed for the β CXCDs with few cross-links or for those containing TEG segments.

Cracking was observed in β CXCD samples cooled below their T_g during DMA experiments due to strong interactions with the metallic supports via hydrogen bonds. This was also confirmed by optical microscopy using glass supports. The β CXCDs demonstrated accelerated healing when heated above room temperature, much like the healing properties of hydrogels containing PEG and β CD segments, which are used in pharmaceutical applications.

The research project then focused on the synthesis and characterisation of nitrated derivatives of β CXCDs, aiming to improve the binder's contribution to the energy of the formulation. The nitration reaction with fuming nitric acid yielded two sets of β NCXCDs differing in terms of their solubility in water and

other organic solvents, and properties correlated to the physicochemical characteristics of the β CXCD precursors. Insoluble β CXCD systems yielded cross-linked derivatives with various degrees of nitration that were insoluble in acetone, whereas water-soluble β CXCD precursors produced β NCXCDs that were soluble in acetone and easy to characterise and process. A purification method adopted from the NC manufacturing process removed acid traces from the nitration reaction more efficiently, stabilising the compound during storage.

The β NCXCDs were characterised by $^1\text{H-NMR}$ and FTIR spectroscopy to determine the degree of nitration, which was found to be dependent on the nitration reaction time, the length of the cross-linker and the cross-linker: β CD feed ratio. This was confirmed by measuring the nitrogen content of the products. The more soluble products generally featured a lower degree of nitration.

The thermal stability of β NCXCDs ($T_{\text{dec}} = 190\text{--}200\text{ }^\circ\text{C}$) was independent of the length of the XEG unit and the XEG: β CD ratio whereas the ΔH_{dec} of each system ($1300\text{--}2100\text{ J g}^{-1}$) was dependent on the length of the XEG segment.

The β NCXCDs retained a certain degree of softness from their β CXCD precursors with T_g values in the range -14 to $+65\text{ }^\circ\text{C}$. The higher T_g values probably reflected the higher polarity of the system, which increases the cohesive energy of the compounds and inhibits the mobility of the XEG chains. One β NCXCD product containing PEG units retained the self-healing ability of its precursor after 4 h at room temperature.

The suitability of β NCXCDs as binders in energetic formulations was determined by conducting compatibility, hazard and stability tests using NATO STANAG and EMTAP protocols. Most of these studies were performed on the β NCPCD derivatives containing PEG segments. The compatibility studies determined the likelihood that the binder would initiate undesirable reactions in the other constituents of the energetic formulations.

Both β CPCD and β NCPCD behaved similarly when tested and were found to be compatible with several pyrotechnic ingredients (including KClO_3 , KNO_3 and

NH₄ClO₄) as well as explosives such as HMX and PETN. The degree of incompatibility determined for RDX, needs further investigation. The different behaviour of mixtures containing HMX and RDX was attributed to the difference in the size of these energetic nitramines, promoting different interactions with the cavities of βCPCDs and βNCPCDs. Only Centralite was compatible with the energetic βNCPCD binders among three common stabilisers used with nitroesters

Small-scale laboratory hazard tests performed on a set of βNCPCD binders with different degrees of cross-linking showed that the most malleable compounds were insensitive to impact and friction with a mallet, but reducing the degree of cross-linking increased their sensitivity to impact. All the compounds changed colour when left for 30 min at 100 °C suggesting they produced NO_x which was subsequently absorbed.

A highly cross-linked βNCPCD sample was found to be sensitive to impact (Fol = 29) but insensitive to ESD stimuli up to 4.5 J. The ESD test result is very significant because nitrated βCD is highly sensitive to ESD (0.0125 J) and the low sensitivity of βNCPCDs indicates they could be promising as a new generation of energetic binders.

Stability tests indicated that softer βNCPCD compounds are unstable when placed at 80 °C for 3 days even in the presence of a stabiliser. This may be due to the inherent viscosity of these materials, which is thought to speed up the degradation of the nitroester groups.

In conclusion, the new inert and nitrated βCD-based binders designed and developed during this PhD project offer a promising alternative to current binders for energetic formulations. The greatest strengths of the project are the use of an environmentally sustainable βCD precursor, the absence of flammable organic solvents in the synthesis method, and the easy synthesis and processability of the inert and energetic products. The highlight of the nitrated derivatives is their insensitivity to ESD at values up to 4.5 J compared to the low value of 0.12555 J for similar compounds reported in literature.

Notably, an inert β CPCD derivative with a PEG: β CD ratio of 3.7:1 is now being exploited by BAE Systems in Glascoed as a potential alternative to NC in propellant formulations.

Recommendations

The scope for future work in the area covered by this PhD project is considerable. Areas worthy of further investigation include, but are not limited to:

1. Investigating the inclusion properties of β CXCDs, which are widely exploited in pharmaceutical research because they can change the physical properties of encapsulated materials. These tests could help to optimise the manufacturing process for energetics containing β CXCDs and their nitrated derivatives. The characterisation of Mw during this project was not ideal due to the limited resources available for this task. Studying the Mw of the products should be extended to determine the effect of the reaction conditions and the consistency of the properties in each trial. GPC/MALDI-TOF (matrix-assisted laser desorption/ionisation time of flight) mass spectrometry could also be applied to confirm the results of the GPC/refractive index studies with the β CXCDs.
2. The phenomenon of thermal healability looks interesting for manufacturing purposes and further investigations of the healing process are needed to determine the degree of healing inherited by the formulations.
3. Curing is another step towards the manufacturing of energetic devices. Appendix A1 describes the first attempted curing experiments in the project to obtain polymer-bonded explosive (PBX) formulations from the remaining free hydroxyl groups in the β CXCDs, although the results are still preliminary.
4. Scaling up the formulations even further (500 g mixes) and investigating the effects of plasticisers, filler particle size distributions and automated mixing

processes on the mechanical properties and sensitivity of pressed/cast PBX pellets.

5. Further compatibility testing is necessary to determine the differences in compatibility between the β CXCDs and β NCXCDs when the XEG: β CD ratio varies. In addition, compatibility with nitroglycerine and NC should be assessed.
6. All forms of analysis should be extended to the level of triplicates in order to increase confidence in the results.
7. Scaling up the synthesis of the energetic derivatives for EMTAP tests should be extended to all compounds in order to correlate the mechanical characteristics and hazard properties of the β NCXCDs. In addition, hazard tests should be extended to real formulations to determine the suitability of the binders for real-world applications.
8. Stabilisation studies were performed on only one β NCXCD compound. Stability tests should be extended to obtain data for all the compounds synthesised in the project, to determine how the rheology of the products affects their stability.

The starting material was β CD cyclodextrin because it is less expensive than γ CD. However, the studies performed with β CD should be replicated with γ CD so that the complexation of energetic molecules with this larger macrocycle can be exploited.

REFERENCES

1. Raymond L Beaugard. The History of Insensitive Munitions. <http://www.insensitivemunitions.org/history/preface/>
2. Akhavan J. Chemistry of Explosives. Chemistry of Explosives. 2004. pp. P001–P004. DOI:10.1039/9781847552020
3. NATO - STANAG 4439 - POLICY FOR INTRODUCTION AND ASSESSMENT OF INSENSITIVE MUNITIONS (IM). 2018.
4. DEPARTMENT OF DEFENSE., TEST METHOD STANDARD. MIL-STD-2105 C HAZARD ASSESSMENT TESTS NON-NUCLEAR MUNITIONS. 2003.
5. Smith P. Coating Technologies for Insensitive Munitions. 2006.
6. Madsen T., DeFisher S., Baker EL., Suarez D., Al-Shehab N., Wilson A., et al. Explosive venting technology for cook-off response mitigation. 2010.
7. Peterson NR., Sweitzer JC. Composite Material Particle Impact Mitigation Sleeve Testing. Procedia Engineering. Elsevier; 1 January 2015; 103: 475–481. DOI:10.1016/J.PROENG.2015.04.062
8. Sharp M., Sloan M. Active Passive Mitigation Devices S3 Assessment.
9. G. G. Ang; Pisharath Sreekumar., Ang HG., Pisharath S. Energetic Polymers - Binders and Plasticizers for Enhancing Performance. Energetic Polymers - Binders and Plasticizers for Enhancing Performance. Wiley-VCH; 2012. 510 p. DOI:10.1002/prop.201280003
10. Fakirov S. Fundamentals of Polymer Science for Engineers. Weinheim, Germany: Wiley-VCH Verlag GmbH & Co. KGaA; 2017. DOI:10.1002/9783527802180
11. Ebewele RO. Polymer science and technology. CRC Press; 2000. 483 p.
12. Guo Q. Polymer morphology : principles, characterization, and processing.
13. Kavesh S., Schultz JM. Meaning and measurement of crystallinity in polymers: A Review. Polymer Engineering and Science. John Wiley & Sons, Ltd; 1 November 1969; 9(6): 452–460. DOI:10.1002/pen.760090612
14. Peters EN. Thermoplastics, Thermosets, and Elastomers-Descriptions and Properties. Mechanical Engineers' Handbook. Hoboken, NJ, USA: John Wiley & Sons, Inc.; 2015. pp. 1–48. DOI:10.1002/9781118985960.meh109
15. Tadmor Z., Gogos CG. Principles of polymer processing. Wiley-Interscience; 2006. 961 p.
16. McKeen LW. The effect of creep and other time related factors on plastics and elastomers. W. Andrew; 2009. 406 p.
17. Sanghavi RR., Asthana SN., Karir JS., Singh H. Studies on thermoplastic elastomers based RDX-propellant compositions. Journal of Energetic Materials. Taylor & Francis Group ; January 2001; 19(1): 79–95. DOI:10.1080/07370650108219393
18. Cooper PW. Explosives engineering. VCH; 1996. 460 p.

19. Junisbekov TM., Kestelman VN., Malinin NI. Stress Relaxation in Viscoelastic Materials. Science Publishers; 2003. 1-82 p.
20. G. G. Ang; Pisharath Sreekumar. Polymers as Binders and Plasticizers - Historical Perspective. Energetic Polymers - Binders and Plasticizers for Enhancing Performance. 2012. 510 p. DOI:10.1002/prep.201280003
21. Bohn M a. NC-based energetic materials - stability , decomposition , and ageing. Nitrocellulose - Supply, Ageing and Characterisation. 2007;
22. Agrawal J. High energy materials. 2010. 495 p. DOI:10.1002/9783527628803
23. Laboratory & RCRA Group Los Alamos. Waste Explosives Treated by Open Detonation at Los Alamos.
24. Persson P-A., Holmberg R., Lee J. Rock blasting and explosives engineering. CRC Press; 1994. 540 p.
25. Ang HG., Pisharath S. Energetic polymers: binders and plasticizers for enhancing performance. Wiley-VCH; 2012. 218 p.
26. NPFC - MIL-DTL-244 - NITROCELLULOSE | E. 2014.
27. Saunders CW., Taylor LT. A review of the synthesis, chemistry and analysis of nitrocellulose. Journal of Energetic Materials. Taylor & Francis Group ; September 1990; 8(3): 149–203. DOI:10.1080/07370659008012572
28. Pourmortazavi SM., Hosseini SG., Rahimi-Nasrabadi M., Hajimirsadeghi SS., Momenian H. Effect of nitrate content on thermal decomposition of nitrocellulose. Journal of Hazardous Materials. 15 March 2009; 162(2–3): 1141–1144. DOI:10.1016/j.jhazmat.2008.05.161
29. Sutton E. From polymers to propellants to rockets - A history of Thiokol. 35th Joint Propulsion Conference and Exhibit. Reston, Virginia: American Institute of Aeronautics and Astronautics; 1999. DOI:10.2514/6.1999-2929
30. Hendel., J. F. Review of solid propellants for space exploration. 1 October 1965;
31. Cesaroni AJ. US 6,740,180 B1: Thermoplastic polymer propellant compositions. US: United States Patent and Trademark Office; 2004.
32. Salazar MR., Kress JD., Lightfoot JM., Russell BG., Rodin WA., Woods L. Low-temperature oxidative degradation of PBX 9501 and its components determined via molecular weight analysis of the Poly[ester urethane] binder. Polymer Degradation and Stability. December 2009; 94(12): 2231–2240. DOI:10.1016/j.polymdegradstab.2009.08.011
33. Chaturvedi S., Dave PN. Solid propellants: AP/HTPB composite propellants. Arabian Journal of Chemistry. Elsevier; 8 January 2015; DOI:10.1016/j.arabjc.2014.12.033
34. Wingborg N. Increasing the tensile strength of HTPB with different isocyanates and chain extenders. Polymer Testing. 2002; 21(3): 283–287. DOI:10.1016/S0142-9418(01)00083-6
35. Keshavarz MH., Klapötke TM. The Properties of Energetic Materials. Berlin, Boston: De Gruyter; 2017. DOI:10.1515/9783110521887

36. GOLDING P., BELLAMY AJ., CONTINI AE., DOSSI E. POLYPHOSPHAZENES. 28 December 2013;
37. Badgujar DM., Talawar MB., Zarko VE., Mahulikar PP. New directions in the area of modern energetic polymers: An overview. *Combustion, Explosion, and Shock Waves*. Pleiades Publishing; 31 July 2017; 53(4): 371–387. DOI:10.1134/S0010508217040013
38. Szejtli J. Introduction and General Overview of Cyclodextrin Chemistry. *Chemical Reviews*. 1998; 98(5): 1743–1754. DOI:10.1021/cr970022c
39. Zheng M., Endo T., Zimmermann W. Enzymatic Synthesis and Analysis of Large-Ring Cyclodextrins. *Australian Journal of Chemistry*. CSIRO PUBLISHING; 2002; 55(2): 39. DOI:10.1071/CH01189
40. Del Valle EMM. Cyclodextrins and their uses: A review. *Process Biochemistry*. 2004; 39(9): 1033–1046. DOI:10.1016/S0032-9592(03)00258-9
41. Challa R., Ahuja A., Ali J., Khar RK. Cyclodextrins in drug delivery: An updated review. *AAPS PharmSciTech*. 2005; 6(2): E329–E357. DOI:10.1208/pt060243
42. Das SK., Rajabalaya R., David S., Gani N., Khanam J., Nanda A. Cyclodextrins-the molecular container. *Research Journal of Pharmaceutical, Biological and Chemical Sciences*. 2013; 4(2): 1694–1720.
43. Redenti E., Szente L., Szejtli J. Drug/cyclodextrin/hydroxy acid multicomponent systems. Properties and pharmaceutical applications. *Journal of Pharmaceutical Sciences*. 2000; 89(1): 1–8. DOI:10.1002/(SICI)1520-6017(200001)89:1<1::AID-JPS1>3.0.CO;2-W
44. Hădărugă NG., Bandur GN., David I., Hădărugă DI. A review on thermal analyses of cyclodextrins and cyclodextrin complexes. *Environmental Chemistry Letters*. 7 September 2018; DOI:10.1007/s10311-018-0806-8
45. Specogna E., Li KW., Djabourov M., Carn F., Bouchemal K. Dehydration, dissolution, and melting of cyclodextrin crystals. *Journal of Physical Chemistry B*. American Chemical Society; 29 January 2015; 119(4): 1433–1442. DOI:10.1021/jp511631e
46. Sabadini E., Cosgrove T., Egidio F do C. Solubility of cyclomaltooligosaccharides (cyclodextrins) in H₂O and D₂O: a comparative study. *Carbohydrate Research*. February 2006; 341(2): 270–274. DOI:10.1016/j.carres.2005.11.004
47. Larsen KL. Large Cyclodextrins. *Journal of Inclusion Phenomena and Macrocyclic Chemistry*. Kluwer Academic Publishers; 2002; 43(1/2): 1–13. DOI:10.1023/A:1020494503684
48. Gattuso G., Gargiulli C., Parisi MF. Threading cyclodextrins in chloroform: A [2]pseudorotaxane. *International Journal of Molecular Sciences*. 2007; 8(10): 1052–1063. DOI:10.3390/i8101052
49. Gattuso G., Nepogodiev SA., Stoddart JF. Synthetic cyclic oligosaccharides. *Chemical Reviews*. 1998; 98(5): 1919–1958. DOI:10.1021/cr960133w
50. Liu L., Guo QX. The driving forces in the inclusion complexation of cyclodextrins. *Journal of Inclusion Phenomena*. 2002; 42(1–2): 1–14. DOI:10.1023/A:1014520830813
51. Bing-Lin He (Ping-Lum Ho), Zhao X Bin. Study of the oxidation of crosslinked β -cyclodextrin polymer and its use in the removal of urea. I. *Reactive Polymers*. 1992; 18(3): 229–235. DOI:10.1016/0923-1137(92)90653-J

52. Mocanu G., Vizitiu D., Carpov A. Cyclodextrin polymers. *Journal of Bioactive and Compatible Polymers*. 2001; 16(4): 315–342. DOI:10.1106/JJUV-8F2K-JGYF-HNGF
53. Oliveira T., Botelho G., Alves NM., Mano JF. Inclusion complexes of α -cyclodextrins with poly(d,l-lactic acid): Structural, characterization, and glass transition dynamics. *Colloid and Polymer Science*. 2014; 292(4): 863–871. DOI:10.1007/s00396-013-3127-2
54. Jana M., Bandyopadhyay S. Molecular Dynamics Study of β -Cyclodextrin–Phenylalanine (1:1) Inclusion Complex in Aqueous Medium. *The Journal of Physical Chemistry B*. American Chemical Society; 8 August 2013; 117(31): 9280–9287. DOI:10.1021/jp404348u
55. Shanmugam M., Ramesh D., Nagalakshmi V., Kavitha R., Rajamohan R., Stalin T. Host–guest interaction of l-tyrosine with β -cyclodextrin. *Spectrochimica Acta Part A: Molecular and Biomolecular Spectroscopy*. Elsevier; 1 November 2008; 71(1): 125–132. DOI:10.1016/J.SAA.2007.10.054
56. Francisco R., Biagi G. Characterization and Synthesis of Cyclodextrin Inclusion Complexes and their Applications as Fluorescent Probes for Sensing Biomacromolecules by Characterization and Synthesis of Cyclodextrin Inclusion. 2012;
57. Rachmawati H., Edityaningrum CA., Mauludin R. Molecular Inclusion Complex of Curcumin– β -Cyclodextrin Nanoparticle to Enhance Curcumin Skin Permeability from Hydrophilic Matrix Gel. *AAPS PharmSciTech*. 29 December 2013; 14(4): 1303–1312. DOI:10.1208/s12249-013-0023-5
58. Giordano F., Novak C., Moyano JR. Thermal analysis of cyclodextrins and their inclusion compounds. *Thermochimica Acta*. December 2001; 380(2): 123–151. DOI:10.1016/S0040-6031(01)00665-7
59. Akira H., Masaoki F., Shun-ichi N. Inclusion of aromatic compounds by a β -cyclodextrin-epichlorohydrin polymer. *Polymer Journal*. 1981. pp. 777–781. DOI:10.1295/polymj.13.777
60. Giglio V., Sgarlata C., Vecchio G. Novel amino-cyclodextrin cross-linked oligomer as efficient carrier for anionic drugs: A spectroscopic and nanocalorimetric investigation. *RSC Advances*. Royal Society of Chemistry; 2015; 5(22): 16664–16671. DOI:10.1039/c4ra16064a
61. Szejtli J., Fenyvesi E., Zoltan S., Zsador B., Tudos F. Cyclodextrin-polyvinyl alcohol polymers and a process for the preparation thereof in a pearl, foil, fiber or block form. 23 June 1981;
62. Cyclodextrin-epichlorohydrin polymers for separating and adsorbing substances. 26 December 1991;
63. Schneider H-J., Hacket F., Rüdiger V., Ikeda H. NMR Studies of Cyclodextrins and Cyclodextrin Complexes. *Chemical Reviews*. 1998; 98(5): 1755–1786. DOI:10.1021/cr970019t
64. ISO 6796:1981 - Polyglycols for industrial use -- Determination of hydroxyl number -- Phthalic anhydride esterification method. <https://www.iso.org/standard/13294.html>
65. ASTM E222-17, Standard Test Methods for Hydroxyl Groups Using Acetic Anhydride Acetylation, ASTM International, West Conshohocken, PA, 2017.
66. ASTM E1899-16, Standard Test Method for Hydroxyl Groups Using Reaction with p-

Toluenesulfonyl Isocyanate (TSI) and Potentiometric Titration with Tetrabutylammonium Hydroxide, ASTM International, West Conshohocken, PA, 2016.

67. Sheremata TW., Hawari J. Cyclodextrins for desorption and solubilization of 2,4,6-trinitrotoluene and its metabolites from soil. *Environmental Science and Technology*. 2000; 34(16): 3462–3468. DOI:10.1021/es9910659
68. Zhao D., Zhao L., Zhu C., Tian Z., Shen X. Synthesis and properties of water-insoluble β -cyclodextrin polymer crosslinked by citric acid with PEG-400 as modifier. *Carbohydrate Polymers*. Elsevier Ltd; 2009; 78(1): 125–130. DOI:10.1016/j.carbpol.2009.04.022
69. Jiang H., Yang Z., Zhou X., Fang Y., Ji H. Immobilization of β -cyclodextrin as insoluble β -cyclodextrin polymer and its catalytic performance. *Chinese Journal of Chemical Engineering*. 2012; 20(4): 784–792. DOI:10.1016/S1004-9541(11)60249-8
70. Zhao D., Zhao L., Zhu CS., Huang WQ., Hu JL. Water-insoluble β -cyclodextrin polymer crosslinked by citric acid: Synthesis and adsorption properties toward phenol and methylene blue. *Journal of Inclusion Phenomena and Macrocyclic Chemistry*. 2009; 63(3–4): 195–201. DOI:10.1007/s10847-008-9507-4
71. Kono H., Nakamura T. Polymerization of β -cyclodextrin with 1,2,3,4-butanetetracarboxylic dianhydride: Synthesis, structural characterization, and bisphenol A adsorption capacity. *Reactive and Functional Polymers*. Elsevier Ltd; 2013; 73(8): 1096–1102. DOI:10.1016/j.reactfunctpolym.2013.04.006
72. Roik N V., Belyakova LA. Thermodynamic, IR spectral and X-ray diffraction studies of the “ β -cyclodextrin-para-aminobenzoic acid” inclusion complex. *Journal of Inclusion Phenomena and Macrocyclic Chemistry*. 27 April 2011; 69(3–4): 315–319. DOI:10.1007/s10847-010-9737-0
73. Maréchal Y., Yves. The molecular structure of liquid water delivered by absorption spectroscopy in the whole IR region completed with thermodynamics data. *Journal of Molecular Structure*. October 2011; 1004(1–3): 146–155. DOI:10.1016/j.molstruc.2011.07.054
74. Krause, Rui; Mamba BB. 9. Cyclodextrin polymers: Synthesis and Application in Water Treatment. *Cyclodextrins: Chemistry and Physics*. 2010;
75. Yi JM., Tang KW. Preparation of insoluble β -cd polymer and its application to enantiomers and isomers separation. *Journal of Central South University of Technology (English Edition)*. 2001; 8(1): 57–59. DOI:10.1007/s11771-001-0026-3
76. Martel B., Ruffin D., Weltrowski M., Lekchiri Y., Morcellet M. Water-soluble polymers and gels from the polycondensation between cyclodextrins and poly(carboxylic acid)s: A study of the preparation parameters. *Journal of Applied Polymer Science*. 2005; 97(2): 433–442. DOI:10.1002/app.21391
77. Davis ME., Gonzalez H., Hwang SSJ. Linear Cyclodextrin Copolymers. Patent US/2006/7091192B1. Int. Appl. C07H 3/00. 2006;
78. Kono H., Nakamura T., Hashimoto H., Shimizu Y. Characterization, molecular dynamics, and encapsulation ability of β -cyclodextrin polymers crosslinked by polyethylene glycol. *Carbohydrate Polymers*. Elsevier Ltd.; 5 September 2015; 128: 11–23. DOI:10.1016/j.carbpol.2015.04.009
79. Wycisk A., Döring A., Schneider M., Schönhoff M., Kuckling D. Synthesis of β -cyclodextrin-based star block copolymers with thermo-responsive behavior. *Polymers*.

2015; 7(5): 921–938. DOI:10.3390/polym7050921

80. Mhlanga SD., Mamba BB., Krause RW., Malefetse TJ. Removal of organic contaminants from water using nanosponge cyclodextrin polyurethanes. *Journal of Chemical Technology & Biotechnology*. Wiley-Blackwell; April 2007; 82(4): 382–388. DOI:10.1002/jctb.1681
81. Kayaci F., Aytac Z., Uyar T. Surface modification of electrospun polyester nanofibers with cyclodextrin polymer for the removal of phenanthrene from aqueous solution. *Journal of Hazardous Materials*. Elsevier B.V.; 2013; 261: 286–294. DOI:10.1016/j.jhazmat.2013.07.041
82. Birck C., Degoutin S., Tabary N., Miri V., Bacquet M. New crosslinked cast films based on poly(vinyl alcohol): Preparation and physico-chemical properties. *Express Polymer Letters*. 2014; 8(12): 941–952. DOI:10.3144/expresspolymlett.2014.95
83. Chen W., Wang C., Yan L., Huang L., Zhu X., Chen B., et al. Improved polyvinylpyrrolidone microneedle arrays with non-stoichiometric cyclodextrin. *Journal of Materials Chemistry B*. 2014; 2(12): 1699–1705. DOI:10.1039/c3tb21698e
84. Radia O., Rogalska E., Moulay-Hassane G. Preparation of meloxicam β -cyclodextrinpolyethylene glycol 6000 ternary system: Characterization, in vitro and in vivo bioavailability. *Pharmaceutical Development and Technology*. Taylor & Francis; 23 October 2012; 17(5): 632–637. DOI:10.3109/10837450.2011.565347
85. Salmaso S., Semenzato A., Bersani S., Matricardi P., Rossi F., Caliceti P. Cyclodextrin/PEG based hydrogels for multi-drug delivery. *International Journal of Pharmaceutics*. 10 December 2007; 345(1–2): 42–50. DOI:10.1016/j.ijpharm.2007.05.035
86. Nielsen TT., Wintgens V., Larsen KL., Amiel C. Synthesis and characterization of poly(ethylene glycol) based β -cyclodextrin polymers. *Journal of Inclusion Phenomena and Macrocyclic Chemistry*. Springer Netherlands; 30 December 2009; 65(3): 341–348. DOI:10.1007/s10847-009-9591-0
87. Cesteros LC., Ramírez CA., Peciña A., Katime I. Poly(ethylene glycol- β -cyclodextrin) gels: Synthesis and properties. *Journal of Applied Polymer Science*. 15 October 2006; 102(2): 1162–1166. DOI:10.1002/app.24390
88. Klaewklod A., Tantishaiyakul V., Hirun N., Sangfai T., Li L. Characterization of supramolecular gels based on β -cyclodextrin and polyethyleneglycol and their potential use for topical drug delivery. *Materials Science and Engineering C*. May 2015; 50: 242–250. DOI:10.1016/j.msec.2015.02.018
89. Meille S V., Allegra G., Geil PH., He J., Hess M., Jin J-I., et al. Definitions of terms relating to crystalline polymers (IUPAC Recommendations 2011). *Pure and Applied Chemistry*. De Gruyter; 3 August 2011; 83(10): 1831–1871. DOI:10.1351/PAC-REC-10-11-13
90. Peppas N. Hydrogels in pharmaceutical formulations. *European Journal of Pharmaceutics and Biopharmaceutics*. 3 July 2000; 50(1): 27–46. DOI:10.1016/S0939-6411(00)00090-4
91. Crini G. Recent developments in polysaccharide-based materials used as adsorbents in wastewater treatment. *Progress in Polymer Science (Oxford)*. 2005; 30(1): 38–70. DOI:10.1016/j.progpolymsci.2004.11.002

92. Van De Manakker F., Vermonden T., El Morabit N., Van Nostrum CF., Hennink WE. Rheological behavior of self-assembling PEG- β -cyclodextrin/ PEG-cholesterol hydrogels. *Langmuir*. 4 November 2008; 24(21): 12559–12567. DOI:10.1021/la8023748
93. Jia Y-GG., Zhu XX. Self-healing supramolecular hydrogel made of polymers bearing cholic acid and β -cyclodextrin pendants. *Chemistry of Materials*. American Chemical Society; 13 January 2015; 27(1): 387–393. DOI:10.1021/cm5041584
94. Jeong D., Joo S-W., Shinde VV., Jung S. Triple-crosslinked β -cyclodextrin oligomer self-healing hydrogel showing high mechanical strength, enhanced stability and pH responsiveness. *Carbohydrate Polymers*. Elsevier; 15 October 2018; 198: 563–574. DOI:10.1016/J.CARBPOL.2018.06.117
95. Guo K., Lin M-S., Feng J-F., Pan M., Ding L-S., Li B-J., et al. The Deeply Understanding of the Self-Healing Mechanism for Self-Healing Behavior of Supramolecular Materials Based on Cyclodextrin-Guest Interactions. *Macromolecular Chemistry and Physics*. John Wiley & Sons, Ltd; 1 May 2017; 218(10): 1600593. DOI:10.1002/macp.201600593
96. Miao T., Fenn SL., Charron PN., Oldinski RA. Self-Healing and Thermoresponsive Dual-Cross-Linked Alginate Hydrogels Based on Supramolecular Inclusion Complexes. *Biomacromolecules*. NIH Public Access; 14 December 2015; 16(12): 3740–3750. DOI:10.1021/acs.biomac.5b00940
97. Poudel AJ., He F., Huang L., Xiao L., Yang G. Supramolecular hydrogels based on poly (ethylene glycol)-poly (lactic acid) block copolymer micelles and α -cyclodextrin for potential injectable drug delivery system. *Carbohydrate Polymers*. 15 August 2018; 194: 69–79. DOI:10.1016/j.carbpol.2018.04.035
98. Burattini S., Greenland BW., Chappell D., Colquhoun HM., Hayes W. Healable polymeric materials: a tutorial review. *Chemical Society Reviews*. 2010; 39(6): 1973. DOI:10.1039/b904502n
99. Binder W (Wolfgang H. Self-healing polymers : from principles to applications. Wiley-VCH; 2013. 425 p.
100. Garcia SJ., Fischer HR. Self-healing polymer systems: properties, synthesis and applications. *Smart Polymers and their Applications*. Woodhead Publishing; 1 January 2014; : 271–298. DOI:10.1533/9780857097026.1.271
101. Kakuta T., Takashima Y., Harada A. Highly elastic supramolecular hydrogels using host-guest inclusion complexes with cyclodextrins. *Macromolecules*. American Chemical Society; 11 June 2013; 46(11): 4575–4579. DOI:10.1021/ma400695p
102. Jeong YK., Kwon TW., Lee I., Kim TS., Coskun A., Choi JW. Hyperbranched β -cyclodextrin polymer as an effective multidimensional binder for silicon anodes in lithium rechargeable batteries. *Nano Letters*. American Chemical Society; 12 February 2014; 14(2): 864–870. DOI:10.1021/nl404237j
103. Klein J. Evidence for reptation in an entangled polymer melt. *Nature*. Nature Publishing Group; 12 January 1978; 271(5641): 143–145. DOI:10.1038/271143a0
104. Muthukumar M., Baumgärtner A. Diffusion of a Polymer Chain in Random Media. *Macromolecules*. American Chemical Society; July 1989; 22(4): 1941–1946. DOI:10.1021/ma00194a071
105. Guo K., Lin M-SS., Feng J-FF., Pan M., Ding L-SS., Li B-JJ., et al. The Deeply Understanding of the Self-Healing Mechanism for Self-Healing Behavior of

- Supramolecular Materials Based on Cyclodextrin–Guest Interactions. *Macromolecular Chemistry and Physics*. Wiley-Blackwell; 1 May 2017; 218(10): 1600593. DOI:10.1002/macp.201600593
106. Hart LR., Harries JL., Greenland BW., Colquhoun HM., Hayes W. Healable supramolecular polymers. *Polymer Chemistry*. 2013; 4(18): 4860. DOI:10.1039/c3py00081h
 107. Tavengwa NT., Hintsho N., Durbach S., Weiersbye I., Cukrowska E., Chimuka L. Extraction of explosive compounds from aqueous solutions by solid phase extraction using β -cyclodextrin functionalized carbon nanofibers as sorbents. *Journal of Environmental Chemical Engineering*. June 2016; 4(2): 2450–2457. DOI:10.1016/j.jece.2016.04.024
 108. Hawari J., Paquet L., Zhou E., Halasz A., Zilber B. Enhanced Recovery of the Explosive Hexahydro-1,3,5-Trinitro-1,3,5-Triazine (RDX) From Soil: cyclodextrin versus anionic surfactants. *Chemosphere*. Pergamon; 1 May 1996; 32(10): 1929–1936. DOI:10.1016/0045-6535(96)00102-6
 109. Ruebner A., Statton GL., Consaga JP. Polymeric cyclodextrin nitrate esters. 2003. p. 10. DOI:10.1074/JBC.274.42.30033.(51)
 110. Cahill S., Bulusu S. Molecular complexes of explosives with cyclodextrins I. Characterization of complexes with the nitramines RDX, HMX and TNAZ in solution by ^1H NMR spin-lattice relaxation time measurements. *Magnetic Resonance in Chemistry*. August 1993; 31(8): 731–735. DOI:10.1002/mrc.1260310808
 111. Cahill S., Owens FJ. Molecular Complexes of Explosives with Cyclodextrins. 2. Preparation and Characterization of a Solid Complex of β -Cyclodextrin with the Nitramine 1,3,3-Trinitroazetidide (TNAZ). *The Journal of Physical Chemistry*. 1994; 98(28): 7095–7100.
 112. Maksimowski P., Rumianowski T. Properties of the Gamma-Cyclodextrin /CL-20 System. *Central European Journal of Energetic Materials*. 2016; 13(1): 217–229. DOI:10.22211/cejem/64973
 113. Maksimowski P., Grzegorzczak A., Cieślak K., Gołofit T., Chmielarek M., Tomaszewski W., et al. γ -Cyclodextrin Nitrate/CL-20 Complex: Preparation and Properties. *Propellants, Explosives, Pyrotechnics*. John Wiley & Sons, Ltd; 15 November 2018; DOI:10.1002/prop.201800301
 114. Consaga JP., Collignon SL. Energetic composites of cyclodextrin nitrate esters and nitrate. Patent US/1992/5114506. *Int. Appl. C06B 25/00*. 1992;
 115. Consaga JP., Plata L., Entz USPD. Chemically reactive fragmentation warhead. 2001; 1.
 116. Romanova LB., Barinova LS., Lagodzinskaya G V., Kazakov AI., Mikhailov YM. Preparation and NMR analysis of β -cyclodextrin nitrates. *Russian Journal of Applied Chemistry*. 2014; 87(12): 1884–1889. DOI:10.1134/S1070427214120155
 117. Zukas JA., Walters WP (William P. Explosive effects and applications. 431 p.
 118. Copperhead Chemical Database. <http://www.copperheadchemical.com/>
 119. Energetic Materials Testing Assessment Policy Manual of Tests (EMTAP) Manual of Tests. 2007.

120. Dossi E., Akhavan J., Gaulter SE., Williams RG., Doe WJ. Cross-linking of Hydroxyl-terminated Polyols with Triethyleneglycol Diglycidyl Ether: An Alternative to Toxic Isocyanates. *Propellants, Explosives, Pyrotechnics*. Wiley-Blackwell; 1 March 2018; 43(3): 241–250. DOI:10.1002/prop.201700220
121. STANAG 4147 (Ed. 2), 2001, “Chemical compatibility of ammunition components with explosives (non-nuclear applications)”.
122. Mazzeu MAC., Mattos E da C., Iha K. Studies on compatibility of energetic materials by thermal methods. *Journal of Aerospace Technology and Management*. 2010; 2(1): 53–58. DOI:10.5028/jatm.2010.02015358
123. Weiss F., Finkelmann H. Lyotropic liquid crystalline epoxide-amine addition polymers. *Colloid & Polymer Science*. 1 October 2003; 281(11): 1007–1014. DOI:10.1007/s00396-003-0951-9
124. Gaidamauskas E., Norkus E., Butkus E., Crans DC., Grinciene G. Deprotonation of β -cyclodextrin in alkaline solutions. *Carbohydrate Research*. 2009; 344(2): 250–254. DOI:10.1016/j.carres.2008.10.025
125. Atkins PW (Peter W., De Paula J. *Atkins’ Physical chemistry*. Oxford University Press; 2010. 972 p.
126. Hădărugă NG., Hădărugă DI. Water content of natural cyclodextrins and their essential oil complexes: A comparative study between Karl Fischer titration and thermal methods. *Food Chemistry*. Elsevier; 15 June 2012; 132(4): 1741–1748. DOI:10.1016/J.FOODCHEM.2011.11.003
127. Zhou G., Zhao T., Wan J., Liu C., Liu W., Wang R. Predict the glass transition temperature and plasticization of β -cyclodextrin/water binary system by molecular dynamics simulation. *Carbohydrate Research*. Elsevier Ltd; 2015; 401: 89–95. DOI:10.1016/j.carres.2014.10.026
128. Rodríguez-Tenreiro C., Alvarez-Lorenzo C., Concheiro Á., Torres-Labandeira JJ. Characterization of cyclodextrincarbopol interactions by DSC and FTIR. *Journal of Thermal Analysis and Calorimetry*. Kluwer Academic Publishers; 2004; 77(2): 403–411. DOI:10.1023/B:JTAN.0000038981.30494.f4
129. Abiad MG., Campanella OH., Carvajal MT. Assessment of Thermal Transitions by Dynamic Mechanical Analysis (DMA) Using a Novel Disposable Powder Holder. *Pharmaceutics*. Multidisciplinary Digital Publishing Institute (MDPI); 24 March 2010; 2(2): 78–90. DOI:10.3390/pharmaceutics2020078
130. Tabary N., Garcia-Fernandez MJ., Danède F., Descamps M., Martel B., Willart J-FF. Determination of the glass transition temperature of cyclodextrin polymers. *Carbohydrate Polymers*. Elsevier; 5 September 2016; 148: 172–180. DOI:10.1016/j.carbpol.2016.04.032
131. van Ekeren PJ., Carton EP. Polyurethanes for potential use in transparent armour investigated using DSC and DMA. *Journal of Thermal Analysis and Calorimetry*. 16 August 2011; 105(2): 591–598. DOI:10.1007/s10973-011-1665-8
132. Sepe MP., Rapra Technology Limited. *Thermal analysis of polymers*. Rapra Technology Ltd; 1997. 120 p.
133. Contini AE., Flood N., McAteer D., Mai N., Akhavan J. Low hazard small-scale synthesis and chemical analysis of high purity nitroglycerine (NG). *RSC Advances*. The Royal

- Society of Chemistry; 13 October 2015; 5(106): 87228–87232.
DOI:10.1039/C5RA17951C
134. Rodin MD., Romanova LB., Darovskih A V., Gorbunova MA., Tarasov AE. Ir-Spectroscopic Method for Determining the Degree of Nitration of β -Cyclodextrin. *Journal of Applied Spectroscopy*. Springer US; 20 September 2018; 85(4): 691–696. DOI:10.1007/s10812-018-0706-5
 135. Kolthoff IM., Sandell EB., Moskovitz B. The Volumetric Determination of Nitrates with Ferrous Sulfate as Reducing Agent. *Journal of the American Chemical Society*. April 1933; 55(4): 1454–1457. DOI:10.1021/ja01331a020
 136. Kwei TK. The effect of hydrogen bonding on the glass transition temperatures of polymer mixtures. *Journal of Polymer Science: Polymer Letters Edition*. June 1984; 22(6): 307–313. DOI:10.1002/pol.1984.130220603
 137. Park SJ., Seo MK. *Solid-Liquid Interface. Interface Science and Technology*. Elsevier; 1 January 2011; 18: 147–252. DOI:10.1016/B978-0-12-375049-5.00003-7
 138. Hansen CM. *Hansen solubility parameters: a user's handbook*. CRC Press; 2007. 519 p.
 139. Vogelsanger B. Chemical Stability, Compatibility and Shelf Life of Explosives. *CHIMIA International Journal for Chemistry*. 1 June 2004; 58(6): 401–408. DOI:10.2533/000942904777677740
 140. Trache D., Tarchoun AF. Stabilizers for nitrate ester-based energetic materials and their mechanism of action: a state-of-the-art review. *Journal of Materials Science*. Springer US; 23 January 2018; 53(1): 100–123. DOI:10.1007/s10853-017-1474-y
 141. Manelis GB. *Thermal decomposition and combustion of explosives and propellants*. Taylor & Francis; 2003. 362 p.
 142. Burov YM. *Thermal Decomposition of Solid Energetic Materials*. http://www.abitura.com/modern_physics/x1.html
 143. Apatoff JB., Norwitz G. *Role of Diphenylamine as a Stabilizer in Propellants; Analytical Chemistry of Diphenylamine in Propellants (A Survey Report)*. 1973.

Appendix A

Table A 1 List of β CPCDs synthesised using PEGDGE as the cross-linker.

Sample ID	Logbook ref.	Feed ratio	β CD (g) ¹	Water (%)	PEGDGE (mL)	NaOH (% w/w)	NaOH (mL)	Time alkox. (h)	T (°C)	Cross-linker addition time.	Time reaction	Yield (%)	Solubility
IP3	β CPCD1	9:1	5.00	N.d	17.4	36	21	0	70	~20min	0.5	1	Water
IP24	β CPCD2	9:1	5.00	N.d	17.4	50	21	0	70	~20min	0.5+4.5 RT	1	Water
IP27	β CPCD3	9:1	5.00	N.d	17.4	5.6	21	0	70	~20min	0.66	88	Insoluble
IP4	β CPCD4	3:1	5.00	N.d	5.8	5.6	21	0	70	~20min	1	5	Water
IP26	β CPCD5	6:1	5.00	N.d	11.6	5.6	21	0	70	~20min	0.66	91	Insoluble
IP28	β CPCD6	9:1	5.00	N.d	17.4	5.6	21	0	70	~20min	1	1	Water
IP1	β CPCD7	9:1	5.00	N.d	17.4	50	21	0	70	~20min	0.5	1	Water
IP2	β CPCD8	9:1	5.00	N.d	17.4	40	21	1	70	~20min	1	1	Water
IP5	β CPCD9	9:1	5.00	N.d	17.4	40	21	1	70	~20min	5	12	Water
IP29	β CPCD10	1:1	5.00	N.d	1.9	40	21	3	70	~20min	1	1	Water
IP6	β CPCD11	5:1	5.00	N.d	9.7	5.6	21	1	70	~20min	5	1	Water

Sample ID	Logbook ref.	Feed ratio	β CD (g) ¹	Water (%)	PEGDGE (mL)	NaOH (% w/w)	NaOH (mL)	Time alkox. (h)	T (°C)	Cross-linker addition time.	Time reaction	Yield (%)	Solubility
IP7	β CPCD12	5:1	5.00	N.d	9.7	5.6	21	0	50	~20min	5	13	Water
IP30	β CPCD13	5:1	5.00	N.d	9.7	5.6	21	0	50	~20min	2	9	Water
IP8	β CPCD14	5:1	5.00	N.d	9.7	5.6	21	16	50	~20min	5	30	Water
IP31	β CPCD15	5:1	5.00	N.d	9.7	5.6	21	16	30	~20min	7.5	23.6	Insoluble
IP32	β CPCD16	5:1	5.00	N.d	9.7	5.6	21	16	30	5 hours	1	23.9	Water
IP9	β CPCD17	5:1	5.00	N.d	9.7	5.6	21	16	30	~20min	6	33.6	Water
IP33	β CPCD18	5:1	5.00	N.d	9.7	5.6	21	16	30	~20min	7	33.2	Water
IP34	β CPCD19	5:1	2.5	N.d	4.8	20	10.5	16	70	~20min	6	15	Water
IP35	β CPCD20	5:1	2.5	N.d	4.8	5.6 KOH	10.5	16	30	5 hours	1.5	Not recovered	Insoluble
IP36	β CPCD21	1:1	2.5	N.d	9.7	5.6	100	16	30	~20min	7.5	not recovered	Water
IP37	β CPCD22	5:1	2.5	N.d	4.8	5.6	10+42.5	16	30	~20min	24	48	Water
IP11	β CPCD23	3:1	2.5	N.d	2.9	5.6	10.5	16	30	~20min	24	68	Water
IP38	β CPCD24	4:1	5.00	N.d	7.7	5.6	21	16	30*	~20min	24	39	Water

Sample ID	Logbook ref.	Feed ratio	β CD (g) ¹	Water (%)	PEGDGE (mL)	NaOH (% w/w)	NaOH (mL)	Time alkox. (h)	T (°C)	Cross-linker addition time.	Time reaction	Yield (%)	Solubility
IP10	β CPCD25	4:1	5.00	N.d	7.7	5.6	21	16	30	~20min	24	36	Water
IP39	β CPCD26	4:1	5.00	N.d	7.7	5.6	21	16	30	7 hours	17	Not recovered	Insoluble
IP40	β CPCD27	3:1	5.00	N.d	5.8	5.6	21	16	30	7 hours	17	48	Water
IP12	β CPCD28	2:1	5.00	N.d	3.9	5.6	21	16	30	7 hours	17	44	Water
IP41	β CPCD29	3.5:1	5.67	0.12	9.7	5.6	21	16	30	7 hours	17	not recovered	Insoluble
IP42	β CPCD30	5:1	5.63	0.12	9.7	5.6	21	16	30	~20min	6	61	Insoluble
IP43	β CPCD31	5:1	5.63	0.12	9.7	5.6	21	16	30	~20min	5	not recovered	Insoluble
IP44	β CPCD32	5:1	5.64	0.12	9.7	5.6	21	16	30	~20min	5	not recovered	Insoluble
IP13	β CPCD33	5:1	4.35	0.13	8.4	5.6	20.7	16	30	~20min	6	68	Water
IP20	β CPCD34	5:1	4.35	0.13	8.4	5.6	20.7	16	30	~20min	6	64	water
IP22	β CPCD35	4:1	4.40	0.12	6.8	5.6	20.8	16	30	~20min	6	63	water
IP15	β CPCD36	4:1	4.40	0.12	6.8	5.6	20.8	16	30	~20min	6	65	water
IP45	β CPCD37	2:1	4.15	0.17	3.2	5.6	18.7	16	30	~20min	6	68	water

Sample ID	Logbook ref.	Feed ratio	β CD (g) ¹	Water (%)	PEGDGE (mL)	NaOH (% w/w)	NaOH (mL)	Time alkox. (h)	T (°C)	Cross-linker addition time.	Time reaction	Yield (%)	Solubility
IP17	β CPCD38	2:1	4.15	0.17	3.2	5.6	18.7	16	30	~20min	6	68	water
IP46	β CPCD39	6:1	4.34	0.13	8.4	5.6	19.8	16	30	~20min	6	gel	Insoluble
IP47	β CPCD40	6:1	4.34	0.13	8.4	5.6	20.7	16	30	~20min	6	37%+gel	Insoluble
IP16	β CPCD41	3:1	4.15	0.17	4.8	5.6	20.7	16	30	~20min	6	73	water
IP48	β CPCD42	3:1	4.15	0.17	4.8	5.6	19.8	16	30	~20min	6	68	water
IP14	β CPCD43	3.8:1	4.34	0.13	8.4	5.6	19.8	16	30	7 hours	6	71	water
IP21	β CPCD44	5:1	4.34	0.13	8.4	5.6	19.8	16	30	~20min	6	68	water
IP25	β CPCD45	3:1	4.34	0.13	5	5.6	19.8	16	30	~20min	6	67	water
IP23	β CPCD46	4:1	4.34	0.13	6.7	5.6	19.8	16	30	~20min	6	69	water
IP19	β CPCD47	5:1	4.34	0.13	8.4	5.6	19.8	16	30	~20min	6	67	water
IP18	β CPCD48	5:1	4.34	0.13	8.4	5.6	19.8	16	30	~20min	6	68	water

1 Dry mass of β CD determined by TGA after sample β CDPCD28.

Table A 2 List of β CHCDs using HEGDGE as the cross-linker.

Sample ID	Logbook ref.	Feed ratio	β CD (g) ¹	Water (%)	HEGDGE (g)	NaOH (% w/w)	NaOH (mL)	Time alkox. (h)	T (°C)	Cross-linker addition time	Time reaction	Yield (%)	Sol.
IH1	β CHCD1	5:1	4.00	0.12	6.9	5.6	19	16	30	~20min	6	68	water
IH2	β CHCD2	4:1	4.00	0.12	5.6	5.6	19	16	30	~20min	6	72	water
IH3	β CHCD3	2:1	4.00	0.13	2.8	5.6	14.3	16	30	~20min	6	65	water
IH4	β CHCD4	3:1	4.00	0.13	4.2	5.6	14.3	16	30	~20min	6	67	water

1 Dry mass of β CD determined by TGA.

Table A 3 List of β CTCDs synthesised using TEGDGE as the cross-linker.

Sample ID	Logbook ref.	Feed ratio	β CD (g)	Water (%)	TEGDGE (g)	NaOH (% w/w)	NaOH (mL)	Time alkox. (h)	T (°C)	Cross-linker addition time	Time reaction	Yield (%)	Sol.
IT5	β CTCD1	9:1	5	N.d	9.35	40	21	1	70	~20min	5	35	Insoluble
IT6	β CTCD2	3:1	5	N.d	3.1	40	21	1	70	~20min	5	40	Insoluble
IT7	β CTCD3	6:1	5	N.d	6.2	40	21	1	70	~20min	5	33	Insoluble
IT8	β CTCD4	5:1	5	N.d	5.76	5.6	21	1	70	~20min	5	10	water
IT9	β CTCD5	5:1	5	N.d	5.76	5.6	21	16	30	~20min	5	38	water

Sample ID	Logbook ref.	Feed ratio	β CD (g)	Water (%)	TEGDGE (g)	NaOH (% w/w)	NaOH (mL)	Time alkox. (h)	T (°C)	Cross-linker addition time	Time reaction	Yield (%)	Sol.
IT1	β CTCD6	5:1	2.00	0.12	2.3	5.6	9.5	16	30	~20min	6	63	water
IT2	β CTCD7	4:1	2.00	0.12	1.84	5.6	9.5	16	30	~20min	6	52	water
IT3	β CTCD8	3:1	2.00	0.12	1.39	5.6	9.5	16	30	~20min	6	56	water
IT4	β CTCD9	2:1	2.00	0.12	0.93	5.6	9.5	16	30	~20min	6	45	water

1 Dry mass of β CD determined by TGA.

Table A 4 Nitration of insoluble β CPCD precursor, sample IP26.

Sample ID	Logbook ref.	Precursor		HNO ₃ %	Volume HNO ₃ (mL)	H ₂ SO ₄ %	Volume H ₂ SO ₄ (mL)	Time (h)	DCM (mL)	Stirr rpm	Yield (%)
		Name	Solubility								
NP9	β NCPCD3	IP26	N	100	0.5	100	0.5	1.0	0.0	200	32 ^{1,2}
NP10	β NCPCD4	IP26	N	100	0.5	100	0.5	2.0	0.0	400	30 ^{1,2}
NP11	β NCPCD5	IP26	N	100	0.5	100	0.5	1.5	1.8	900	44 ^{1,2}
NP12	β NCPCD6	IP26	N	100	0.5	100	0.5	1.5	0.0	900	37 ^{1,2}
NP13	β NCPCD7	IP26	N	100	0.5	100	0.5	1.5	1.8	900	90
NP14	β NCPCD8	IP26	N	100	0.5	100	0.5	2.0	1.8	900	87

1 Low degree of nitration, gum-like β CPCD precursors.

2 Purification process affected the yield of the reaction.

Table A 5 Nitration of insoluble β CTCD precursors.

Sample ID	Logbook ref.	Precursor		HNO ₃ %	Volume HNO ₃ (mL)	H ₂ SO ₄ %	Volume H ₂ SO ₄ (mL)	Time (h)	DCM (mL)	Stirr rpm	Yield (%)
		Name	Solubility								
NT5	β NCTCD1	IT5	N	95	1.0	0	0.0	1.0	0.0	200	87

NT6	β NCTCD2	IT5	N	100	1.0	0	0.0	1.0	0.0	200	80
NT7	β NCTCD3	IT5	N	100	0.5	100	0.5	1.0	0.0	200	35
NT8	β NCTCD4	IT5	N	100	0.5	100	0.5	0.5	1.8	400	85
NT9	β NCTCD5	IT5	N	100	0.5	100	0.5	1.0	0.0	900	88
NT10	β NCTCD6	IT7	N	100	0.5	100	0.5	1.0	0.0	900	88
NT11	β NCTCD7	IT6	N	100	0.5	100	0.5	1.0	0.0	900	84
NT12	β NCTCD8	IT5	N	100	0.5	100	0.5	1.0	1.8	900	86
NT13	β NCTCD9	IT6	N	100	0.5	100	0.5	1.0	1.8	900	91
NT14	β NCTCD10	IT7	N	100	0.5	100	0.5	1.0	1.8	900	92

Table A 6 Nitration of β CPCD precursors.

Sample ID	Logbook ref.	Precursor name	HNO ₃		Mass of precursor (mg)	Volume HNO ₃ (mL)	H ₂ SO ₄		Time (h)	DCM (mL)	Stirr rpm	Yield ¹		Sol
			Sol.	%			%	(mL)				Mass mg	%	
NP14	β NCPCD1	IP5	Y	100	200	0.5	100	0.5	0.5	1.8	200	163		
NP15	β NCPCD2	IP5	Y	95	200	1	0	0	1	0	200	199		

Sample ID	Logbook ref.	Precursor name	HNO ₃		Mass of precursor (mg)	Volume HNO ₃ (mL)	H ₂ SO ₄		Time (h)	DCM (mL)	Stirr rpm	Yield ¹		Sol
			Sol.	%			%	(mL)				Mass mg	%	
NP7	βNCPCD3	IP26	N	100	200	0.5	100	0.5	1	0	200			purification is difficult, insoluble precursor
NP8	βNCPCD4	IP26	N	100	200	0.5	100	0.5	2	0	400			purification is difficult, insoluble precursor
NP9	βNCPCD5	IP26	N	100	200	0.5	100	0.5	1.5	1.8	900	70		purification is difficult, insoluble precursor
NP10	βNCPCD6	IP26	N	100	3000	0.5	100	0.5	1.5	0	900	300		purification is difficult, insoluble precursor
NP11	βNCPCD7	IP26	N	100	200	0.5	100	0.5	1.5	1.8	900	103		purification is difficult, insoluble precursor
NP12	βNCPCD8	IP26	N	100	200	0.5	100	0.5	2	1.8	900	169		purification is difficult, insoluble precursor
NP18	βNCPCD9	IP8	Y	100	200	1			1		700	180		

Sample ID	Logbook ref.	Precursor name	HNO ₃		Mass of precursor (mg)	Volume HNO ₃ (mL)	H ₂ SO ₄		Time (h)	DCM (mL)	Stirr rpm	Yield ¹		Sol
			Sol.	%			%	(mL)				Mass mg	%	
NP19	βNCPCD10	IP8	Y	95	200	1			1		700	187		
NP20	βNCPCD11	IP8	N	100	200	1			1		700			almost nothing recovered (filter paper problem)
NP21	βNCPCD12	IP11	Y	100	200	1			1		700	190		
NP22	βNCPCD13	IP10	Y	100	1000	5			1+(15min dis)		700	1070		
NP16	βNCPCD14	βCPCD27	Y	100	1000	5			1		700	1230		
NP23	βNCPCD15	IP10	Y	100	200	1			1		700	103		
NP24	βNCPCD16	IP10	Y	100	200	1			1		700	117		compound is not easy to purify cloud solution
NP25	βNCPCD17	IP13/20 blend	Y	100	1000	5			1		700	451		
NP13	βNCPCD18	IP13/20 blend	Y	100	500	2.5			1		700	476		

Sample ID	Logbook ref.	Precursor name	HNO ₃		Mass of precursor (mg)	Volume HNO ₃ (mL)	H ₂ SO ₄		Time (h)	DCM (mL)	Stirr rpm	Yield ¹		Sol
			Sol.	%			%	(mL)				Mass mg	%	
NP26	βNCPCD19	IP13/20 blend	Y	100	2000	10			1		700	1637		
NP27	βNCPCD20	IP13/20 blend	Y	100	1000	10			1		700	656		
NP28	βNCPCD21	IP13/20 blend	Y	100	1000	10			1		700	395		
NP29	βNCPCD22	IP13/20 blend	Y	100	500	5			1		700	NA		samples damaged trying to use Na ₂ CO ₃
NP30	βNCPCD23	IP13/20 blend	Y	100	500	5			1		700	NA		
NP31	βNCPCD24	IP13/20 blend	Y	100	300	2.1			1		700	150		
NP32	βNCPCD25	IP13/20 blend	Y	100	300	2.1			1		700	98		
NP33	βNCPCD26	IP13/20	Y	100	300	2.1			1		700	72		

Sample ID	Logbook ref.	Precursor name	HNO ₃		Mass of precursor (mg)	Volume HNO ₃ (mL)	H ₂ SO ₄		Time (h)	DCM (mL)	Stirr rpm	Yield ¹		Sol
			Sol.	%			%	(mL)				Mass mg	%	
		blend												
NP5	βNCPCD27	IP13/20 blend	Y	100	2000				1		700	1301		N% 6.2
NP6	βNCPCD28	IP13/20 blend	Y	100	2000	14			1		700	1755		N% 6.6
NP34	βNCPCD29	IP21	Y	100	2000	14			1		700	1562		
NP17	βNCPCD30	IP18/19 blend	Y	100	2500X4	17.5X4			1		700	9000		
NP2	βNCPCD31	IP23	Y	100	2500	17.5			1		700	2760		N% 6.8
NP4	βNCPCD32	IP17	Y	100	2100	14.7			1		700	1556		N% 7
NP3	βNCPCD33	IP25	Y	100	2200	15			1		700	2294		N% 8.7
NP1	βNCPCD34	IP18	Y	100	6000	28			1		700	4764	62	

1 Where yield is not reported, masses are less than required to determine the nitrogen content, thus were not calculated.

Table A 7 Nitration of β CHCD precursors.

Sample ID	Logbook ref.	Precursor name	Solubility	Mass of precursor (mg)	Volume 100% HNO ₃ (mL)	Time (h)	Stirr	Yield		N (%)	
								rpm	Mass		(%)
									mg		
NH1	β NCHCD1	IH1	Y	2000	14	1	700	1683	60	8.2	
NH2	β NCHCD2	IH2	Y	2060	14	1	700	1897	71	7.1	
NH3	β NCHCD3	IH3	Y	2000	14	1	700	1798	62	9.0	
NH4	β NCHCD4	IH4	Y	2000	14	1	700	1939	66	7.4	

Table A 8 Nitration of soluble β CTCD precursors.

Sample ID	Logbook ref.	Precursor name	HNO ₃		Mass of precursor (mg)	Volume HNO ₃ (mL)	H ₂ SO ₄	Volume H ₂ SO ₄ (mL)	Time (h)	DCM (mL)	Stirr rpm	Yield ¹		N (%)
			%	Sol.			%							
								Mass mg				(%)		
NT5	β NCTCD1	NT5	N	95	200	1	0	0	1	0	200	170		
NT6	β NCTCD2	NT5	N	100	200	1	0	0	1	0	200	112		
NT7	β NCTCD3	NT5	N	100	200	0.5	100	0.5	1	0	200	146		
NT8	β NCTCD4	NT5	N	100	200	0.5	100	0.5	0.5	1.8	400	148		
NT9	β NCTCD5	NT5	N	100	200	0.5	100	0.5	1	0	900	103		

NT10	βNCTCD6	NT7	N	100	200	0.5	100	0.5	1	0	900	157		
NT11	βNCTCD7	NT6	N	100	200	0.5	100	0.5	1	0	900			
NT12	βNCTCD8	NT5	N	100	200	0.5	100	0.5	1	1.8	900	126		
NT13	βNCTCD9	NT6	N	100	200	0.5	100	0.5	1	1.8	900	110		
NT14	βNCTCD10	NT7	N	100	200	0.5	100	0.5	1	1.8	900	196		
NT1	βNCTCD11	NT10	Y	100	1000	7	0	0	1	0	700	1038	74	8.2
NT2	βNCTCD12	NT11	Y	100	1000	7	0	0	1	0	700	886	60	9.4
NT3	βNCTCD13	NT12	Y	100	1000	7	0	0	1	0	700	884	60	9.3
NT4	βNCTCD14	NT13	Y	100	1000	7	0	0	1	0	700	870	68	6.2

¹Where yield is not reported, masses are less than required to determine the nitrogen content, thus were not calculated.

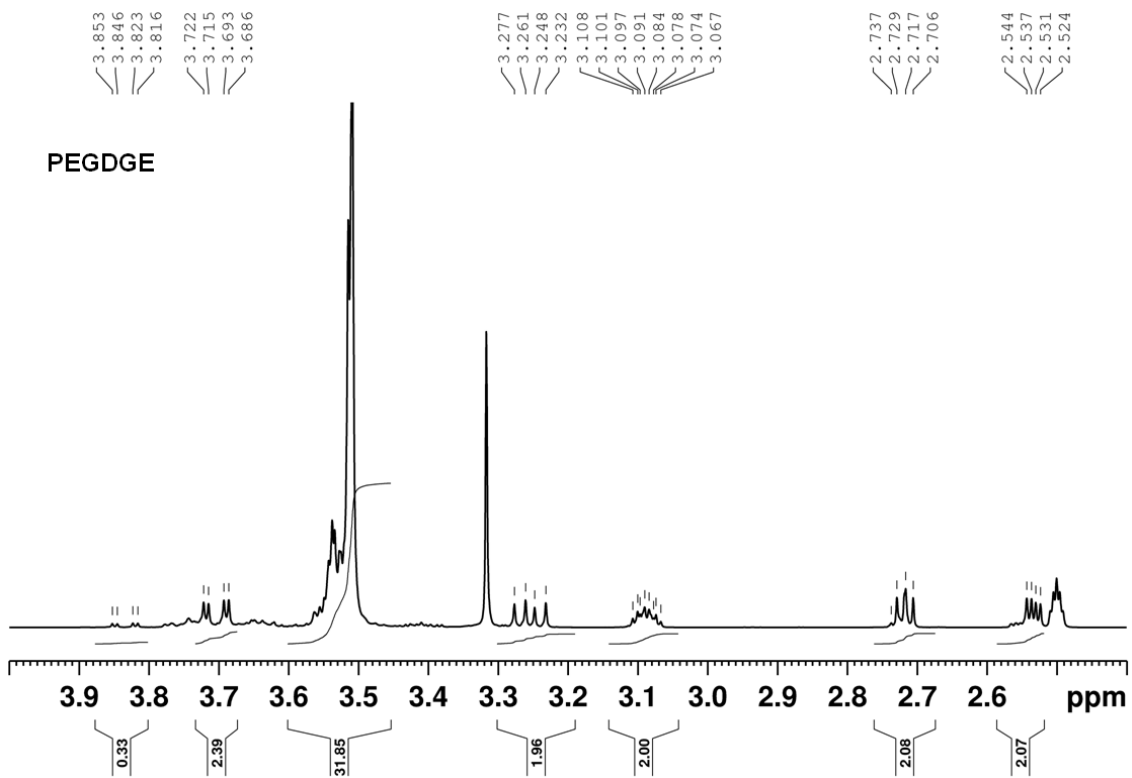


Figure A 1 $^1\text{H-NMR}$ spectrum of PEGDGE in DMSO-d_6 .

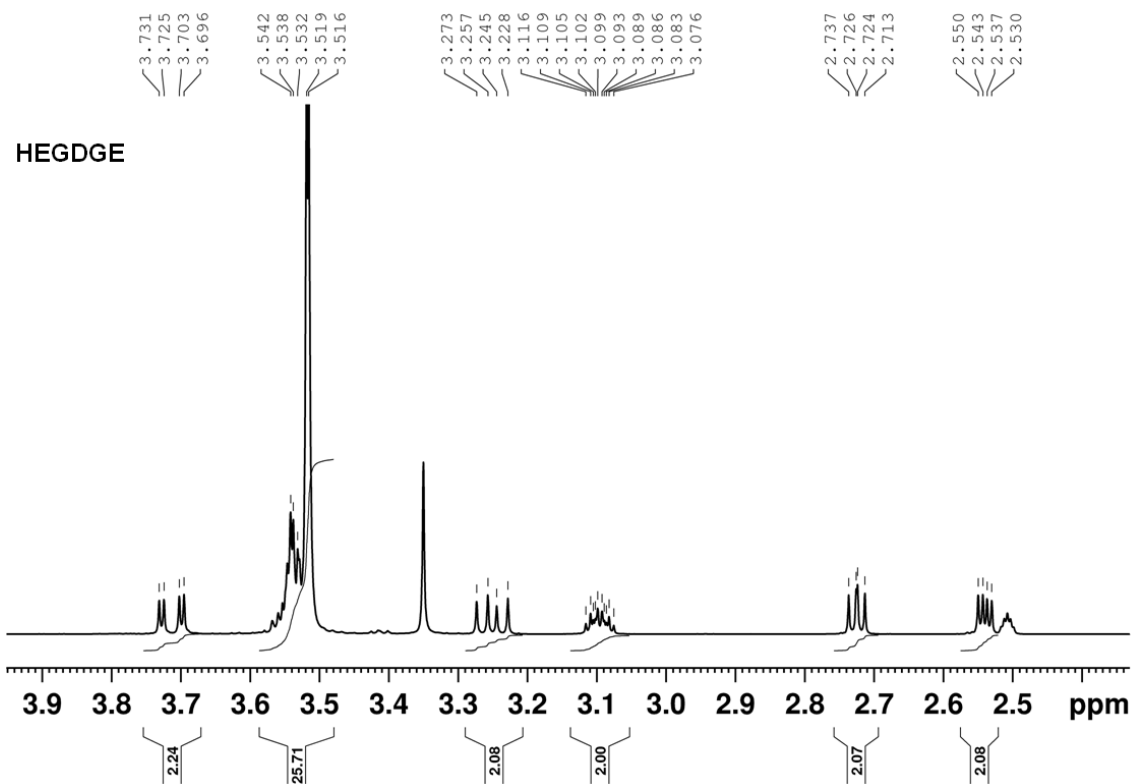


Figure A 2 ^1H -NMR spectrum of HEGDGE in DMSO-d_6 .

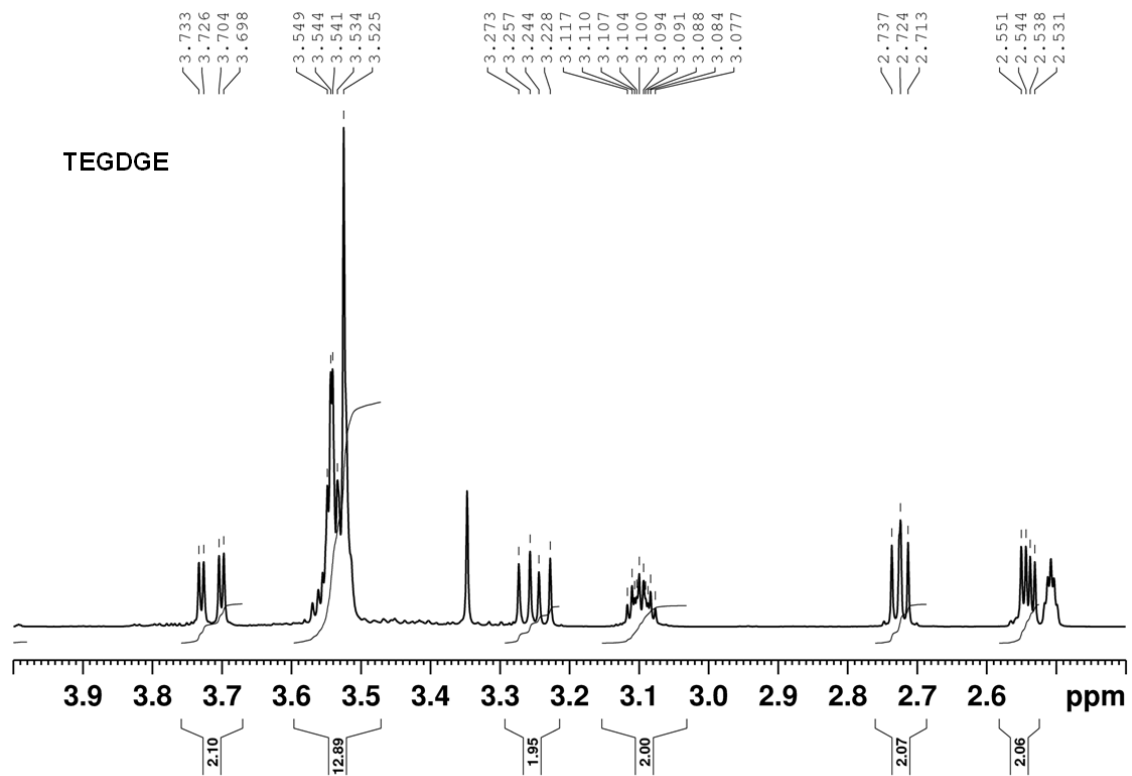


Figure A 3 $^1\text{H-NMR}$ spectrum of TEGDGE in DMSO-d_6 .

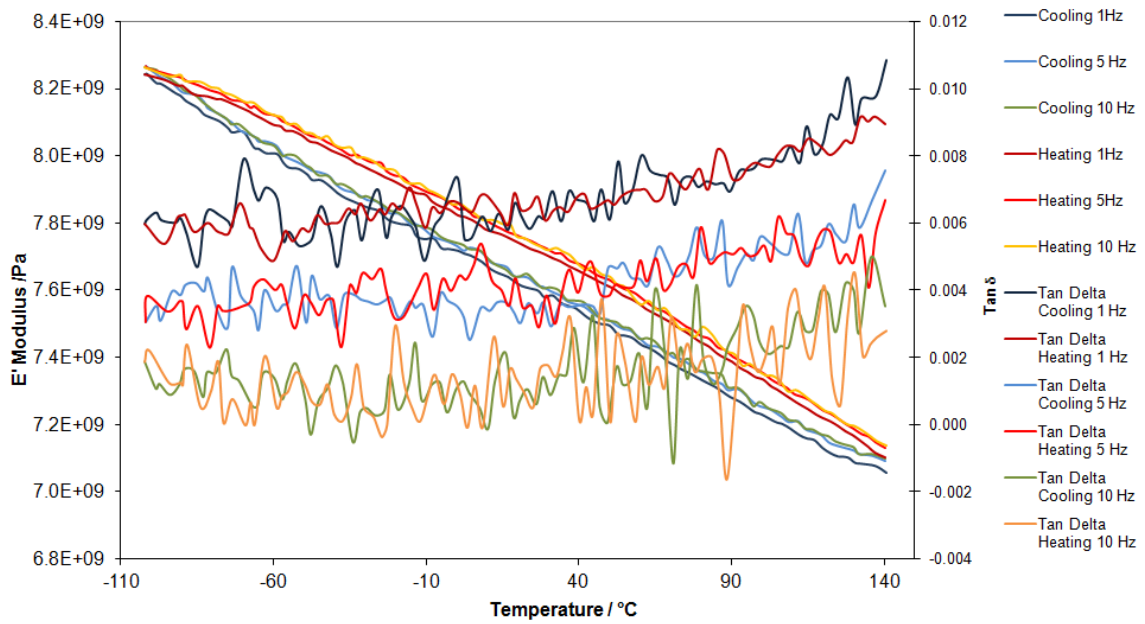


Figure A 4 DMA showing variation in the storage modulus (E') and tanδ of βCD at 1, 5 and 10 Hz (10 °C min⁻¹, third temperature cycle from -100 to 140 °C, aluminium pocket).

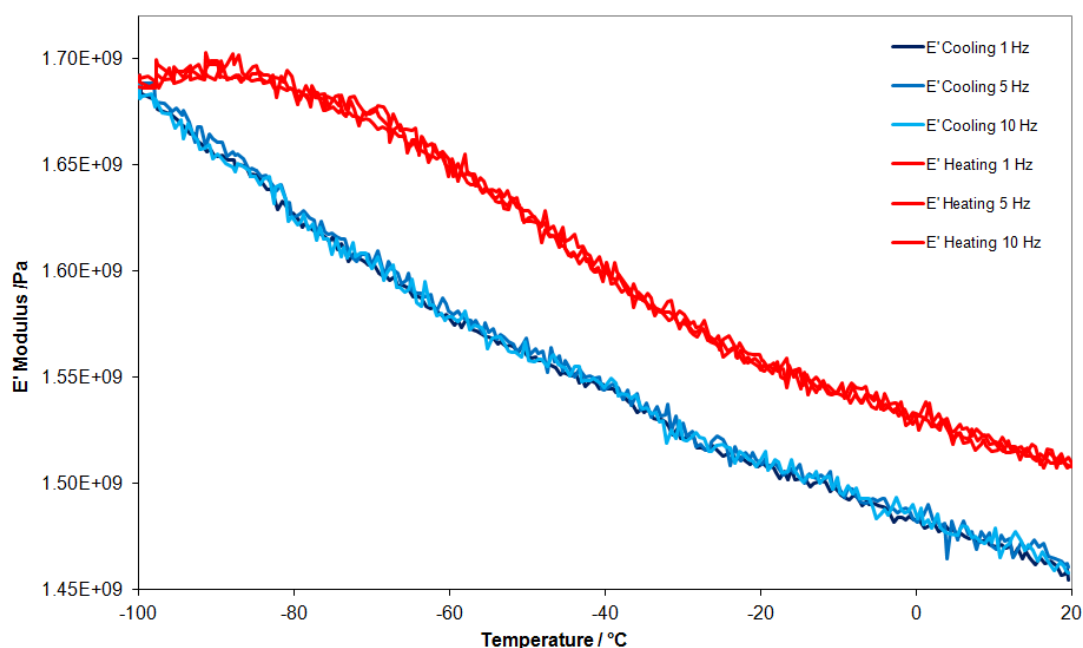


Figure A 5 DMA showing variation in the storage modulus (E') of the aluminium support ($10\text{ }^{\circ}\text{C min}^{-1}$, 1 Hz, third temperature cycle from -100 to $140\text{ }^{\circ}\text{C}$, aluminium pocket).

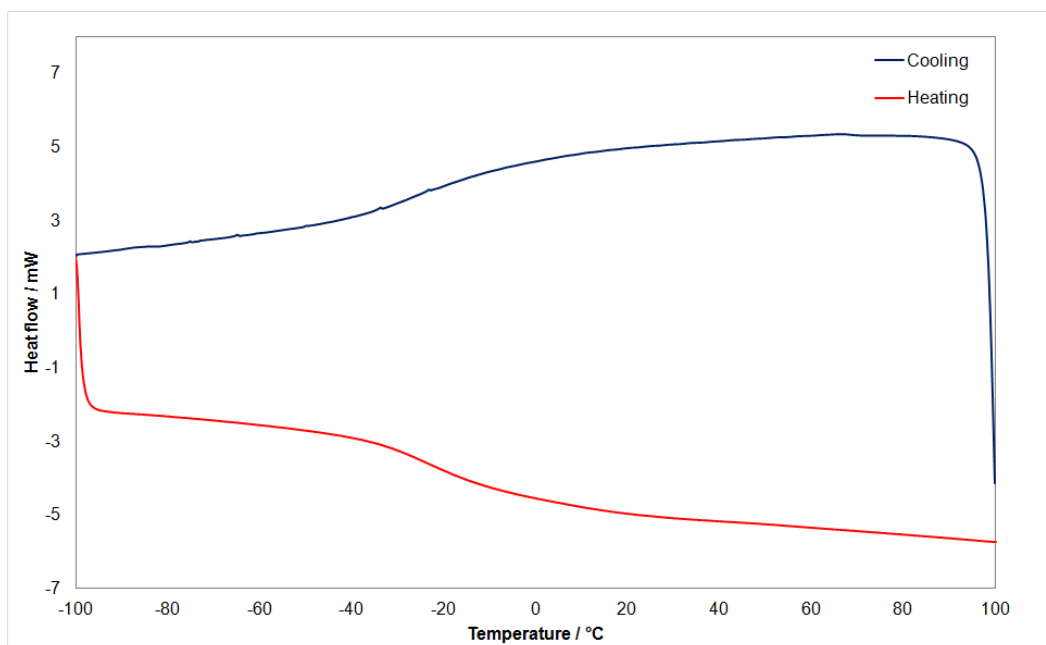


Figure A 6 DSC showing cooling of IP13 from -100 to $100\text{ }^{\circ}\text{C}$ ($10\text{ }^{\circ}\text{C min}^{-1}$, third temperature cycle, aluminium crucible).

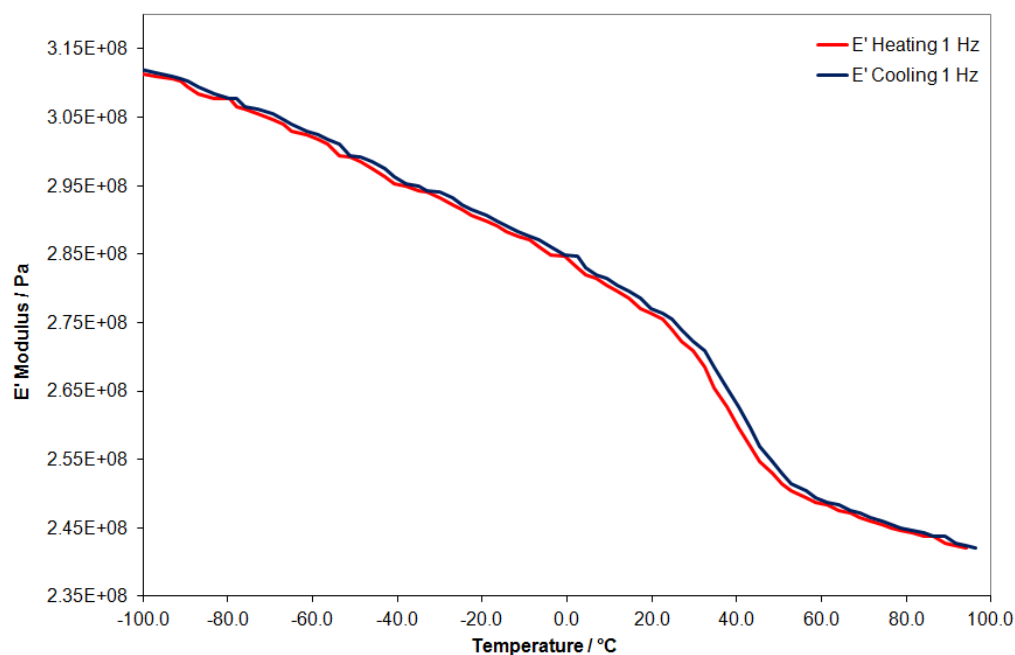


Figure A 7 DMA showing variation in the storage modulus (E') of the aluminium support and PTFE ($10\text{ }^{\circ}\text{C min}^{-1}$, 1 Hz, third temperature cycle from -100 to $140\text{ }^{\circ}\text{C}$, aluminium pocket).

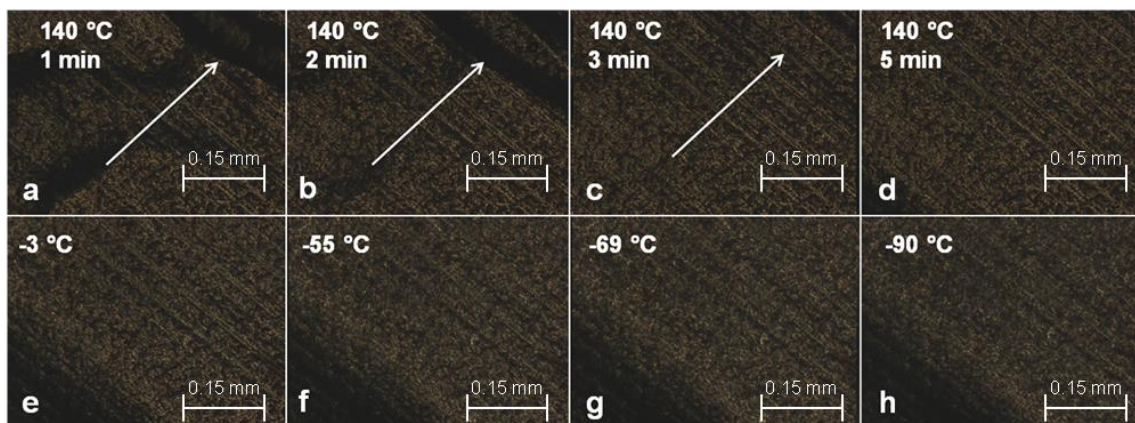


Figure A 8 Optical microscope images of IP9 (PEG: β CD ratio = 3.5) placed on PTFE tape. The sample was annealed at $140\text{ }^{\circ}\text{C}$ for 5 min, top row (a-d), to remove any physical defects (a-b, black shades). The arrow indicates the disappearance of the black shades. The bottom row (e-h) shows the cooling phase captured at -3 , -55 , -69 and $-90\text{ }^{\circ}\text{C}$ and confirms the absence of cracking. The dark shapes on the bottom left of the picture represent condensed water in the cooling chamber.

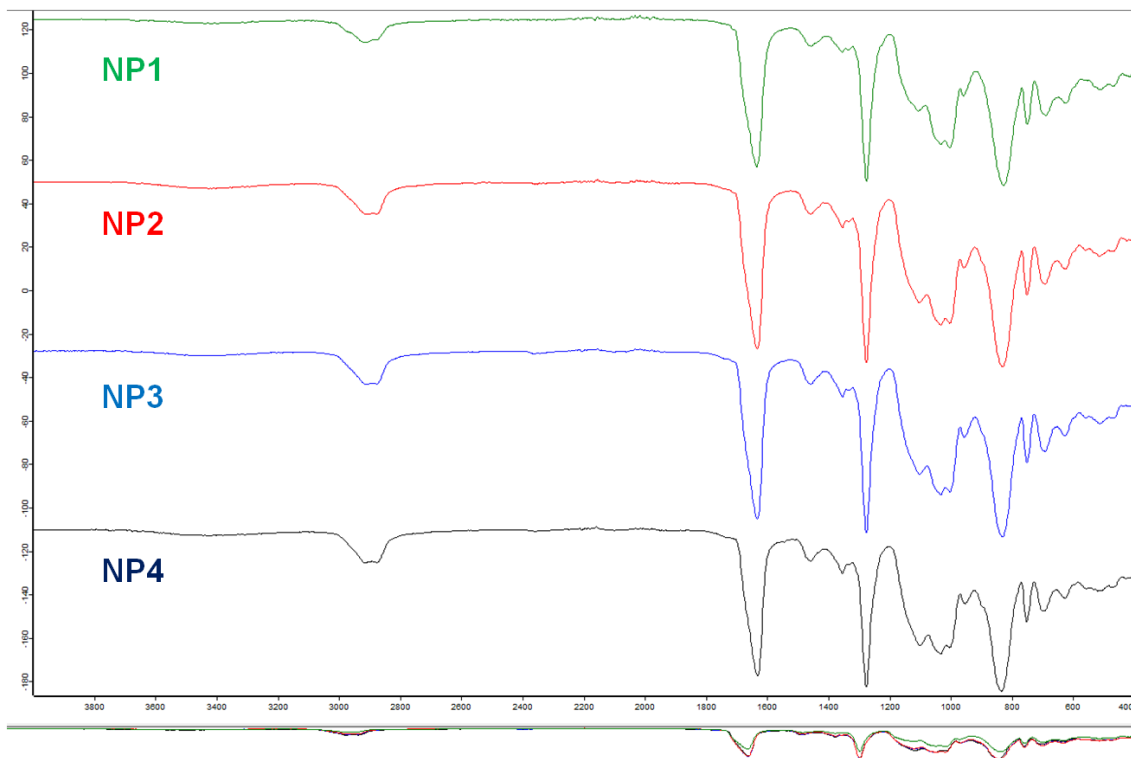


Figure A 9 FTIR spectra of the β NCPCD samples NP1–NP4 containing PEG spacer units.

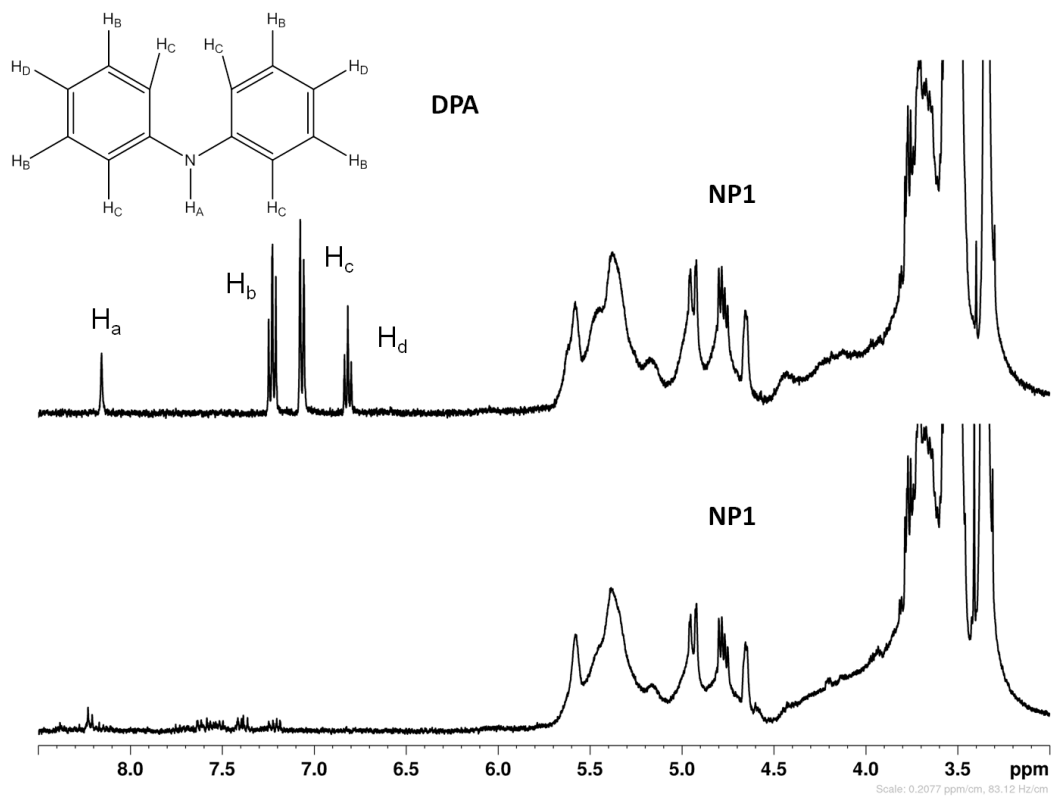


Figure A 10 ¹H NMR spectra of (a) NP1 + 1% w/w DPA at time 0, and (b) NP1 + 1% w/w DPA at time 3 d at 80 °C in DMSO-d₆.

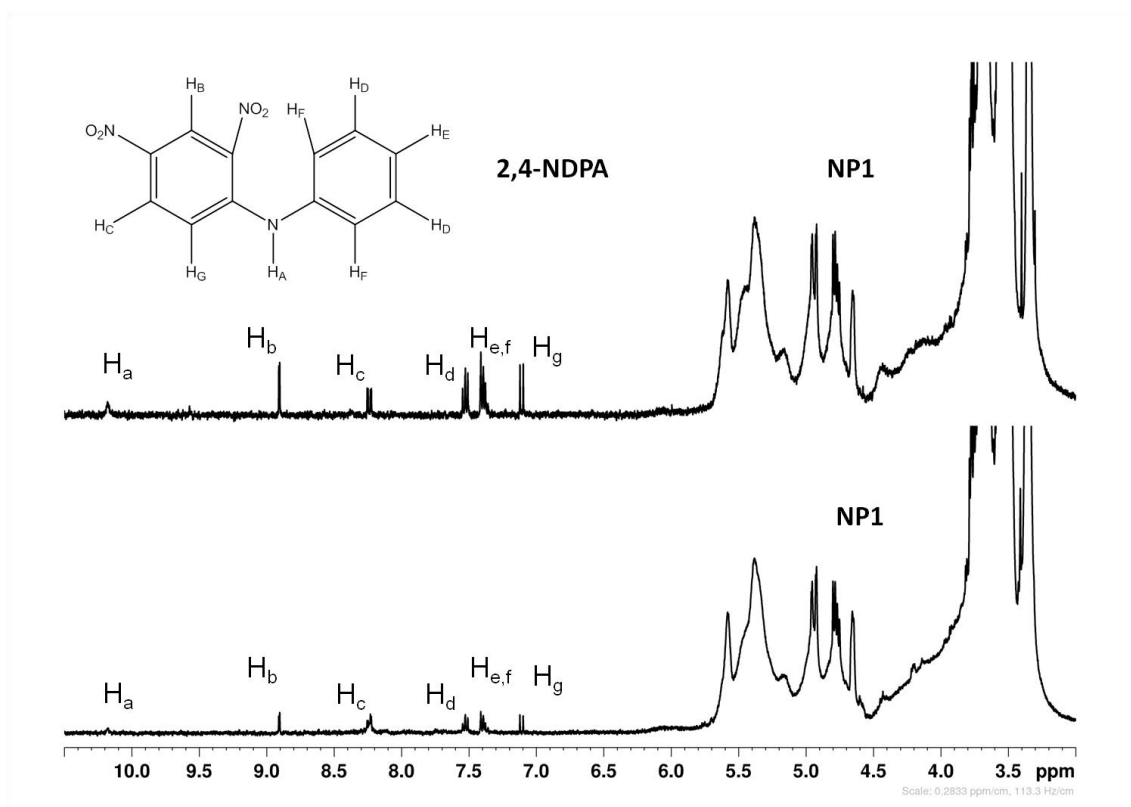


Figure A 11 ^1H NMR spectra of (a) NP1 + 1% w/w 2,4-NDPA at time 0, and (b) NP1 + 1% w/w 2,4-NDPA at time 3 d at 80 °C in DMSO-d_6 .

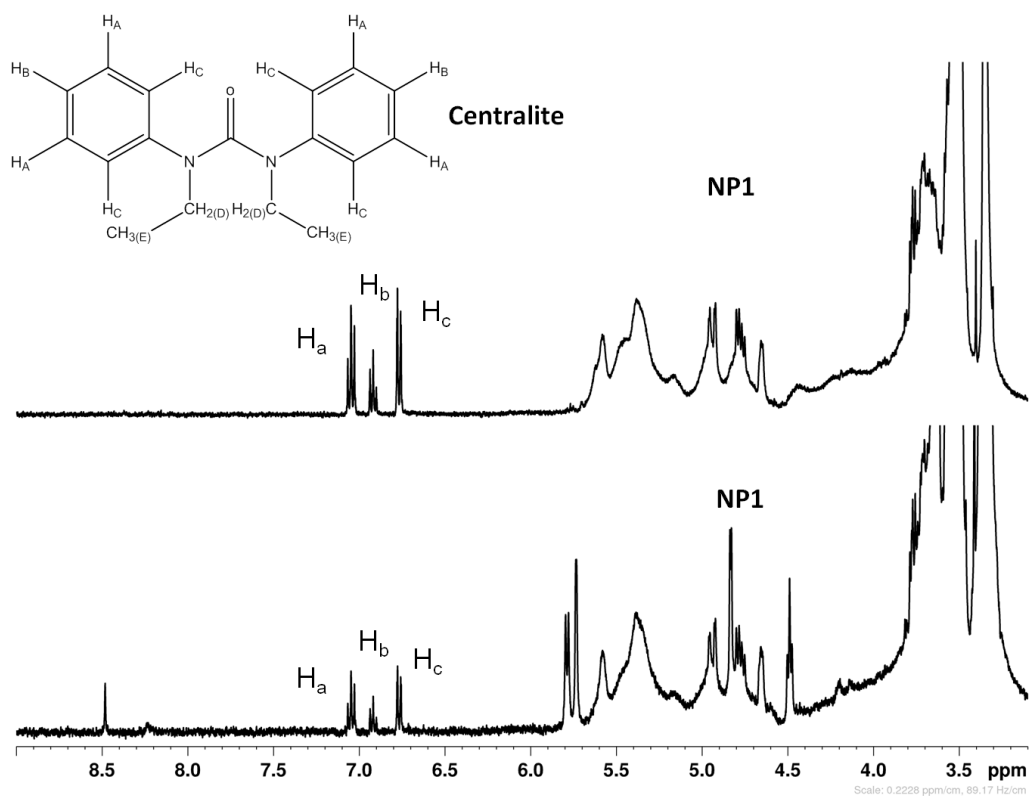


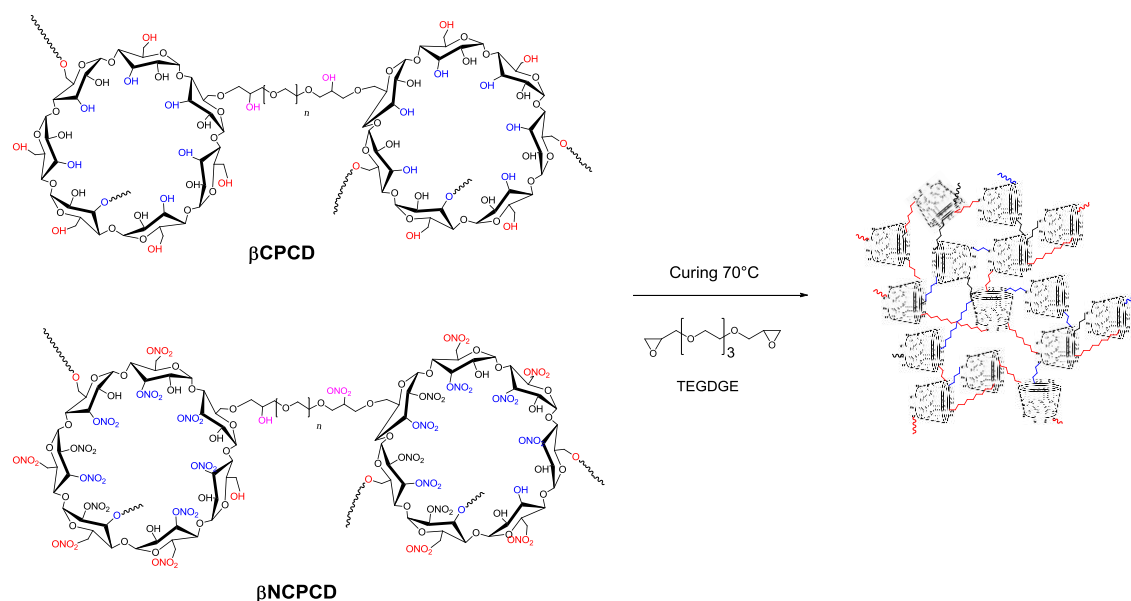
Figure A 12 ^1H NMR spectra of (a) NP1 + 1% w/w Centralite at time 0 and (b) NP1 + 1% w/w Centralite a time 3 d at 80 °C in DMSO- d_6 .

A.1 Preliminary curing tests of inert βCXCDs and energetic βNCXCDs

Initial tests were performed on inert βCPCD and energetic samples βNCPCD to investigate further cross-linking in the presence of TEGDGE. The curing tests at 70 °C were designed to check the possibility that cured products could be used during the formulation process.

Preliminary curing tests using inert IP18 and nitrated NP1 samples (PEG: βCD ratio = 4.1) were performed with TEGDGE as the curing agent at a βCPCD :TEGDGE ratio of 1:0.2 (Figure A 13). The curing mixtures were prepared by dissolving IP18 or NP1 and the cross-linker in acetone. The samples were stirred for 10 min, the acetone was removed under high vacuum at 40 °C and the samples were left to cure in sealed flasks in the oven at 70 °C for 20 days. The analysis of the sample involved checking the solubility of a

small fraction of the curing samples and analysing the consumption of the cross-linker by $^1\text{H-NMR}$ spectroscopy.



Scheme A 1 Schematic representation of the curing of βCPCD and βNCPCD binders using TEGDGE as the cross-linker.

A visible change in the colour of the mixture was observed after 2 days at 70°C (Figure A.13b) which was attributed to the ageing of the compounds in the oven. The IP18 sample became partially insoluble in water after 3 days. Characterisation by $^1\text{H-NMR}$ revealed that the cross-linker was consumed and/or degraded under curing conditions, suggesting that cross-linking had occurred.

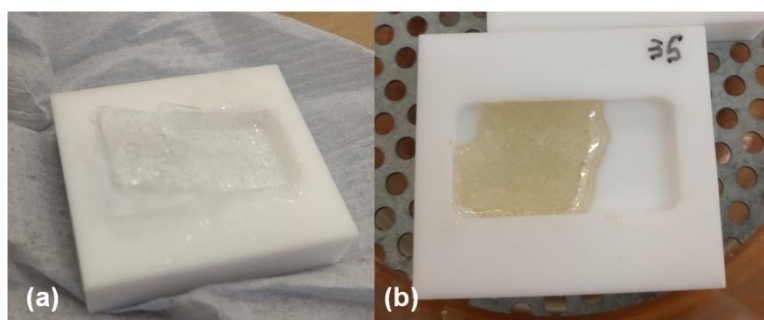


Figure A 13 (a) IP18 before curing and (b) after curing for 2 days at 70°C .

A colour change was also observed after curing NP1 for 1 day at 70°C (Figure A.14b,c). This was attributed primarily to the degradation of the nitrate esters, in

addition to the ageing of the compound in the oven. The NP1 sample was still soluble in acetone after 3 days. Characterisation by $^1\text{H-NMR}$ revealed that the cross-linker was consumed and/or degraded under curing conditions, suggesting that no cross-linking occurred.

Additional curing tests for the βCXCDs and βNCXCDs are necessary, potentially including the use of curing accelerators.

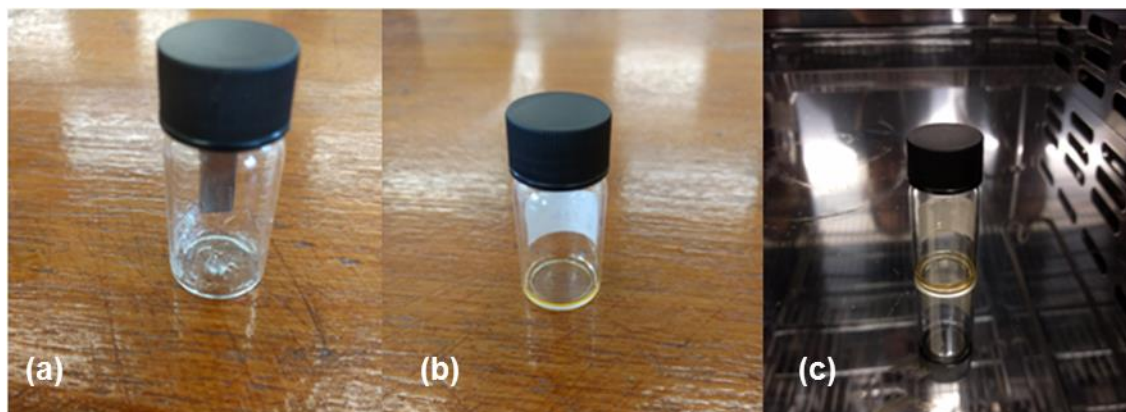


Figure A 14 Comparison of (a) NP1 and the NP1/TEGDGE curing mixture at (b) the mixing time, and (c) after 20 days at 70 °C.

Nitrated Cross-linked β -Cyclodextrin Binders Exhibiting Low Glass Transition Temperatures

Federico Luppi^{+, [a]}, Hamish Cavaye^{+, [a]} and Eleftheria Dossi^{+, * [a]}

Abstract: Polymeric binders such as β -cyclodextrins (β CDs) are used to bind with other constituents of energetic formulations and to prevent accidental ignition. One of the advantages of β CDs is the ability to tune their properties by chemical modification. Here, we synthesised nitrated cross-linked β CDs (β NCXCDs) to produce new binders for energetic formulations. The cross-linking of β CD with non-toxic triethylene glycol diglycidyl ether (TEGDGE, X=T) and poly(ethylene glycol) diglycidyl ethers (PEGDGE, X=P) yielded soft, water soluble oligomeric compounds (β CXCDs) which can improve the processability of energetic formulations and contribute to their desensitisation. When the PEGDGE cross-linker was used, lower glass transition temperatures were achieved, which extended the operative range of the β CPCD binder to -20°C . The analogous ni-

trated systems (β NCXCDs) were therefore synthesised using a 1:1 (v/v) ratio of 98% sulfuric acid/100% nitric acid or 100% fuming nitric acid, increasing their solubility in acetone and tetrahydrofuran. The nitrated derivatives were characterised by decomposition temperatures (200°C) and energies (up to 1750 J g^{-1}) comparable to nitrocellulose. Moreover, the glass transition of the inert β CXCDs at low temperatures ($<0^{\circ}\text{C}$) was conserved in the corresponding nitrated β NCXCDs, ensuring the desensitisation of energetic compositions even at low temperatures. This is the first time that nitrated derivatives of β CD with glass transition temperatures below 0°C have been reported, suggesting such derivatives could make suitable replacements for nitrocellulose and other binders in energetic formulations.

Keywords: cross-linked β -cyclodextrin · diglycidyl ethers · energetic binder · low T_g

1 Introduction


Synthetic and semi-synthetic polymeric binders are important components of most energetic formulations [1]. The role of the binder is to improve the overall mechanical properties of the formulation and to coat the energetic molecules, thus shielding them from accidental stimuli and environmental degradation. Nitrocellulose, produced by the nitration of natural cellulose, is the most frequently used semi-synthetic polymer in energetic formulations [1].

During the past three decades, cyclodextrins (CDs) have been introduced as energetic binders in a small number of studies because they are natural molecules with a composition similar to cellulose and they have useful molecular inclusion properties [1,2]. Typical CDs are cyclic compounds containing six, seven or eight sugar rings (α , β and γ CDs, respectively) linked together via α -glycosidic bonds. They are particularly useful in the food, cosmetic and pharmaceutical industries because they form complexes within their toroidal cavities with a wide range of molecules [2]. The physical properties of the CDs can be tuned to satisfy specific applications such as shielding other molecules from external stimuli [2,3], which is important in explosive applications [4–5]. The availability of hydroxyl functional groups allows the functionalisation of the macrocycles to further tune their physicochemical properties [2,3].

The inclusion properties of β CD and γ CD binders can lead to stabilisation of energetic molecules because these molecules have larger cavities than α CDs [3–5]. Furthermore, nitrated cyclodextrins (NCDs) have been developed as energetic components, although fully-nitrated cyclodextrins are sensitive to electrostatic discharge (ESD), e.g. β CD nitrated to 85% is sensitive to ESD ignition at 0.0125 J [6]. To reduce the ESD hazard, pre-functionalisation before nitration can be achieved using inert molecules as cross-linkers [7,8]. NCDs initially cross-linked with epichlorohydrin in NaOH, polyallylamine in KOH or isocyanate in DMSO, are less sensitive to ESD ignition at 0.1288 J [8], which is a 10-fold reduction in sensitivity. In contrast, longer inert cross-linkers such as poly(ethylene glycol) (PEG) have been used in CD systems for pharmaceutical applications, resulting in the formation of insoluble gels [9,10]. Water-

[a] F. Luppi,⁺ H. Cavaye,⁺ E. Dossi⁺
Centre for Defence Chemistry, Cranfield University, Defence Academy of United Kingdom, Shrivenham, SN6 8LA, UK
*e-mail: f.luppi@cranfield.ac.uk
hamish.cavaye@stfc.ac.uk
e.dossi@cranfield.ac.uk

[*] The manuscript was written with contributions from all authors. All authors have approved the final version of the manuscript.

 Supporting information for this article is available on the WWW under <https://doi.org/10.1002/prop.201800137>

soluble CD polymers were obtained when acyl chloride PEG derivatives were used [11] but to the best of our knowledge these derivatives have never been converted to nitrated derivatives.

One of the most important properties of binders in energetic formulations is the glass transition temperature (T_g), at which the rubbery binder becomes glassy and brittle. PEG-based cross-linkers are favoured for their low glass transition temperatures because this increases the operative temperature range within which the cross-linked materials can successfully contribute as a binder [12] and desensitise the energetic formulation. The replacement of highly toxic cross-linkers with non-toxic materials is one of the requirements for new energetic formulations. The REACH regulation of the European Union, has introduced restrictions on the usage of certain isocyanates to improve the protection of human health and the environment from the risks that can be posed by chemicals [13,14]. In this context, the use of CDs and non-toxic ethylene glycol diglycidyl ethers ensures relatively mild and environmentally sustainable cross-linking conditions: CDs are obtained from natural and sustainable sources, water is used as the reaction solvent, and the reaction temperatures are kept low. The formation of stable ether linkages (C–O–C) between CDs and the diglycidyl ethers also supports further functionalisation such as the nitration of the cross-linked cyclodextrins (CXCDs). Several nitration methods for pure or cross-linked CDs have been reported, ranging from pure nitric acid or nitric/sulfuric acid mixtures to stronger and more advanced systems such as nitration in liquid CO_2 with nitrogen pentoxide [8,15]. The latest methods achieve full nitration whereas earlier methods resulted in up to 90% nitration of the available hydroxyl groups [15]. The complexation of explosive molecules in the CD cavities also reduces the sensitivity of the explosive to external stimuli [8].

Here we report the synthesis of a β CXCD system and its nitrated derivative β NCXCD using TEGDGE and PEGDGE cross-linkers. The two cross-linkers were chosen as soft segments for their low glass transition temperatures of -80 and -68°C , respectively [16,17]. We selected β CD for the initial tests because it is less expensive than γ CD. However, the γ CD cavity would encapsulate larger energetic molecules and more tests using γ CD will be published in the future. All β CXCDs were subsequently nitrated to determine the impact of the β NCXCD systems on degradation energies and the glass transition temperature. We also carried out preliminary studies to determine the degree of compatibility between the inert and nitrated products and energetic fillers.

2 Experimental Section

2.1 Materials

The β CD ($\geq 97\%$, Sigma-Aldrich) was used from stock (TGA, 13% water content). Polyethylene glycol diglycidyl ether (PEGDGE 500 Mw, Sigma-Aldrich), sodium hydroxide (Fisher Chemicals), acetylated dialysis membrane (2000 MWCO, Sigma-Aldrich), tetra-*n*-butylammonium bromide (TBAB, Sigma-Aldrich), and triethylene glycol (TEG, Sigma-Aldrich) were obtained from commercial sources and used without further purification. Triethylene glycol diglycidyl ether (TEGDGE, 262.0 g/mol) was synthesised as previously described [14]. The β CXCD cross-linking ratio was determined by ^1H NMR.

2.2 Characterisation

NMR spectra were recorded on a Bruker Ascend (400 MHz) with a BBFO probe in deuterated dimethyl sulfoxide (DMSO-d_6) solution using tetramethylsilane (TMS) as an internal reference. Spectra were also recorded in deuterated water (D_2O) with 3-(trimethylsilyl)-1-propane-sulfonic acid sodium salt as an internal reference. Peak multiplicities were described as follows: singlet (s), doublet (d), triplet (t), multiplet (m), doublet of doublet (dd), and broad (br). Thermal properties were determined by DSC using a Mettler Toledo DSC822 or DSC30 with heating and cooling rates of $10^\circ\text{C min}^{-1}$ and a flow of dry nitrogen. The reported values were the measurements performed on samples with a mean weight of 10 mg for inert materials and low temperature, whereas 1 mg was used to assess the decomposition temperature of energetic materials. Yields were measured as mass of products over mass of reactants. Gel Permeation Chromatography (GPC) measurements were performed in tetrahydrofuran (THF) at 35°C , using Agilent PLgel 10 μm mixed B columns and Agilent polystyrene calibration kit (M_w 500– 6.9×10^6).

2.3 Synthesis of β CXCDs

The β CD (5–5.6 g, 3.8–4.4 mmol) was dissolved in 5.6–50% w/w NaOH (21.0 mL) and stirred mechanically for 0–16 h. Diepoxide (TEGDGE $n=3$ or PEGDGE $n=9$) (17.4–5.8 mL, 13.2–36.9 mmol) was then added dropwise in 20 min with vigorous stirring. The reaction mixture was heated to 30– 70°C for 30 min with vigorous stirring. After cooling for 20 min, the mixture was neutralised with 6 M HCl. The purification method depended on the solubility of the product in water. The volume of solvent for soluble products was reduced and the crude solute was precipitated in acetone three times. The solid was then collected and dissolved in distilled water and dialysed against water using a cellulose membrane (2000 MWCO) for 5 days. The insoluble products

were filtered from the crude reaction mixture and washed with acetone. The insoluble solid was then collected and suspended in distilled water and dialysed against water using a cellulose membrane (2000 MWCO) for 5 days. The dialysis water was replaced every day. The dialysed solid was collected and the water was evaporated under reduced pressure. The final product was characterised by ^1H NMR and DSC. ^1H NMR (400 MHz, DMSO- d_6 , ppm): δ = 5.9–5.6 (br m, $\text{OH}-\text{C}_2$, $\text{OH}-\text{C}_3$), 5.1–4.8 (m, $\text{H}-1$), 4.7–4.5 (br m, OH_A , OH_B and OH_C), 4.4 (br m, $\text{OH}-\text{C}_6$), 4.0–3.2 (br m, $\beta\text{CD}-\text{OCH}_2-(\text{CH}-\text{OH})-\text{CH}_2-\text{O}-\text{CH}_2-\text{CH}_2$). DSC ($10^\circ\text{C min}^{-1}$, N_2) 240–250 $^\circ\text{C}$ (dec) (See Supporting Information).

2.4 Synthesis of βNCXCDs

Nitric acid (95–100% 0.5–1 mL) or 100% nitric acid/100% sulfuric acid mixture (50:50 v/v, 1 mL) was poured into a round-bottomed flask and cooled to below 10°C in ice water. Dichloromethane (DCM) (1.8 mL) was added when route 2 reported later in the paper (Figure 2) was followed. The bath was removed and βCXCD ($X=\text{P}$ and T , 200.0 mg) was added in small fractions over 5 min, ensuring that the temperature remained below 10°C . The crude slurry or solution was then left stirring at room temperature for 1 h. The reaction mixture was poured into ice/water (10 mL) and the solid was dissolved in acetone (5 mL) and precipitated in water (100 mL). The clean product was collected, dissolved in acetone and dried under vacuum. Small portions necessary for characterisation were taken and the rest was stored under DCM. The ^1H NMR analysis was performed in acetone- d_6 and DMSO- d_6 . DSC ($10^\circ\text{C min}^{-1}$, N_2) 197–210 $^\circ\text{C}$ (dec) (See Supporting Information).

3 Results and Discussion

3.1 Synthesis of βCXCDs

Several βCXCDs were synthesised at 70°C to determine the effect of different parameters on the yield of the reaction and the physicochemical properties of the products. The cross-linked compounds were recovered after cooling the reaction mixture followed by neutralisation with 6 M HCl. The final products were obtained by precipitation from water in acetone followed by dialysis against water using a cellulose membrane with a molecular weight cut-off (MWCO) of 2000 for 5 days.

The cross-linking reaction involved the alkoxidation of βCD combined with diglycidyl ethers of two different lengths: PEGDGE with $n=9$ repeating ethylene glycol units and TEGDGE with $n=3$ ethylene glycol units. The hydroxide (OH^-) ions from the basic medium (NaOH) reacted first with the hydroxyl groups of the βCDs to form alkoxides, and the latter then reacted with the epoxide ring of the diglycidyl ether molecule. The hydroxyl groups of the βCDs would not

react at room temperature with the epoxides. Heating the reaction mixture (up to 70°C) under variable basic conditions (5.6% w/w, 40% w/w and 50% w/w) led to the partial substitution of all three hydroxyl groups attached to C-2, C-3 and C-6 atoms of βCD units in βCXCDs as from ^1H -NMR characterisation in dimethylsulfoxide (DMSO); this is discussed later in this paper. As a general rule for the reactivity of βCD hydroxyl groups, the primary hydroxyl groups attached to C-6 atom (Figure 1), are considered the most reactive [18–20]. The difference of reactivity of the primary and secondary hydroxyl groups of βCD cannot be assessed by the authors in these earlier studies due to the overlap of the hydroxyl proton signals in the NMR analyses. The number of unreacted hydroxyl groups attached to C-2 and C-3 atoms was evaluated by ^1H -NMR spectroscopy in dimethylsulfoxide (DMSO) and was found to depend on the concentration of NaOH. The least concentrated NaOH solution (5.6% w/w) promoted more cross-linkages whereas stronger NaOH solutions (40–50% w/w) inhibited the formation of the cross-linked product (Table 1) because of i) the higher amount of degraded cross-linker by the reaction conditions discussed in the following paragraph and ii) the suppressed formation of βCD -alkoxide in the very viscous reaction mixtures.

Under the basic cross-linking conditions we used, a competitive side reaction occurs and the degradation of the diepoxide cross-linker produces a tetra-hydroxyl by-prod-

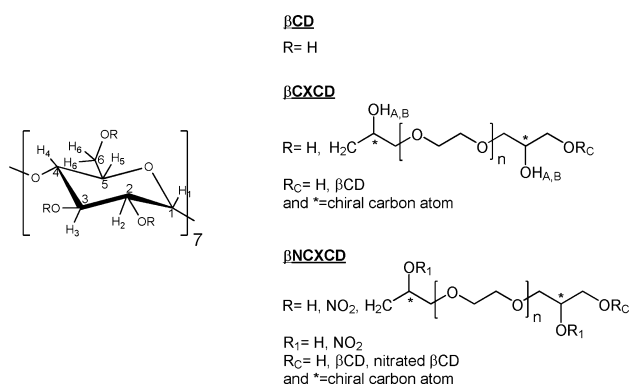


Figure 1. Proposed chemical structure of βCD , βCXCD and βNCXCD ($X=\text{T,P}$) with numbered H and C atoms.

Table 1. Effect of NaOH concentration on the properties of βCPCDs .

Sample ¹	NaOH ² (% w/w)	Reaction time (h)	Yield ³ (%)	T _g ($^\circ\text{C}$)	Water solubility
βCPCD1	50.0	1.00	< 1	–	Y
βCPCD2	40.0	1.00	< 1	–	Y
βCPCD3	5.6	0.66	88	–30	N

¹ PEGDGE: βCD ratio = 9:1, ² Reaction temperature = 70°C , ³ Yield measured as mass of products/mass of reactants.

uct, thus affecting the yield of the reaction and physical properties of the final product. The effect of the NaOH concentration was investigated at 70 °C for short reaction times (≤ 1 h) (Table 1) and this had a significant influence on the reaction. When the NaOH concentration was low, the reaction become more efficient and reached the gelation point accompanied by the appearance of a solid product and the increasing of the viscosity of the reaction mixture, whereas strong NaOH solutions delayed the formation of gels and affected the yield of the reaction due to faster cross-linker degradation.

We also investigated the effect of the number of ethylene glycol units in the cross-linker when the cross-linker: β CD ratio was maintained at 9:1, and 40% w/w NaOH was used for all the reactions. The trend of the reactions suggested that TEGDGE produces gels more quickly than PEGDGE. Given this result and the insoluble nature of the gels produced with TEGDGE, we decided to focus on the longer cross-linker (PEGDGE), which was expected to confer better mechanical properties upon the cross-linked products.

Another parameter that affects the cross-linking of β CD is the time needed to prepare its alkoxide. Initial trials suggested that leaving the β CD stirring in basic conditions for 16 h leads to better yields of soluble products (Table 2). It is therefore necessary to allow the cyclodextrin to form the alkoxidic groups prior to the addition of the cross-linker as discussed below. Indeed, the alkoxide promoted successful ether linkage formation between cyclodextrin and PEGDGE (see the Supporting Information).

Table 2. Role of the temperature on the yield of β CPCDs.

Sample	T (°C)	Yield (%)	T _g (°C)	Water solubility
β CPCD4 ¹	70	1	–	Y
β CPCD5 ¹	50	13	+6	Y
β CPCD6 ²	50	30	–18	Y
β CPCD7 ²	30	34	–22	Y

¹ Cross-linker: β CD = 5:1, 0 h alkoxide formation, 5 h reaction time,

² Cross-linker: β CD = 5:1, 16 h alkoxide formation, 5 h reaction time.

Higher temperatures affect the kinetics of cross-linking by increasing the rate of cross-linking and also by accelerating the degradation of the cross-linker. Two sets of trials were carried out using the following conditions: a low concentration of NaOH (5.6% w/w), a cross-linker: β CD ratio of 5:1, 0 or 16 h for the formation of the alkoxide and 5 h for the cross-linking reaction itself. The longer time for alkoxide formation was set at 16 h based on the results discussed above. The cross-linker: β CD ratio was set to 5:1 to prevent gelation, which occurred at the higher ratio of 9:1. The data summarised in Table 2 suggest that the cross-linker is more stable at 30 °C, but higher temperatures such as 50 °C and

70 °C reduce the yield due to the loss of cross-linker in the competitive degradation reaction.

The effect of the cross-linker: β CD ratio was investigated under the optimal conditions determined thus far, i.e. 5.6% w/w NaOH, 30 °C, 16 h for the formation of the alkoxide and 5 h for the completed cross-linking reaction (Table 3). The thermal properties of the cross-linked products at low temperatures were affected, i.e. lower amounts of cross-linker resulted in products with higher degree of crystallinity and higher T_g. The ratio of cross-linker: β CD in the cross-linked product is lower than in the initial feed of the reaction. The difference is caused by the degradation of the cross-linker as mentioned above and the NMR analysis of the compounds is discussed in detail later, in the section dealing with characterisation.

Table 3. Effect of cross-linker: β CD ratio on the properties of β CPCDs.

Sample ¹	Cross-linker: β CD ratio feed	Cross-linker: β CD ratio by NMR	Yield (%)	T _g (°C)	Water solubility
β CPCD7	5:1	3.75:1	34	–22	Y
β CPCD8	4:1	3:1	36	–13	Y
β CPCD9	3:1	2.25:1	68	–3	Y
β CPCD10	2:1	1.5:1	44	+8	Y

¹ 5.6% (w/w) NaOH, 30 °C, 16 h alkoxide formation, 5 h reaction time.

A final investigation demonstrated that the duration of the addition of the cross-linker to the reaction mixture also influenced the reaction yield. If prolonged addition times were used, a small proportion of cross-linker was lost in the competing degradation reaction. Further studies are needed to determine the optimal conditions to improve the yield of water-soluble samples ($\leq 68\%$ at present). Higher yields were achieved only for insoluble gels. The cross-linking of β CPCDs therefore requires further optimisation. The samples obtained in these early experiments were used for the nitration reactions described in the following section.

The images of β CPCD7 and its precursor β CD were compared by scanning electron microscopy (SEM) and the corresponding images are provided in the Supporting Information. The images show the homogeneity of the surface of the β CPCDs, whereas the β CDs have a crystalline appearance.

3.2 Synthesis of β NCXCDs

The β CXCDs were functionalised with nitro groups to form energetic derivatives that can contribute energy to explosive formulations. The nitration of a set of water-soluble β CPCDs and insoluble β CTCD precursors with variable phys-

ical properties was carried out using the reaction conditions shown in Figure 2.

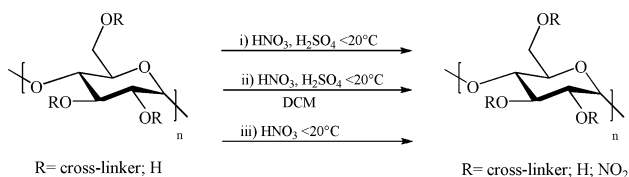


Figure 2. Overview of the synthesis of β NXCDCs.

In initial tests we evaluated the following nitration methods: (i) using 1:1 98% sulfuric acid/100% nitric acid; (ii) two-phase nitration, using 1:1 98% sulfuric acid/100% nitric acid followed by dichloromethane (DCM); and (iii) using 100% fuming nitric acid as the nitrating phase. DCM did not improve the control and/or efficiency of the nitration reaction because the β NXCDCs were insoluble in DCM and were not extracted from the acidic water phase during the reaction. Therefore, DCM was not included in subsequent experiments. Attempts to nitrate insoluble gel compounds also achieved no control of the nitration reaction, and thus the physicochemical and hazard properties of the products were unpredictable, so these precursors were also abandoned.

The β CXCDCs were difficult to dissolve in the mixed acids and their conversion to analogous nitrated products was compromised. The sulfate esters [21,22] of β CXCDCs formed in these nitration conditions are expected to affect their solubility and consequently the efficiency of the nitration reaction. In contrast, the β CXCDCs dissolved efficiently in the fuming nitric acid within the 1 h duration of the nitration reaction. Table 4 summarises the data obtained when 100% fuming nitric acid was used as the nitrating agent. All β NCPCDCs were soluble in organic solvents such as acetone and THF, suggesting good processability, which is important in energetic formulations because the different components must be mixed thoroughly. The β NCPCDCs were purified by re-precipitation from acetone in water and their thermal stability was satisfactory, as shown by their high decomposition energy and negative T_g values. A nitrated sample β NCPCDC1 was examined by gel permeation chromatog-

raphy (GPC) in THF and compared with poly(styrene) standards. The results $M_n=7350$ Da and $M_w=15140$ Da, confirmed the polymeric nature of the sample (see Supporting Information).

Like the β CPCDCs precursors, the T_g of the nitrated products was dependent on the number of soft ethylene glycol units in the cross-linker. The T_g increased when less PEGDGE was used (Table 4) and we speculate from very preliminary modelling [23] investigation on nitrated CDs that the polar nitro groups could inhibit the mobility of the polymeric chains. On the other hand, the large number of OH to ONO₂ (nitrate) transformations contributed to the overall energy of the system. The decomposition temperature (T_{dec}) stabilised at 196 °C, which is similar to nitrocellulose samples with a 12.5% nitrogen content [24]. As expected, the energy of the system was also affected, with higher decomposition energies (ΔH_{dec}) such as 1750 Jg⁻¹ for sample β NCPCDC3. The thermal properties of the β NCPCDCs can be tuned to give the desired product for specific applications. A very small, second-order transition was observed in all thermograms at ~80 °C, which was attributed to the glass transition of the rigid β CD units in the cross-linked systems.

When TEGDGE was used as the cross-linker, both the β CTCD precursors and the β NCTCDs derivatives were insoluble gels. The β NCTCDs were characterised by low T_g values, thermal stability and relatively low decomposition energies compared to the analogous β NCPCDCs (Table 4). Although the cross-linker: β CD ratio was 9:1 to guarantee low transition temperatures, the degree of nitration was lower in these materials due to the inability of the acids to penetrate the polymer structure and efficiently nitrate the hydroxyl groups of the β CD units. The nitration of the same β CTCD resulted in the synthesis of β NCTCDs with variable properties. This highlights the lack of control over the nitration of insoluble products. Also, it was difficult to purify the insoluble β NCTCDs from the acid traces. The stability of these products and their hazard properties is strongly affected by the efficiency of the purification process.

3.3 Chemical Characterisation

The cross-linked products we synthesised were characterised by ¹H NMR spectroscopy in deuterated dimethylsulf-

Table 4. Thermal properties of β NXCDC oligomers.

Nitrated sample ¹	Precursor Name	cross-linker: β CD	Reaction time (h)	T_g (°C)	T_{dec} (°C)	ΔH_{dec} (Jg ⁻¹)
β NCPCDC1	β CPCDC7	5:1	1.0	-20	202	1500
β NCPCDC2	β CPCDC8	4:1	1.0	14 ²	197	1640
β NCPCDC3	β CPCDC9	3:1	1.0	19	199	1750
β NCTCD1	β CTCD1	9:1	1.0	-21	210	530
β NCTCD2	β CTCD1	9:1	1.0	-20	208	650

¹ Using 200 mg of precursor and 1 mL 100% HNO₃, ² Very broad transition; more investigation needed.

oxide (DMSO- d_6) and deuterated water (D_2O) as solvents. DMSO- d_6 was used to investigate the reactivity of the hydroxyl groups of the β CDs at 4.4–5.5 ppm (Figure 3 and 4).

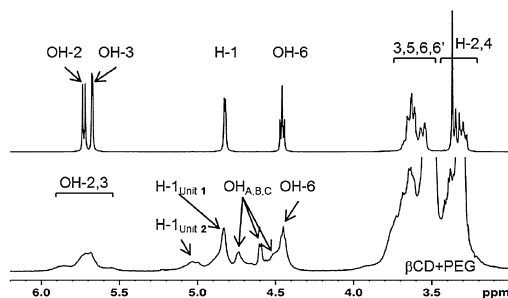


Figure 3. 1H NMR spectrum of β CD and β CPCD8 in DMSO- d_6 , suggesting the assignment of the proton of the OR groups when no substitution occurs. The OH_C assignment is expected when $R_1 = H$.

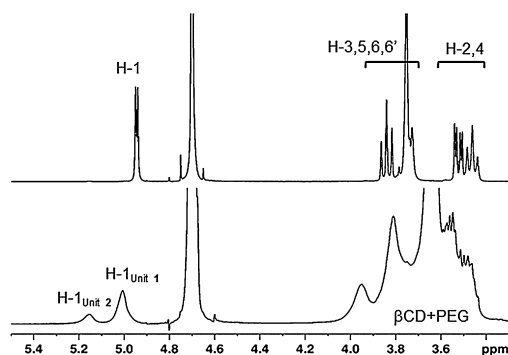


Figure 4. 1H -NMR spectra of β CD (top) and β CPCD8 (bottom) in D_2O .

The spectrum of the β CPCDs shows broadened peaks due to the larger cross-linked molecules, when compared to the spectrum of pure β CD [2]. New peaks appear in the spectrum (Figure 4) and are attributed to the three hydroxyl groups (OH_A , OH_B and OH_C when $R_C = H$) on the cross-linking units. Due to the similar environments in the compound, many signals overlap. The water peak which overlaps the signals of the product at 3.3–3.4 ppm in DMSO- d_6 moves in the hydrogen-deuterium oxide (HDO) when D_2O is used, allowing us to determine the cross-linking ratio as reported below.

The cross-linker: β CD ratio in β CPCDs was calculated [11] from the 1H NMR in D_2O (Figure 4).

- Integral 1 at 4.8–5.1 ppm = $n_{\beta CD}$ H-1 protons

- Integral 2 at 3.2–4.0 ppm = $6n_{\beta CD}$ H-2 to H-6 protons + $44n_{cross-linker}$ protons

The results show that the cross-linker is not consumed in the competing degradation reaction at 30 °C, allowing the reactants to react in a quasi-stoichiometric manner (25% lower than the anticipated theoretical value, Table 3).

The β NCTCDs and β NCPCDs were characterised by 1H NMR in acetone- d_6 and DMSO- d_6 . The spectra recorded in DMSO- d_6 were compared with those of the starting oligomers and with a sample of nitrated β CD (β NCD) synthesised under the same conditions [15]. Figure 5 shows the 1H NMR spectra of β NCD and β NCXCD in DMSO- d_6 .

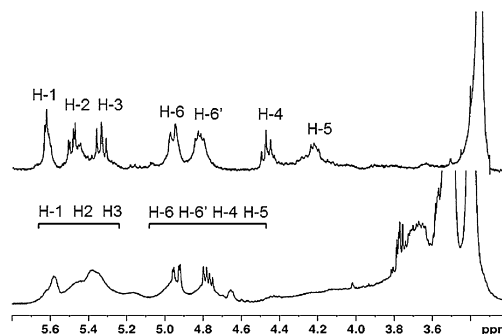


Figure 5. 1H NMR spectra of β NCD (top) and β NCPCD1 (bottom) in DMSO- d_6 . In the β NCPCD1 spectrum (bottom), the signals near the water peak are assigned to protons that are not near the nitrate groups.

The β NCPCD1 signals were broader due to the polymeric nature of this product. The broadness of the peaks and the down field shift of the signals compared to β CPCD reflect the complex chemical environment present in this energetic polymer. The different degrees of nitration on the cyclodextrin units result in overlapping signals representing protons close to the nitrate groups. The reference peak of proton H-1 close to the glycoside bond is present at 5.60 ppm. The broad signals at 5.55–5.10 ppm can be assigned to protons H-2 and H-3 attached to asymmetric carbon atoms 2 and 3, whereas the signals at 5.10–4.60 ppm can be assigned to CH_2 , which is adjacent to nitrate groups in both β CD and the cross-linker units. Finally, the signals at 4.6–4.0 ppm can be assigned to CH_2 protons belonging to both β CD and the cross-linker units that are not adjacent to a nitrate group, but close enough to be influenced by them. The signals between 3.8 ppm and 3.2 ppm can be assigned to the methylene of the ethylene glycol units which are farthest from and least affected by the nitrate groups.

The degree of nitration in β NCD was determined using a previously described analytical method [15] and was nearly 90%. The degree of nitration in the β NCPCDs will be assessed in future studies based on iron sulfate titration and comparison with ion chromatography data.

3.4 Thermal Characterisation

The T_g of the β CXCDs and β NCXCDs was determined by differential scanning calorimetry (DSC) within the temperature range -100°C to 100°C at $10^\circ\text{C min}^{-1}$ and the results are reported in Tables 1–4. The T_g of the β CXCDs ranged between -22°C and $+8^\circ\text{C}$ and increased in line with the proportion of β CD because the cross-linker introduces more mobility into the system. The glass transitions reported for a similar cross-linked system based on a carboxylic acid PEG linker ranged from -20°C to -16°C [11]. These values are consistent with the properties gained by the cross-linked system studied herein.

The low T_g of the β CXCD precursors was transferred to the β NCXCD derivatives and ranged from -20°C to $+19^\circ\text{C}$ (Table 4). This transition is particularly wide compared to the non-nitrated precursor (Figure 6) and the material begins to soften at very low temperatures. The T_g midpoint is difficult to determine in the nitrated product due to the broadness of the transition, which may reflect the sum of different arrangements of the entangled cross-linker chains in the compound. Dynamic mechanical analysis (DMA) of β CXCD and β NCXCD samples is currently underway and the results will be published in a separate article.

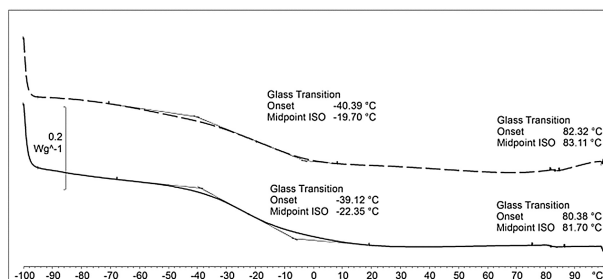


Figure 6. DSC thermogram of the glass transition of β PCPD8 (solid line) and β NCPCD1 (dashed line) between -100°C and 100°C .

All β NCPCDs derived from water-soluble β PCPD precursors showed similar thermal stabilities, with decomposition occurring at $\sim 200^\circ\text{C}$. This is comparable with the decomposition of nitrocellulose [24]. The decomposition energy fell within the range 1500 – 1750 J g^{-1} (Figure 7).

The energy released by the β NCXCDs was similar to that released by nitrocellulose samples with a nitrogen content of 12.5%, measured using the same method [24]. As expected, cross-linking affected the maximum nitrogen content of the β NCXCDs, which declined with the increasing content of inert ethylene glycol chains. DSC revealed that the β NCXCD systems displayed lower decomposition energies than the β NCD sample with 90% nitration (1880 J g^{-1}). Micro-calorimetry measurements will be performed in the future to measure the decomposition energy of the β NCXCDs and the effective release of energy from these systems.

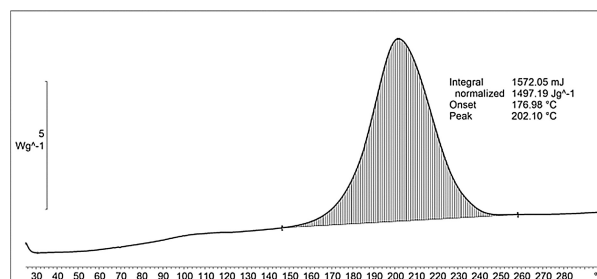


Figure 7. DSC thermogram of the decomposition of β NCPCD1.

The attempted nitration of insoluble β CXCD products also yielded compounds with a decomposition event at $\sim 200^\circ\text{C}$, but the decomposition energy was 500 – 800 J g^{-1} . This reduction in energy probably reflects the presence of fewer nitrate groups after nitration given the less accessibility to the hydroxyl groups of β CXCDs and a higher proportion of cross-linker in the system.

3.5 Compatibility Assessments

Initial compatibility tests based on DSC were carried out to determine whether contact between the β NCPCDs and energetic ingredients in a formulation could lead to undesirable or unexpected hazards. Sample β NCPCD1 was mixed with energetic fillers such as oxidisers, pyrotechnics and high explosives, and preliminary DSC compatibility tests were carried out according to STANAG 4147 Test 4 [25]. Any chemical interaction between the ingredients should lead to a change in the decomposition profile of the formulation. The thermal decomposition of the single ingredients and their mixture was compared (Table 5). The compounds were mixed in a 1:1 w/w ratio (total amount 1.0 mg) and heated from 30 to 500°C at a rate of 2°C min^{-1} .

Sample β NCPCD1 was tested with oxidisers such as ammonium dinitramide (ADN), potassium chlorate (KClO_3), ammonium perchlorate (NH_4ClO_4) and ammonium nitrate

Table 5. Summary of compatibility tests using β NCPCD1.

Energetic Name	Mixture			Change in shape
	T_{deg} ($^\circ\text{C}$)	T_{deg} ($^\circ\text{C}$)	ΔT ($^\circ\text{C}$)	
ADN	174	161	-13	Significant
KNO_3^1	-	-	-	Minor
NH_4ClO_4	300	242	-58	Significant
NH_4NO_3^1	-	-	-	Significant
KClO_3^1	-	-	-	-
Red Phosphorous	400	404	+4	Minor
PETN	185	187	-2	None
HMX	279	279	0	Minor
RDX	225	210	-15	Minor

¹ No degradation observed.

(NH_4NO_3). No changes in either the decomposition temperature (T_{dec}) or the curve shape were observed for mixture $\beta\text{NCPCD1}/\text{KClO}_3$ compared to the thermogram of the pure oxidiser (Table 5). We found that βNCPCD1 is not compatible with NH_4ClO_4 or NH_4NO_3 and that ADN shifted the T_{dec} by -13°C and changed the shape of the curve. Further vacuum stability tests are needed to confirm compatibility with ADN. Sample βNCPCD1 showed good compatibility with pyrotechnics such as red phosphorous. All thermograms are provided in the Supporting Information.

Sample βNCPCD1 also showed good compatibility with symmetric nitro-esters such as pentaerythritol tetranitrate (Figure 8) suggesting that βNCPCDs could potentially be combined with nitroglycerine in double-based and triple-based propellants [26].

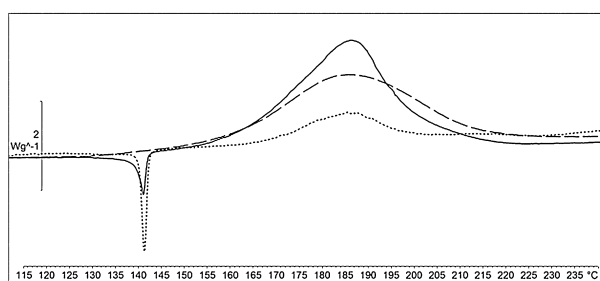


Figure 8. Thermograms of pentaerythritol tetranitrate (dotted line), βNCPCD1 (dashed line) and the mixture (solid line) at 2°C min^{-1} .

Nitramines such as RDX and HMX were also tested for compatibility with βNCPCD1 . Although the T_{deg} of RDX was 15°C lower when mixed with βNCPCD1 , the degradation of HMX was not affected (Figure 9).

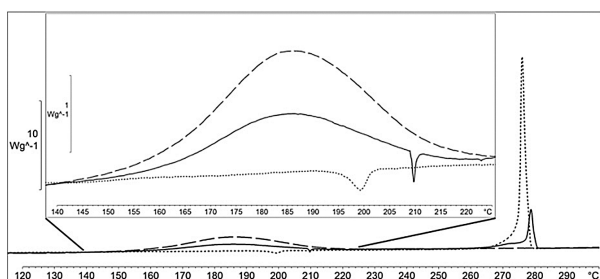


Figure 9. Thermograms of HMX (dotted line), βNCPCD1 (dashed line) and the mixture (solid line) at 2°C min^{-1} .

The small amount of HMX used in the test underwent degassing within the degradation temperature range of βNCPCD1 . The phenomenon was detected by DSC as an endothermic peak at 210°C . The measurement was repeated several times and the endothermic peak shifted at different temperatures every time, supporting the degassing hypothesis.

4 Conclusions

The synthesis of βCXCD systems from βCD and diglycidyl ethers yielded cross-linked insoluble or water-soluble derivatives with low T_g values down to -30°C , the first such observation for this type of product. The physicochemical properties of the products were affected by several reaction parameters, including the temperature, cross-linker: βCD ratio, concentration of NaOH, time allowed for the formation of βCD alkoxide, and the duration of reaction with the cross-linker. The cross-linking reaction parameters were tuned to obtain soft, soluble precursors to make the subsequent nitration reaction safer and more consistent. The polymers were water soluble if prepared with a PEGDG-E: βCD ratio of up to 5:1 at 30°C . The T_g of the cross-linked materials was primarily affected by the quantity and length of PEG spacer present in the system.

The βNCPCDs retained some of the mechanical properties of the precursor systems. The T_g was maintained below 0°C after the nitration of βPCPD derivatives made of high βCD :cross-linker ratio. The presence of polar nitrate groups on the cross-linked molecules increased the packing density of the molecules and thus reduced their freedom, increasing the T_g . Thermal analysis revealed that the nitrated products soften from -60°C in a linear manner. The thermal stability and energy released by the βNCPCDs is similar to that observed for nitrocellulose samples with a nitrogen content of 12.5–13.5% making them promising nitrocellulose substitutes in energetic compositions. The further processing of βNCXCDs using the same purification methods applied to nitrocellulose would improve the thermal stability even more.

Initial compatibility tests indicated that βNCPCDs may be suitable binders in formulation with selected energetics. The reaction will need to be scaled up for proper compatibility and Energetic Materials Testing and Assessment Policy (EMTAP) tests to determine the sensitivity of the new nitrated cross-linked compounds to ESD.

5 Recommendations/Future work

The assessment of the properties of the new nitrated cross-linked β -cyclodextrins developed in this work is in progress. Investigation of the change of properties with time and overall ageing of the nitrated binder as well as their compatibility with stabilisers/plasticisers is recommended. The cross-linking reaction of βCD with TEGDGE and other ethylene glycol diglycidyl ethers is currently investigated.

Supporting Information

The following files are available free of charge.

Acknowledgements

This project was funded through the Weapons Science and Technology Centre (WSTC) by the Defence Science and Technology Laboratory (Dstl). The authors would like to thank Roxel UK for kindly providing the ADN sample and BAES Land for assistance in the exploitation of this work.

References

- [1] H. G. Ang, S. Pisharath, *Energetic Polymers*, Wiley-VCH, 2012.
- [2] J. Szejtli, Introduction and General Overview of Cyclodextrin Chemistry, *Chem. Rev.* **1998**, *98*, 1743–1753.
- [3] H. J. Schneider, F. Hacket, V. Rüdiger, NMR Studies of Cyclodextrins and Cyclodextrin Complexes, *Chem. Rev.* **1998**, *98*, 1755–1786.
- [4] S. Cahill, S. Bulusu, Molecular Complexes of Explosives with Cyclodextrins, *Magn. Reson. Chem.* **1993**, *31*, 731–735.
- [5] P. Maksimowski, T. Rumianowski, Properties of the Gamma-Cyclodextrin/CL-20 System, *Cent. Eur. J. Energ. Mater.* **2016**, *13*, 217–229.
- [6] J. P. Consaga, Composites of Cyclodextrin Nitrate Ester Plasticizers, United States Patent, 5,114,506, United States Dept. of the Navy, USA **1992**.
- [7] J. P. Consaga, Chemically Reactive Fragmentation Warhead, United States Patent, 6,293,201 B1, United States of America, Secretary of the Navy, USA **2001**.
- [8] A. Ruebner, G. L. Statton, J. P. Consaga, Polymeric Cyclodextrin Nitrate Esters, United States Patent, 6,527,887, Mach I, Inc., USA **1991**.
- [9] G. Mocanu, D. Vizitiu, A. Carпов, Cyclodextrin Polymers, *J. Bioact. Compat. Polym.* **2001**, *16*, 315–342.
- [10] C. Rodriguez-Tenreiro, C. Alvarez-Lorenzo, A. Rodriguez-Perez, A. Concheiro, J. J. Torres-Labandeira, New Cyclodextrin Hydrogels Cross-linked with Diglycidylethers with a High Drug Loading and Controlled Release Ability, *Pharm. Res.* **2006**, *23*, 121–130.
- [11] T. T. Nielsen, V. Wintgens, K. L. Larsen, C. Amiel, Synthesis and characterization of poly(ethylene glycol) based β -cyclodextrin polymers, *J. Inclusion Phenom. Macrocyclic Chem.* **2009**, *65*, 341–348.
- [12] P. Golding, A. J. Bellamy, A. E. Contini, E. Dossi, Polyphosphazenes, Patent WO, WO/2013/190260 A3, Int. Appl. PCT/GB2013/000276, The Secretary of State for Defence, UK; Cranfield University **2013**.
- [13] Regulation (EC) No 1907/2006 of the European Parliament and of the Council of 18 December 2006 concerning the Registration, Evaluation, Authorisation and Restriction of Chemicals (REACH), establishing a European Chemicals Agency, 2006.
- [14] E. Dossi, J. Akhavan, S. E. Gaultier, R. G. Williams, W. J. Doe, Cross-linking of Hydroxyl-terminated Polyols with Triethylene-glycol Diglycidyl Ether: An Alternative to Toxic Isocyanates, *Propellants Explos. Pyrotech.* **2018**, *43*, 241–250.
- [15] L. B. Romanova, L. S. Barinova, G. V. Lagodzinskaya, A. I. Kazakov, Y. M. Mikhailov, Preparation and NMR Analysis of β -Cyclodextrin Nitrates, *Russ. J. Appl. Chem.* **2014**, *87*, 1884–1889.
- [16] W. J. Doe, New PBX formulations free of toxic isocyanates, MSc Thesis, Cranfield University, Shrivvenham, UK, **2012**.
- [17] G. Tripodo, C. Wischke, A. Lendlein, Highly Flexible Poly(ethyl-2-cyanoacrylate) Based Materials Obtained by Incorporation of Oligo(ethylene glycol)diglycidylether, *Macromol. Symp.* **2011**, *309/310*, 49–58.
- [18] R. Khan, P. Forgo, K. J. Stine, V. T. D'Souza, Methods for Selective Modifications of Cyclodextrins, *Chem. Rev.* **1998**, *98*, 1977–1996.
- [19] E. Gaidamuskas, B. Norkus, E. Botkus, D. C. Crans, G. Grinciene, Deprotonation of β -cyclodextrin in alkaline solutions, *Carbohydr. Res.* **2009**, *344*, 250–254.
- [20] P. Mischnick, D. Momcilovic, Chemical Structure Analysis of Starch and Cellulose Derivatives, *Adv. Carbohydr. Chem. Biochem.* **2010**, *64*, 117–210.
- [21] G. Norwitz, Spectrophotometric Determination of sulfate in propellants and nitrocellulose, Department of the Army Frankford Arsenal, AMS code 4931.OM.6350, Philadelphia, 1970, <http://www.dtic.mil/dtic/tr/fulltext/u2/711884.pdf> (cited October **2017**).
- [22] A. G. Bricknell, L. W. Trevoay, J. W. T. Spinks, A study of the sulfate in nitrocellulose using S35O4 – as tracer, *Can. J. Chem.* **1957**, *35*, 704–14.
- [23] Porter, D. Group Interaction Modelling of Polymer Properties; Marcel Dekker: New York, **1995**.
- [24] S. M. Pourmortazavi, S. G. Hosseini, M. Rahimi-Nasrabadi, S. S. Hajimirsadeghi, H. Momenian, Effect of nitrate content on thermal decomposition of nitrocellulose, *J. Hazard. Mater.* **2009**, *162*, 1141–1144.
- [25] NATO Standardization Agreement STANAG 4147, Chemical Compatibility of Ammunition Components with Explosives and Propellants (Non-Nuclear Application), **1992**.
- [26] J. Akhavan, *The Chemistry of Explosives*, The Royal Society of Chemistry, Cambridge, **1998**.

Received: May 1, 2018

Revised: July 18, 2018

Published online: September 4, 2018



Material Properties

Thermomechanical characterisation of cross-linked β -cyclodextrin polyether binders

Federico Luppi, Guillaume Kister, Mark Carpenter, Eleftheria Dossi*

Centre for Defence Chemistry, Cranfield University, Defence Academy of the United Kingdom, Shrivenham, SN6 8LA, UK

ARTICLE INFO

Keywords:

Differential scanning calorimetry
Dynamic mechanical analysis
Polyethylene glycol
Processability
Self-healing
Adhesiveness

ABSTRACT

Cyclodextrins are promising building blocks for the synthesis of industrial binders. A new binder was prepared by cross-linking β -cyclodextrin with variable amounts of polyethylene glycol diglycidyl ether (40–60% w/w) to produce a soft polyether network that was soluble in water and alcohol, and the thermomechanical properties of the binder were determined. Increasing the amount of cross-linker reduced the glass transition temperature of the binder, as determined by differential scanning calorimetry and dynamic mechanical analysis. Cooling experiments revealed sudden stress relief below the glass transition temperature, reflecting the de-bonding of the polymer from the metallic supports. This was prevented by contact with polytetrafluoroethylene tape. Optical microscopy confirmed the stress relief in the form of cracking, and revealed self-healing by reptation, promoted by a higher cross-linker content and temperature. The information gained on the influence of the support medium on the thermomechanical properties of the cross-linked β -cyclodextrins can be used by industry for optimising manufacture and storage methods for new binders.

1. Introduction

Binders are typically large molecules that are used to bond the particulate components in formulations and improve the physicochemical properties of the mixture. The paint manufacturing industry is historically one of the major investors in the development of new polymeric binders in order to improve the cohesion of pigment particles and adhesion to the coated substrate following evaporation of the solvent [1–3]. The electronics industry uses binders to improve the conductivity and mechanical strength of electrodes in batteries [4–6]. Binders are also used in rocket manufacturing to improve the safety and ballistic performance of propellants [7,8]. Finally, medical researchers seek biocompatible binders that facilitate controlled drug release [9]. Most current binders are derived from petrochemical resources and there is a strong demand for more sustainable alternatives [4,10–12].

Cyclodextrins (CDs) are polysaccharides derived from starch that provide a promising set of sustainable building blocks for the synthesis of new binders, particularly in the pharmaceutical industry [14]. As shown in Fig. 1, these toroidal macrocycles comprise six, seven or eight glucopyranose units to form α , β and γ CDs, respectively [14]. CDs have the ability to complex small molecules and alter their physicochemical properties, allowing the controlled release of drugs [15,16] or the entrapment and inactivation of toxins [17]. The many hydroxyl groups

carried by CDs are easily derivatised to yield binders that can be used to manufacture electrodes [18–20] or drug products [21–24]. Polymeric derivatives of all three types of CDs can respond to external stimuli such as pH or temperature, and safely deliver their cargoes of drugs to target organs [25–27]. In order to process the encapsulated drugs, crystalline CDs have been chemically modified to allow the incorporation of drugs during extrusion [26–28]. CDs were cross-linked with either multifunctional isocyanate or ethylene glycol diepoxides to form insoluble hydrogels, which can easily be formulated into pills or capsules [15,29–32]. These hydrogels are thermoresponsive and some of them self-heal following physical damage [31,33]. The self-healing mechanism relies on the supramolecular interactions in the hydrogel, such as hydrogen bonding promoted by the hydroxyl groups in the polymer [34] and interactions between CD macrocycles and the polyether chains [35–37]. Furthermore, the soft hydrogel matrix allows the polymer chains to diffuse and re-bond in a damaged area [38–40]. The self-repair of damaged synthetic materials typically involves physical flow of the material at or near the damaged area followed by reversible covalent bonding or supramolecular chemistry, which also includes metal-ligand coordination, π - π stacking and ionic interactions [41].

Most self-repairing CD systems show a high degree of cross-linking and are insoluble in water and common organic solvents. This limits their use as binders because post-synthesis reactions cannot be achieved

* Corresponding author.

E-mail address: e.dossi@cranfield.ac.uk (E. Dossi).

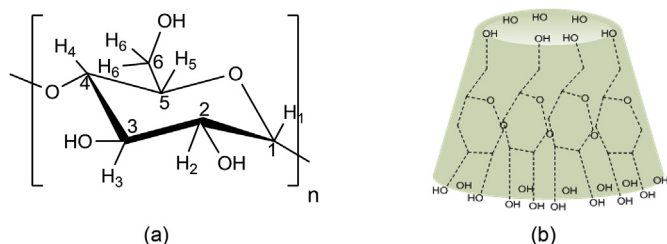


Fig. 1. a) Chemical structure of α ($n = 6$), β ($n = 7$) and γ ($n = 8$) cyclodextrins. b) Toroid structure of a cyclodextrin molecule [13].

without modifying the chemical structure, and the hydrogel becomes brittle because it cannot dissipate mechanical stress when swollen [42]. To address these drawbacks, we recently synthesised water and alcohol soluble cross-linked β CDs using polyethylene glycol diglycidyl ether (β CPCDs) [13]. Here, the thermomechanical properties of the cross-linked β CPCD system are characterized and the thermosensitive, self-healing and adhesive behaviour of the synthetic materials investigated by differential scanning calorimetry (DSC) and dynamic mechanical analysis (DMA). These experiments provide more information about these new binders and will facilitate the development of appropriate manufacturing and storage methods.

2. Materials

The β CPCD samples were synthesised from β CD ($\geq 97\%$ purity, Sigma-Aldrich) prepared as a stock (13% water content, determined by thermogravimetric analysis) and polyethylene glycol diglycidyl ether (PEGDGE, Sigma-Aldrich, $M_w = 500$ Da, polydispersity index = 1.7), as previously described [13]. The chemical structure and purity of all precursors and products were assessed by proton nuclear magnetic resonance (^1H NMR) spectroscopy and DSC. The PEGDGE/ β CD ratios used are reported in Table 1, and the PEG/ β CD ratio in the cross-linked products was determined by ^1H NMR, as previously described [35]. The physical appearance of the cross-linked products was influenced by the proportion of PEGDGE: cross-linked malleable products were generated when the PEGDGE content exceeded 50% w/w (Fig. 2a, sample β CPCD1), whereas powdery products were generated when less PEGDGE was present (Fig. 2b, sample β CPCD3).

3. Experimental

3.1. Dynamic mechanical analysis

The thermomechanical properties of the β CPCD products were determined by DMA using a Perkin Elmer DMA8000 device. The samples underwent a controlled sinusoidal displacement of 0.05 mm at frequencies of 1, 5 and 10 Hz in the single cantilever clamping bending

Table 1

Dynamic mechanical analysis and differential scanning calorimetry data for β CPCD samples and their precursors.

Sample	PEGDGE: β CD (% w/w)	Cracking temperature ^a (°C)	E' drop (%)	T _g (°C)	
				DMA ^b	DSC ^c
β CD	–	–	–	–	83
PEGDGE	100/0	–70	23	–60/–25	–73/–41/–20 ^d
β CPCD1	60–40	–42	33	41	–17
β CPCD2	55–45	–31	21	75	–8
β CPCD3	40–60	+42	11	93	+96

^a The third cooling cycle at 1 Hz.

^b The $\tan\delta$ peak.

^c Midpoint.

^d The $\tan\delta$ peaks of the three major transitions of PEGDGE.

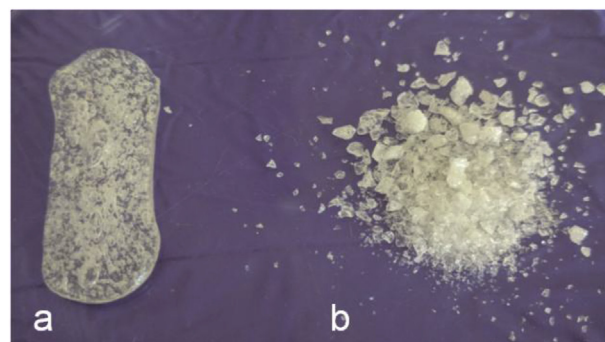


Fig. 2. Physical characteristics of β CPCD: a) malleable β CPCD1, and b) powdery β CPCD3.

configuration. The storage modulus (E'), loss modulus (E'') and damping factor ($\tan\delta$) were monitored as a function of temperature and time. The free sample length between the vibrating and fixed cantilever clamps was ~ 15 mm. The test temperature was cycled three times between -100 and 140 °C at a rate of either 2 or 10 °C min^{-1} . Each material was tested in triplicate under each condition.

The cross-linked β CPCD samples were incapable of self-support and were, therefore, tested in aluminium pockets (Fig. 3a), a stainless steel mesh (Fig. 3b), or aluminium pockets with polytetrafluoroethylene (PTFE) tape (Fig. 3c) with the aim of assessing the debonding effect of the polymer on the support. The aluminium pockets recommended by Perkin Elmer consisted of rectangular shims (30×14 mm) cut from a 0.1 mm thick aluminium strip (supplied by RS) and then folded lengthwise to form the pockets. Approximately 25 mg of the cross-linked β CPCD sample was placed in the centre of each pocket. PTFE tape (30×15 mm) was used to fold the sample in the pocket and assess the bonding interaction between the sample and the metallic support during cooling. Rectangular strips of type 18 mesh (30×15 mm) were cut from a 0.65 mm thick sheet (supplied by RS). Approximately 30 mg of the crosslinked β CPCD material was spread around and in the centre of the mesh strips.

3.2. Differential scanning calorimetry

Thermal analysis of the β CPCD samples and their precursors was carried out using a Mettler Toledo DSC3+ device. 10 mg of the material was placed in a 40 μl aluminium pan with a pierced lid. The DSC chamber was continuously purged with N_2 gas at a flow rate of 50 ml min^{-1} . The test temperature was cycled three times between -100 and 140 °C. The variation of the heat flow in the samples was recorded as a function of temperature and time.

3.3. Optical microscopy

The dynamic physical properties of the β CPCD materials under the influence of temperature were investigated by optical microscopy using a Leica DM microscope fitted with a temperature-controlled stage (Linkam THMS 600). The temperature was changed using a T95 controller and an automated LNP95 liquid N_2 pump (both from Linkam). The material was placed on a 0.5 mm thick quartz microscopy cover slip. The slide was placed in a carrier within the stage to allow visual scanning. The stage was cooled to -100 °C and then heated to 100 °C at either 2 or 10 °C min^{-1} . To prevent condensation forming on the windows of the cold stage, the interior was purged with dry N_2 gas prior to cooling. A digital Qicam Fast 1394 CCD camera (QImaging) was used to continuously record any changes in the samples during the temperature cycle. The sample was illuminated by a white light source set in transmission mode.

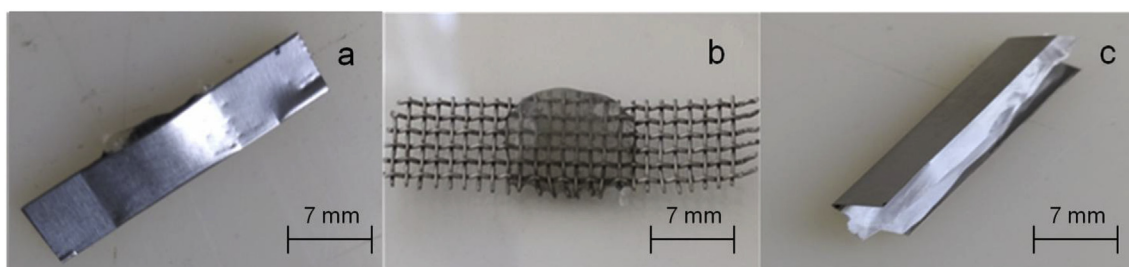


Fig. 3. Photographs of β CD samples supported by a) an aluminium pocket, b) a stainless-steel mesh, and c) an aluminium pocket wrapped in PTFE tape.

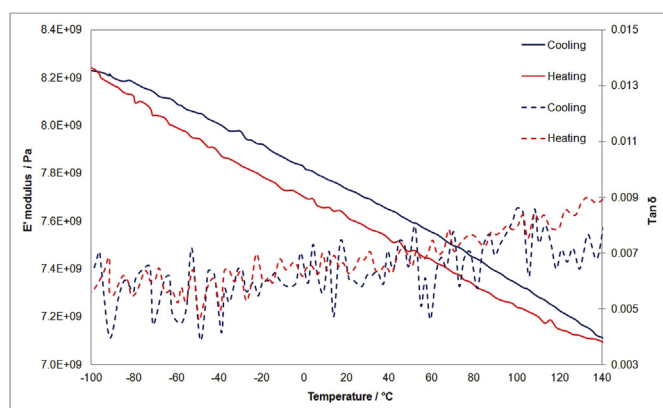


Fig. 4. Dynamic mechanical analysis showing the variation of the storage modulus (E') (solid lines) and $\tan\delta$ (dashed lines) of β CD ($10^\circ\text{C min}^{-1}$, 1 Hz, third temperature cycle from -100°C to 140°C , aluminium pocket).

4. Results and discussion

4.1. Precursor analysis – β CD

DMA was used to determine the storage modulus (E') and damping factor ($\tan\delta$) of β CD over three heating/cooling cycles from -100°C to 140°C at $10^\circ\text{C min}^{-1}$. The last cycle is shown in Fig. 4. The E' value was slightly higher during the first thermal cycle compared to the second and third cycles, reflecting the presence of synthesis-dependent stresses. There were no significant differences between the second and third thermal cycles, which are shown in the Supporting Information (SI).

The E' values of the pure β CD sample were inversely related to the temperature, whereas the $\tan\delta$ values remained relatively constant during each temperature cycle, showing there was no phase transition. This is consistent with earlier experiments that defined β CD as a crystalline compound [14]. Minor hysteresis was observed between cooling and heating. The lower E' value during heating reflects the higher degree of relaxation in the material at high temperatures. Therefore, the higher E' value during cooling is due to the stress created by the high cooling rate.

The variation in E' and $\tan\delta$ was also investigated as a function of the oscillation frequency. The increase in frequency during the temperature cycle had no significant influence on either value. The corresponding thermogram is shown in the SI. A phase transition indicated by DSC at 83°C (Fig. 5) persisted at temperature cycles up to 140°C . Earlier reports attributed this phenomenon to the dissolution of β CD crystals in the water present in the sample [43]. Molecular dynamics simulations predicted a glass transition temperature (T_g) for β CD of 61°C [44] whereas others reported a measured T_g value of 216°C [45].

4.2. Precursor analysis – PEGDGE cross-linker

DMA was also used to determine the thermomechanical properties

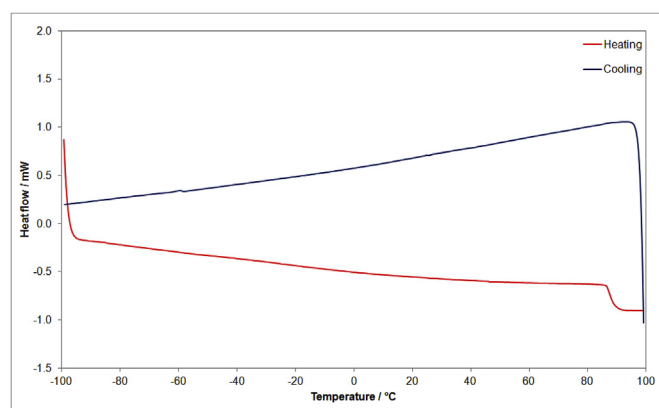


Fig. 5. Differential scanning calorimetry thermogram of β CD ($10^\circ\text{C min}^{-1}$, third temperature cycle from -100°C to 100°C).

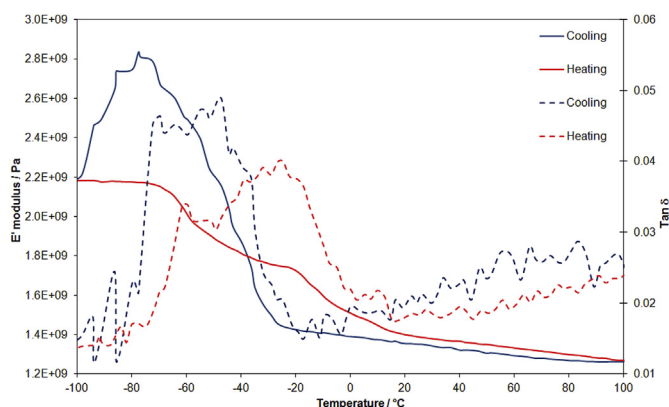


Fig. 6. Dynamic mechanical analysis showing the variation of the storage modulus (E') (solid lines) and $\tan\delta$ (dashed lines) of PEGDGE ($10^\circ\text{C min}^{-1}$, 1 Hz, third temperature cycle from -100°C to 100°C , aluminium pocket).

of the PEGDGE cross-linker, again with three heating/cooling cycles from -100°C to 140°C at $10^\circ\text{C min}^{-1}$. There was no significant difference between the thermal cycles so only the third cycle is shown in Fig. 6. The E' value fell during heating, with two main transitions at -70°C and -22°C , corresponding to the glass transitions of the PEGDGE sample. The broad and ladder-like decline in E' reflects the specific properties of this commercial product, a blend of polyethylene glycol (PEG) chains with an average molecular weight of 500 Da and a polydispersity index of 1.7.

Previous studies have shown that the T_g of PEGDGE is inversely related to its polydispersity because the shortest polymer chains act as a plasticiser, reducing the brittleness, lowering the tensile strength and increasing impact strength of the material overall [46,47]. During cooling, PEGDGE underwent a single glass transition event, increasing its stiffness. However, the rapid increase in E' from about -30°C was followed by a sudden drop at about -75°C , the latter corresponding to

28% of the maximum E' value. This phenomenon also occurred in tests conducted at the lower heating/cooling rate of 2 °C min^{-1} . DMA was used to test the aluminium support in order to eliminate artefacts caused by the machine and/or support matrix (SI). The E' value of the support showed linear variation within the experimental temperature range, suggesting that the observed phenomenon is caused by the viscoelastic behaviour of the PEGDGE and its strong interaction with the supporting pocket. Hydroxyl, epoxy and carboxyl functionalities in a polymer allow the formation of hydrogen bonds with metal and glass [48]. The strong adhesive interactions and the change in the stiffness of the PEGDGE sample during the glass transition promote internal stress which is suddenly released, initiating cracking and de-bonding of the sample from the support, recorded as a sudden drop in the E' value. The physical damage (such as cracking) that emerged during the cooling cycle provided an interesting initial assessment of the adhesive strength between the sample and different support matrices. The same thermal profile during the second and third cycles confirmed that PEGDGE recovers its initial mechanical properties when heated above the T_g in each cycle, and the process is, therefore, reversible.

The effect of the oscillation frequency on the mechanical properties of PEGDGE was tested at 1, 5 and 10 Hz. The E' curves at 1 and 10 Hz are shown in Fig. 7. The cooling and heating curves at both frequencies diverge at the point of glass transition. During heating, the glass transition of the compound is complete at $\sim 25\text{ °C}$, as confirmed by the small decrease in E' and the overlapping of the curves at different frequencies. The T_g is directly proportional to the frequency during both heating and cooling, and thus increases at higher frequencies [49,50]. The drop in the E' values caused by cracking is also influenced by the oscillation frequency: the E' peak at 1 and 5 Hz occurs at -78 °C whereas the 10 Hz peak occurs at -70 °C .

The cracking of the PEGDGE samples was analysed by DSC with a temperature cycle between -100 and 100 °C . The heat flow variation in the sample during the third temperature cycle is shown in Fig. 8. DSC revealed a thermal transition during the cooling interval from -23 to -50 °C reflecting both the crystallisation and vitrification of the blend. Therefore, the mechanical phenomenon observed by DMA is likely to occur when the PEGDGE becomes fragile following crystallisation of the longer chains (-34 °C) and vitrification of the shorter chains (-42 °C). The lower baseline heat flow adsorption after the crystallisation peak from -22 °C possibly indicates the presence of a glass transition due to the middle-length and shorter polymer chains that act as a plasticiser, as reported for PEG [51]. During heating, the heat flow adsorption of the PEGDGE increases between -70 and 10 °C in a multi-step transition that represents the combination of longer polymer chains melting ($\sim 1\text{ °C}$) and the increased mobility of the middle length and shorter chains after the glass transition. Notably, the phase transformation

measured by DMA occurred at a higher temperature compared to that recorded by DSC (Table 1), probably reflecting the oscillation frequency applied to each sample and the different sample masses used in the two analytical techniques.

4.3. Analysis of the β CPCD product in aluminium pockets

The characteristics of the precursors allowed selection of suitable methods for the analysis of β CPCD product samples. First, DMA and DSC were used to determine how the amount of PEGDGE cross-linker (ranging from 40% to 60%) affected the thermomechanical properties of β CPCD, initially with the samples held in aluminium pockets as recommended for materials incapable of self-support. The DMA and DSC data for β CD, PEGDGE and β CPCD are compared in Table 1.

The E' and $\tan\delta$ values for β CPCD1 containing 60% PEG units during the third temperature cycle from -100 to 140 °C are shown in Fig. 9. There were no significant differences in either value when comparing the three temperature cycles, suggesting that the cross-linked system is not affected by the thermal history of the sample, as observed for PEGDGE (SI). The PEG chains dominated the behaviour of the cross-linked samples, with a notable shift in the transitions towards positive temperature values. During heating, DMA revealed a gradual stepwise decrease in E' between the temperature extremes, with a major step at 55 °C coinciding with a $\tan\delta$ peak. This broad transition was frequency dependent, suggesting it represented a glass transition event for β CPCD1 (SI). The softening of the β CPCD1 product was represented by a change in the slope of the E' curve at -10 °C , matching with the onset of the $\tan\delta$ peak, and this relates to the viscoelasticity of the PEG soft segments.

With an aluminium support in place, the DMA thermogram for β CPCD1 showed a similar profile to PEGDGE during the cooling phase, which can be attributed to the cracking of the sample. A sudden drop in E' from its maximum value to 31% occurs at around -42 °C . The temperature at which cracks begin to appear in the β CPCD1 sample was not significantly dependent on the oscillation frequency, whereas cracking of the PEG chains shifted from -78 °C at 1 Hz in PEGDGE to -70 °C at 10 Hz. The lower mobility of the β CPCD1 samples reflects the existence of a cross-linked matrix compared to the viscous PEGDGE liquid, which has a higher adhesive surface area.

The DMA curves of samples β CPCD1 (60% w/w PEGDGE) and β CPCD3 (40% w/w PEGDGE) are compared in Fig. 10. When the PEG content was lower, the β CPCD cracked at a much higher temperature (35 °C) and the E' value dropped to 10% of its maximum, far below the 30% of maximum observed for the sample with a higher PEG content. A low PEG content appears to increase the brittleness of the sample and reduces its viscoelastic behaviour, also reducing its binding strength given that the drop in E' is related to the strength of adhesion to the metallic support. The glass transitions determined from the peak $\tan\delta$ values shift to higher temperatures when the PEG content is low. The absence of first-order transitions in the β CPCD samples during cooling was confirmed by DSC (Fig. 11 and SI) suggesting that β CPCD products are completely amorphous at temperatures between -100 and 100 °C .

4.4. Analysis of the β CPCD product on a steel mesh support

The way in which β CPCD1 (60% w/w PEGDGE) and β CPCD3 (40% w/w PEGDGE) interacted with a stainless-steel mesh in lieu of the aluminium pocket was also investigated. The samples were spread over the mesh prior to analysis (Fig. 1b). The glass transition of β CPCD1 as determined by DMA was interrupted by stress relaxation at 15 °C (Fig. 12). The relaxation declined between the thermal cycles but was still present during the third cycle (SI). Cracking was still observed during cooling, but the phenomenon was less severe when compared to the sample held in an aluminium pocket (Fig. 12). The cracking also manifested itself over a wider temperature range (-14 °C to -70 °C) compared to the sudden drop observed with the aluminium pocket. The

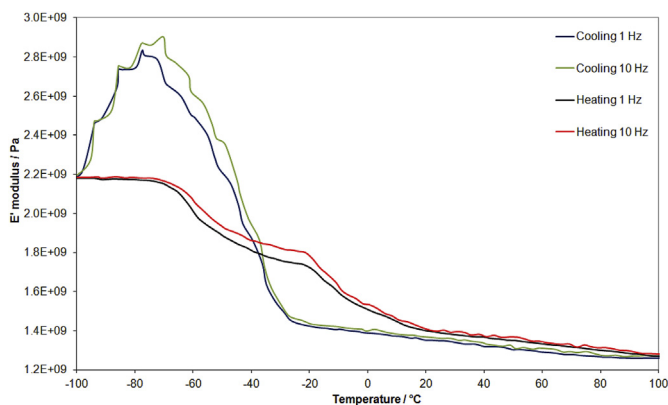


Fig. 7. Dynamic mechanical analysis showing the variation of the storage modulus (E') of PEGDGE with frequency (1 and 10 Hz) during cooling (blue and green lines) and heating (black and red lines) (10 °C min^{-1} , third temperature cycle from -100 °C to 100 °C , aluminium pocket).

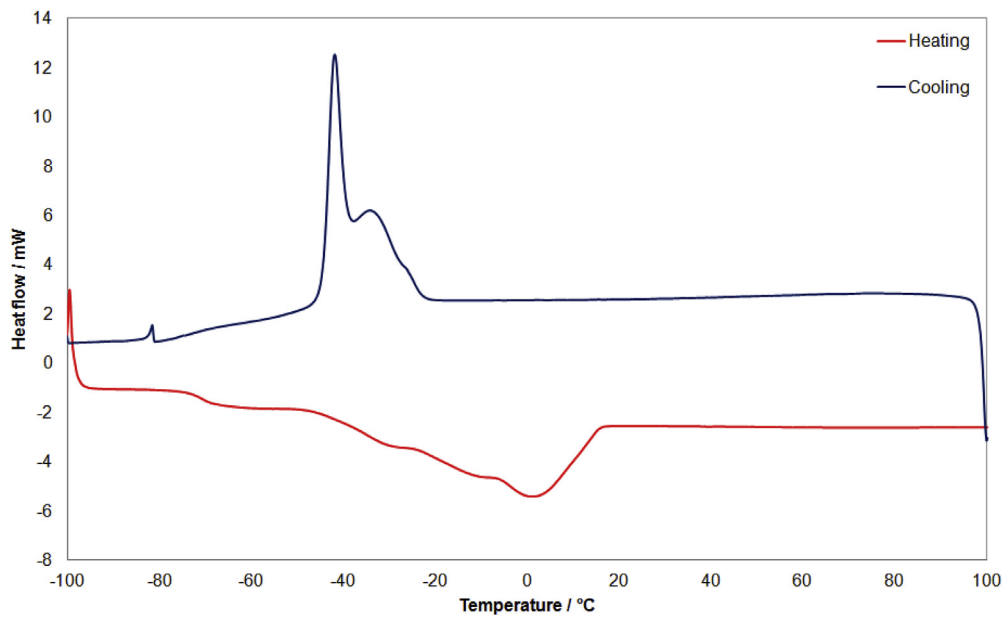


Fig. 8. Differential scanning calorimetry thermogram of PEGDGE from -100°C to 100°C ($10^{\circ}\text{C min}^{-1}$, third temperature cycle, aluminium crucible).

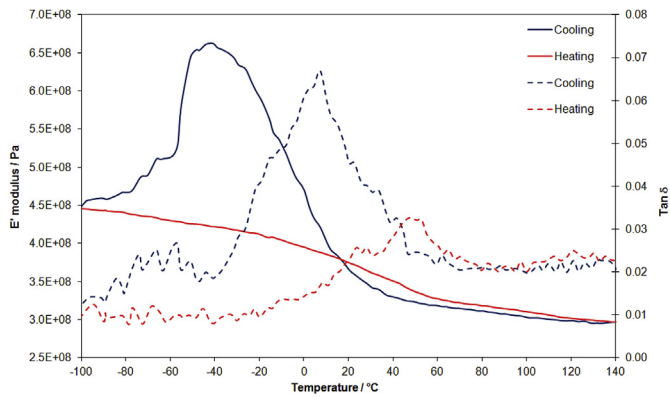


Fig. 9. Dynamic mechanical analysis showing the variation of the storage modulus (E') (solid lines) and $\tan\delta$ (dashed lines) of βCPCD1 ($10^{\circ}\text{C min}^{-1}$, 1 Hz, third temperature cycle from -100°C to 140°C , aluminium pocket).

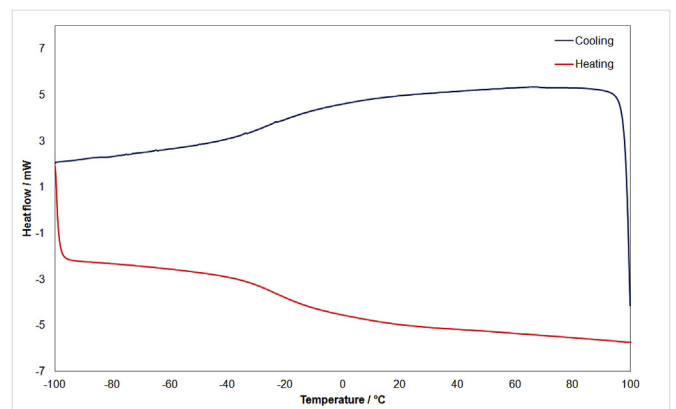


Fig. 11. Differential scanning calorimetry thermogram of βCPCD1 from -100°C to 100°C ($10^{\circ}\text{C min}^{-1}$, third temperature cycle, aluminium crucible).

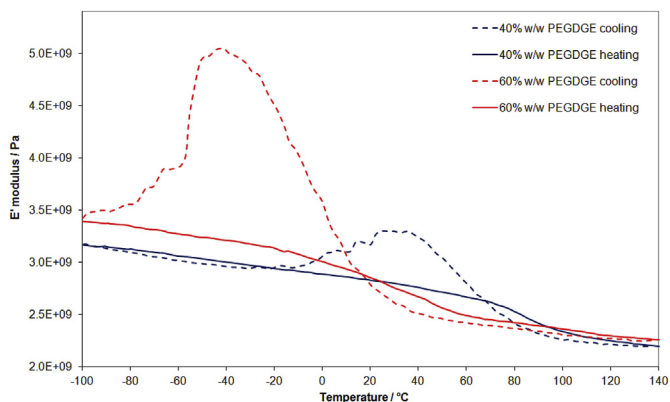


Fig. 10. Dynamic mechanical analysis showing the variation of the storage modulus (E') and $\tan\delta$ of βCPCD1 (60% w/w PEGDGE, solid and dotted red lines) and βCPCD3 (40% w/w PEGDGE, solid and dotted blue lines) ($10^{\circ}\text{C min}^{-1}$, 1 Hz, third temperature cycle from -100°C to 140°C , aluminium pocket).

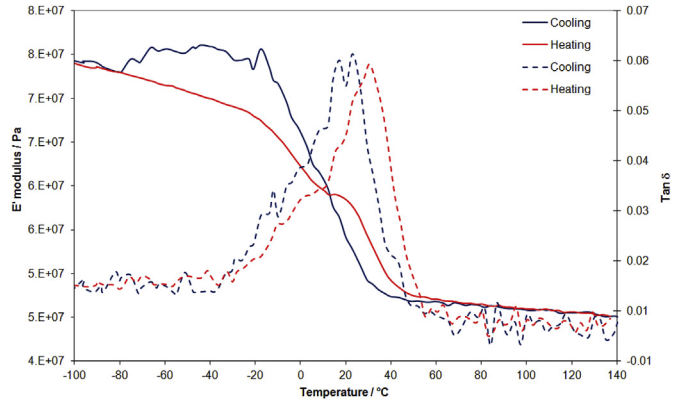


Fig. 12. Dynamic mechanical analysis showing the variation of the storage modulus (E') (solid lines) and $\tan\delta$ (dashed lines) of βCPCD1 ($10^{\circ}\text{C min}^{-1}$, 1 Hz, third temperature cycle from -100°C to 140°C , stainless-steel mesh).

characteristic drop in E' began at about -17°C and reached 3% of the maximum value. The drop was visible during each cycle, confirming the stress relaxation effect that occurs with each round of heating. The metallic mesh changes the manner in which the stress introduced

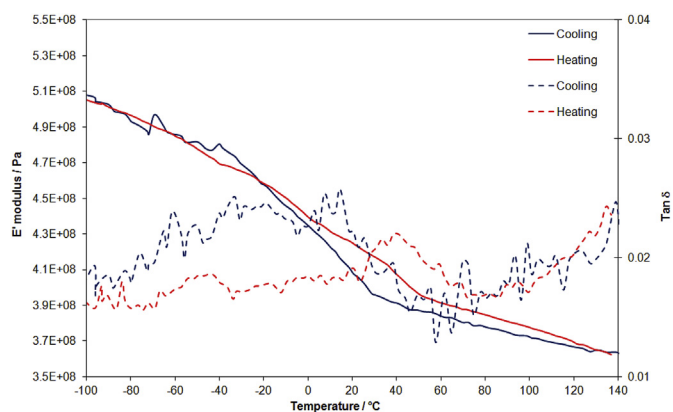


Fig. 13. Dynamic mechanical analysis showing the variation of the storage modulus (E') (solid lines) and $\tan\delta$ (dashed lines) of β CPCD1 ($10^\circ\text{C min}^{-1}$, 1 Hz, third temperature cycle from -100°C to 140°C , aluminium pocket and PTFE tape).

during each cooling cycle is dissipated. The mesh has a greater surface area to which the β CPCD1 can bind (362 mm^2) compared to the aluminium pocket (180 mm^2) but, nevertheless, allows stress to be dissipated within the bulk sample much more effectively.

4.5. Analysis of the β CPCD product in aluminium pockets with PTFE tape

Finally, to confirm that the drop in the E' values during cooling was due to the de-bonding of the sample from its support, PTFE tape was used to hold β CPCD1 samples within an aluminium pocket, thus allowing the samples to contract freely with the decreasing temperature. Preliminary DMA characterisation of the PTFE tape (blank) showed a softening at the onset temperature of 18°C (SI). The absence of adhesion between β CPCD1 and the support when enclosed by PTFE tape was confirmed by the drop in E' during cooling as shown in Fig. 13. The hysteresis between the heating and cooling curves during the same temperature cycle diminished with each cycle. Therefore, the PTFE tape almost completely eliminated the de-bonding phenomenon and the formation of thermal stress in the sample during the cooling phase. The T_g of β CPCD1 under these conditions was 41°C , identical to the value recorded in the aluminium pocket without tape, confirming that the experimental setup does not affect the T_g .

4.6. Analysis of the β CPCD product by optical microscopy

Optical microscopy was used to characterise in more detail the cracking that occurred in the β CPCD1 product during cooling (Fig. 14). A glass support was considered adequate as a transparent substitute for

the metallic support used to investigate the adhesion of the compound. The sample was cooled from 25°C (Fig. 14a) and began to crack at about -55°C (Fig. 14b), with the cracks propagating further as the temperature was reduced to -100°C (Fig. 14c and d). The same sample was then heated to 100°C and the cracks began to self-repair, starting at 0°C (Fig. 14e) until complete healing was observed at about 80°C (Fig. 14h).

During a second thermal cycle on the same sample, cracking began at -58°C and initiated at a different location (Fig. 15c). This confirms the evidence provided by the similar E' value profiles in each thermal cycle, i.e. the thermal history of the sample is erased by heating, as previously reported for a hydrogel CD/PEG system [33]. In the second cycle, sample healing occurred at about 80°C as in the first run (Fig. 15h). Furthermore, β CPCD1 placed on PTFE tape showed no evidence of cracking during the cooling phase, confirming that stress relief by cracking was due to the bonding of β CPCD1 to the glass support (SI).

This experiment confirmed the self-healing of the compound and explained why the E' curves are identical during multiple temperature cycles. The self-healing behaviour is thought to reflect the reformation of hydrogen bonds and host-guest interactions, as seen in CD hydrogel systems due to the reduction of the viscosity of the cross-linked system when heated above T_g [33,52–54]. The physical transformation occurs at the onset of material flow behaviour, allowing the crack to be filled in, and probably involves a rheological model involving the snake-like displacement of the polymeric chains, described as reptation [55].

The rupture strength of sample β CPCD1 was qualitatively assessed by intentionally cutting the sample (Fig. 16b). Both parts were subsequently re-joined and annealed in the oven at 70°C for 30 min (Fig. 16c). The joined parts were found to be cohesive after this qualitative test (Fig. 16d). The sample was gripped at its extremities and pulled gently. The sample showed considerable elongation. Diffusion of the polymeric chains by reptation and the reforming of hydrogen bonds in the fracture allowed the material to qualitatively self-repair and self-heal. In future work, the self-healing capabilities of this compound will be assessed in more detail.

5. Conclusions

The thermomechanical properties of a new cross-linked binder based on β CD and PEG segments were assessed by DSC and DMA. The cross-linking improved the processability of the material compared to crystalline β CD, which has unsuitable physical properties for a binder. All cross-linked β CPCD products showed viscoelastic responses similar to those observed for the pure cross-linker. The viscoelasticity was directly related to the proportion of cross-linker in the β CPCD system, with T_g values as low as -17°C (determined by DSC) when cross-linker content was $> 50\%$ w/w. DMA revealed a sudden drop in E' during the

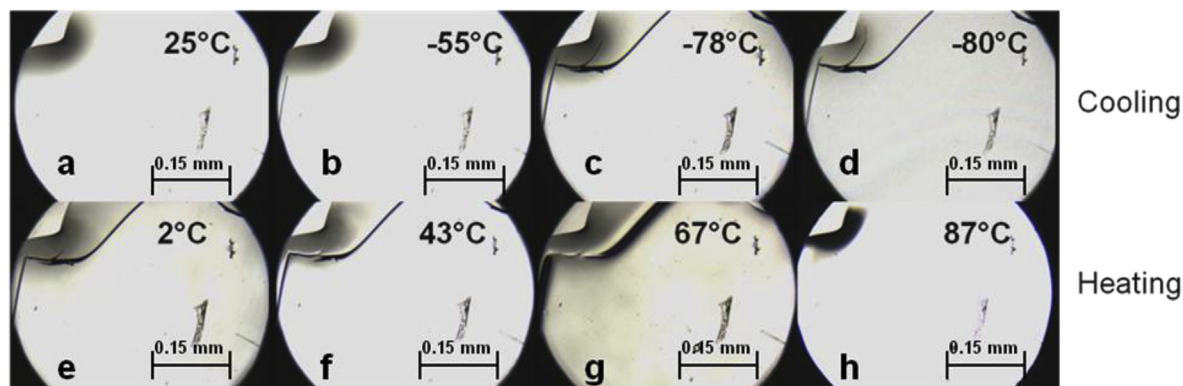


Fig. 14. Optical microscope images of β CPCD1 (60% w/w PEGDGE) during the first temperature cycle from -100 to 100°C . The top row (a–d) shows the cooling phase captured at 25, -55 , -78 and -80°C , and the bottom row (e–h) shows the heating phase captured at 2, 43, 67 and 87°C .

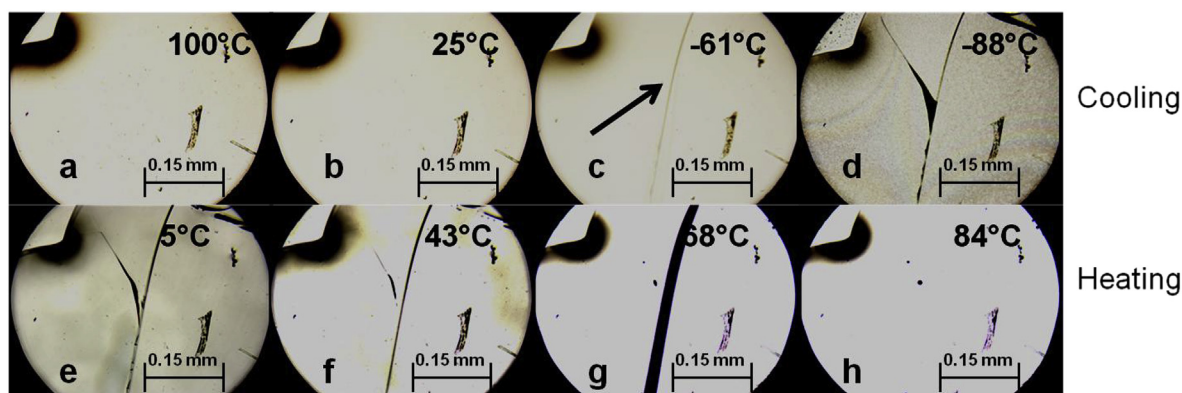


Fig. 15. Optical microscope images of β CPCD1 (60% w/w PEGDGE) during the second temperature cycle from -100 to 100 °C. The top row (a–d) shows the cooling phase captured at 100, 25, -61 and -88 °C, and the bottom row (e–h) shows the heating phase captured at 5, 43, 68 and 84 °C.

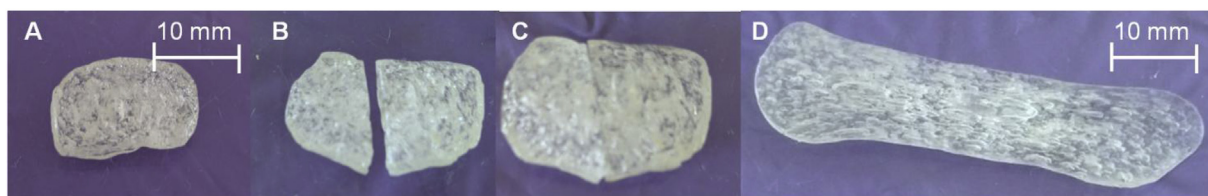


Fig. 16. Self-healing of β CPCD1 (60% w/w PEGDGE). a) Sample after solvent evaporation. b) Sample after cutting. c) The parts are placed in contact. d) The sample is heated to 70 °C for 30 min and pulled by the extremities.

cooling sequence, and the amplitude of the drop was directly proportional to the amount of cross-linker present. This phenomenon is thought to reflect the de-bonding of β CPCD from the metallic support when the sample was cooled below T_g . The adhesiveness of the material was drastically reduced when folded in PTFE film, indicating that the adhesive strength is due to the ability to form hydrogen bonds with the metallic support. Optical microscopy confirmed that the adhesiveness between the samples and the support, combined with the changes in viscoelasticity of the PEG and β CPCD segments at temperatures below T_g , produced mechanical stress that resulted in the propagation of cracks in the cross-linked material. Interestingly, the damaged β CPCD structure was able to restore its integrity by self-healing, which began at 0 °C and achieved complete self-repair at about 80 °C. The results show that the thermomechanical properties of the β CPCD system are superior to those of pure β CD. The influence of the support matrix on the thermomechanical properties of β CPCD could facilitate the development of optimal manufacturing and storage methods for new binders.

Funding

This project was funded through the Weapons Science and Technology Centre (WSTC) by the UK Defence Science and Technology Laboratory (DSTL).

Appendix A. Supplementary data

Supplementary data to this article can be found online at <https://doi.org/10.1016/j.polymertesting.2018.11.034>.

References

- [1] K.K. Sutna, S. Jacob, R. Joseph, Paint formulation using water based binder and property studies, *Macromol. Symp.* 277 (2009) 144–151, <https://doi.org/10.1002/masy.200950318>.
- [2] F.F. Abdel-Mohsen, H.S. Emira, A study of the effects of different binders and fillers on the properties of flame retardant paints, *Pigment Resin Technol.* 36 (2007) 67–73, <https://doi.org/10.1108/03699420710733493>.
- [3] V. Alvarez, M. Paulis, Effect of acrylic binder type and calcium carbonate filler amount on the properties of paint-like blends, *Prog. Org. Coating* 112 (2017) 210–218, <https://doi.org/10.1016/j.porgcoat.2017.07.023>.
- [4] B. Andres, C. Dahlström, N. Blomquist, M. Norgren, H. Olin, Cellulose binders for electric double-layer capacitor electrodes: the influence of cellulose quality on electrical properties, *Mater. Des.* 141 (2018) 342–349, <https://doi.org/10.1016/j.matdes.2017.12.041>.
- [5] D. Mazouzi, Z. Karkar, C.R. Hernandez, P.J. Manero, D. Guyomard, L. Roué, B. Lestriez, Critical roles of binders and formulation at multiscales of silicon-based composite electrodes, *J. Power Sources* 280 (2015) 533–549, <https://doi.org/10.1016/j.jpowsour.2015.01.140>.
- [6] J.E.S. Technol, N. Choi, S. Ha, Y. Lee, J.Y. Jang, M. Jeong, W.C. Shin, M. Ue, Recent progress on polymeric binders for silicon anodes in lithium-ion batteries, *J. Electrochem. Sci. Technol.* 6 (2015) 35–49, <https://doi.org/10.5229/JECST.2015.6.2.35>.
- [7] G.G. Ang, Pisharath Sreekumar, Polymers as binders and plasticizers - historical perspective, *Energ. Polym. - Bind. Plast. Enhancing Performance.* 37 (2012) 510, <https://doi.org/10.1002/pep.201280003>.
- [8] S. Chaturvedi, P.N. Dave, Solid propellants: AP/HTPB composite propellants, *Arab. J. Chem.* (2015), <https://doi.org/10.1016/j.arabjc.2014.12.033>.
- [9] N. Bertrand, P. Colin, M. Ranger, J. Leblond, Designing Polymeric Binders for Pharmaceutical Applications, in: 2013: pp. 483–517. doi:10.1039/9781849737821-00483.
- [10] P. Tourneroche, J.C. Gelin, M. Sahli, T. Barrière, Development and thermo-physical characterization of polymers/metallic powder mixtures for MIM application, *Procedia Eng* 81 (2014) 2530–2536, <https://doi.org/10.1016/j.proeng.2014.10.362>.
- [11] A. Royer, T. Barrière, J.C. Gelin, Development of bio-sourced binder to metal injection moulding, *AIP Conf. Proc.* AIP Publishing LLC, 2016, p. 020009, <https://doi.org/10.1063/1.4963413>.
- [12] S. Vasantrao Patil, S. Laxman Ghatage, S. Shankar Navale, N. Kadar Mujawar, Natural binders in tablet formulation, *Int. J. PharmTech Res.* 6 (2014) 1070–1073 https://www.researchgate.net/publication/265644099_Natural_Binders_in_Tablet_Formulation.
- [13] F. Luppi, H. Cavaye, E. Dossi, Nitrated cross-linked β -cyclodextrin binders exhibiting low glass transition temperatures, *Propellants, Explos. Pyrotech.* (2018), <https://doi.org/10.1002/pep.201800137>.
- [14] J. Szejtli, Introduction and general overview of cyclodextrin chemistry, *Chem. Rev.* 98 (1998) 1743–1754, <https://doi.org/10.1021/cr970022c>.
- [15] R. Challa, A. Ahuja, J. Ali, R.K. Khar, Cyclodextrins in drug delivery: an updated review, *AAPS PharmSciTech* 6 (2005) E329–E357, <https://doi.org/10.1208/pt060243>.
- [16] E.M.M. Del Valle, Cyclodextrins and their uses: a review, *Process Biochem.* 39 (2004) 1033–1046, [https://doi.org/10.1016/S0032-9592\(03\)00258-9](https://doi.org/10.1016/S0032-9592(03)00258-9).
- [17] R. Solaro, E. Dossi, E. Chiellini, G. Mazzanti, New multifunctional polymeric materials for the treatment of chronic uremia, *J. Bioact. Compat. Polym.* 12 (1997) 27–46, <https://doi.org/10.1177/088391159701200103>.
- [18] Y.K. Jeong, T.W. Kwon, I. Lee, T.S. Kim, A. Coskun, J.W. Choi, Hyperbranched β -cyclodextrin polymer as an effective multidimensional binder for silicon anodes in lithium rechargeable batteries, *Nano Lett.* 14 (2014) 864–870, <https://doi.org/10.1021/nl404237j>.

- [19] J. Wang, Z. Yao, C.W. Monroe, J. Yang, Y. Nuli, Carbonyl- β -cyclodextrin as a novel binder for sulfur composite cathodes in rechargeable lithium batteries, *Adv. Funct. Mater.* 23 (2013) 1194–1201, <https://doi.org/10.1002/adfm.201201847>.
- [20] F. Zeng, W. Wang, A. Wang, K. Yuan, Z. Jin, Y.S. Yang, Multidimensional polycation β -cyclodextrin polymer as an effective aqueous binder for high sulfur loading cathode in lithium-sulfur batteries, *ACS Appl. Mater. Interfaces* 7 (2015) 26257–26265, <https://doi.org/10.1021/acsami.5b08537>.
- [21] W. Chen, C. Wang, L. Yan, L. Huang, X. Zhu, B. Chen, H.J. Sant, X. Niu, G. Zhu, K.N. Yu, V.A.L. Roy, B.K. Gale, X. Chen, Improved polyvinylpyrrolidone micro-needle arrays with non-stoichiometric cyclodextrin, *J. Mater. Chem. B* 2 (2014) 1699–1705, <https://doi.org/10.1039/c3tb21698e>.
- [22] V. Giglio, C. Sgarlata, G. Vecchio, Novel amino-cyclodextrin cross-linked oligomer as efficient Carrier for anionic drugs: a spectroscopic and nanocalorimetric investigation, *RSC Adv.* 5 (2015) 16664–16671, <https://doi.org/10.1039/c4ra16064a>.
- [23] R. Solaro, S. D'Antone, L. Bemporad, E. Chiellini, New polyfunctional derivatives of β -cyclodextrin suited for the formulation of drug release systems, *J. Bioact. Compat. Polym.* 8 (1993) 236–250, <https://doi.org/10.1177/088391159300800303>.
- [24] O. Radia, E. Rogalska, G. Moulay-Hassane, Preparation of meloxicam- β -cyclodextrin-polyethylene glycol 6000 ternary system: characterization, in vitro and in vivo bioavailability, *Pharmaceut. Dev. Technol.* 17 (2012) 632–637, <https://doi.org/10.3109/10837450.2011.565347>.
- [25] Y.Y. Liu, X.D. Fan, Synthesis and characterization of pH- and temperature-sensitive hydrogel of N-isopropylacrylamide/cyclodextrin based copolymer, *Polymer (Guildf)* 43 (2002) 4997–5003, [https://doi.org/10.1016/S0032-3861\(02\)00350-6](https://doi.org/10.1016/S0032-3861(02)00350-6).
- [26] J.-T. Zhang, S.-W. Huang, J. Liu, R.-X. Zhuo, Temperature sensitive poly[N-isopropylacrylamide-co-(acryloyl- β -cyclodextrin)] for improved drug release, *Macromol. Biosci.* 5 (2005) 192–196, <https://doi.org/10.1002/mabi.200400167>.
- [27] V. Bennevault, C. Huin, P. Guégan, K. Evgeniya, X.P. Qiu, F.M. Winnik, Temperature sensitive supramolecular self assembly of per-6-PEO- β -cyclodextrin and α,ω -di-(adamantylethyl)poly(N-isopropylacrylamide) in water, *Soft Matter* 11 (2015) 6432–6443, <https://doi.org/10.1039/c5sm01293g>.
- [28] J. Thiry, F. Krier, S. Ratwatté, J.M. Thomassin, C. Jerome, B. Evrard, Hot-melt extrusion as a continuous manufacturing process to form ternary cyclodextrin inclusion complexes, *Eur. J. Pharmaceut. Sci.* 96 (2017) 590–597, <https://doi.org/10.1016/j.ejps.2016.09.032>.
- [29] H. Kono, T. Nakamura, H. Hashimoto, Y. Shimizu, Characterization, molecular dynamics, and encapsulation ability of β -cyclodextrin polymers crosslinked by polyethylene glycol, *Carbohydr. Polym.* 128 (2015) 11–23, <https://doi.org/10.1016/j.carbpol.2015.04.009>.
- [30] S.K. Osman, G.M. Soliman, M. Amin, A. Zaky, Self-assembling hydrogels based on β -Cyclodextrin polymer and poly (ethylene glycol) bearing hydrophobic moieties for protein delivery, *Int. J. Pharm. Pharmaceut. Sci.* 6 (2014) 591–597.
- [31] F. Van De Manakker, T. Vermonden, N. El Morabit, C.F. Van Nostrum, W.E. Hennink, Rheological behavior of self-assembling PEG- β -cyclodextrin/PEG-cholesterol hydrogels, *Langmuir* 24 (2008) 12559–12567, <https://doi.org/10.1021/la8023748>.
- [32] S. Salmaso, A. Semenzato, S. Bersani, P. Matricardi, F. Rossi, P. Caliceti, Cyclodextrin/PEG based hydrogels for multi-drug delivery, *Int. J. Pharm.* 345 (2007) 42–50, <https://doi.org/10.1016/j.ijpharm.2007.05.035>.
- [33] Y.G. Jia, X.X. Zhu, Self-healing supramolecular hydrogel made of polymers bearing cholic acid and β -cyclodextrin pendants, *Chem. Mater.* 27 (2015) 387–393, <https://doi.org/10.1021/cm5041584>.
- [34] F. Herbst, D. Döhler, P. Michael, W.H. Binder, Self-healing polymers via supramolecular forces, *Macromol. Rapid Commun, Wiley-VCH Verlag GmbH & Co. KGaA, Weinheim, Germany*, 2013, pp. 203–220, <https://doi.org/10.1002/marc.201200675>.
- [35] T.T. Nielsen, V. Wintgens, K.L. Larsen, C. Amiel, Synthesis and characterization of poly(ethylene glycol) based β -cyclodextrin polymers, *J. Inclusion Phenom. Macrocycl. Chem.* 65 (2009) 341–348, <https://doi.org/10.1007/s10847-009-9591-0>.
- [36] H.-J. Schneider, F. Hacket, V. Rüdiger, H. Ikeda, NMR studies of cyclodextrins and cyclodextrin complexes, *Chem. Rev.* 98 (1998) 1755–1786, <https://doi.org/10.1021/cr970019t>.
- [37] T. Miao, S.L. Fenn, P.N. Charron, R.A. Oldinski, Self-healing and thermoresponsive dual-cross-linked alginate hydrogels based on supramolecular inclusion complexes, *Biomacromolecules* 16 (2015) 3740–3750, <https://doi.org/10.1021/acs.biomac.5b00940>.
- [38] K. Guo, M.S. Lin, J.F. Feng, M. Pan, L.S. Ding, B.J. Li, S. Zhang, The deeply understanding of the self-healing mechanism for self-healing behavior of supramolecular materials based on cyclodextrin–guest interactions, *Macromol. Chem. Phys.* 218 (2017) 1600593, <https://doi.org/10.1002/macp.201600593>.
- [39] H. Fujita, Y. Einaga, Self diffusion and viscoelasticity in entangled systems I. Self-diffusion coefficients, *Polym. J.* 17 (1985) 1131–1139, <https://doi.org/10.1295/polymj.17.1131>.
- [40] M. Muthukumar, A. Baumgärtner, Diffusion of a polymer chain in random media, *Macromolecules* 22 (1989) 1941–1946, <https://doi.org/10.1021/ma00194a071>.
- [41] Y. Yang, X. Ding, M.W. Urban, Chemical and physical aspects of self-healing materials, *Prog. Polym. Sci.* 49–50 (2015) 34–59, <https://doi.org/10.1016/j.progpolymsci.2015.06.001>.
- [42] X. Zhao, Multi-scale multi-mechanism design of tough hydrogels: building dispersion into stretchy networks, *Soft Matter* 10 (2014) 672–687, <https://doi.org/10.1039/C3SM52272E>.
- [43] E. Specogna, K.W. Li, M. Djabourov, F. Carn, K. Bouchemal, Dehydration, dissolution, and melting of cyclodextrin crystals, *J. Phys. Chem. B* 119 (2015) 1433–1442, <https://doi.org/10.1021/jp511631e>.
- [44] G. Zhou, T. Zhao, J. Wan, C. Liu, W. Liu, R. Wang, Predict the glass transition temperature and plasticization of β -cyclodextrin/water binary system by molecular dynamics simulation, *Carbohydr. Res.* 401 (2015) 89–95, <https://doi.org/10.1016/j.carres.2014.10.026>.
- [45] C. Rodríguez-Tenreiro, C. Alvarez-Lorenzo, Á. Concheiro, J.J. Torres-Labandeira, Characterization of cyclodextrin-carbopol interactions by DSC and FTIR, *J. Therm. Anal. Calorim.* 77 (2004) 403–411, <https://doi.org/10.1023/B:JTAN.0000038981.30494.f4>.
- [46] S.K. Behera, D. Saha, P. Gadige, R. Bandyopadhyay, Effects of polydispersity on the glass transition dynamics of aqueous suspensions of soft spherical colloidal particles, *Phys. Rev. Mater.* 1 (2017) 055603, <https://doi.org/10.1103/PhysRevMaterials.1.055603>.
- [47] S.J. Li, S.J. Xie, Y.C. Li, H.J. Qian, Z.Y. Lu, Influence of molecular-weight polydispersity on the glass transition of polymers, *Phys. Rev. E* 93 (2016) 012613, <https://doi.org/10.1103/PhysRevE.93.012613>.
- [48] B. ESCAIG, Binding metals to polymers. A short review of basic physical mechanisms, *Le J. Phys. IV.* 03 (1993), <https://doi.org/10.1051/jp4:19937120> C7-753-C7-761.
- [49] Y. Bai, L. Jin, Characterization of frequency-dependent glass transition temperature by Vogel-Fulcher relationship, *J. Phys. D Appl. Phys.* 41 (2008) 152008, <https://doi.org/10.1088/0022-3727/41/15/152008>.
- [50] G. Kister, E. Dossi, Cure monitoring of CFRP composites by dynamic mechanical analyser, *Polym. Test.* 47 (2015) 71–78, <https://doi.org/10.1016/j.polymertesting.2015.08.009>.
- [51] N. Tabary, M.J. Garcia-Fernandez, F. Danède, M. Descamps, B. Martel, J.F. Willart, Determination of the glass transition temperature of cyclodextrin polymers, *Carbohydr. Polym.* 148 (2016) 172–180, <https://doi.org/10.1016/j.carbpol.2016.04.032>.
- [52] M.D. Hager, P. Greil, C. Leyens, S. Van Der Zwaag, U.S. Schubert, Self-healing materials, *Adv. Mater.* 22 (2010) 5424–5430, <https://doi.org/10.1002/adma.201003036>.
- [53] S.R. White, B.J. Blaiszik, S.L.B. Kramer, S.C. Olugebefola, J.S. Moore, N.R. Sottos, Self-healing polymers and composites, *Am. Sci.* 99 (2011) 392–399, <https://doi.org/10.1179/095066010X12646898728408>.
- [54] A. Klawek, V. Tantisaiyakul, N. Hirun, T. Sangfai, L. Li, Characterization of supramolecular gels based on β -cyclodextrin and polyethyleneglycol and their potential use for topical drug delivery, *Mater. Sci. Eng. C* 50 (2015) 242–250, <https://doi.org/10.1016/j.msec.2015.02.018>.
- [55] J. Klein, Evidence for reptation in an entangled polymer melt, *Nature* 271 (1978) 143–145, <https://doi.org/10.1038/271143a0>.